2000

Modelling machine induced noise and vibration in a ship structure

Wang, Weihui

MODELLING MACHINE INDUCED NOISE AND VIBRATION IN A SHIP STRUCTURE

by

WEI-HUI WANG

A thesis submitted to the University of Plymouth
In partial fulfilment for a degree of

DOCTOR OF PHILOSO .PHY

Department of Mechanical and Marine Engineering

In collaboration with

The Seventh Peace Preservation Police Corps
Taiwan, ROC

August 2000

Copyright Statement

This copy of the thesis has been supplied on condition that anyone who consults it is understood to recognize that its copyright rests with its author and that no quotation from the thesis and no information derived from it may be published without the author's prior written consent.

ABSTRACT

Modelling Machine Induced Noise and Vibration in a Ship Structure

by

Wei-Hui Wang

Most high speed vessels are fitted with powerful high speed engines which are installed in confined spaces and, as a consequence, cause an extremely high level of noise and vibration. Often structure-borne sound power is transmitted to a sound carrying structure from a source via a number of contact points. In turn, the noise and vibration are propagated in the structure and could possibly cause an undesired noise radiation.

In this study, a model for predicting power flow based on the mobility theory has been addressed. The unique parts of the study include the establishment of the relationship of mobility functions with respect to four-pole parameters and the dynamic stiffness coefficients of a coupled machine/mount/foundation system. Also expressions to represent the sound input power, the output power and the transmitted power in relation to mobility functions are clarified.

From a detailed analysis of relevant literature, it is shown that no validated models for predicting the propagation of structure-borne noise within the intermediate frequency range of 125 Hz to 1kHz exist. As a consequence, a new numerical stress wave model has been developed to bridge this knowledge gap. This innovative approach extends the earlier works of Cremer, Heckl and Ungar in the field of stress wave propagation.

Finally, a novel holistic model has been developed to line up the transmission, propagation and radiation predictions of a machine induced noise and vibration in ship's structure to take in account the fluid-structure interaction effect. A number of experiment measurements have been performed to validate the established models. From the comparisons, the prediction models are shown to be credible with an accuracy higher than 95 per cent.

The established models are of a generic nature and can be applicable to diverse engineering fields regarding to the predictions of structure-borne noise and vibration transmission, propagation and radiation. Applications of these models to characterize the vibration reduction countermeasures, as in the case of resilient mounts and squeeze-film damping plates, from a machine are also discussed.

CONTENTS

LIST OF FIGURES

CHAPTER 5

CHAPTER 6

LIST OF TABLES

NOMENCLATURE

A_{ijr}	Modal constant of r^{th} mode
B	Bending rigidity of beam
B'	Bending stiffness per unit length
c	Sound speed in surrounding fluid
c_B	Bending wave speed
c_{Lb}	Longitudinal wave speed in beam
c_{Lp}	Longitudinal wave speed in plate
c_T	Torsional wave speed in beam
c_{eq}	Equivalent viscous damping
E	Young's modulus
F_1	Force at input side
F_2	Force at output side
F_i^m	Force at point m in direction i
$\hat{F}$	Force amplitude
$\{F_k\}$	Known force vector
$\{F_u\}$	Unknown force vector
F_y	Shear force
f	Exciting frequency in Hertz
f_n	Natural frequency in Hertz
G	Shear modulus
$G(\vec{r}, \vec{r}_s)$	Green's function
G_{ff}	Force spectrum density function
G_{fv}	Cross power spectrum density function
G_{vv}	Velocity spectrum density function
$H_0^{(2)}$	Hankel function
H_{tF}	Transfer or frequency response function for force excitation
H_{tv}	Transfer or frequency response function for velocity excitation
h	Hysteresis damping coefficient; Thickness of plate/beam
h_{ij}	Hysteresis damping coefficient
j	Unit imaginary number
K	Shear rigidity
k	Stiffness coefficient
k_{ij}	Stiffness coefficient
$n(\vec{r}_s)$	Normal direction vector at $\vec{r}_s$
M	Mobility
M_{ii}	Point mobility

M_{ij}	Mobility matrix element; Transfer mobility
M_z	Bending moment
M_{ij}^{mk}	Mobility matrix element
m	Mass
m′	Mass per unit length
m″	Mass per unit area
m_{ij}	Mass coefficient
P	Power
$P(\vec{r})$	Underwater acoustic pressure at $\vec{r}$
p	Sound pressure
Q	Shear force in plate
R	Receptance
R_{ij}	Receptance coefficient
r	Distance from excitation point
$\vec{r}$	Position vector in water
$\vec{r}_{ij}$	Displacement vector from nodal point i to nodal point j
$\vec{r}_s$	Position vector on immersed hull surface
S	Cross-sectional area
S_s	Immersed hull surface area
S_{ij}	Dynamic stiffness function
T	Torsional rigidity
t	Time
V_1	Velocity at input side
V_2	Velocity at output side
V_+	Amplitude of progressive wave velocity along positive x axis
V-	Amplitude of progressive wave velocity along negative x axis
V_j	Amplitude of decayed near-field wave velocity along negative x axis
V_{-j}	Amplitude of decayed near-field wave velocity along positive x axis
V_j^k	Velocity at point k in direction j
$\{v_k\}$	Known velocity vector
$\{v_u\}$	Unknown velocity vector
$\hat{X}$	Response amplitude
x	vibration response
x_i	Displacement of interior structure as well as tangential displacement on the water contactin surface
x_n	Normal displacement of surface contacted with ambient water
w_z	Angular velocity about z axis
$\{Y\}$	Modal displacement vector
Z_{ii}	Point impedance coefficient

Z_{ij}	Transfer impedance coefficient
v_y	Velocity along y axis
α_{ij}	Four-pole parameters
$[\Phi]$	Normalized modal matrix
ϕ	Phase angle
ϑ'_z	Rotary mass moment of inertia about z axis
κ	Shear distribution factor
k	Wave number
ρ_p	Density of plate material
η	Structural damping loss factor; Lateral displacement
η_r	Structural damping loss factor of rth mode
σ	Radiation efficiency
μ	Poisson's ratio
λ_B	Bending wavelength
λ_r	rth damped eigenvalue
ω	Exciting frequency in radian per second
ω_n	Natural frequency in radian per second
ω_r	Undamped natural frequency of rth mode

GLOSSARY

BE	Boundary Element
BEM	Boundary Element Method
CLF	Coupling Loss Factor
DAA	Doubly Asymptotic Approximation
FE	Finite Element
FEM	Finite Element Method
FEA	Finite Element Analysis
FFT	Fast Fourier Transform
MDOF	Multi-Degrees of Freedom
NR	Noise Reduction
rpm	revolutions per minute
SDOF	Single Degree of Freedom
SEA	Statistical Energy Analysis
SPL	Sound Pressure Level
TDOF	Two Degrees of Freedom

ACKNOWLEDGEMENTS

The candidate wishes to express his most sincere thanks to his supervisor, Dr.R.Sutton, for his helpful suggestions, encouragement and stimulation throughout the course of this study. Similar, gratitude are extenuated to Dr. B. Dobson for many fruitful suggestions and constructive criticisms.

The author is pleased to acknowledge the contribution of my colleagues Professor R. J. Shyu, as Head of the Department of Naval Architecture, NTOU, and Professor K. Y. Wu, who provided many worthwhile discussions. Thanks are also extended to his assistants T. C. Yang and J. H. Liou, for the valuable assistance in experiments and Li Shiou Yu and Ya Wen Chuang for the typewriting support during the final months of the study.

The author is also indebted to the Seventh Peace Preservation Police Corps, Taiwan, ROC from her provision of the patrol vessel for the investigation and the National Science Council of the Republic of China for the support for this study.

Finally, the author washes to express unaffected and profound gratitude to his wife, Jenny, son, George, and daughter, Michelle for their patience, tolerance and support.

AUTHOR'S DECLARATION

I declare that the work submitted is the result of my own investigations and has not been submitted in support of a Candidature for any other degree of this or any other University

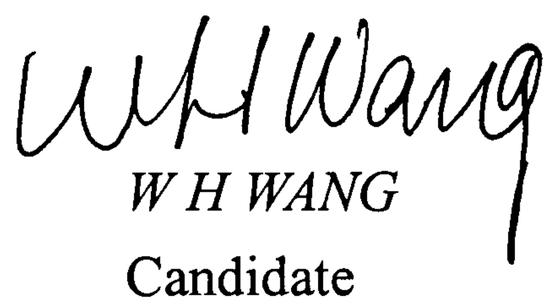

W H WANG

Candidate

CHAPTER 1

INTRODUCTION

1.1 The Structure-Borne Noise Source

Noise in a ship can be a problem. For reasons of comfort and habitability, the control of structure-borne noise is of paramount importance in the design of high performance ships. Effective noise control has been one of the most difficult objectives to accomplish in ship building. In essence, noise is acoustic energy in air radiated from vibratory solid bodies. Therefore, to control noise is to reduce vibration. Vibrations are generated from periodical mechanical forces such as impact, torsion, shearing, bending, etc., produced by various machinery. They propagate via connecting junctions to beams, plates, shells, etc., to all structural parts of a ship. During propagation, vibration waves transmit in two principal modes, the longitudinal mode along the propagation orientation, and the transverse mode in all directions normal to the propagation orientation. In a ship structure, these two modes constantly transform in fraction into each other at the perpendicular joint of two structural members.

For instance, consider two beams A and B perpendicularly cross jointed. A longitudinal wave propagation in beam A reaches the junction. There a major portion of the incoming wave continues its journey in beam A, and a fraction of the wave is scattered into beam B, with the vibration mode changing to transversal one. The magnitude of the scattered fraction depends on the frequency of the wave, the nature of the connecting joint, the fixtures and materials of either beams, etc. To complicate the matter further, as the vibration waves encounter the material discontinuities in the structure, some reflections will occur. In summary, there are vibrations with various frequencies, amplitudes,

oscillation orientations, and phases existing in a ship structure. As those vibrations transmit throughout the ship structure, the transversal modes radiate acoustic energy into the air in direct contact with the structural solid surfaces. Thus, in a noisy compartment, for example, it is often difficult to identify the specific noise sources.

As ships adopt lighter weight structure to improve their speed performance, this causes stronger structural vibrations and louder noises. Especially for those fast patrol boats, where the structure is super light, with comparatively more powerful propulsion engines confined in relatively smaller spaces, the vibrations and noises become unbearable. The noise sources generated by the mechanical forces or the forces acting directly on structural parts of a machine are called structure-borne noise sources. From an onboard measurement survey of structure-borne noise level of sources, such as the main diesel engine, the reduction gear, the generator and the exhaust pipe etc, onboard a fast vessel, it has been found that the main diesel engine is often the most dominant one, Wang (1996).

Naturally, it is desirable to contain the vibrations at the origin. To this day, resilient mounts are utilized between the engine block and the base structure as the vibration isolator. But in reality, there is no resilient material in the world capable of isolating the entire vibration power by its molecular friction mechanism alone. Thus, a large portion of the vibration power does pass through the mounts into the structure. Then every portion of the structure is a noise source. To analyse and describe the whole picture is a mission next to impossible.

However, with sufficient knowledge of the vibration transmission mechanisms in the structure, a simplified model may be constructed and an approximate solution may be obtained for this noise control problem.

1.2 Noise Source Transmission in Structure

Structure-borne sound power is predominantly transmitted to a sound carrying structure from a source via a number of contact points. In turn, the noise and vibrations are propagated in the structure possibly causing sensitive equipment to vibrate or to cause

undesired radiated noise. In principle, this may be avoided by measures at source, in transmission, during propagation or at radiation. It is, of course, preferable to cope with the problems at the generation sites and thereby avoid more comprehensive and expensive measures later in the chain. To this end, the resilient mounts are utilized as an effective countermeasure to reduce noise and vibration power transmitted from the source to sound receiver.

In reviewing noise transmission paths, it is noted that from the machinery room compartment to other areas of a ship, there are three parallel paths : air, water, and structure, the latter being the most important. While structure-borne noise is familiar, it takes an uncommon form in ship hulls : compared to industrial environments, the hull is relatively homogeneous and long wave-guide and whose transmission characteristics are affected by spatially periodic stiffening frames. Furthermore, the waterborne path is intimately coupled to the structure-borne path, partially short-circuiting structural impedance discontinuities such as bulkheads, which, in the atmosphere, would constitute effective barriers to structure-borne noise propagation. Another peculiarity of a hull is that, over much of the relevant frequency range, radiation loading is associated with inertia forces, exerted by the entrained mass of water, which modify the hull plating response. Because of the high sound velocity of water, the coincidence frequency of surface ship hull plating lies in the ultrasonic range. Flexural waves therefore radiate from areas where wave number conversion occurs, viz. drive points and impedance discontinuities. Once launched, the waterborne acoustic signal suffers propagation losses which are small compared to those encountered in the atmosphere.

Noise propagation in ship structures as well as the choice of appropriate steps for control/reduction are intimately related. Figure 1.1 shows the relation between each step on structure-borne noise transmission in ships.

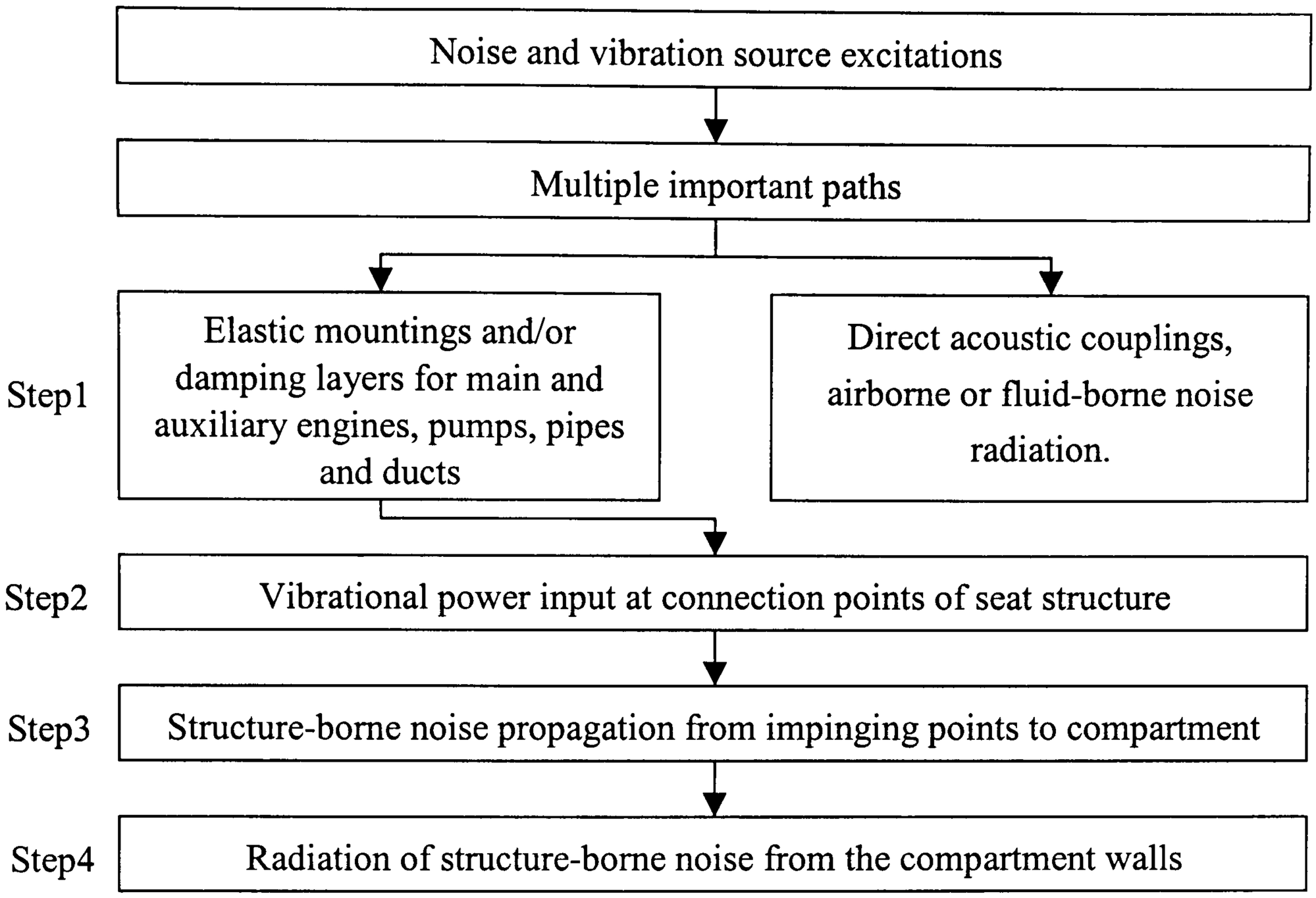

Figure 1.1 Relation between each step on structure-borne noise transmission

Machines fitted to a ship structure generate unwanted vibrations, therefore, they are often mounted on the structures via vibration ioslators as a vibration control measure. In practice, machines are mounted on large flexible structures (referred to as the seating) which may have many modes of vibration, therefore, it is not convenient to consider each mode separately. For this situation, the dispersion properties of elastic waves in rib-stiffened plate systems need to be determined for application with geometries typical of a ship's structure.

1.3 Background and Objective of the Study

Operational motions of engine and other machinery start vibrations, and the resilient mounts under the machinery seatings initiate the noise control reduction efforts. The effectiveness of the mounts can be defined in terms of the force or velocity at the machine seating. But the vibration force and the velocity may not be in phase. Besides, a large response in a structure does not always lead to a high level radiated noise. Here a more appropriate method to describe the vibration condition is adopted for each machine. The

effectiveness of isolation is defined as the measure of the power transmitted to the structure. This single quantity includes both the vibration parameters of force and velocity. An important reason for using the concept of power is that it provides a means of comparing the effects of both translational and rotational excitations. Minimizing the power transmitted through an isolator is also consistent with the first step in any vibration control exercise, ie, to deal with the problem at the source. Normally, the resilient mounts are composed of elastic and viscoelastic materials and designed in various configurations.

The vibration power fed into a structure for a multipoint mounting system can be calculated by utilizing the concept of effective mobility of the source /mount /receiver system and the source characterization as a force or a velocity. Furthermore, if the relations between the mobility function pertaining to the coupled and decoupled source/ mount/ receiver systems can be derived, then the effectiveness and performance of the mount can be identified. To achieve a successful design and an appropriate selection of the mount, sensitivity analyses of the mobility function value with respect to the dynamic properties should be undertaken.

Owing to the complexity of a ship structure, the effectiveness of the structure-borne noise isolation measure should be tightly dependent on the propagation wave patterns.

Besides considering the resilient engine mounts, a model of structure-borne noise propagation in the foundation structure has to be developed. In most cases, however, the foundation is formed in branch structure, which means the interactions between the contact points may be reduced due to intermediate stiffeners and/or energy transmission to adjacent structural parts, Cremer et al (1988). The main reason of this phenomenon has been found to be the standing wave effect in the complex branch structure. Basically, a structure which is excited, e.g. by means of a point force, will disperse motion. To describe the dynamic behaviour of the structure, the transfer mobility function matrix approach is used in the study.

Both in the predictions of the effect of design modifications for vibration isolation and in predictions of structure-borne noise propagation through complex systems, the structural characteristics of the source and the receiver are required. The quantity primarily sought is the active sound power transmitted to the supporting structure. The aim of this research investigation is to establish a new holistic model to line up the transmission, propagation and radiation predictions of a machine induced noise and vibration in a ship's structure that takes into account the fluid-structure interaction effect.

To achieve the above, the research objectives are:

(a) Engine or machine characterization as a velocity source coupled with mobility data in order to obtain convenient measurements and power calculations;

(b) Develop models for transfer mobilities and transmissibilities from engine to foundation;

(c) Numerical analysis and validation of the results by experimental measurements;

(d) Establish a model of propagation of structure-borne noise and vibration from the engine or machine foundation;

(e) Numerical analysis based on the stress wave model for the sound and vibration distribution in the ship's structure by using a computer package and self-generated software;

(f) Develop a combined finite element and boundary element method in dealing with the prediction of underwater sound radiation.

(g) Validation of the analysis accuracy by undertaking experiment measurements.

It is intended that the developed model will be suitable for use in the design stage of such, or similar, marine craft and to assist in the reduction of vibratory noise in existing ones.

1.4 Contributions of this Research Work

The contributions to knowledge that have been made as a result of this research study are as follows:

(a) Establishment of the relations of the mobility functions with respect to the four-pole

parameters and the dynamic stiffness coefficients of a coupled machine/mount /foundation system.

(b) Clarification of the expressions to represent the sound input power, the output power and the transmitted power in relation to mobility functions of a coupled machine/mount /foundation system.

(c) Development of a new numerical stress wave model to predict the propagation of structure-borne noise within the intermediate frequency range of 125 Hz to 1 kHz where existed a knowledge gap in the pervious literature.

(d) Accomplishment of a holistic model to line up the transmission, propagation and radiation predictions of a machine induced noise and vibration in ship's structure to take in account the fluid-structure interaction effect.

1.5 Outline of the Report

In more detail, the works carried out in this study are summarized in Table 1.1. In which the stress wave finite element method (FEM) is developed by continuing the previous work by Cremer et al (1998). An interface program to link the finite element and boundary element software is also developed. In the transfer mobility prediction model, the establishment of the relations of the mobility functions with respect to the four-pole parameters and the dynamic stiffness coefficients is a unique contribution.

Table 1.1 Summary of the works carried out in this study

Application / Model	Mobility and Transmission					Structure-Borne Sound Propagation			Underwater Acoustic Radiation	
	Beam	Plate	Test Rig (I)	Test Rig (II)	Patrol vessel	Test Rig (I)	Test Rig (II)	Patrol vessel	Test Rig(II)	Spherical shell
FEM (ANSYS)	√	√	√	√	√			√		
FEM/BEM			√	√		√	√		√	√
Stress wave FEM	√	√								
Analytical	√									√
Experimental Measurement	√	√	√	√					√	

A literature survey in those areas where vibrational power transmitted from machines into various ship structures and prediction models for propagation of structure-borne noise in ships is given in Chapter 2. The survey clearly reveals the fact that there are not enough validated models for predicting the propagation of structure-borne noise within the medium frequency range, i.e. from 125Hz to 1kHz, present in the published literature. Thus this gap in knowledge needs to be bridged.

The mobility model to calculate the transmitted power flow to the foundation structure from a machine is introduced and developed in Chapter 3. A mobility theory is offered in this Chapter for evaluating the point and transfer mobilities of various machine-isolator-receiving structure systems. It is the predominant and important aspect to cope with the machine induced structure-borne noise and vibration problems.

In order to evaluate the mobility reduction behaviour of structure-borne sound transfer from a marine engine via resilient mounts, the concept of mechanical four-pole parameters, which represent the physical state at a junction, is adopted to explain the sound attenuation

theory of a resilient mount.

A coupling model, combining finite element method (FEM) and boundary element method (BEM), is developed in Chapter 4 for the purpose of predicting the sound propagation in a ship structures to take into account for the fluid-structure interaction effect. In the derivations of the transfer matrices of a finite beam and a finite rectangular plate element, a stress wave model has derived. A FORTRAN program is developed based on this stress wave model. This program is especially suitable for analysing structure-borne noise and vibration within medium frequency range in a more efficient way. The validations of the developed stress wave model and the coupled FEM/BEM model are given in this Chapter. Also, the developed coupled FEM/BEM model has applied to study the machine induced underwater radiation problem.

In Chapter 5, the experimental model studies for measuring point and transfer moiblities from a machine to foundation are described. Validation of the four-pole parameters model is made by comparing the measurement results on two different scale engine room models. Also, the investigations of the effect of the resilient mounts in the attenuation of structure-borne noise power transmission are discussed.

A mobility study on the improved engine room structure by using squeeze film damping plates in a patrol vessel is also exhibited in Chapter 5. The improved radiated cabins' noise levels from the machines were discussed by measurements.

In Chapter 6, an application of the coupled FEM/BEM model to predict a machine induced underwater acoustic radiation is performed on the scale engine room model. Experimental measurement for validation was also given.

The discussion and the conclusions of this work are presented in Chapter 7. Recommendations for further work are also given.

Some of the chapters have appendices related to them. In connection with Chapter 5,

Appendix A details derivations of the transfer function matrix of finite rectangular element for the elastic bending wave. Furthermore, in Chapter 4, the discretization model of the Helmholtz equation by boundary element method is given in Appendix B. Also, there is a requirement to consider the Green's function for the solution of Helmholtz equation, this is discussed in Appendix C.

Appendix D are the technical papers published during the progress of this study.

Finally, shown in Appendix E is the FORTRAN program written for analysing the structure-borne noise propagation based on the stress wave model described in Chapter 4.

CHAPTER 2.

OVERVIEW OF THE FIELD OF RESEARCH

2.1 General Background

The interest in acoustics and structural dynamics has increased in Naval Architecture Engineeing during the last decade. The possibilities of looking into the details of sound and vibration transmission, propagation and radiation to , in and from the solid structures have also been enhanced due to the rapid progress of advanced electronic devices, such as the piezoelectric accelerometer, the impedance head, the hammer kit, the hydrophone, the digital sound level meter and the fast Fourier transformer. Owing to the increased complexity with respect to both technical equipment and constructions as well as to the environment demand sophisticated methods are required to predict the consequences of planned alterations and to validate by measurements.

Many noise problems do not surface until the ship is in operation. Simple as well as inexpensive methods to rectify the undesirable situations must be sought. Otherwise, it may be extremely difficult to get a solution. In addition, the assembly of different subsystems can lead to unintended sound and vibration problems despite the fact that each subsystem works extremely well separately. Therefore, all parts of the sound and vibration chain are important and should be equivalently treated.

The following summary is a short version of the research works done on the problem, providing a general background of this study. The references are arranged more or less in accordance with the steps outlined in Fig1.1.

The works of Middleton (1976), Kihlman (1978), and Plunt (1982) have discussed the possible ways in which the structure-borne noise source strength could be defined and measured. They concluded that the practical methods, available for the noise level prediction in buildings and ships, were those which define source strength of machinery by reference to the response of a typical foundation to the force source. Machinery impedance methods might appear to offer some assistance in the derivation of the vibration source strength of a prime mover or other item of machinery. Classical impedance theories treat vibration generators as ideal elements such as force sources or velocity sources. Real machines tend not to fall neatly into these categories because the machine itself is a structure. Large machines, such as main engines, appreciably affect the structure of the ship. The source strength of an engine could be quantified by measuring the velocity or acceleration response of the bed plate in the test house when the engine is undergoing land trial. However, the information would only be useful if the characteristics of the bed plate could be defined and compared with the characteristics of the ship's hull.

The transmission in turn, is completely determined by the source strength together with the dynamic characteristics of the source, of the receiver and of the coupling elements in between the two subsystems. A series of research works, such as Pinnington (1980, 1987, 1988), Pinnington and White (1981), Pinnington and Pearce (1990), Dobson et al. (1993); Janssen and Buiten (1973), Buiten (1976), Ohlrich (1979, 1980), Petersson (1980, 1983), Petersson and Plunt (1980, 1981, 1982a, 1982b), Plunt (1983), Plunt and Jensen (1983), have been undertaken in United Kingdom and Nordic Co-operative Organization respectively since 1980. Such works concentrated on investigating the parameters controlling power transmission from a vibrating machine to an extensive receiving structure, such as a ship hull, via spring-like vibration isolators. Part of the work was an investigation looking into convenient ways of representing a machine as a source of vibration power. Two simple models of a machine were developed, namely a mass and a finite beam. For the first one, a mass was used to represent a machine at low frequencies, when it moves as a rigid body. This model was used by Pinnington and White (1981), which was applied to an experimental investigation of power transmission from a mass

excited by a force, the mass being coupled to a long finite beam by a rubber spring. The rubber spring represented a machine isolator, and the long finite beam, represented an extensive receiving structure. At low frequencies a machine can be considered as a rigid mass, but at higher frequencies it vibrates in its natural modes of vibration, therefore impossible to accurately model it with a simple element. Thus a free-free beam has been chosen, at this first instance, to characterise a resonant machine source. This choice is simple enough to permit mathematical analysis, yet it has the necessary feature to provide an understanding of power transmission from a resonant machine source. Furthermore, the theory of Pinnington (1980), Pinnington and White (1981) considered the power input to, and transmitted from, a short finite beam connected to a semi-infinite beam by a spring-like isolator. The semi-infinte beam was the simplest way in which to represent the receiving structure. For the second one, the theory considered power transmitted from a short finite beam connected to a long finite beam by a spring-like isolator. In this case the long finite beam, having many resonances, represents an extensive but finite receiving structure. Experiments were then carried out with physical models of the above two configurations, and the measurements of peak and frequency average power were compared with the predictions. Most experimental measurements in these research works were undertaken in a laboratory. While in the case of a ship structure, the characterization of power flow of structure-borne noise source by measurements will be much more complicated.

Heckl (1976) pointed out that the behaviour of elastic mounts at low frequencies was fairly well understood and it was possible to predict their performance provided the stiffness of the mount and the impedances of the structures on both sides of the mount were known. For higher frequencies, elastic mounts must be considered as wave-guides having higher order resonances. It was shown that the first higher order resonance depends mainly on the mass of the resilient element. It was also shown that for large resiliently mounted engines at medium and higher frequencies (100-500 Hz) the sound transmission through the surrounding air can be more prominent than that through a good resilient mount.

Kihlman (1982) developed a simple model to calculate the vibrational power fed into a structure for a multipoint mounting system based on the concept of effective overall mobility of the source and the foundation and the effective transfer mobility of the vibration isolators. However, the vibration source was considered to be under rigid body motion only.

Horner (1990), Horner and White (1990, 1991) have developed the models to determined the wave type, either flexural or longitudinal wave, which carry most vibrational power through bends or joints in beam-like structures. By establishing the wave type which predominantly carries power transmission, it is then possible to apply the most suitable vibration control measure. Gibbs and Tattersall (1987) considered all modes of vibration, including compression, torsion and bending, both for the incident and generated waves of vibrational energy transmission at a corner-junction of square section rods.

At the beginning of the 1980's, Goyder and White's works (1980a, 1980b, 1980c) studied the phenomena of wave propagation and power flow in the far field of an infinite plate with a single infinite line-beam. Such a structure is excited by forces or torques applied to the beam at the driving point. In the far field, power transmitted by flexural waves in the beam is radiated into the plate but power transmitted by torsional waves in the beam is not radiated. The general conclusion from their analysis is that the power flowing into the system is controlled by the beam while the subsequent flow of power throughout the structure is governed by the plate. Also the plate carries a cylindrical wave with a strong directivity. However, their method is hardly applicable to the vibrational power flow analysis of real ship structure, as the later is composed of plate-stiffener combination with limited plate extent and multiple stiffeners.

Regarding the development of the measurement technique of power flow, Pavic (1976) examined the signal propagation characteristics in both nondispersive and dispersive media based on the signal coherence at two different points along propagation paths. In propagation along nondispersive paths, coherence was achieved by characteristic time lag

shifting and crosscorrelation analysis was used. For dispersive paths in which the coherence of the traveling signal was degraded along the path and conventional crosscorrelation ceased to be useful as a method of analysis, Pavic showed that the coherence between the signals can be restored by applying some transformation to the spectra of the signals. The resultant simplified power flow measurement methods and the conceptual design of analog electronic measuring devices could be applicable in some special cases of flexural vibrations in both beams and plates. The finite difference approach was chosen for obtaining spatial derivatives of kinematical quantities relevant to power flow determination.

The two processes, i.e., generation and transmission of the noise in ship structure are not independent. Knowledge of the mechanisms governing the generation as well as the dynamic characteristics of the source allows for an approximate description of the source strength. Verheij (1976) discussed an experimental method in which the internal excitation of a machine was replaced by an equivalent external force. Application of this method to three diesel engines for the octave bands with central frequencies from 125 to 2kHz showed that the real excitation may be replaced by an external equivalent force, which generates within 3dB the same response as that of the running engine, for various receiver positions, various sound transmission paths, various ways of mounting and various enviroments. There are some limitations of such a method: (1) the vibrational energy should be distributed over the respective transmission paths in the same ratio; (2) the equivalent forces measured with the aid of a loudspeaker should be easily recognizable by their narrow band signature of the open circuit voltage of a reciprocal transducer in the mechano-electrical two-port system, whereas for broad band sources this will be less easy; (3) the transmission system would be reciprocal.

The works of Cremer et al (1988) have dealt with analysis of the propagation of structure-borne noise in vehicles and buildings, especially concentrating on the propagation wave pattern for the fundamental structure such as simple infinite (or semi-infinite) beam, thin plate or shell.

Nilsson (1976, 1977, 1981) investigated the propagation of the structure-borne noise in the superstructures for typical medium-sized tankers. It was found that the attenuation of structure-borne noise was sufficiently well described by a simple flexual wave model for a frequency range of 31.5-4kHz. After Sawley (1969) and Lyon (1975) developed a framework of the study of the energy flow of structural vibration systems called Statistical Energy Analysis (SEA), Jensen (1976) discussed the possibility of calculating expected vibration amplitude distribution throughout a ship's structure with a higher degree of accuracy using a power flow model based on SEA. The comparison between measured and calculated values of the insertion loss on a ship model section has shown that the agreement was reasonable; somewhere acceptable and elsewhere poor. The experimental investigation on the ship structure model has shown that it is hardly appropriate to limit the SEA model of a ship section to include only flexual vibration modes in the structure. At last, when the intention is to carry out a complete analysis of the structure-borne noise propagation in complicated steel plate construction (composed of combinations of plates joined in either T-junction, L-junctions or cruciform junctions), it is necessary to consider the flexual wave combined with longitudinal and shear wave transmission through the hull plate sections simultaneously. The main problems involved in the application of SEA for prediction of noise level concerning structure-borne noise propagation, as pointed out by Sawley (1969), Kihman and Plunt (1976) and Irie and Takagi (1978), was in getting proper input data to the calculation.

Sound radiation as a result of structure-borne vibration has been treated by Gophey (1967), Ginsberg and Rosenkilde (1986), Cremer et al. (1988), Chen and Ginsberg (1988) and Fahy (1989). Fahy explained that sound radiation from vibrating surfaces could be expressed in terms of the distribution of normal surface velocity. Analysis of sound radiation from planar surfaces by means of far-field evaluation of the Rayleigh integral and synthesis of travelling wave Fourier components were presented in such a way that the equivalence of these dual approaches could be appreciated. Gophey derived a regular integral equation from the classical Helmholtz integral and a numerical quadrature technique, successfully solved the integral equation to obtain the distributions of pressure

and velocity over a vibrating surface submerged in an unbounded acoustic medium. The acoustic radiation from an elastic plate driven by an underwater shock (Ginsberg and Rosenkilde, 1986)or by a central point force (Chen and Ginsberg, 1988) was numerically solved by the Doubly Asymptotic Approximation (DAA) model which took the fluid-structure interaction into consideration. The results showed that the pressure distribution was not in good accord with the displacement. The main reason is that in the formulation of DAA model the numerical error for displacement is of the first order whilst that for pressure, which is proportional to the velocity, is of the second order.

2.2 Special Topics

There are some subjects of particular interest as this study is concerned. The relevant references are assembled accordingly.

2.2.1 Multi-Point Transmission

The classical approach for calculating structure-borne noise and vibration transmission is based on the assumption of a velocity source performing rigid body motions. Thus a multi-point coupling between the source and the receiving structure may be considered as a combination of separate poles according to Pinnington and Pearce in 1990. For a machine mounted at four sites there will be four possible modes of motion; the monople motion with all sites moving in phase, two dipoles with opposite pairs moving in anti-phase (rocking about two perpendicular axes), and a quadrupole in which diagonal pairs move in anti-phase.

Although it was possible to handle mathematically all six degrees of freedom in motion as well as the potential coupling between them, the unwieldiness of the classical approach grows rapidly as the number of degrees of freedom included increases (Timoshenko and Young, 1955). It is therefore customary to simplify the transmission problem to only one degree of freedom. The rigid body motion treatment underlying this approach is often questionable. Instead it is usually necessary to treat both the source and the receiving structure as continuous systems for low frequencies. Such a description of linear source

and receiver systems is conveniently obtained by means of the concept of mobility which, most often, is more preferable than the mechanical impedance in dealing with structure-borne sound and vibration transmission problems.

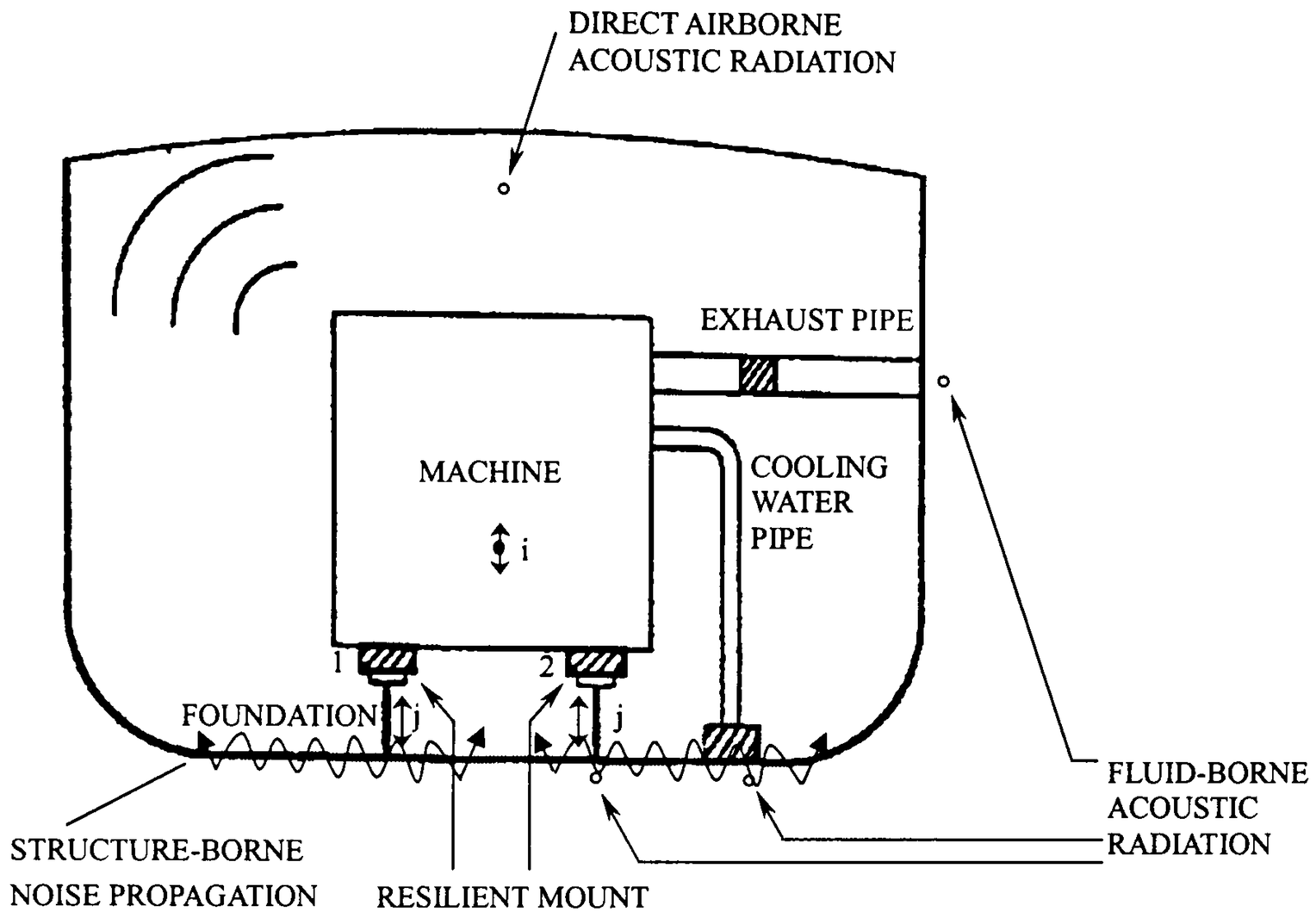

Figure 2.1 Possible acoustic transmission paths

The source and receiver structures are commonly coupled to each other at several discrete points as shown in Figure 2.1. The word "point" herein is used in a somewhat extended meaning, denoting an area with its dimensions smaller than a fraction of the governing wavelength. The physical coupling of the structural subsystems is often constituted by relatively small elastic elements (chocks, isolators, etc) called the transmission elements. For a general system, the subsystems are thus consisting the source (including possible feet), the transmission elements and the receiver. If no transmission elements are present, the interface between the source and the receiver is located below the feet. Of course, there are other possible assembly variations, but the one described facilitates a unified treatment of rigid and resilient installations.

In the general case, the interaction between the different contact points as well as between the different components of motion must be taken into account. For the wide frequency band of interest, the handling of the general matrix formulation results in an excessive task

since not only the contact points between the source and the receiver can be quite numerous, but also the six components of motion relative to Cartesian axes and excitation at each connection must be taken into account.

A large number of works concerning developing the methodology and describing experimental methods for the determination of structure-borne noise and vibration transmission have been reported. It is also shown that in the experimental situation the benefits of the mobility representation are apparent.

Ohlrich (1979, 1980) compared the dynamic characteristics of four types of bedplates used for engine mounting in ships and revealed that the characteristic of the bedplates has a local effect to the structure-borne noise control in the frequency range from 20Hz to 20kHz of interest for shipboard acoustics. The bedplate structure is composed of two parallel platestrips supported by girders and frames, which may from an integral part of the double-bottom structure in a ship. The results presented were derived from experiments on models of 5-frame bottom sections of ships. Also the vibration transmission from the bedplate to the hull structure by applying a harmonic point force excitation normal to the bedplate in a single point was discussed. This relationship is an important factor for the prediction of engine-generated noise in remote areas.

In 1980 to 1983, Petersson(1980, 1983), Petersson and Plunt (1981, 1982a, 1982b), Plunt and Jensen (1983) and Plunt (1983) applied the effective mobility concept to the analysis of a structure-borne sound power transmission between coupled structures via multi-paths from a machine. Also the methods for determing the effective mobilities in the transmission of vibrations between complex structures connected at several points were developed. The general moblilty matrix of multi-point, coupled structures can be formulated into a $6N \times 6N$ matrix, where N is the number of contact points. The effective moblilty represents the ratio of the total velocity due to all applied forces to the force acting at a contact point to be considered. Thus it is possible to neglect the influence of some element in the mobility matrix and to rearrange the general mobility matrix into some

corresponding effective mobilities. Some results from full scale measurements of point and transfer mobilities on the feet of shipboard diesel engine and the foundations were presented and some possible simplifications of the mobility description of these structures were discussed. The measurements were performed for the frequency range 50-3200Hz. The examples of measured point and transfer mobilities for the structures in their studies showed that the point mobilities were generally greater than the transfer mobilities because of the inhomogeneity of the sturctures. Also, the point mobilities were found to be mainly determined by the local dynamic properties of the structure. Accordingly, the effective point mobilities of complex, inhomogeneous structures can be approximated by the corresponding ordinary point mobilities in many case. For homogeneous structure and structures where there are no strong discontinuities between the contact points, at which the source and the receiving structure are connected, the interaction between the points must be taken into account. However, the effective point mobility can be approximated in such cases by the ordinary point mobility multiplied by different correction factors. The agreements between the measurement mobility results and the results from the estimation precedures were very good. Besides, in the utilization of the effective moblilties as the descriptive parameters to evaluate the structure-included acoustic engergy input on the combination of diesel engine---coupling elements---foundation structure, the prediction models of structure-borne noise power transmission still need the appropriate source velocity data.

Verheij (1986) made some significant contributions to the methodolgy for analysing the multi-path sound transfer in resilient mounting systems in ships, and for improving such systems in an economical way by using the experimental methods of reciprocal transfer function measurement for quantifying the sound transfer path. The concept of this approach for the path analysis is that, the measurements were performed with the engine stopped, whereas the machinery noise is simulated by excitation upon the outside of the engine with a number of incoherent exciters. It is assumed that for the frequency range where the engine no longer vibrates as a rigid body, the internal excitation may be modelled with sufficient accuracy by this artificial excitation. Only by using this artificial

excitation does it become practicable to interrupt sound transfer path, e.g. by removing a flexible pipe coupling. If then for constant excitation the sound transfer to a distant position decreases, it is certainly a quantitative indication for the relative importance of the interrupt path. An essential step simplifying these experiments is to perform the transfer measurements reciprocally. The great advantage of this approach might be that the predominant transfer paths can be detected with relatively simple experiments. Moreover, a quantitative insight is obtained as to what extent a certain resilient mounting system can be improved without modifying the paths through the mounts and through the air.

The sound source under investigation was 4MW medium-speed propulsion diesel engine onboard a twin propeller passenger and car-ferry. Measurements had been performed both at sea during a normal service trip and at the yard before the ship went into service. During the measurements at sea, the two outer of the four main engines were in service. They were running deliberately at different speeds to facilitate source identification. The engine close to the receiver location was running at 512 rpm, the more distant engine at 480 rpm. The receiver location for determining the sound transfer to the accommodation, was on the hull at approximately 10m above the tanktop of the double bottom in the engine room. To characterise the total sound transfer to this location, the open circuit voltage of a reciprocal electrodynamic vibration exciter was used. It's response at sea was completely determined by the nearest main engine for the frequency range of the path analysis, i.e., the 63Hz-1kHz octave bands.

More recently, Koh (1992) recognised that for the study of machine-induced vibration problems, considering resonance responses of the coupled systems as well as the interactions among governing degrees-of-freedom, a more detailed model is necessary. The unifying concept of time-averaging vibrational power was utilized to examine the vibration transmission from a machine source to flexible beam and plate-like seating structures via the translational and rotational motions as well as the coupling between these motions, for the case when the seating structures were subjected to co-located simultaneously acting sinusoidal force and moment excitations. For linear structures subjected to simultaneously

acting force and moment excitations, the driving point coupling mobility function always exist, except for the special case when the excitation point coincides with a symmetrical point of the mode shape. These coupling mobility functions contribute to vibrational power components transmitting to the structures as important as the direct force and / or moment mobility functions. Thus the cancellation among the transmitted vibrational power components to the seat structure is possible, which constitutes a special vibration control technique. Koh proposed this vibration control technique to reduce the unwanted machine-induced vibration levels on the seat structure, at a specific frequency, by means of controlling the rate of the applied moment to the applied force via suitably designed force and moment seatings attached to the mounting point. This control technique is most suitable for the case of a low to medium constant speed machine mounted on a flexible seating structure.

2.2.2 Mobility Prediction

The mechanical point mobility at a point of a structure is defined as the complex ratio between the velocity and the force acting at the same point. The moment mobility may analogously be defined as the ratio between the angular velocity and the moment. Generally the magnitude and the phase of both the velocity (angular velocity) and the force (moment) are required. The force and moment mobility functions are completely determined by the dynamic characteristics of the actual structure, such as the mass (inertia), the stiffness and the losses (internal losses as well as coupling or radiation losses).

In case where the subsystems (machinery, foundation) are connected at several points, as shown in Figure 2.1, the so-called transfer mobilities must also be defined. These transfer mobilities are defined as the ratio of the velocity component at point k to the force component acting at point m. Generally, there are six independent components of motion at a point, three translations and three rotations. Accordingly there must be transfer mobilities defined between all six components, obviously including point mobilities. Thus O'Hara (1967) generally defined the elements in a total mobility matrix as:

$$M_{ij}^{mk} = \frac{V_j^k}{F_i^m} \quad , \quad (m,k=1,2,\ldots,N\,; \qquad i,j=1,2,\ldots,6) \tag{2.1}$$

Where F_i^m is the force at point m in the direction i and V_j^k the velocity at point k in the direction j due to this force. For the linear systems, the reciprocity principle should be valid, which means that the indices could be transposed but with the restriction that both the point indices and the direction indices are transposed simultaneously, i.e.,

$$M_{ij}^{mk} = M_{ji}^{km} \tag{2.2}$$

For continuous systems where the number of degrees of freedom are infinite, the mobility can be deduced from the wave equation. Such a deduction can be rather complicated, especially for finite structures in resonances. Generally, the mobility can only be expressed in a closed form for infinite system. However, there are special cases often of great practical importance for first order calculations and estimations. Figure 2.2 presents a typical mobility plot. The mobility of an infinite elementary structure is called the characteristic mobility. Whilst finite structures possess more or less recurrent resonances. The expressions of the mobility are quite complicated, since they are mainly determined by these resonances. In many cases, it is not even possible to find practically useful expressions unless special methods for the determination of the eigen-functions are used.

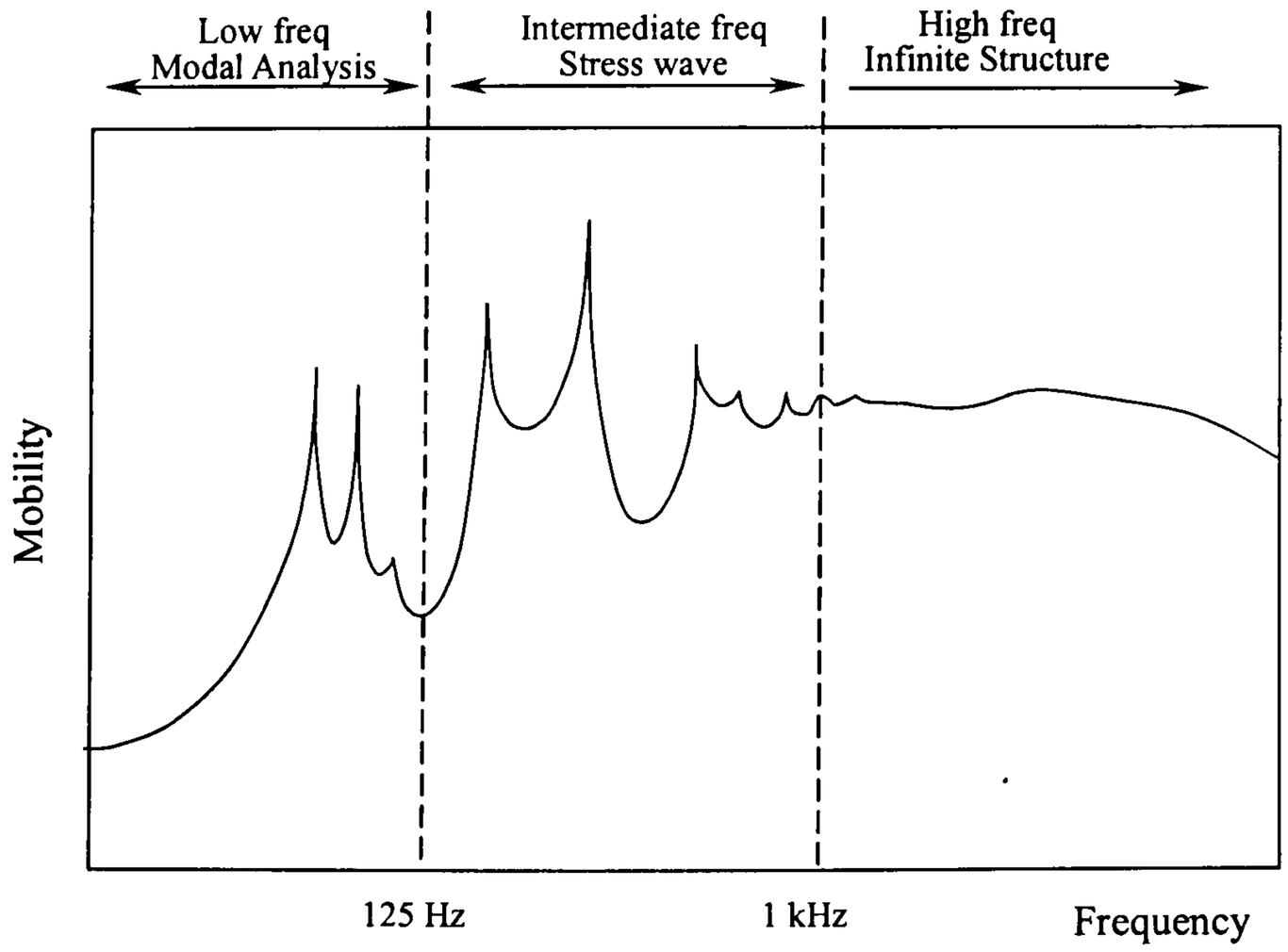

Figure 2.2 Typical mobility plot

The mobility (or the inverse quantity of mechanical impedance) has been derived for a number of systems that are either of infinite or semi-infinite in extent. Two compilations of expressions were given by Cremer et al. (1988) and Pinnington (1988). For a limited number of finite systems, closed form expressions representing the mobility have been estabilshed, such as by Snowdon (1968). However, in the general case of a finite system, the mobility is not obtainable in closed form.

For the low frequency region the mobility may be estimated using a series solution approach (Cremer et al., 1988), or a finite element analysis (Hale and Meirovitch, 1980). But, to consider a moderate number of eigen-functions (modes) contributing to the dynamic behaviour of the system, the numerical work required is very time-consuming. Moreover, the fineness of the finite element mesh needed is related to the maximum frequency of interest, which in sound and vibration problems can be relatively high. Naturally, the physical size of the system under consideration also put a limit to this approach.

Damping is the removal of energy from a vibratory system. The energy loss is either transmitted away from the system by some mechanism of radiation or dissipated within the system. Most measurements of damping are performed under conditions of cyclic or near cyclic oscillation. Usually, the decay of free oscillation is observed directly, or by measurements of steady-state forced vibration at (or in the vicinity of) resonance. In both cases the total energy removed in a cycle can be inferred, but the results are seldom precise enough to provide a detailed picture of how the instantaneous rate of energy removal fluctuates within a single cycle. Apart from the correct data input problems, the handling of amplitude and frequency dependent losses can be rather intricate (Crandall, 1970). Surveys and discussions of the different mechanisms governing the damping are found in the works of Crandall (1970), Unger (1973), Bert (1973), Nashif et al. (1985) and Sun and Lu (1995).

Another approach which has become increasingly attractive is the synthesis of experimental and numerical methods owing to the development of the Fast Fourier

Transform (FFT)-technique. The modal parameters were extracted from a few transfer function measurements and a complete mobility matrix was found numerically by Ewins (1980) and Goyder (1980). Unfortunately, it is found that such an approach is critically dependent on the measurement technique and the subsequent analysis of the results, and misleading conclusions can be reached (Ewins and Griffin, 1981). The discrepancies between measurement and analysis are due to localised errors (loss of stiffness at joints, etc), or to more general factors (such as incorrect values of elastic modulus or material density etc), or to the case that the location of the response points used in the modal test does not coincide exactly with any of the mesh of grid points used in the analytical model. In addition, the extraction of the modal parameters can be very cumbersome for heavily damped systems or for cases of high modal density with strong coupling (Looser, 1982).

For the high frequency region of the non-resonant system, i.e., where the modal density of built-up structures is generally high, Skudrzyk (1980) and Cremer et al. (1988) discussed the validity that the mobility of the actual finite system can be approximated by the mobility of the corresponding infinite system. It was demonstrated for some structure configurations for which expressions giving the frequency for the onset of the infinite system behaviour were proposed by Goyder and White (1980a). Moreover, as frequency increases, the mobility is determined better by the dynamic characteristics of a small substructure surrounding the point under consideration. This means that the infinite system behaviour and thereby the mobility may be estimated for the structural element within the nearest discontinuities (Bishop and Mahalingam, 1981).

Consequently, the prediction of the mobility is most difficult in the mid-frequency range. However, if details of the vibrations are not of interest but rather the average dynamic behaviour of the system is under consideration, the mobility can be derived from that of the corresponding infinite system (Skudrzyk, 1980).

The inadequate understanding of the numerous mechanisms governing the losses of a structural system, both with respect to the dissipation and to the coupling or radiation to

external systems, makes the prediction of the mobility more difficult. This in turn, is essential for the determination of the structure-borne noise and vibration power transmission. Thus, in general, such predictions still, to a great extent, must be based on experience and empirically acquired data.

The problems in predicting the real part or mobility, i.e., that part associated with the power transmission, were discussed by Goyder and White (1980a, 1980b, 1980c) and Pinnington (1980). For the low and mid-frequency regions, the real part of the mobility of the finite system is normally, on the average, less than predicted on the assumption of an infinite behaviour, and is approximately equal to that value at high frequencies.

2.2.3 Prediction Method for Propagation of Structure-Borne Noise in Ship

The majority of prediction methods for structure-borne noise propagation are basically empirical and written in computer software programs which are easy and inexpensive to operate. This approach views previous ships as full-scale models for future similar ones, meanwhile trying to find rules for arranging experimental findings and for translating them into reliable predictions. The accuracy of these programs is satisfactory for standard ship designs. In principle, this approach comes down to asking what is the difference in acoustical effect between a new ship and ships that could be investigated. However, parameter studies and prediction for non-standard ship design cannot be accommodated using these methods. Among these, probably the most well-known is the method proposed by Janssen and Buiten (1973). Also further developments of this method, where more detailed data for the reductions in velocity levels per deck and per frame were taken into account by Buiten (1976) and Plunt (1980), are available. Common to all these empirical methods is the requirement that a velocity level for the foundation of the source is used as the input data.

Other prediction methods are, in general, based on the Statistical Energy Analysis (SEA) method (Lyon, 1975) or the so-called waveguide methods (Nilsson, 1978a). Such methods, which describe the propagation of structure-borne noise in a ship structure, have certain

limitations in the low frequency region, i.e., below the first few plate resonances (Nilsson, 1980). The first resonance frequency can be fairly high for a plate element in the tanktop construction or in the engine foundation. This naturally causes uncertainties for the predicated noise levels in the octave bands with centre frequencies at and below 125 Hz. However, Nilsson (1976, 1978b, 1981) has developed a method for extending the waveguide model for calculating the attenuation of structure-borne sound in the junction between a plate panel and a boundary stiffener in a ship structure.

The SEA provides a means for high-frequency vibration prediction by estimating the equilibrium energies of a network of subsystems which are subjected to an assumed distribution of external sources of time-stationary vibrational power input. It offers a good tool to analyse and predict acoustic and vibration transmissions in coupled systems. From the practical point of view, the capital element for applying SEA is the determination of the coupling loss factors (CLF). Theoretical estimations of CLF has been obtained in simple cases from wave propagation in infinite coupled beams by Gibbs and Tattersall (1987). The SEA approach for analysing complicated structures with many resonant modes in every frequency band considered has been developed by Lyon (1975). It was applied firstly to predict a ship's noise level by Plunt (1980). Other studies by Sawley (1969), Jensen (1976), Kihlman and Plunt (1976), and Irie and Takagi (1978) also reported positive results from the use of the method on marine vessels. They use the transmitted structure-borne noise power, which is not directly measurable, as the quantity to describe the source strength. However, knowing the mobilities of the foundation and the machinery as well as the velocity level of the contact points of the freely suspended machinery, it is possible to calculate the input power.

The waveguide method or the grillage method has been developed by Nilsson (1977, 1978 a&b, 1980, 1981) for the calculation of the attenuation of the structure-borne noise in a ship structure, which is modelled by a grillage consisting of the plates between two successive frames. The moments and rotation at the plate junctions are calculated. In this method the input power to the plates is given by the product of the moment and the angular

velocity. Accordingly, the primary quantity for the description of the source is the fore-and-aft directed moment, transmitted from the engine to the foundation. Direct measurements of these moments are very complicated to perform. Nilsson investigated various methods to decrease the noise levels in the accommodation spaces in superstructure by model tests. The attenuation of structure-borne sound in the propagation path between source and receiver is increased by means of damping layers, resilient mounts and changed boundary conditions between main deck and superstructure. Damping layers were found to have only a local effect. Resilient mounts between superstructure and main deck can reduce the noise levels in the superstructure by the order of 10 dB(A).

More recently, Cabos and Jokat (1998) proposed a Noise Finite Element Method (Noise-FEM) to predict the propagation of structure-borne noise in complex structure by using the concept of "sound temperature" and "sound conductivities". The sound temperature is defined as the mean energy per mode of a subsystem that is capable of vibration. The sound temperature can determine the direction of sound energy flux. The sound conductivities rspresent the coefficients of energy flux in different directions of a subsystem considering the losses at discontinities and the changed coupling loss factors. To derive the conductivities relation, methods combining the acoustical waveguide model, the power flow finite element analysis and the SEA are used. Once the sound conductivities are determined, a power balance equation can be solved with the aid of the method of finite elements. The result is the sound temperature distribution and hence the energy distribution based on the given power fed into the system. Owing to the sound temperature just represents a mean energy per mode, thus when applying the Noise-FEM to analyse the structure-borne sound of a container ship ECOBOX 42, larger deviations of the noise level generally occur in the lower frequency range (below 160 Hz) compared with measurements.

2.3 Summary of the Field of Previous Research

A number of the methods for previous activities regarding the prediction and control of structure-borne noise induced by a onboard machine have been proposed. These research

works can be categorised as calculation methods about structure-borne sound propagation in the ship's structure, the methodologies for determining structure-borne sound transmission from engine to foundation, and the measures for reducing the structure-borne sound transmission. Comparisons of what each process does and how these methods have been applied are summarized in Table 2.1. The review clearly highlights the fact that there are very few validated models for predicting the propagation of structure-borne noise within the medium frequency range, i.e., from 125 Hz to 1 kHz, and thus served as the impetus for this research work reported herein.

Table 2.1 Comparsion of the methods for previous activities concerning the prediction and control of structure-borne noise

Calculation of structure-borne sound propagation in the ship structure	
Calculation methods	**Description**
1.Empirical methods (Janssen and Butien, 1973; Plunt, 1980; Buiten, 1976)	Statistical approach of previous ships as full-scale models to find the propagation rules of vibration velocity different of sound transmission through different parts of the hull for frequency range 32Hz-8kHz. Input data is the shaft speed, shaft power, main structure characteristics and the velocity levels of engine and foundation.
2.Statistical energy analysis (Jensen, 1976; Sawley, 1969; Kihlman and Plunt, 1976; Irie and Takagi, 1978)	High-frequency vibration prediction by estimating the equilibrium energies of a network of subsystems. Input data is the transmitted power (velocity levels and effective mobility of foundation) from sources.
3.Grillage method (Nilsson, 1977, 1978b, 1981)	The calculation of the attenuation of the structure-borne noise power flow, represented by the velocity squared, in the vertical direction in a ship structure is determined by the propagation of flexural waves in the plate elements between two successive frames. Based on the prediction model it is found that the velocity level of a deck is a function of the input data at the source, wave numbers, masses, losses and dimensions of the plate elements in the structure. The input data is the transmitted moments (angular velocity and moment mobility of foundation).
4.Noise Fininite Element Method(Cabos and Jokat,1998)	Applied the concept of sound temperature and sound conductivities and combined the acoustical waveguide method, the power flow finite element method and the statistical energy analysis to calculate the structure-borne noise propagation in complex structures. The input data is the transimitted power fed into the structure system.
Determination of structure-borne sound transmission from engine to foundation	
Methods	**Description**
1.Petersson and Plunt's method (1981, 1982a, 1982b)	Applied the effentive mobility concept to analyse structure-borne sound power transmission between coupled structures via multi-paths from a machine. Besides the full scale measurements of point and transfer mobilities on the feet of shipboard diesel engine and foundation, the source velocity is needed for transmitted power calculation.
2.Verheij's method (1986)	Facilitate source and path identification by using the experimental method of reciprocal transfer function measurement. Linear structural system is assumed.
3.Koh's method (1992)	The unifying concept of time-averaged vibrational power was used to examined the vibration transmission from a machine source to flexible beam and plate-like seating structures via the translational and rotational motions as well as the coupling between these motions.
Reduction of structure-borne sound power transmission by changes in design of foundations	
Methods	**Description**
1.Empirical methods (Middleton, 1976; steenhoek, 1976; Besio and Loredan, 1993)	Undertook model and /or full-scale experiments to measure the velocity levels at various foundations and the hull.
2.Partly theoretical methods (Heckl, 1976; Petersson, 1983)	Predicting the behaviour of elastic mounts at low frequencies (<100 Hz) fairly well provided the stiffness of the mount and the impedances of structures on both sides of the mount were known. For higher frequencies (>500Hz) elastic mounts must be considered as wave-guides having higher order resonances. The first higher order resonance dependends mainly on the mass of resilient element. At medium frequencies (100-500Hz) the sound transmission through air cavity beneath the engine can be more important than that through a good resilient mount.

CHAPTER 3

THEORY OF MOBILITY

AND

POWER FLOW TRANSMISSION

The mobility of a structure is the ratio between velocity and force for simple harmonic vibration in the range of linear behaviour. The term point mobility is used where velocity and force are at the same position and in the same direction. The term transfer mobility is used when velocity and force are at different positions and/or in different directions.

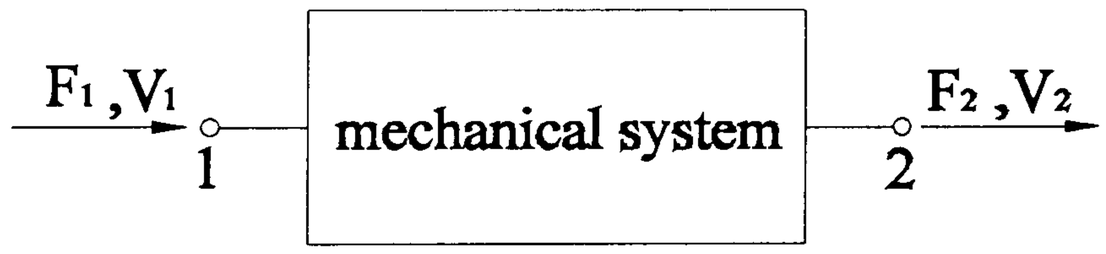

Figure 3.1 Input and output of a mechanical system

Assumed that a mechanical system as shown in Figure 3.1, with instantaneous forces F_1 and F_2 applied at the input and output respectively resulting in corresponding instantaneous velocities V_1 and V_2. The ratio $\frac{V_1}{F_1} = M_{11}$ is the point mobility at 1 and $\frac{V_2}{F_1} = M_{21}$ is the transfer mobility at 2 induced by force acting at 1. For linear system the transfer mobilities M_{21} and M_{12} are reciprocal, i.e. $M_{21} = M_{12}$. The velocity vector $\begin{Bmatrix} V_1 \\ V_2 \end{Bmatrix}$ is related to the force vector $\begin{Bmatrix} F_1 \\ F_2 \end{Bmatrix}$ by the full mobility matrix, i.e.

$$\begin{Bmatrix} V_1 \\ V_2 \end{Bmatrix} = \begin{bmatrix} M_{11} & M_{12} \\ M_{21} & M_{22} \end{bmatrix} \begin{Bmatrix} F_1 \\ F_2 \end{Bmatrix} \tag{3.1}$$

In this Chapter consideration is given to developing the theory of mobility prediction and power flow transmission.

3.1 Mobility of Single Degree of Freedom (SDOF) Vibration Model

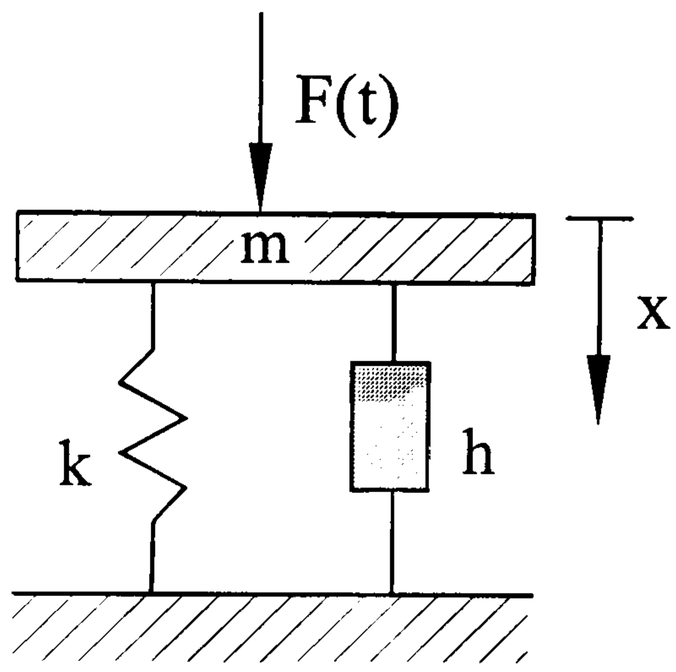

Figure 3.2 Single degree of freedom spring-mass-hysteresis damping system

Consider a single degree of freedom spring-mass-hysteresis damping system, as shown in Figure 3.2, with mass, damping and stiffness coeffcients denoted by m, h, and k, respectively. If the system is subjected to a harmonic exciting force, i.e., $F(t) = F_0 e^{j\omega t}$, then the equation of motion for the response x(t) can be expressed as

$$m\ddot{x} + \frac{h}{\omega}\dot{x} + kx = F(t) \tag{3.2}$$

Thus for the harmonic excitation, where $\dot{x} = j\omega x$, equation (3.2) becomes

$$m\ddot{x} + k(1 + j\eta)x = F_0 e^{j\omega t} \tag{3.3}$$

where $\eta = \frac{h}{k}$ is called the structural damping loss factor. The quantity $k(1 + j\eta)$ is called the complex stiffness.

The mobility of the system is

$$M(\omega) = \frac{\dot{x}(t)}{F(t)} = j\omega R(\omega) = \frac{j\omega}{[(k - \omega^2 m) + j\eta k]} = \frac{j\omega}{m[(\omega_n^2 - \omega^2) + j\eta\omega_n]} \tag{3.4}$$

where

$$R(\omega) = \frac{x(t)}{F(t)} = \frac{1}{[(k - \omega^2 m) + j\eta k]} \quad : \text{ receptance}$$

$$\omega_n = \left(\frac{k}{m}\right)^{\frac{1}{2}} = 2\pi f_n \quad : \text{ natural frequency}$$

The mobility of such a damped system is always a complex quantity and is frequency dependent. Evidently, the mobility is influenced by the system parameters, namely mass, damping and stiffness. If the damping ratio is small then the mobility has the following characteristics:

1. As $\omega >> \omega_n$,

$$M(\omega) \approx -\frac{j}{m\omega} \tag{3.5}$$

In this situation, the mobility is said to be mass dependent only.

2. As $\omega = \omega_n$,

$$M(\omega) = \frac{1}{\eta} \tag{3.6}$$

At resonance, the mobility is said to be damping dependent only.

3. As $\omega << \omega_n$,

$$M(\omega) \approx \frac{j\omega}{k} \tag{3.7}$$

In this case, the mobility is stiffness dependent only.

Taking logarithms and absolute values on both sides of equations (3.5) to (3.7), the following relations is obtained:

$$\log|M(\omega)| = \log\left(\frac{1}{\omega m}\right) = -\log(m) - \log(\omega), \qquad \text{for } \omega >> \omega_n \tag{3.8}$$

$$\log|M(\omega)| = \log\left(\frac{1}{\eta}\right), \qquad \text{for } \omega = \omega_n \tag{3.9}$$

$$\log|M(\omega)| = \log\left(\frac{\omega}{k}\right) = \log(\omega) - \log(k), \qquad \text{for } \omega << \omega_n \tag{3.10}$$

Equations (3.8) to (3.10) show that providing M(ω) and ω expressed in logarithmic coordinates, they have linear relations in the very high and very low frequency ranges as shown in Figure3.3.

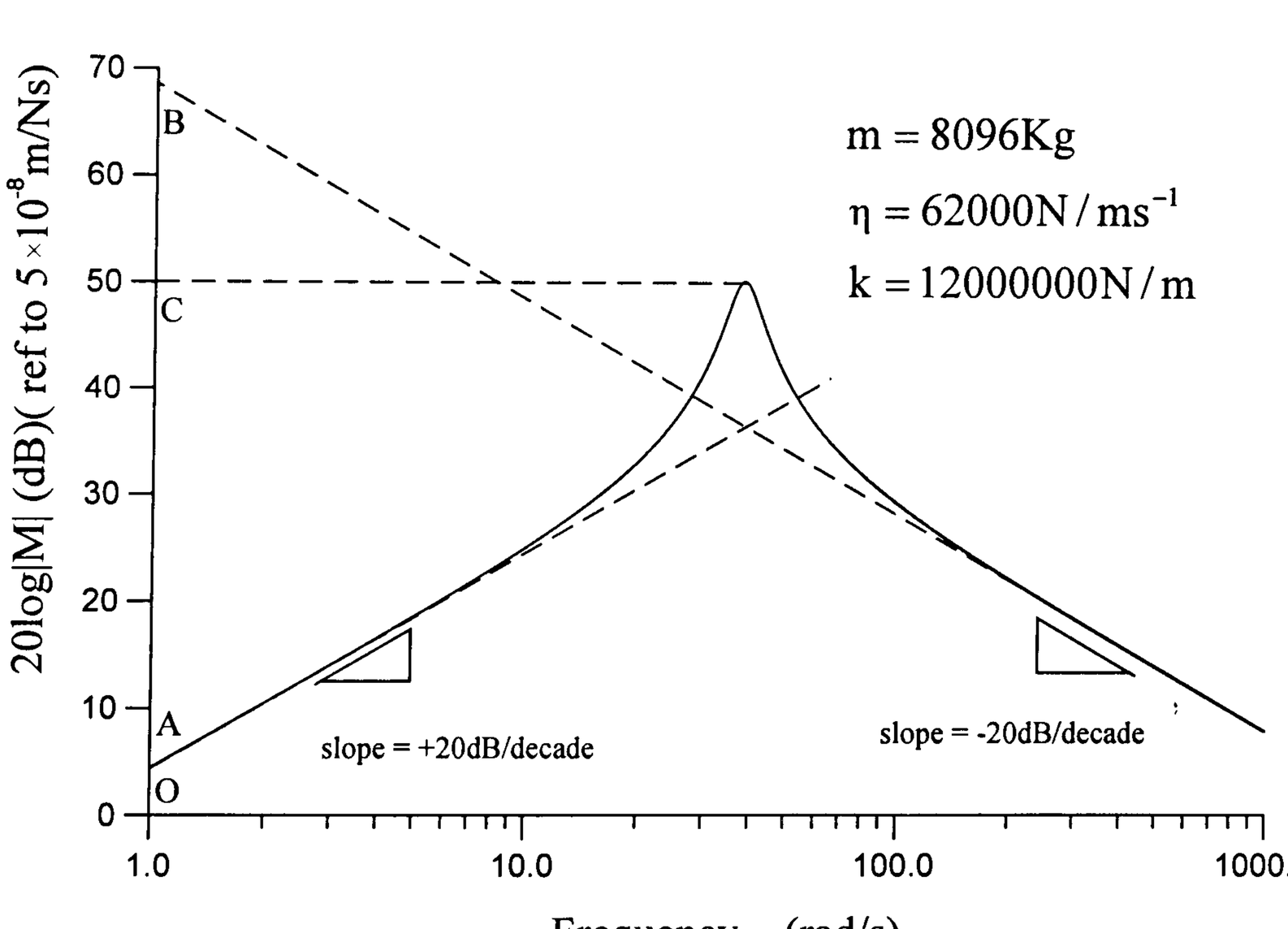

Figure 3.3 Characteristics of mobility spectrum for a SDOF system

These correspond to "mass-like" and "spring-like" behaviour as would be expected. Figure 3.3 represents the mobility spectrum of a SDOF system with m=8,096 kg, η=62,000

Ns/m, k=12,000,000 N/m and $\omega_n = 38.5$ rad/s.

In Figure 3.3, it is seen firstly that the magnitude of mobility spectrum curve approaches a straight line with slope equaling +20 dB/decade in the lower frequency region. The intersection distance $\overline{OA}$ along the ordinate axis is,

$$\overline{OA} = \log\left|M(\omega)\right|_{\log(\omega)=0} = -\log(k) \tag{3.11}$$

or

$$k = \left[\left|M(\omega)\right|_{\log(\omega)=0}\right]^{-1} \tag{3.12}$$

Secondly, in the mobility spectrum curve has a peak value $\overline{OC}$ at resonance, that is,

$$\overline{OC} = \log\left|M(\omega_n)\right| = \log(\frac{1}{\eta}) \tag{3.13}$$

or

$$\eta = \left[\left|M(\omega_n)\right|\right]^{-1} \tag{3.14}$$

Finally, the mobility spectrum curve approaches another straight line with slope equaling -20 dB/decade in the higher frequency region. The intersection distance $\overline{OB}$ along the ordinate axis is

$$\overline{OB} = \log\left|M(\omega)\right|_{\log(\omega)=0} = -\log(m) \tag{3.15}$$

or

$$m = \left[\left|M(\omega)\right|_{\log(\omega)=0}\right]^{-1} \tag{3.16}$$

Equations (3.11), (3.13) and (3.15) constitute the bases for the data checking methods of the mobility measurements.

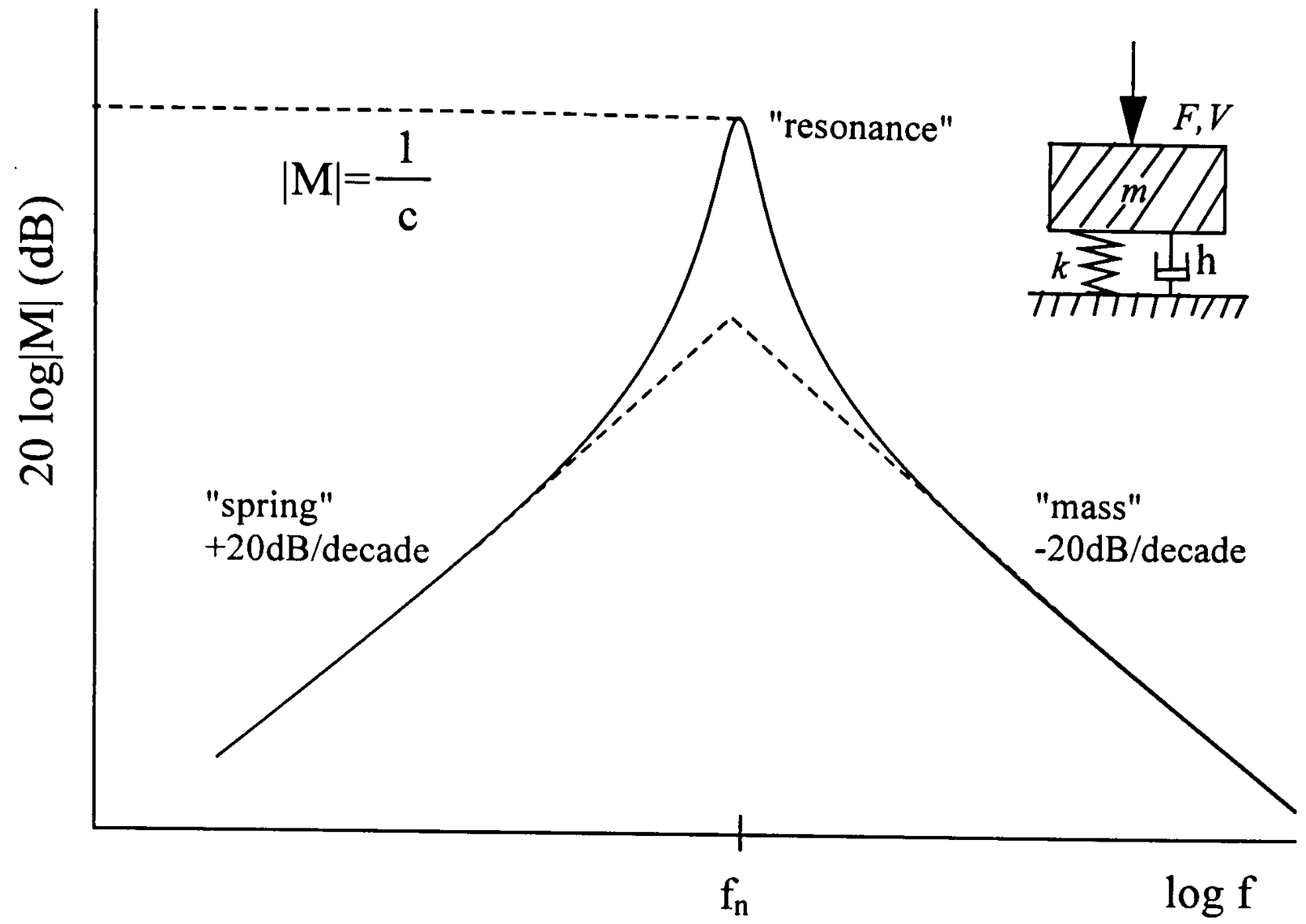

(a) Excited on mass (rigid foundation)

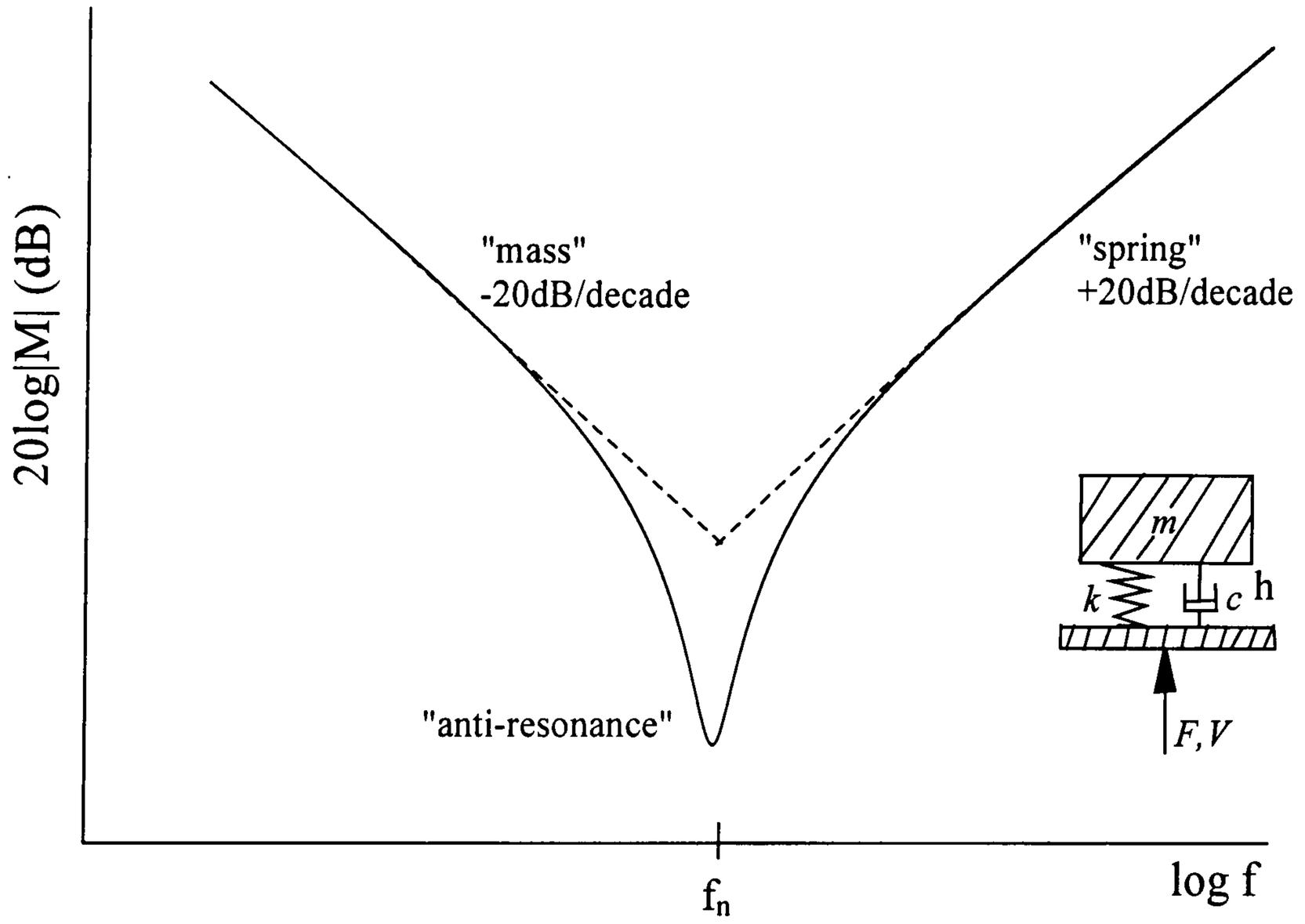

(b) Excited on spring

Figure 3.4 Mobility of general SDOF system

For generality, the mobility curve of SDOF spring-mass-dashpot system can be shown as Figure 3.4. Figure 3.4(a) represents the driving point mobility for excitation on the mass. The height of the maximum in the mobility curve is determined by the damping. The lower the damping, the higher the $|M|_{max}$. For $f >> f_n$ the curve shows "mass-behaviour", i.e.,

$|M| \approx 1/\omega\, m$ (slope -20dB/decade) and for $f << f_n$ the curve shows "spring-behaviour", i.e., $|M|_{max} \approx \omega / k$ (Slope +20dB/decade). The mobilities in the ranges of "spring-behaviour" and "mass-behaviour" are symmetrical about the axis $f=f_n$ with equal magnitude but opposite slopes.

Figure 3.4 (b) shows the driving point mobility for excitation on the lower side of the spring. There is now an "anti-resonance" at f_n, giving a minimum mobility. Now the mass-behaviour is seen for $f<<f_n$. For the " tuning" frequency such a spring-mass system may apply a high dynamical load using a relatively small mass. This set-up can be used for vibration suppression, especially on resonant structures.

3.2 Mobility of Two Degrees of Freedom (TDOF) Vibration Model

A two degrees of freedom vibration system, as shown in Figure 3.5, is represented by two discrete lumped mass m_1 and m_2 and linked by two pairs of massless spring and hysteresis damper in series. The spring constants are k_1 and k_2 and structural damping loss coefficients are h_1 and h_2 respectively.

When the exciting forces F_1 and F_2 are applied at mass 1 and mass 2 respectively, then the equations of motion for mass 1 and 2 are:

$$[m]\{\ddot{x}\} + \frac{1}{\omega}[h]\{\dot{x}\} + [k]\{x\} = \{F(t)\} \tag{3.17}$$

where [m], [h] and [k] are the 2×2 mass, damping and stiffness matrices, respectively. $\{\ddot{x}\}$, $\{\dot{x}\}$ and $\{x\}$ are the acceleration, velocity and displacement vector,respectively. $\{F(t)\}$ is the exciting force vector. Their expanded forms are:

$$[m] = \begin{bmatrix} m_{11} & m_{12} \\ m_{21} & m_{22} \end{bmatrix} \quad , \quad [h] = \begin{bmatrix} h_{11} & h_{12} \\ h_{21} & h_{22} \end{bmatrix} \quad , \quad [k] = \begin{bmatrix} k_{11} & k_{12} \\ k_{21} & k_{22} \end{bmatrix} \quad ,$$

$$\{\ddot{x}\} = \begin{Bmatrix} \ddot{x}_1 \\ \ddot{x}_2 \end{Bmatrix} \quad , \quad \{\dot{x}\} = \begin{Bmatrix} \dot{x}_1 \\ \dot{x}_2 \end{Bmatrix} \quad , \quad \{x\} = \begin{Bmatrix} x_1 \\ x_2 \end{Bmatrix} \quad ,$$

and

$$\{F\} = \begin{Bmatrix} F_1 \\ F_2 \end{Bmatrix}$$

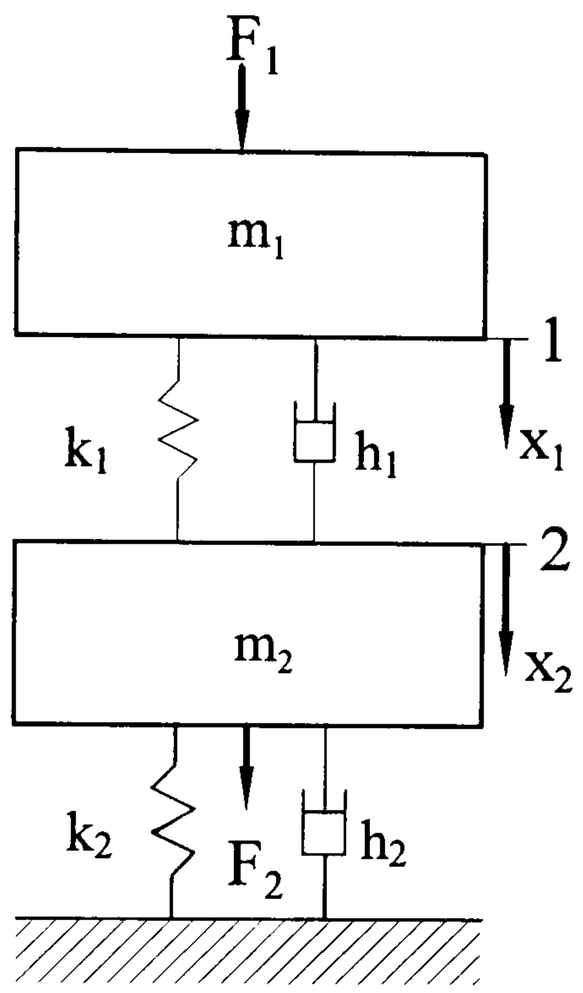

Figure 3.5 Gerneral two degrees of freedom system

For discrete lumped mass system,

$$m_{11} = m_1 \quad , \quad m_{12} = m_{21} = 0 \quad , \quad m_{22} = m_2 .$$

By equilibrium relations, h_{ij} and k_{ij} are found to be:

$$h_{11} = h_1 \quad , \quad h_{12} = h_{21} = -h_1 \quad , \quad h_{22} = h_1 + h_2$$

and

$$k_{11} = k_1 \quad , \quad k_{12} = k_{21} = -k_1 \quad , \quad k_{22} = k_1 + k_2$$

The expanded form of equation (3.18) is

$$\begin{bmatrix} m_{11} & m_{12} \\ m_{21} & m_{22} \end{bmatrix} \begin{Bmatrix} \ddot{x}_1 \\ \ddot{x}_2 \end{Bmatrix} + \begin{bmatrix} h_{11} & h_{12} \\ h_{21} & h_{22} \end{bmatrix} \begin{Bmatrix} x_1 \\ x_2 \end{Bmatrix} + \begin{bmatrix} k_{11} & k_{12} \\ k_{21} & k_{22} \end{bmatrix} \begin{Bmatrix} x_1 \\ x_2 \end{Bmatrix} = \begin{Bmatrix} F_1(t) \\ F_2(t) \end{Bmatrix} \qquad (3.18)$$

When harmonic forcing functions are applied, i.e.,

$$F_i(t) = \hat{F}_i e^{j\omega t}, \qquad i = 1,2. \tag{3.19}$$

then the vibration displacements can be represented as

$$x_i(t) = \hat{X}_i e^{j\omega t}, \qquad i = 1,2. \tag{3.20}$$

in which $\hat{X}_1$, $\hat{X}_2$ are called complex response amplitudes. Substituting equation (3.19), (3.20) into (3.18), and defining the dynamic stiffness functions $S_{ij}(\omega)$ of the system as

$$S_{ij}(\omega) = -\omega^2 m_{ij} + jh_{ij} + k_{ij} \quad , \qquad i,j = 1,2 \tag{3.21}$$

then, equation (3.16) becomes

$$S_{ij}(\omega)\hat{X}_j = \hat{F}_i \quad , \qquad i,j = 1,2 \tag{3.22}$$

The response amplitudes can be solved from equation (3.22) as

$$\hat{X}_j = S_{ij}^{-1}(\omega)\hat{F}_i \quad , \qquad i,j = 1,2. \tag{3.23}$$

or

$$\hat{X}_1(\omega) = \frac{S_{22}(\omega)\hat{F}_1 - S_{12}(\omega)\hat{F}_2}{S_{11}(\omega)S_{22}(\omega) - S_{12}(\omega)S_{21}(\omega)} \tag{3.24a}$$

$$\hat{X}_2(\omega) = \frac{-S_{21}(\omega)\hat{F}_1 + S_{11}(\omega)\hat{F}_2}{S_{11}(\omega)S_{22}(\omega) - S_{12}(\omega)S_{21}(\omega)} \tag{3.24b}$$

The vibration velocity vector is

$$V_i = \dot{X}_i(t) = j\omega\hat{X}_i e^{j\omega t} = \hat{V}_i e^{j\omega t} \quad , \qquad i = 1,2. \tag{3.25}$$

where

$$\hat{V}_1(\omega) = j\omega\hat{X}_1 = j\omega\frac{S_{22}(\omega)\hat{F}_1 - S_{12}(\omega)\hat{F}_2}{S_{11}(\omega)S_{22}(\omega) - S_{12}(\omega)S_{21}(\omega)} \tag{3.26a}$$

$$\hat{V}_2(\omega) = j\omega\hat{X}_2 = j\omega\frac{-S_{21}(\omega)\hat{F}_1 + S_{11}(\omega)\hat{F}_2}{S_{11}(\omega)S_{22}(\omega) - S_{12}(\omega)S_{21}(\omega)} \tag{3.26b}$$

Then the mobility matrix of a TDOF system is related by:

$$\begin{Bmatrix} V_1 \\ V_2 \end{Bmatrix} = \begin{bmatrix} M_{11} & M_{12} \\ M_{21} & M_{22} \end{bmatrix} \begin{Bmatrix} F_1 \\ F_2 \end{Bmatrix} \tag{3.27}$$

where the mobility functions M_{ij} (i=1,2 and j=1,2) can be expressed in terms of the dynamic stiffness functions:

$$M_{11} = \frac{j\omega S_{22}(\omega)}{S_{11}(\omega)S_{22}(\omega) - S_{12}(\omega)S_{21}(\omega)} \tag{3.28a}$$

$$M_{12} = \frac{-j\omega S_{12}(\omega)}{S_{11}(\omega)S_{22}(\omega) - S_{12}(\omega)S_{21}(\omega)} \tag{3.28b}$$

$$M_{21} = \frac{-j\omega S_{21}(\omega)}{S_{11}(\omega)S_{22}(\omega) - S_{12}(\omega)S_{21}(\omega)} \tag{3.28c}$$

$$M_{22} = \frac{j\omega S_{11}(\omega)}{S_{11}(\omega)S_{22}(\omega) - S_{12}(\omega)S_{21}(\omega)} \tag{3.28d}$$

Expanding equation (3.27) and rearranging gives:

$$\begin{Bmatrix} V_1 \\ F_1 \end{Bmatrix} = \begin{bmatrix} \alpha_{11} & \alpha_{12} \\ \alpha_{21} & \alpha_{22} \end{bmatrix} \begin{Bmatrix} V_2 \\ F_2 \end{Bmatrix} \tag{3.29}$$

where α_{ij} are the four-pole parameters and can be expressed in terms of mobility fumctions as:

$$\alpha_{11} = \frac{M_{11}}{M_{12}}, \quad \alpha_{12} = \frac{M_{12}M_{21} - M_{11}M_{22}}{M_{21}}, \quad \alpha_{21} = \frac{1}{M_{12}}, \quad \alpha_{22} = -\frac{M_{22}}{M_{12}} \tag{3.30}$$

For the linear system with proportional damping, there exists the symmetry properties for m_{ij}, h_{ij} and k_{ij}, therefore, the dynamic stiffness S_{ij} and the transfer mobility M_{ij} are also symmetrical.

3.3 Mobility of Multidegrees of Freedom (MDOF) Vibration Model

Consider an N degrees of freedom system with structural or hysteresis damping. The equation of motion can be expressed as:

$$[m_{ij}]_{NXN}\{\ddot{X}\}_{NXl} + j[h_{ij}]_{NXN}\{\dot{X}\}_{NXl} + [k_{ij}]_{NXN}\{X\}_{NXl} = \{F\}_{NXl} \tag{3.31}$$

where the mass matrix $[m_{ij}]$, the damping matrix $[h_{ij}]$ and the stiffness matrix $[k_{ij}]$ are $N \times N$ matrices.

When the exciting force vector {F} equals zero, equation (3.31) becomes the equation of motion for the free vibration of a linear dynamic system. There exists the mass normalized modal matrix $[\Phi]$, in which the rth damped eigenvalue is

$$\lambda_r^2 = \omega_r^2(1 + j\eta_r) \tag{3.32}$$

where

ω_r : the undamped natural frequency of the rth mode;

η_r : the structural damping loss factor of the rth mode.

For a linear dynamic system, the mass normalized modal matrix $[\Phi]$ possesses the following orthorgonality properties,

$$[\Phi]^T[m][\Phi] = [I] = \begin{bmatrix} \ddots & & \\ & M_r = 1 & \\ & & \ddots \end{bmatrix} \tag{3.33a}$$

$$[\Phi]^T[k_{ij}][\Phi] = \begin{bmatrix} \ddots & & \\ & \omega_r^2 & \\ & & \ddots \end{bmatrix} \tag{3.33b}$$

$$[\Phi]^T[h_{ij}][\Phi] = \begin{bmatrix} \ddots & & \\ & \eta_r\omega_r^2 & \\ & & \ddots \end{bmatrix} \tag{3.33c}$$

The response {X} can be expressed as a linear combination of modal shapes, i.e.,

$$\{X\}=[\Phi]\{Y\} \tag{3.34}$$

where $\{Y\}$ is called modal displacement vector. Substitute equation (3.34) into equation (3.31) then multiply both sides by $[\Phi]^T$, equation (3.31) becomes:

$$[\Phi]^T[m_{ij}][\Phi]\{\ddot{Y}\}+j[\Phi]^T[h_{ij}][\Phi]\{\dot{Y}\}+[\Phi]^T[k_{ij}][\Phi]\{Y\}=[\Phi]^T\{F\} \tag{3.35}$$

By utilizing the orthogonality relations, equation (3.35) can be simplified and decoupled as:

$$\{Y\}+j\left[\ddots\ \eta_r\omega_r^2\ \ddots\right]\{Y\}+\left[\ddots\ \omega_r^2\ \ddots\right]\{Y\}=[\Phi]^T\{F\}=[F_{eq}] \tag{3.36}$$

If there is a single force F_j applied at the jth degree of freedom, then the external modal force is

$$\{F_{eq}\}=\begin{bmatrix}\Phi_{11} & \Phi_{21} & \cdots & \Phi_{j1} & \cdots & \Phi_{N1}\\ \Phi_{12} & \Phi_{22} & \cdots & \Phi_{j2} & \cdots & \Phi_{N2}\\ \vdots & \vdots & & \vdots & & \\ \Phi_{1r} & \Phi_{2r} & \cdots & \Phi_{jr} & \cdots & \Phi_{Nr}\\ \vdots & \vdots & & \vdots & & \\ \Phi_{1N} & \Phi_{2N} & \cdots & \Phi_{jN} & \cdots & \Phi_{NN}\end{bmatrix}\begin{Bmatrix}0\\0\\\vdots\\F_j\\\vdots\\0\end{Bmatrix}=\begin{Bmatrix}\phi_{j1}F_j\\\phi_{j2}F_j\\\vdots\\\phi_{jr}F_j\\\vdots\\\phi_{jN}F_j\end{Bmatrix} \tag{3.37}$$

The solution of the rth modal displacement in equation (3.36) is obtained as:

$$Y_r=\frac{\Phi_{jr}F_j}{(\omega_r^2-\omega^2+j\eta_r\omega_r^2)} \tag{3.38}$$

where ω is the excitation frequency of the external force F_j.

By equation (3.34) the displacement of the ith degree of freedom is:

$$X_i=\Phi_{i1}Y_1+\Phi_{i2}Y_2+....+\Phi_{ir}Y_r+....\Phi_{iN}Y_N \tag{3.39}$$

Substituting equation (3.38) into equation (3.39), the receptance coefficient can be expressed as:

$$R_{ij}(\omega)=\frac{X_i}{F_j}=\sum_{r=1}^{N}\frac{A_{ijr}}{\omega_r^2-\omega^2+j\eta_r\omega_r^2} \tag{3.40}$$

where

$A_{ijr}=\Phi_{ir}\,\Phi_{jr}$: the modal constant.

Therefore the mobility coefficient can then be written as:

$$M_{ij}(\omega) = \sum_{r=1}^{N} \frac{j\omega A_{ijr}}{(\omega_r^2 - \omega^2) + j\eta_r\omega_r^2} \tag{3.41}$$

From equation (3.41), it is seen that the mobility coefficient of an N degrees of freedom system can be expressed as the sum of the N modal mobilities.

In reality, a mechanical structure system has an infinite number of degrees of freedom. It can be approximated by a N degrees of freedom system, with approximations being made to the higher modes. For the mobility of the real system, a residual term C+jD has to be added to equation (3.41),

$$M_{ij}(\omega) = \sum_{r=1}^{N} \frac{j\omega A_{ijr}}{(\omega_r^2 - \omega^2) + j\eta_r\omega_r} + (C + jD) \tag{3.42}$$

3.4 Mobility of Infinite Beam and Plate Model

Not only for beams, but also for structures like plates, cylinders, etc., the asymptotic approximation obtained by averaging over frequency is nearly equal to the mobility of the corresponding infinitely extended system, as shown by Skudrzyd (1980) and Cremer et al. (1988). Such infinite system mobilities are often applied in machinery acoustics calculations. The reason is that, for many problems a detailed frequency analysis is not relevant. Often the noise spectrum is broadband and/or varying with rotation speed. If such an excitation generates structural responses in the frequency range far above the lowest eigenfrequency, a change of structural design parameters would affect many relevant eigenfrequencies simultaneously. Averaging over frequency bands is then profitable in analysis procedures.

The driving point mobilities for infinite beams and plates are respectively given by Cremer et al. (1988):

$$M_{b\infty} = \frac{0.19(1-j)}{\rho_b S\sqrt{c_{Lb} h f}} \tag{3.43}$$

$$M_{P\infty} = \frac{0.125}{\sqrt{B' m''}} \approx \frac{0.453}{\rho_p c_{Lp} h^2} \approx \frac{5.41}{\omega \rho_p \lambda_B^2 h} \tag{3.44}$$

where m'' : mass per unit area; B' : bending stiffness per unit width; ρ_b : density of beam; ρ_p : density of plate material; c_{Lp}, c_{Lb} : longitudinal wave speed in plate and beam respectively; h : thickness of plate/beam; λ_B : bending wavelength.

Figure 3.6 shows the frequency behaviour of 20 log $|M|$ for a mass, a spring, an infinite beam and an infinite plate. Note that, for $|M|_{P\infty}$ to be approximately valid not only averaging over frequencies is required, but also the driving point has to be at least a distance of $\lambda_B/2$ away from plate boundaries.

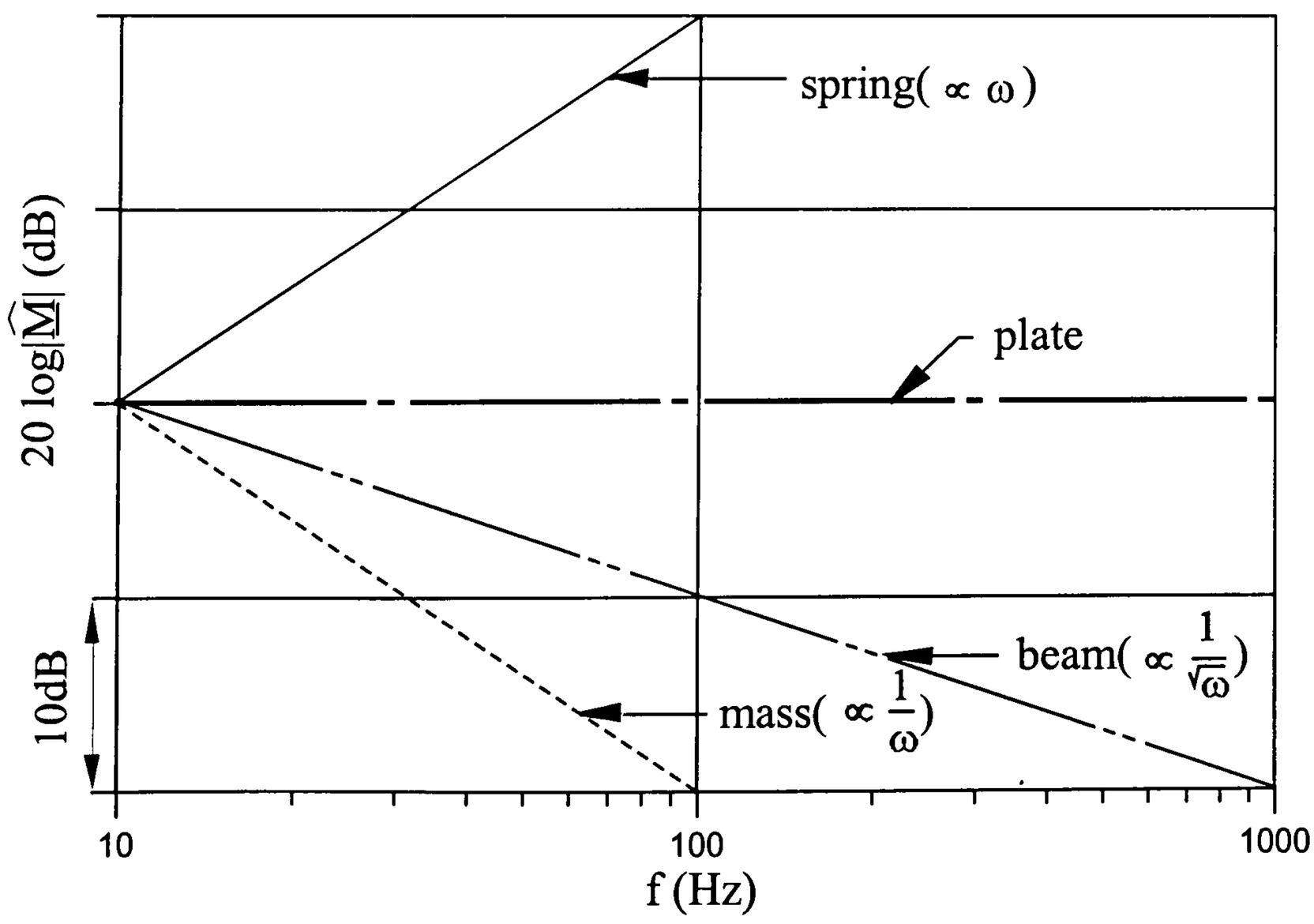

Figure 3.6 Mobility from idealized structural elements and infinite beam and plate

3.5 Mobility of Multipole Coupling System

Structure-borne noise excitation caused by mechanical coupling between an engine and a hull structure via a resilient mount can be represented as shown in Figure 3.7. By assuming that it can be simplified to a 1-direction coupling then it may be modelled as an isolator suspension system.

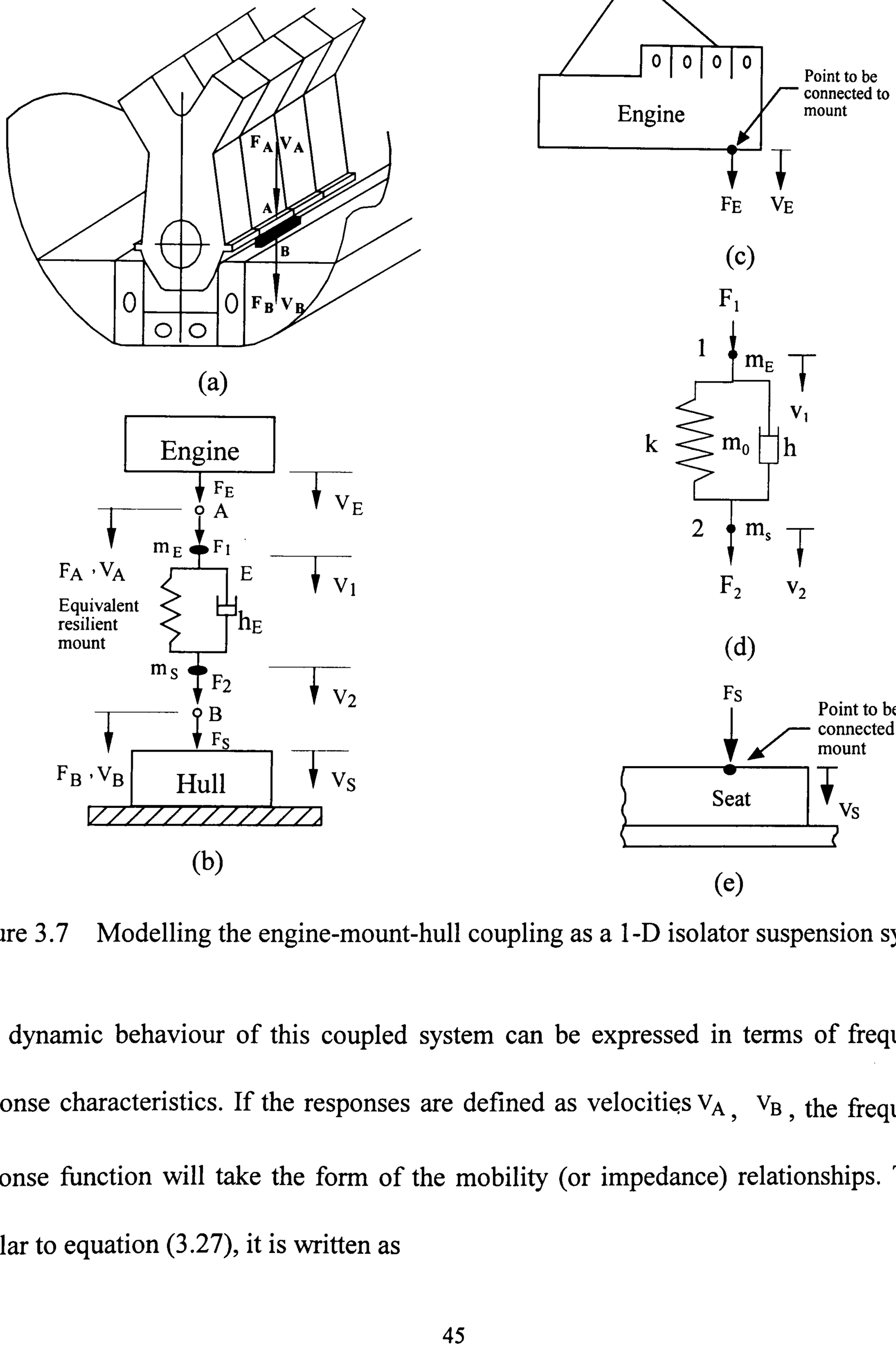

Figure 3.7 Modelling the engine-mount-hull coupling as a 1-D isolator suspension system

The dynamic behaviour of this coupled system can be expressed in terms of frequency response characteristics. If the responses are defined as velocities V_A, V_B, the frequency response function will take the form of the mobility (or impedance) relationships. Thus, similar to equation (3.27), it is written as

$$\begin{Bmatrix} V_A \\ V_B \end{Bmatrix} = \begin{bmatrix} M_{AA} & M_{AB} \\ M_{BA} & M_{BB} \end{bmatrix} \begin{Bmatrix} F_A \\ F_B \end{Bmatrix} \quad \text{or} \quad \begin{Bmatrix} F_A \\ F_B \end{Bmatrix} = \begin{bmatrix} Z_{AA} & Z_{AB} \\ Z_{BA} & Z_{BB} \end{bmatrix} \begin{Bmatrix} V_A \\ V_B \end{Bmatrix} \tag{3.45}$$

where the mobility matrix $[M] = \begin{bmatrix} M_{AA} & M_{AB} \\ M_{BA} & M_{BB} \end{bmatrix}$ is the inverse of the impedance matrix

$[Z] = \begin{bmatrix} Z_{AA} & Z_{AB} \\ Z_{BA} & Z_{BB} \end{bmatrix}$, i.e.,

$$[M] = [Z]^{-1} \tag{3.46}$$

From equation (3.46), the driving point impedance Z_{AA}, the receiving point impedance Z_{BB} and the transfer impedance Z_{AB} or Z_{BA} can be expressed as,

$$Z_{AA} = \frac{M_{BB}}{M_{AA}M_{BB} - M_{AB}M_{BA}} \tag{3.47a}$$

$$Z_{BB} = \frac{M_{AA}}{M_{AA}M_{BB} - M_{AB}M_{BA}} \tag{3.47b}$$

$$Z_{AB} = Z_{BA} = \frac{-M_{AB}}{M_{AA}M_{BB} - M_{AB}M_{BA}} \tag{3.47c}$$

where

$$M_{AA} = \frac{V_A}{F_A}, \quad M_{BB} = \frac{V_B}{F_B}, \quad M_{AB} = \frac{V_A}{F_B}, \quad M_{BA} = \frac{V_B}{F_A}. \tag{3.48}$$

F_A, F_B and V_A, V_B are the forces and velocities at the engine side and seating side of the equivalent resilient mount respectively. M_{AA}, M_{BB} are the point mobilities and M_{AB}, M_{BA} are the transfer mobilities of the engine-mount-hull coupled suspension system. According to the relations in (3.48) all of these mobility spectra can be measured by accelometer transducers mounted on point A and B with an exciting force, such as an impulse, applied at point A and B.

Through the relations of velocity consistency and force equilbrium at the junctions, the mobility functions M_{AA}, M_{BB}, M_{AB}, M_{BA} can be analyzed and combined from the individual mobility characteristics of the separate subsystems, such as engine, resilient mount and seating structure, as shown in Figure 3.7 (c) (d) (e).

Considering the individual hoisted engine system shown in Figure 3.7 (c), if F_E and V_E are respectively the exciting force and velocity response at the site on the engine bed which is connected to the mount, then the relation between F_E and V_E is,

$$V_E = M_E F_E \tag{3.49}$$

The point mobility M_E of the engine can be expressed as,

$$M_E = \frac{j\omega}{[(k_E - \omega^2 m_E) + jh_E]} \tag{3.50}$$

where m_E, k_E and h_E are the effective mass, stiffness and damping coefficients of the engine respectively, at the point to be linked to the mounts.

For the individual resilient mount subsystem shown in Figure 3.7 (d), this can constitute a two degrees of freedom system and the relation of equation (3.27) holds as well. Equations (3.28a) to (3.28d) can be utilized to attain the mobility functions of such a separate resilient mount. While in this case the added effective masses of the engine and the seating structure at the junction points have to be considered. That is:

$$M_{11} = \frac{j\omega S'_{22}(\omega)}{S'_{11}(\omega)S'_{22}(\omega) - S'_{12}(\omega)S'_{21}(\omega)} \tag{3.51a}$$

$$M_{12} = \frac{-j\omega S'_{12}(\omega)}{S'_{11}(\omega)S'_{22}(\omega) - S'_{12}(\omega)S'_{21}(\omega)} \tag{3.51b}$$

$$M_{21} = \frac{-j\omega S'_{21}(\omega)}{S'_{11}(\omega)S'_{22}(\omega) - S'_{12}(\omega)S'_{21}(\omega)} \tag{3.51c}$$

$$M_{22} = \frac{j\omega S'_{11}(\omega)}{S'_{11}(\omega)S'_{22}(\omega) - S'_{12}(\omega)S'_{21}(\omega)} \tag{3.51d}$$

where

$$S'_{1j} = -\omega^2(m_{1j} + m_E) + jh_{1j} + k_{1j} \quad , \quad j = 1, 2 \tag{3.52a}$$

$$S'_{i2} = -\omega^2(m_{i2} + m_S) + jh_{i2} + k_{i2} \quad , \quad i = 1, 2 \tag{3.52b}$$

By a similar consideration, the separate individual seating structure, as Figure 3.7 (e), has the relation:

$$V_S = M_S F_S \tag{3.53}$$

and the point mobility function of the seating structure will be:

$$M_S = \frac{j\omega}{[(k_S - \omega^2 m_S) + j\omega h_S]} \tag{3.54}$$

By connecting the engine, mount, and seat structure together in series, equation (3.27) holds. Considering the relations of force equilibrium and velocity compatibility at the junction point A between the engine and the mount:

$$V_E = V_1 = V_A \tag{3.55}$$

$$F_A = \frac{V_A}{M_{AA}} = \frac{V_E}{M_E} + \frac{V_1}{M_{11}} \tag{3.56}$$

it yields the relation

$$M_{AA} = \frac{M_E M_{11}}{M_E + M_{11}} \tag{3.57}$$

Similarly, by the relations at the junction point B between the mount and the seat :

$$V_S = V_2 = V_B \tag{3.58}$$

$$F_B = \frac{V_B}{M_{BB}} = \frac{V_S}{M_S} + \frac{V_2}{M_{22}} \tag{3.59}$$

one has

$$M_{BB} = \frac{M_S M_{22}}{M_S + M_{22}} \tag{3.60}$$

Then, the transfer mobilities M_{AB} and M_{BA} are found, by equations (3.51b) and (3.51c), to be

$$M_{AB} = \frac{-j\omega S'_{12}(\omega)}{S'_{11}(\omega)S'_{22}(\omega) - S'_{12}(\omega)S'_{21}(\omega)} \tag{3.61a}$$

$$M_{BA} = \frac{-j\omega S'_{21}(\omega)}{S'_{11}(\omega)S'_{22}(\omega) - S'_{12}(\omega)S'_{21}(\omega)} \tag{3.61b}$$

The comparison of the results calculated from equations (3.57), (3.60), (3.61a) and (3.61b) with those by measurements following the relations of equation (3.48) will be carried out to check the validity of the current model.

3.6 Vibrational Power Input to a Receiving Structure from Engine

The instantaneous vibration power input (P_{inst}) to a structure is defined as the product of the excitation force (F) and the associated velocity (V). For a harmonic excitation $|F|\sin\omega t$ applying at a point on a structure of mobility, $M = |M|e^{j\phi}$, it causes a velocity $|V|\sin(\omega t + \phi)$ at that point, where ϕ is the phase angle between the driving excitation force and the associated velocity. The instantaneous vibration power input will be:

$$(P_{inst}) = F\,V^* = |F||V|\sin\omega t \sin(\omega t + \phi) \tag{3.62}$$

where V^* is the conjugate of complex velocity V.

In general, it is of greater interest to know the time averaged power input (P). It is calculated by integrating equation (3.62) over one period of vibration to yield:

$$(P) = \frac{1}{T}\int_0^T |F||V| \sin \omega t \sin(\omega t + \phi) dt = \frac{1}{2}|F||V| \cos\phi \tag{3.63}$$

The averaged power input is related to the phase angle ϕ. If $\phi = \frac{\pi}{2}$ i.e., undamped, then the averaged power (P)=0.

At any point on a structure, the velocity and force is related via frequency response mobility (or impedance) functions, so that equation (3.63) may be rewritten in the following forms:

$$(P) = \frac{1}{2}|F|^2 \, Re[M] \tag{3.64}$$

or

$$(P) = \frac{1}{2}|V|^2 \, Re[Z] \tag{3.65}$$

where Re[M] and Re[Z] are the real part of the point mobility function and the point impedance at the excitation site, respectively. The choice of which equation to apply in a practical situation is controlled by the nature of the vibration source and the ability to measure either the force or velocity. In many cases, equation (3.65) can be applied if a machine is unaffected by the method of attachment, such that it behaves on site as if it were freely suspended. For a machine mounted on an isolation system, this condition is usually fulfilled velocity source.

The above equations are applicable only to a harmonically varying point force. In general, machinery is supported at a number of sites and each site will have some contact area over which both direct forces and moments may be transmitted. This will lead to a very

complicated set of inter-related expressions for the total input power. Suppose that there are N coordinates involved in the coupling of the machine to the sub-structure, then it will be necessary to define an N ×N matrix of mobility functions. Equations (3.64) and (3.65) are rewritten in matrix form as:

$$(P) = \frac{1}{2}\{F\}^T \mathrm{Re}[M]\{F\} \tag{3.66}$$

or

$$(P) = \frac{1}{2}\{V\}^T \mathrm{Re}[Z]\{V\} \tag{3.67}$$

Prediction, or measurement, of (P) value via these full matrix relationships can be extremely difficult. This is particularly true in situations where moment excitations represent a major source of the resultant vibrational power.

From expressions (3.66) and (3.67), it is clear that the power injected into a structure by the machine is dictated by the excitation force or velocity exerted by a machine and the mobility or impedance characteristics of the supporting structure. The characterization of an engine as a " velocity source" will now be considered .

There are many techniques available for modelling engineering structures in order to predict the mobility frequency response functions. These include finite element analysis, experimental modal analysis and analytical techniques based upon the use of infinite structures. Finite element analysis and experimental modal analysis are limited in their application to frequencies whose behaviour can be described as "moda". For a finite element model, this implies that the use of many degrees of freedom may lead to difficulties and can be a serious concern. It has been shown (Pinnington,1980) that relatively simple models of "patches" around mounting sites can be used to predict the

higher frequency performance of a seating structure. The introduction of realistic damping (which is essential if one is seeking to estimate the mathematically real component of the mobility function) into the preliminary modelling phase of a finite element idealization also poses a problem in many instances. However, it is possible to introduce a form of modal damping, extracted from experimental observations, into the calculations of frequency domain data based upon a finite element model.

In practical measurements by utilizing a FFT analyser, the power can be found by using the force spectrum density function G_{ff} , or the vibration velocity spectrum density function G_{vv}, or the cross power spectrum density function G_{fv} , which can be expressed as:

$$P(\omega) = G_{ff}\ Re[M] = Re[G_{fv}] = G_{vv}\ Re[Z] \tag{3.68}$$

The driving point impedance matrix, the receiving point impedance matrix and the transfer impedance matrix for well-installed system can be obtained in the same way as equations (3.47a) to (3.47c), i.e.,

$$[Z_{input}] = [Z_{AA}] = \frac{[M_{BB}]}{[M_{AA}][M_{BB}] - [M_{AB}][M_{BA}]} \tag{3.69a}$$

$$[Z_{output}] = [Z_{BB}] = \frac{[M_{AA}]}{[M_{AA}][M_{BB}] - [M_{AB}][M_{BA}]} \tag{3.69b}$$

$$[Z_{transmit}] = [Z_{BA}] = [Z_{AB}] = \frac{-[M_{AB}]}{[M_{AA}][M_{BB}] - [M_{AB}][M_{BA}]} \tag{3.69c}$$

Substituing $[Z_{input}]$, $[Z_{output}]$ and $[Z_{transmit}]$into equation (3.68), the input power, output power and transmitted power can be calculated respectively, i.e.,

$$(P_{input}) = G_{v_A v_A}\ Re[Z_{input}] \tag{3.70a}$$

$$(P_{output}) = G_{v_B v_B}\ Re[Z_{output}] \tag{3.70b}$$

$$(P_{transmit}) = G_{v_A v_A} \, Re[Z_{transmit}] \tag{3.70c}$$

Thus the general methodlogy for obtaining the power fed into a receiving structure from the excitation sources of a engine via the contact points is derived. More details concerning the transfer mobility reduction of the structure-borne sound transmitted from a marine engine will be discussed later.

3.7 Logic of Structure-Borne Sound Reduction

The low noise design problem for a simple engine room onboard a vessel is schematically shown in Figure 3.8. The primary noise generating mechanism is the main engine that injects vibrations into the structure via the mounts and foundations. These vibrations will be transmitted throughout the structure and eventually radiate sound to the surroundings.

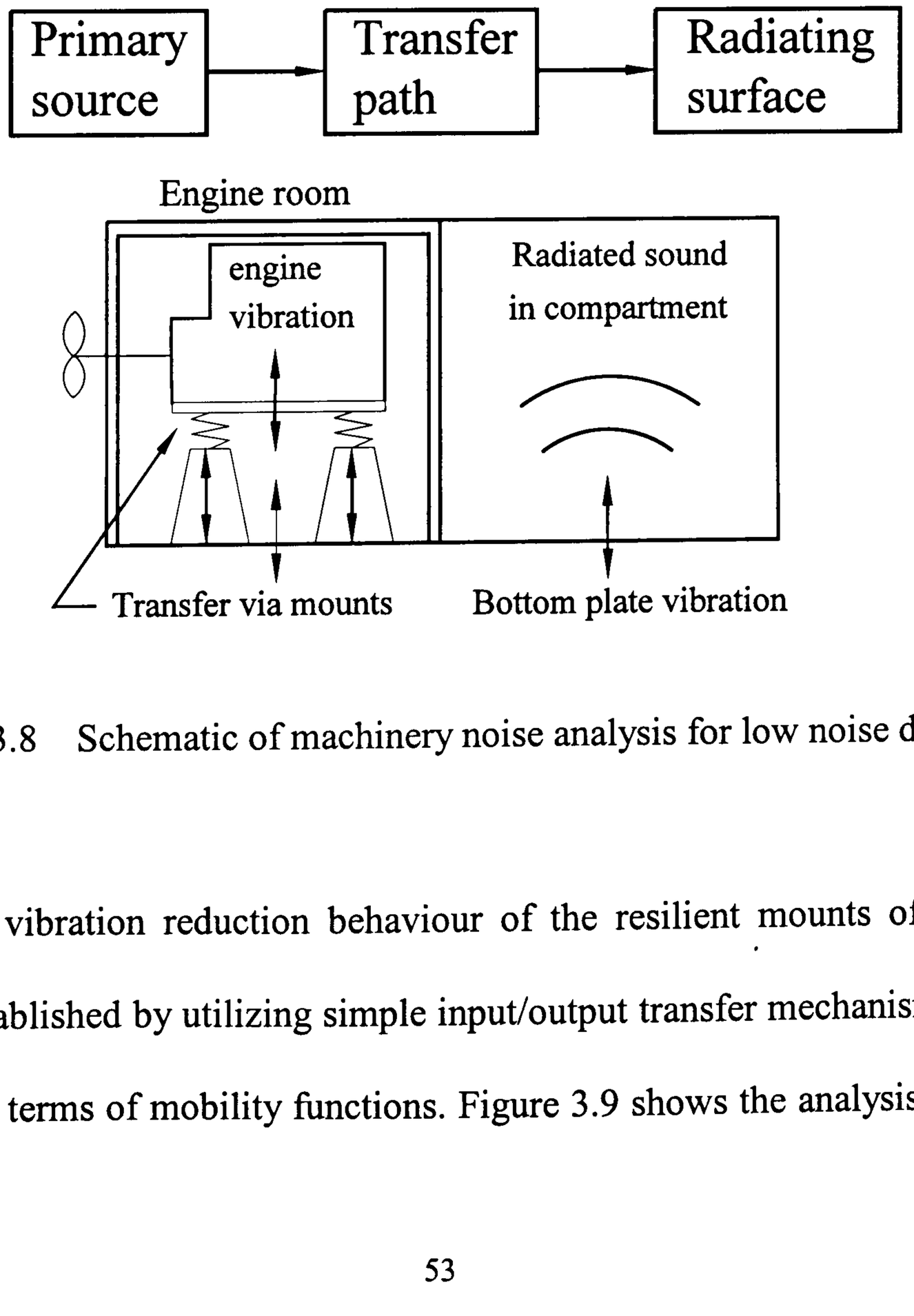

Figure 3.8 Schematic of machinery noise analysis for low noise design

To simulate the vibration reduction behaviour of the resilient mounts of a machine, a model can be established by utilizing simple input/output transfer mechanisms, which may be represented in terms of mobility functions. Figure 3.9 shows the analysis models which

can be used to model the structure-borne sound transfer between the primary source and the radiating surface. For a uni-directional simple harmonic excitation force F_1, the engine structure vibrates with a simple harmonic velocity V_1 at the driving point. Structural waves propagate from the excitation point to the adjacent bottom plate, where bending waves generate a velocity field $V_2(x,y)$. This vibration field radiates a sound field $p(x,y,z)$.

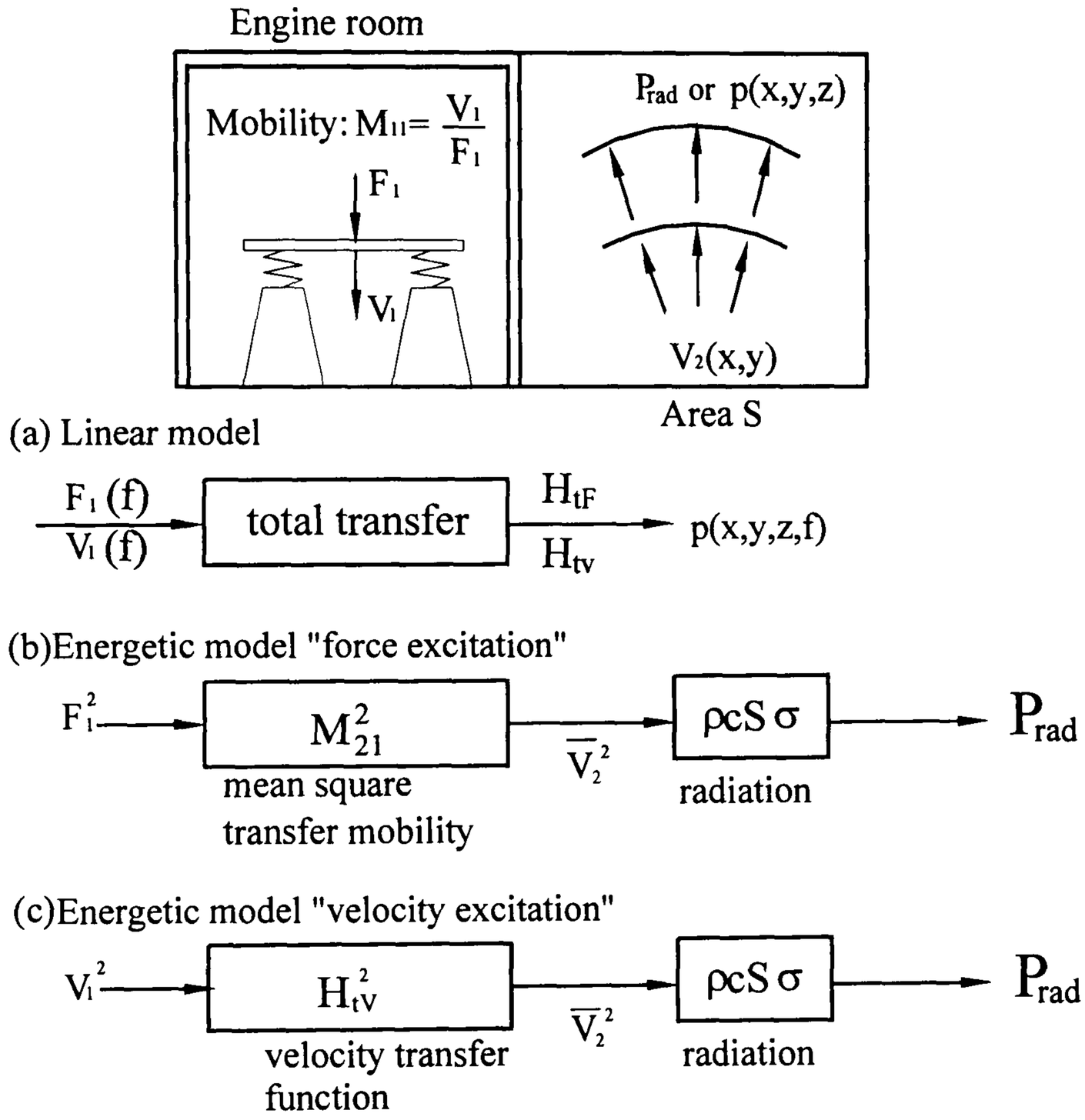

Figure 3.9 Schematic for the analysis of structure-borne noise transfer

The linear equations which relate the radiated sound pressure with the force and the velocity at the driving point are (Verheij,1995):

$$p(x,y,z,f) = H_{tF}F_1(f) \tag{3.71}$$

$$p(x,y,z,f) = H_{tV}V_1(f) \tag{3.72}$$

here H_{tF} and H_{tV} are so-called frequency response functions, describing the sound

transfer for force and velocity excitation respectively. Basically, these frequency response functions have a complex value at each frequency, indicating the magnitude and the phase of the vibration.

The force and velocity at the diving point are related as

$$M_{11} = \frac{V_1}{F_1} \tag{3.73}$$

here M_{11} is called driving point mobility. It is a measure of the vibration velocity for a given force F_1.

In many practical situations instead of linear equations, equations in terms of mean square quantities or so-called " energetic " quantities are used. In principle, these formulations are exact, if derived directly from equations (3.71) and (3.72). However, for practical purposes, approximations of transfer functions are used. Those functions relate e.g. 1/3-octave band levels of F_1^2 and V_1^2 with the radiated sound power P_{rad} (Verheij,1995). In the scheme of Figures 3.9(b) and 3.9(c), the " energetic " models are presented. The transmission chain is divided into two blocks. The first block represents the structure and gives the ratio between the spatially averaged mean square velocity $\overline{V_2^2}$ of the bottom surface and F_1^2 or V_1^2:

$$M_{21}^2 = \frac{\overline{V_2^2}}{F_1^2} \quad , \quad H_{tV}^2 = \frac{\overline{V_2^2}}{V_1^2} \tag{3.74}$$

The function M_{21}^2 is called the mean square transfer mobility and the function H_{tV}^2 is called the velocity transfer function.

The second block represents the sound radiation and gives the ratio between the radiated sound power and $\overline{V_2^2}$:

$$\frac{P_{rad}}{V_2^2} = \rho c S \sigma \tag{3.75}$$

The right side of equation (3.75) contains the characteristic impedance ρc of the surrounding fluid (air, water, etc), the area S of the radiating surface, and the radiation efficiency σ. σ is a measure of the efficiency with which a structure converts vibrations into sound.

The factors which determine the sound transfer is influenced by design as seen in Figure 3.9 and from the following equations:

$$\frac{P_{rad}}{F_1^2} = (M_{21}^2 S\sigma)\rho c = (M_{11}^2 H_{tV}^2 S\sigma)\rho c \tag{3.76}$$

$$\frac{P_{rad}}{V_1^2} = (H_{tV}^2 S\sigma)\rho c \tag{3.77}$$

If the nature of the excitation is such that for different engine design F_1 is unaffected, equation (3.76) implies that sound reduction is obtained by:

(a) decrease of driving point mobility ;

(b) reduction of radiating surface area;

(c) decrease of velocity transfer function;

(d) decrease of radiation efficiency.

If the nature of the excitation is such that for different engine designs V_1 is unaffected, equation (3.77) implies that sound reduction is obtained by:

(a) reduction of radiating surface area;

(b) decrease of velocity transfer function;

(c) decrease of radiation efficiency.

A design measures to decrease S significantly, have very limited applications. However measures to decrease M_{11} and are H_{tV}^2 are very important and will be discussed extensively in this study.

3.8 Velocity Transfer Function and Transfer Mobility

The velocity transfer function H_{tV}^2, defined in equation (3.74), depends strongly on the size and nature of the structure. For noise reduction purposes, the main interest is in the eigenfrequency range. Here again the discussion will be limited to the elementary case of a finite plate. In principle, H_{tV}^2 can be calculated with the aid of an eigenfunction model by the finite element method. Again it can be said that, if in the intermediate frequency range (from 100 Hz to 1 kHz) of interest a large number of eigenfrequencies is involved, the calculations become time consuming. Moreover, from the view point of the designer it is important to look at some smoothed data and to understand the relation between the design parameters and these data.

To derive a simple expression for H_{tV}^2 on a plate, the following assumptions are made:

(a) the plate length and width are large compared with λ_B ;

(b) many weakly damped resonances occur simultaneouly ;

(c) results are for frequency bands that contain at least 3-5 eigenfrequencies.

In that case the velocity distribution over the plate is approximately homogeneous (so called diffuse field).

At equilibrium, the power injected into the plate is equal to the power dissipated by the plate.

$$(P_{in})=(P_{diss}) \tag{3.78}$$

From equations (3.62) and (3.63), the power injected by a point source into the plate at a single frequency is given by :

$$(P_{in}) = \frac{1}{2}\mathrm{Re}\{F_1 V_1^*\} = F_{1,rms}^2\,\mathrm{Re}\{M_{11}\} = V_{1,rms}^2\,\mathrm{Re}\{\frac{1}{M_{11}}\} \tag{3.79}$$

where $F_{1,rms}$ is the root-mean-square of F_1. For averaging over frequencies, M_{11} may be replaced by $M_{P\infty}$. Using equations (3.44) and (3.79) this leads to :

$$(P_{in}) = \frac{0.453F_{1,\Delta f}^2}{\rho_p c_{LP} h^2} = 2.2\rho_p c_{LP} h^2 V_{1,\Delta f}^2 \tag{3.80}$$

where c_{LP} is the longitudinal wave speed of the plate; h is the thickness of the plate; ρ_P is the density of the plate; $V_{1,\Delta f}^2$ is the driving point velocity within the frequency band Δf.

The power dissipation from the plate is caused by material damping, by energy transport across the plate boundaries into the support, and by sound radiation from the plate. The well known parameter which includes all these damping mechanisms is the (apparent) loss factor η. For each frequency or frequency band it was defined by Verheij (1995) as:

$$\eta(f) = \frac{P_{diss}}{\omega m'' S\overline{V_2^2}} = \frac{\text{energy dissipation per vibration period}}{2\pi(\text{reversible) mechancial energy}} \tag{3.81}$$

where m'' is the mass per unit area of the plate. In equation (3.81) it is assumed that the total mechanical energy (i.e. the sum of kinetic and potential energy) is twice the kinetic energy, i.e.

$$E = m'' S\overline{V_2^2} \tag{3.82}$$

Therefore, the dissipated power may be written as:

$$P_{diss} = \eta\omega m'' S\overline{V_2^2} \tag{3.83}$$

Using equations (3.78), (3.80) and (3.83), the second equation of (3.74) becomes

$$H_{tV}^2(f) = \frac{0.35 c_{LP} h}{fS\eta(f)} \tag{3.84}$$

Figure 3.10 shows the effect on H_{tV}^2 of different loss factor. It is seen that at low frequencies $H_{tV}^2 >> 1$. The frequency at which $H_{tV}^2 = 1$ decreases with increasing η and decreasing plate thickness.

The square transfer mobility M_{21}^2, defined by the first equation of (3.74), in the eigenfrequency range follows from equations (3.78), (3.79), (3.83) and putting $\mathrm{Re}\{M_{11}\} = M_{P\infty}$:

$$M_{21}^2 = \frac{\overline{V_{2,\Delta f}^2}}{F_{1,\Delta f}^2} = \frac{M_{P\infty}}{\eta\omega m'' S} \approx \frac{2.85}{\eta f \rho_p^2 c_{LP} h^3 S} \tag{3.85}$$

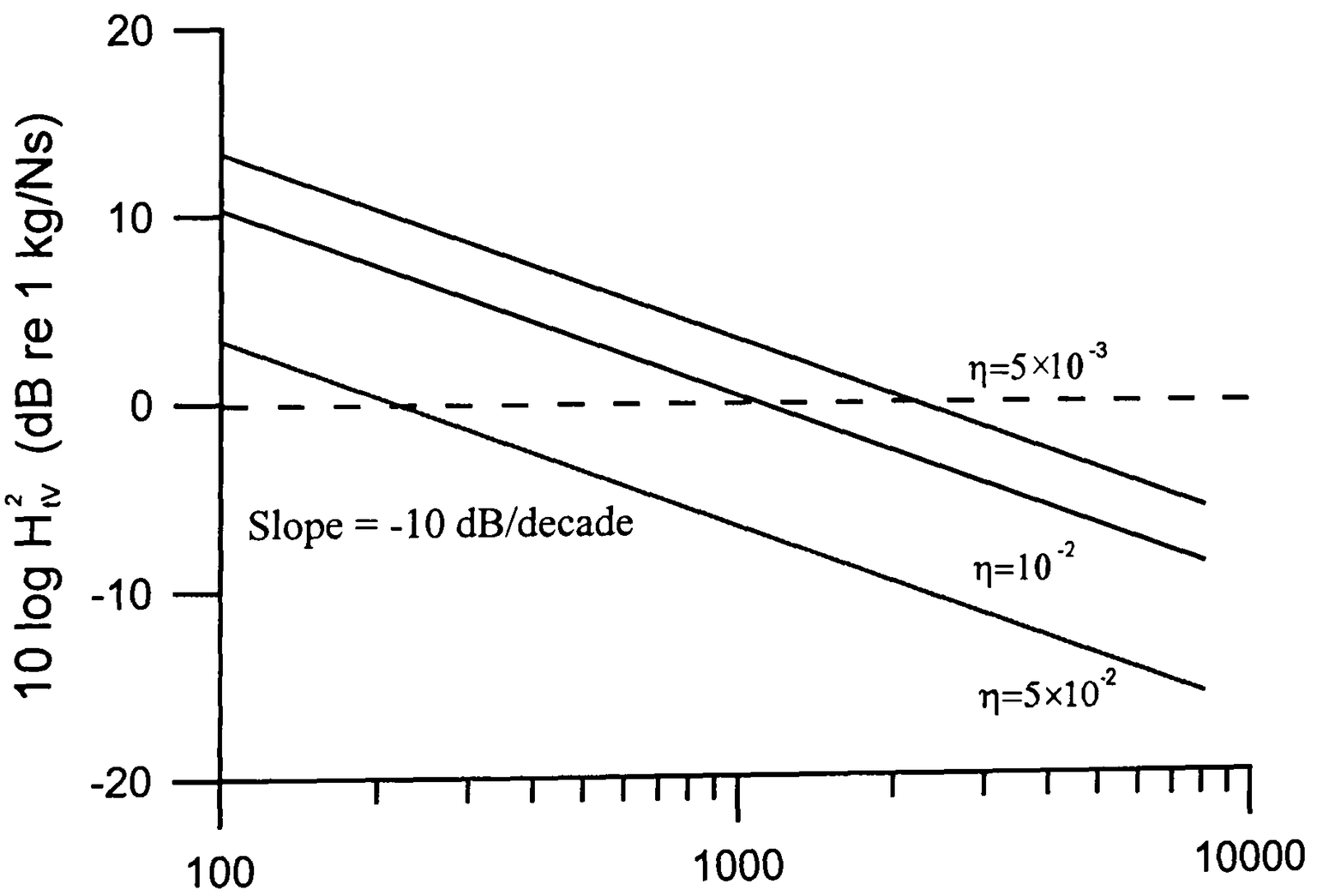

Figure 3.10 Velocity transfer function of a steel plate (480mm×340mm×5mm) of different loss factor

Comparing equation (3.84) and (3.85) reveals that the influence of damping upon H_{tV}^2 and M_{21}^2 is the same, but the influence of plate thickness variation is quite different. Therefore, it is of vital importance for a designer to distinguish the source (or component) type which drives the structure and to determine either equation (3.76) or equation (3.77) to apply.

3.9 Mechanical Four-Pole Parameters Method in System Mobility Evaluation

In 1970's, a powerful method used to calculate the transmission and isolation of structure-borne vibration and noise has been successfully developed. This is the so-called mechanical four-pole parameters method (Cremer et.al.,1988). It has been applied in the vibration and noise control field by Snowdon (1971).

3.9.1 Basic Theory of the Four-Pole Parameters Method

The mechanism of high frequency noise transmission through a mechanical system such as an elastic mount can be characterized in terms of the parameters at each end as shown in Figure 3.1. This allows physical insight into how high frequency noise generated by the input end transmits through the elastic mount, and hence how it may be suppressed at the output end. To keep the analysis simple in the first instance, only two parameters at each end are considered. These are the complex frequency functions of force and velocity. The matrix equation relating velocities and forces to point and transfer mobilities for a general system is equation (3.27), repeated here for clarity,

$$\begin{Bmatrix} V_1 \\ V_2 \end{Bmatrix} = \begin{bmatrix} M_{11} & M_{12} \\ M_{21} & M_{22} \end{bmatrix} \begin{Bmatrix} F_1 \\ F_2 \end{Bmatrix} \tag{3.86}$$

The main advantage of the mobility method is that system components can be coupled by way of these functions that are defined at the interfaces between components. This technique is used to investigated the effects of fitting a simple compliant element between

the engine and seat.

Expanding equation (3.86) and rearranging gives:

$$\begin{Bmatrix} V_1 \\ F_1 \end{Bmatrix} = \begin{bmatrix} \alpha_{11} & \alpha_{12} \\ \alpha_{21} & \alpha_{22} \end{bmatrix} \begin{Bmatrix} V_2 \\ F_2 \end{Bmatrix} \tag{3.87}$$

The coefficients α_{11}, α_{12}, α_{21}, α_{22}, in equation (3.87) are called the four-pole parameters (Cremer er.al.,1988). Their definitions are:

$$\alpha_{11} = \left.\frac{V_1}{V_2}\right|_{F_2=0}, \quad \alpha_{12} = \left.\frac{V_1}{F_2}\right|_{V_2=0}, \quad \alpha_{21} = \left.\frac{F_1}{V_2}\right|_{F_2=0}, \quad \alpha_{22} = \left.\frac{F_1}{F_2}\right|_{V_2=0} \tag{3.88}$$

$V_2=0$ means that the output end is fixed, while $F_2=0$ means that the output end is free. From equation (3.88), it can be seen that α_{11} and α_{22} are dimensionless, α_{12} has the dimension of mobility and α_{21} has the dimension of impedance.

In general, all four-pole parameters are frequency dependent complex quantities. They are relevant to the characteristics of the mechanical system itself. Expanding equation (3.87), the driving point mobility can be obtained as:

$$M_{11} = \frac{V_1}{F_1} = \frac{\alpha_{11}V_2 + \alpha_{12}F_2}{\alpha_{21}V_2 + \alpha_{22}F_2} = \frac{\alpha_{11}M_{22} + \alpha_{12}}{\alpha_{21}M_{22} + \alpha_{22}} \tag{3.89}$$

where $M_{22} = V_2 / F_2$ is the receiving point mobility. Reciprocally, the driving point impedance is:

$$Z_{11} = \frac{F_1}{V_1} = \frac{\alpha_{21}V_2 + \alpha_{22}F_2}{\alpha_{11}V_2 + \alpha_{12}F_2} = \frac{\alpha_{21} + \alpha_{22}Z_{22}}{\alpha_{11} + \alpha_{12}Z_{22}} \tag{3.90}$$

where $Z_{22} = \frac{F_2}{V_2}$ is the receiving point impedance. Also, the transfer mobilities and impedances can be derived as:

$$M_{12} = \frac{V_1}{F_2} = \alpha_{11} M_{22} + \alpha_{12} \tag{3.91}$$

$$M_{21} = \frac{V_2}{F_1} = \frac{M_{22}}{\alpha_{21} M_{22} + \alpha_{22}} \tag{3.92}$$

and

$$Z_{12} = \frac{F_1}{V_2} = \alpha_{21} + \alpha_{22} Z_{22} \tag{3.93}$$

$$Z_{21} = \frac{F_2}{V_1} = \frac{Z_{22}}{\alpha_{11} + \alpha_{12} Z_{22}} \tag{3.94}$$

The force and velocity transmissibilities are defined and expressed as:

$$T_{F_{12}} = \left|\frac{F_2}{F_1}\right| = \left|\frac{1}{\alpha_{21} M_{22} + \alpha_{22}}\right| = \left|\frac{Z_{22}}{\alpha_{21} + \alpha_{22} Z_{22}}\right| \tag{3.95}$$

$$T_{V_{12}} = \left|\frac{V_2}{V_1}\right| = \left|\frac{M_{22}}{\alpha_{11} M_{22} + \alpha_{12}}\right| = \left|\frac{1}{\alpha_{11} + \alpha_{12} Z_{22}}\right| \tag{3.96}$$

By equations (3.95) and (3.96), the system transmissibilities can be found provided the four-pole parameters and the receiving point mobility or impedance are known.

3.9.2 Connection of Mechanical Four-Pole Systems

Analogous to an electric circuit system, there are two basic types of connection for the mechanical four-pole systems, namely the series and parallel connections. If the output end of one system is rigidly joined to the input end of another system, it is said to be in series connection. While the input (output) ends of two or more mechanical systems are rigidly joined together and move with the same velocity, then it is said to be in parallel connection.

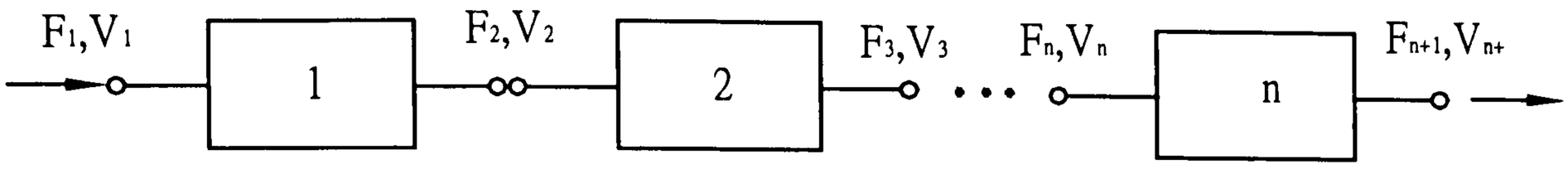

Figure 3.11 Four-pole subsystems in series connection

As the four-pole mechanical subsystems are connected in series, as shown in Figure 3.11, then the output of one subsystem is just the input of the subsequently adjacent subsystem.

For each subsystem, the matrix form expression in terms of the four-pole parameters is:

$$\begin{Bmatrix} V_1 \\ F_1 \end{Bmatrix} = \begin{bmatrix} \alpha'_{11} & \alpha'_{12} \\ \alpha'_{21} & \alpha'_{22} \end{bmatrix} \begin{Bmatrix} V_2 \\ F_2 \end{Bmatrix}$$

$$\begin{Bmatrix} V_2 \\ F_2 \end{Bmatrix} = \begin{bmatrix} \alpha''_{11} & \alpha''_{12} \\ \alpha''_{21} & \alpha''_{22} \end{bmatrix} \begin{Bmatrix} V_3 \\ F_3 \end{Bmatrix}$$

$$\vdots$$

$$\begin{Bmatrix} V_n \\ F_n \end{Bmatrix} = \begin{bmatrix} \alpha^n_{11} & \alpha^n_{12} \\ \alpha^n_{21} & \alpha^n_{22} \end{bmatrix} \begin{Bmatrix} V_{n+1} \\ F_{n+1} \end{Bmatrix}$$

Therefore,

$$\begin{Bmatrix} V_1 \\ F_1 \end{Bmatrix} = \begin{bmatrix} \alpha'_{11} & \alpha'_{12} \\ \alpha'_{21} & \alpha'_{22} \end{bmatrix} \begin{bmatrix} \alpha''_{11} & \alpha''_{12} \\ \alpha''_{21} & \alpha''_{22} \end{bmatrix} \cdots \begin{bmatrix} \alpha^n_{11} & \alpha^n_{12} \\ \alpha^n_{21} & \alpha^n_{22} \end{bmatrix} \begin{Bmatrix} V_{n+1} \\ F_{n+1} \end{Bmatrix} \tag{3.97}$$

For example, if there only two subsystems connected in series, then

$$\begin{Bmatrix} V_1 \\ F_1 \end{Bmatrix} = \begin{bmatrix} \beta_{11} & \beta_{12} \\ \beta_{21} & \beta_{22} \end{bmatrix} \begin{Bmatrix} V_3 \\ F_3 \end{Bmatrix} \tag{3.98}$$

in which

$$\begin{bmatrix} \beta_{11} & \beta_{12} \\ \beta_{21} & \beta_{22} \end{bmatrix} = \begin{bmatrix} \alpha'_{11}\alpha''_{11} + \alpha'_{12}\alpha''_{21} & \alpha'_{11}\alpha''_{12} + \alpha'_{12}\alpha''_{22} \\ \alpha'_{21}\alpha''_{11} + \alpha'_{22}\alpha''_{21} & \alpha'_{21}\alpha''_{12} + \alpha'_{22}\alpha''_{22} \end{bmatrix} \tag{3.99}$$

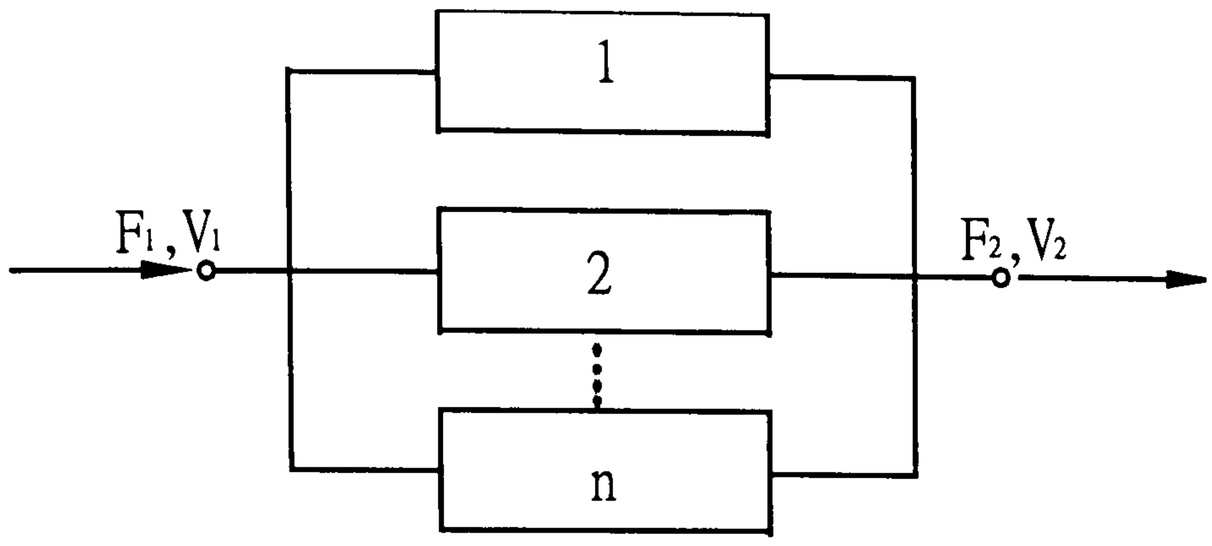

Figure 3.12 Four-pole subsystems in parallel connection

Figure 3.12 shows the n subsystems in parallel connection, in which the terminal input or output forces of the system is equal to the sum of the input and output forces of each individual subsystems. Then

$$\begin{Bmatrix} V_1 \\ F_1 \end{Bmatrix} = \begin{bmatrix} \beta_{11} & \beta_{12} \\ \beta_{21} & \beta_{22} \end{bmatrix} \begin{Bmatrix} V_2 \\ F_2 \end{Bmatrix} \tag{3.100}$$

where

$$\beta_{11} = \frac{A}{B} \quad , \quad \beta_{12} = \frac{1}{B} \quad , \quad \beta_{21} = \frac{AC - B^2}{B} \quad , \quad \beta_{22} = \frac{C}{B} \tag{3.101}$$

and

$$A = \sum_{i=1}^{n} \frac{\alpha_{11}^{i}}{\alpha_{12}^{i}} \quad , \quad B = \sum_{i=1}^{n} \frac{1}{\alpha_{12}^{i}} \quad , \quad C = \sum_{i=1}^{n} \frac{\alpha_{22}^{i}}{\alpha_{12}^{i}} \tag{3.102}$$

For example, if the system is composed of two subsystems in parallel connection, then

$$A = \frac{\alpha'_{11}\alpha''_{12} + \alpha'_{12}\alpha''_{11}}{\hat{\alpha}'_{12}\hat{\alpha}''_{12}} = \frac{\varphi}{\varepsilon} \tag{3.103a}$$

$$B = \frac{\alpha'_{12} + \alpha''_{12}}{\alpha'_{12}\alpha''_{12}} = \frac{\theta}{\varepsilon} \tag{3.103b}$$

$$C = \frac{\alpha'_{22}\alpha'_{12} + \alpha'_{12}\alpha''_{22}}{\alpha'_{12}\alpha''_{22}} = \frac{\lambda}{\varepsilon} \tag{3.103c}$$

Thus

$$\beta_{11} = \frac{A}{B} = \frac{\varphi}{\theta}, \qquad \beta_{12} = \frac{AC - B^2}{B} = \frac{\varphi\lambda - \theta^2}{\varepsilon\theta}$$
$$\beta_{21} = \frac{1}{B} = \frac{\varepsilon}{\theta}, \qquad \beta_{22} = \frac{C}{B} = \frac{\lambda}{\theta} \tag{3.104}$$

where

$$\varphi = \alpha'_{22}\alpha''_{12} + \alpha'_{12}\alpha''_{22} \tag{3.105a}$$

$$\theta = \alpha'_{12} + \alpha''_{12} \tag{3.105b}$$

$$\varepsilon = \alpha'_{12}\alpha''_{12} \tag{3.105c}$$

$$\lambda = \alpha'_{11}\alpha''_{12} + \alpha'_{12}\alpha'' \tag{3.105d}$$

3.10 Explanation of Reduction in Transfer Mobility by Inserting an Isolator

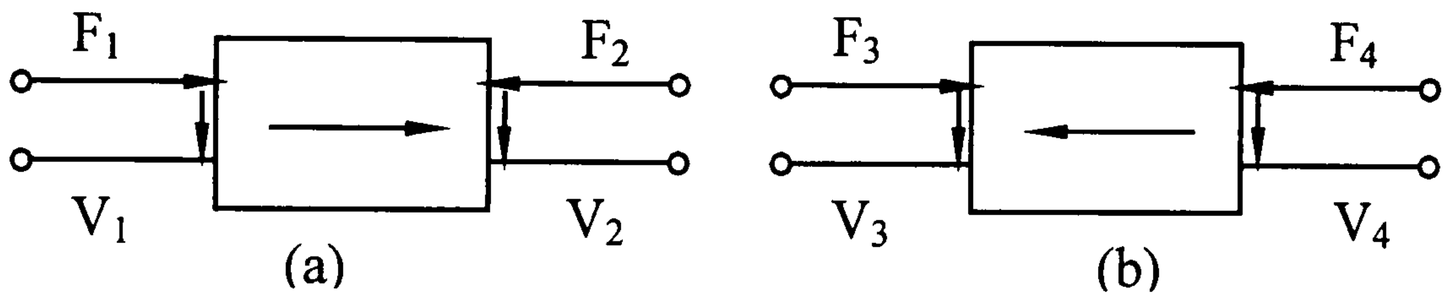

Figure 3.13 Mobility of intergrated system combined by mobility matrices of the subsystems

Suppose the two ends of the subsystems a, b are 1,2 and 3,4 respectively, as shown in Figure 3.13, where F represents the force and V represents the velocity. When the subsystems are linked together, then V_3=V_2 and $F_3 = -F_2$, equation (3.97) the becomes:

$$\begin{Bmatrix} V_1 \\ F_1 \end{Bmatrix} = \begin{bmatrix} \alpha_{11} & \alpha_{12} \\ \alpha_{21} & \alpha_{22} \end{bmatrix} \begin{Bmatrix} V_2 \\ F_2 \end{Bmatrix} = \begin{bmatrix} \alpha_{11} & \alpha_{12} \\ \alpha_{21} & \alpha_{22} \end{bmatrix} \begin{bmatrix} \alpha_{33} & \alpha_{34} \\ -\alpha_{43} & -\alpha_{44} \end{bmatrix} \begin{Bmatrix} V_4 \\ F_4 \end{Bmatrix} = \begin{bmatrix} \alpha'_{11} & \alpha'_{14} \\ \alpha'_{41} & \alpha'_{44} \end{bmatrix} \begin{Bmatrix} V_4 \\ F_4 \end{Bmatrix} \tag{3.106}$$

It requires that F_4=0 since 4 is the receiving point and 1 is the driving point. Thus,

$$\frac{1}{\alpha'_{41}} = M_{41} = \frac{V_4}{F_4} \tag{3.107}$$

From equation (3.106)

$$\alpha'_{41} = \alpha_{21}\alpha_{33} - \alpha_{22}\alpha_{43} = \frac{M_{22} + M_{33}}{M_{12}M_{34}}$$

or

$$M_{41} = \frac{M_{12}M_{34}}{M_{22} + M_{33}} \tag{3.108}$$

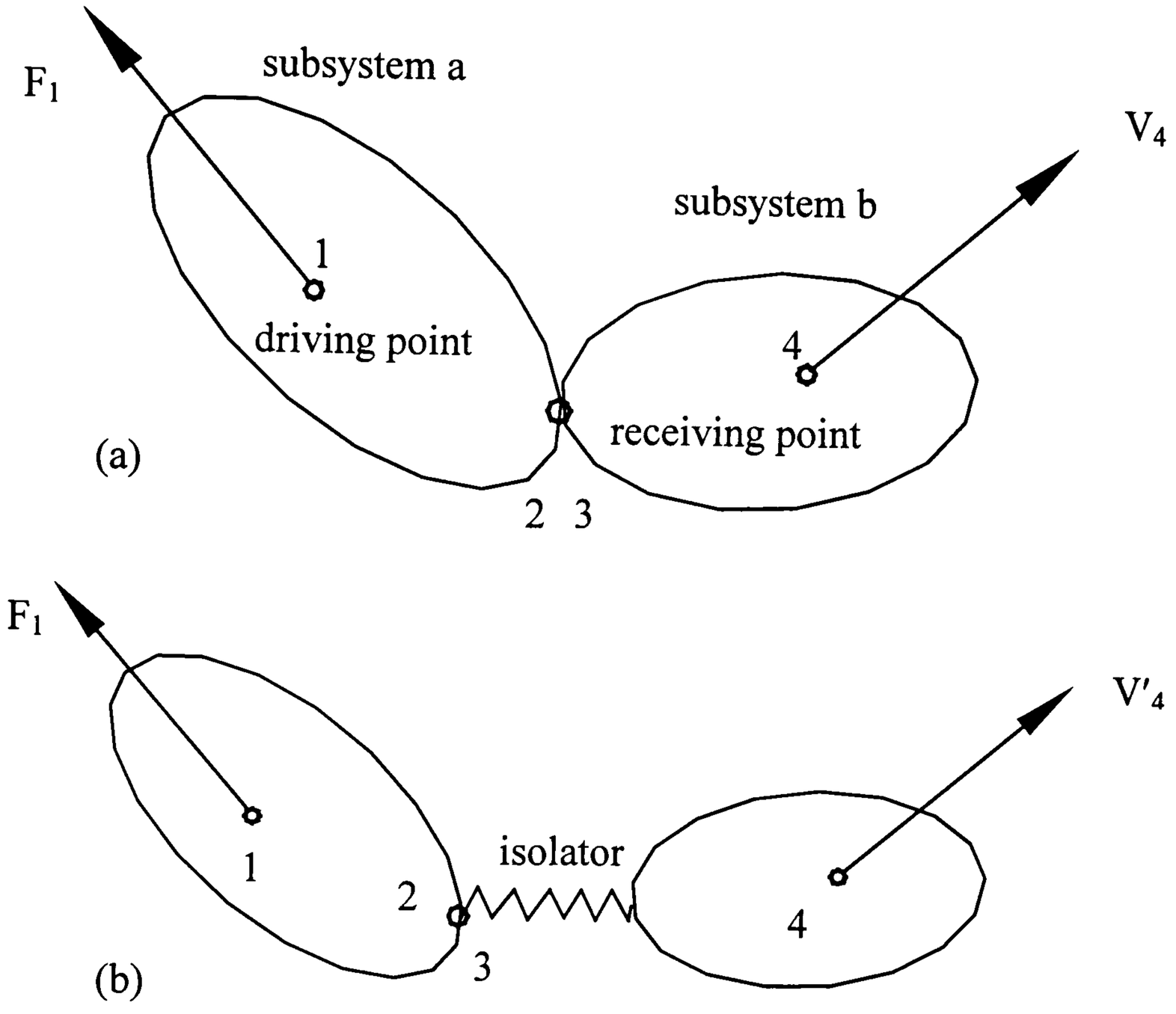

Figure 3.14 System before and after installation of isolator

Form equation (3.108), it can be seen that the transfer mobility of the combined system (M_{41}) is not a simple additive combination of the transfer mobilties (M_{12} and M_{34}) of the two subsystems. The linking point mbilities (M_{22} and M_{33}) of the subsystems play a vital role in determining the total transfer mobility. As an isolator is connected to the input end of the subsystem b, such as in Figure 3.14 (b) which represents the improved system of Figure 3.14 (a), the mobility M_{33} would increase significantly. It follows from equation

(3.108) that the total transfer mobility M_{41} is reduced. In other words, to reduce the total transfer mobility, it requires the introduction of a larger mobility than the original one. This is the reason of the basic principle for a good structure-borne noise attenuation result that, the structure on both sides of a resilient mount must be properly designed with smaller mobility than that of the mount itself. Simply said, the desired mobility changes for the coupled machine---resilient mount---foundation structure in series system should be "heavy-compliant-heavy" and/or "stiff-compliant-stiff".

Thus, the evaluation model and control principle (equation (3.108)) for structure-borne sound tramission from engine to the receiving structure have been established. Besides this, numerical model for the analysis of the transfer function of a complicated stiffened-plate structure like a ship will describe in the next Chapter.

CHAPTER 4

STRUCTURE-BORNE VIBRATION AND NOISE PROPAGATION IN A SHIP STURCTURE

In most cases the engine foundation and hull structure are composed of beams and plates. Once the vibrational power flow feeding in the receiving structure from an engine via the contact points, the structure-borne sound and vibration can propagate in the structure. Structure-borne noise implies elastic waves in the sound frequency range. Besides the longitudinal waves, there are many transverse wave patterns existing in the stiffened-plate structure during the noise propagation, such as bending waves, shear waves and torsional waves etc. Structure-borne noise propagation is more complicated than sound propagating in fluid. To analyse the structure-borne noise propagation, the FEM for the lower frequency range and the SEA model for the higher frequency range can be applied. While in the medium frequency range there is a knowledge gap. If the FEM is used to solve this medium frequency propagation problem, it can be assumed as a rule of thumb that, in the discretization process, about ten elements are needed per wavelength. In the case of a container ship of length 250 m in the range of frequencies around 1 kHz, it leads to FE models with over 10^6 degrees of freedom, which is pointed out by Cabos and Jokat (1998). It sounds to be an impractical model of computation. Thus an innovative numerical model based on the stress wave concept is developed as follows.

4.1 Wave Propagation in a Finite Beam

4.1.1 Elastic Bending Wave in a Finite Beam

For the radiation of airborne noise or hydroacoustics, the elastic bending wave in a stiffened plate structure is the most important wave pattern owing to its larger lateral displacement. The one dimensional bending wave equation in a beam of finite length can be expressed as (Cremer et al, 1988):

$$\frac{B}{m'}\frac{\partial^4 v_y}{\partial x^4}+\frac{\partial^2 v_y}{\partial t^2}-\left[\frac{\vartheta_z'}{m'}+\frac{B}{K}\right]\frac{\partial^4 v_y}{\partial x^2\partial t^2}+\frac{\vartheta_z'}{K}\frac{\partial^4 v_y}{\partial t^4}=0 \qquad (4.1)$$

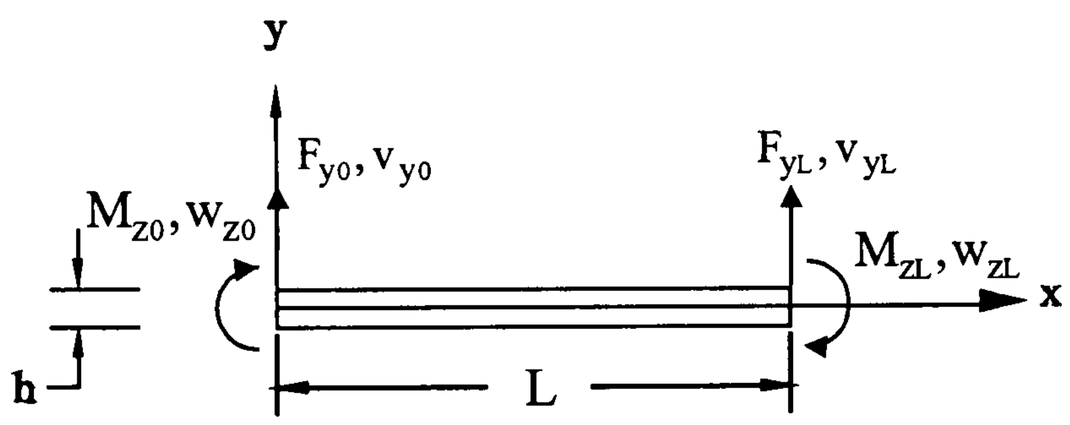

Figure 4.1 Coordinate system of a beam

where the coordinate system is shown in Figure 4.1, and the symbols are:

B = bending rigidity of a rectangular beam $= EI = \frac{1}{12}Ebh^3$ (N-m^2)

m' = mass per unit length $= \rho s$ (kg / m)

v_y = velocity along y axis (m / sec)

w_z = angular velocity about z axis (rad / s)

F_y = force along y axis (N)

M_z = moment about z axis (Nm)

ϑ_z' = $I\rho dx$ = rotary mass moment of inertia of dx about z (kg-m)

K = $\frac{Gs}{\kappa}$ = the shear rigidity (N – m)

E = Young's modulus (N / m^2)

S = cross-sectional area (m^2)

h = thickness of plate or web height of beam (m)

κ = shear distribution factor (m^{-1})

μ = Poisson's ratio

t = time (sec)

The first two terms of equation (4.1) correspond to the differential equation for pure bending waves. The other three terms represent the corrections. The first of these, with the coefficient ϑ'_z / m' (which is equal to the square of the radius of gyration), would occur by itself if only rotational inertia were considered, and the second would occur by itself if only shear deformations were taken into account. For homogeneous structures, these two parts are not independent of each other. First of all,

$$\frac{\vartheta'_z}{m'} = \frac{I}{S}$$

and secondly,

$$\frac{B}{K} = \frac{IE\kappa}{SG}$$

In the case of a steel beam, if the bending wavelength to the web height ratio is less than 6 then the last three terms in equation (4.1) should be maintained. Otherwise, Cremer et al, pointed out that there exists an error of around 10% to the solution of phase velocity. The phase velocity C_B and the elastic wavelength λ_B can be expressed as:

$$C_B = (\frac{B}{m'})^{1/4} (\omega)^{1/2} \qquad (4.2)$$

$$\lambda_B = \frac{2\pi C_B}{\omega} \qquad (4.3)$$

where ω is the circular frequency of the bending wave.

For a 3% error of phase velocity, the ratio of λ_B/h should be greater than 10, thus according to equation (4.3) the frequency range has to be less than 3.2 kHz for a steel beam of the scantling for ship structure type (Wang, 1996). In these cases equation (4.1) can be reduced to the pure bending wave equation:

$$B\frac{\partial^4 v}{\partial x^4} + m'\frac{\partial^2 v}{\partial t^2} = 0 \tag{4.4}$$

In an actual vibration carrying structure, there always exists the boundaries. The boundaries may change the wave direction, phase and amplitude, furthermore, they may even change the wave pattern. To consider the progressive wave, the reflection wave and exponentially decayed near-field wave due to the boundaries, the solution of equation (4.4) with a circular frequency ω is:

$$v = v_+ e^{-jkx} + v_- e^{jkx} + v_{-j} e^{-kx} + v_j e^{kx} \tag{4.5}$$

where

$v = v(t)$ has the form of harmonic function of time

$$k = \text{ bending wave number} = \frac{2\pi}{\lambda_B} = \frac{\omega}{C_B} = (\omega^2 m'/B)^{1/4} \tag{4.6}$$

v_+ = amplitude of the progressive wave along the positive x direction

v_- = amplitude of the progressive wave along the negative x direction

v_{-j} = amplitude of the decayed near-field wave along the positive x direction

v_j = amplitude of the decayed near-field wave along the negative x direction

From equation (4.5) and the fundamental theory of plate, the angular velocity w, the bending moment M_z and the shear force F_y can be obtained from the following relations:

$$w = \frac{\partial v}{\partial x}\ , \quad M_z = -\frac{B}{j\omega}\frac{\partial w}{\partial x} = -\frac{B}{j\omega}\frac{\partial^2 v}{\partial x^2}\ , \quad F_y = -\frac{\partial M_z}{\partial x}\ , \quad \frac{\partial F_y}{\partial x} = -j\omega m' v \qquad (4.7)$$

If the state parameters of both ends of a beam element of length L are $\langle v_{y_0}, w_{z_0}, F_{y_0}, M_{z_0} \rangle$ and $\langle v_{y_L}, w_{z_L}, F_{y_L}, M_{z_L} \rangle$, then the transfer relationships between the end parameters can be represented by:

$$\begin{Bmatrix} v_{y_0} \\ w_{z_0} \\ v_{y_L} \\ w_{z_L} \end{Bmatrix} = \begin{bmatrix} M_{11} & M_{12} & M_{13} & M_{14} \\ M_{21} & M_{22} & M_{23} & M_{24} \\ M_{31} & M_{32} & M_{33} & M_{34} \\ M_{41} & M_{42} & M_{43} & M_{44} \end{bmatrix} \begin{Bmatrix} F_{y_0} \\ M_{z_0} \\ F_{y_L} \\ M_{z_L} \end{Bmatrix} \qquad (4.8a)$$

or

$$\{v_{NP}\} = [M_{ij}]\ \{F_{NP}\} \qquad (4.8b)$$

where $[M_{ij}]$, (i, j = 1, 2,3.4), is called the complex transfer matrix or mobility matrix,

$\{v_{NP}\} = \begin{Bmatrix} v_{y_0} \\ w_{z_0} \\ v_{y_L} \\ w_{y_L} \end{Bmatrix}$ is the nodal velocity vector, and $\{F_{NP}\} = \begin{Bmatrix} F_{y_0} \\ M_{z_0} \\ F_{y_L} \\ M_{y_L} \end{Bmatrix}$ is the nodal force vector

Setting $v = v_{y_0}$ and $w = w_{z_0}$ at x=0; $v = v_{y_L}$ and $w = w_{z_L}$ at x = L, from these four conditions it can be collected as a matrix equation :

$$\begin{Bmatrix} v_{y_0} \\ w_{z_0} \\ v_{y_L} \\ w_{z_L} \end{Bmatrix} = \begin{bmatrix} 1 & 1 & 1 & 1 \\ -jk & jk & -k & k \\ e^{-jkL} & -e^{jkL} & e^{-kL} & e^{kL} \\ -jke^{-jkL} & jke^{jkL} & -ke^{-kL} & ke^{KL} \end{bmatrix} \begin{Bmatrix} v_+ \\ v_- \\ v_{-j} \\ v_j \end{Bmatrix} \qquad (4.9a)$$

or $\{v_{NP}\} = [A]\{v_{coeff}\}$ (4.9b)

where

$$\{v_{coeff}\} = \begin{Bmatrix} v_{+} \\ v_{-} \\ v_{-j} \\ v_{j} \end{Bmatrix}$$

$$[A] = \begin{bmatrix} 1 & 1 & 1 & 1 \\ -jk & jk & -k & k \\ e^{-jkL} & -e^{jkL} & e^{-kL} & e^{kL} \\ -jke^{-jkL} & jke^{jkL} & -ke^{-kL} & ke^{kL} \end{bmatrix}$$

then

$$\{v_{coeff}\} = [A]^{-1}\{v_{NP}\} \tag{4.10}$$

From equation (4.8b), (4.9b) and (4.10)

$$\{F_{Np}\} = [M_{ij}]^{-1}\{v_{NP}\} = [M_{ij}]^{-1}[A]\{v_{coeff}\}$$

or $$\{F_{NP}\} = [\beta]\{v_{coeff}\} \tag{4.11}$$

Where $$[\beta] = [M_{ij}]^{-1}[A]$$

or $$[M_{ij}] = [A][\beta]^{-1} \tag{4.12}$$

Using the relationships in equation (4.7) and setting $F_{y_0} = 1$, $M_{z_0} = 0$, $F_{y_L} = 0$ and $M_{z_L} = 0$ into equation (4.8a), B_{1j} can be derived.

Similarly, by setting $F_{y0} = 0$, $M_{zo} = 1$, $F_{yL} = 0$, $M_{z_L} = 0$; $F_{y_0} = 0$, $M_{z_0} = 0$, $F_{y_L} = 1$, $M_{z_L} = 0$; and $F_{y0} = 0$, $M_{zo} = 0$, $F_{yL} = 0$, $M_{z_L} = 1$ respectively, the transfer functions β_{2j}, β_{3j} and β_{4j} can be obtained. The complete relation between the nodal force vector and the velocity coefficient vector is listed in matrix form as:

$$\begin{Bmatrix} F_{y_0} \\ M_{z_0} \\ F_{y_L} \\ M_{z_L} \end{Bmatrix} = \begin{bmatrix} \frac{Bk^3}{\omega} & -\frac{Bk^3}{\omega} & -\frac{Bk^3}{j\omega} & \frac{Bk^3}{j\omega} \\ \frac{Bk^2}{j\omega} & \frac{Bk^2}{j\omega} & -\frac{Bk^2}{j\omega} & -\frac{Bk^2}{j\omega} \\ \frac{Bk^3 e^{-jkL}}{\omega} & -\frac{Bk^3 e^{-jkL}}{\omega} & -\frac{Bk^3 e^{-kL}}{j\omega} & \frac{Bk^3 e^{xL}}{j\omega} \\ \frac{Bk^2 e^{-jkL}}{j\omega} & \frac{Bk^2 e^{-jkL}}{j\omega} & -\frac{Bk^2 e^{-kL}}{j\omega} & -\frac{Bk^2 e^{-xL}}{j\omega} \end{bmatrix} \begin{Bmatrix} v_+ \\ v_- \\ v_{-j} \\ v_j \end{Bmatrix} \tag{4.13}$$

From equation (4.12), the final form of $[M_{ij}]$ can be derived as:

$$[M_{ij}] = \frac{j\omega}{Bk^2} \begin{bmatrix} 1 & 1 & 1 & 1 \\ -jk & jk & -k & k \\ e^{-jkL} & -e^{jkL} & e^{-kL} & e^{kL} \\ -jke^{-jkL} & jke^{jkL} & -ke^{-kL} & ke^{KL} \end{bmatrix} \begin{bmatrix} jk & -jk & -k & k \\ 1 & 1 & -1 & 1 \\ jke^{-jkL} & -jke^{jkL} & e^{-kL} & e^{kL} \\ e^{-jkL} & e^{jkL} & -e^{-kL} & -e^{kL} \end{bmatrix} \tag{4.14}$$

This forms the mobility matrix of a beam element of finite length for pure bending wave propagation.

4.1.2 Longitudinal Stress Wave in a Finite Beam

If two straight beams are joined at right angles, the bending waves propagating in one beam may be partly changed to the longitudinal waves in another beam. Thus, in a grillage structure, the longitudinal wave and torsional wave are capable of coupling with the bending wave in the beam elements joined at right angle. For the longitudinal stress wave propagation in a finie beam, the governing equation of propagating velocity v_x can be expressed as (Cremer et al, 1988):

$$E\frac{\partial^2 v_x}{\partial x^2} = \rho\frac{\partial^2 v_x}{\partial t^2} \tag{4.15}$$

If the longitudinal wave velocity has the form of harmonic function of time, then the solution of equation (4.15) can be express as:

$$v_x(x) = v_+ e^{-jkx} + v_- e^{jkx} \tag{4.16}$$

where

k= the longitudinal wave number $= \frac{2\pi}{\lambda_L} = \frac{\omega}{C_L} = \omega(E/\rho)^{-1/2}$ (4.17)

and the coordinate system, the longitudinal nodal forces and velocities of a finite beam element are shown in Figure 4.2

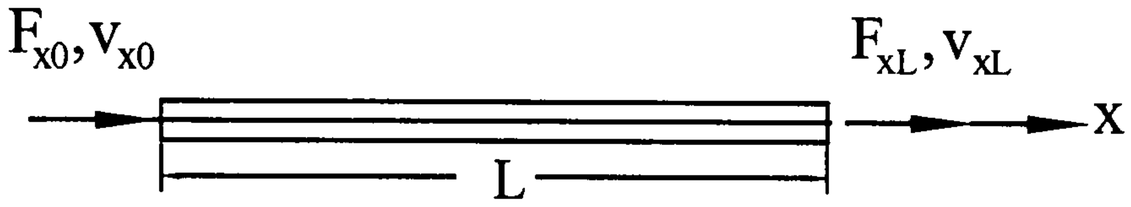

Figure 4.2 Longitudinal nodal force and velocity of bar element

In equation (4.16), the representation has considered the wave field on a rod to be composed of forward and backward propagating waves, where v_+ and v_- are unknown for the present.

Taking into account the relations of nodal velocities,

$$\begin{Bmatrix} v_{x0} \\ v_{xL} \end{Bmatrix} = \begin{bmatrix} 1 & 1 \\ e^{-j\kappa L} & e^{j\kappa L} \end{bmatrix} \begin{Bmatrix} v_+ \\ v_- \end{Bmatrix} \tag{4.18a}$$

or

$$\{ v_{NP} \} = [A] \{ v_{coeff} \} \tag{4.18b}$$

Define the mobility matrix $[M_{ij}]$, which relates to the longitudinal wave propagation in a finite rod as :

$$\begin{Bmatrix} v_{x0} \\ v_{xL} \end{Bmatrix} = \begin{bmatrix} M_{11} & M_{12} \\ M_{21} & M_{22} \end{bmatrix} \begin{Bmatrix} F_{x0} \\ F_{xL} \end{Bmatrix} \tag{4.19a}$$

$$\{ v_{NP} \} = [M_{ij}] \{ F_{NP} \} \tag{4.19b}$$

The corresponding force that acts in the beam is given by :

$$F(x) = Z\left(v_{+} e^{-j\kappa x} - v_{-} e^{j\kappa x}\right) \tag{4.20}$$

where Z is the driving point impedance at free end and

$$Z = C_L \rho S = \sqrt{E\rho}\, S \tag{4.21}$$

From equation (4.20)

$$F_{x0} = Z\left(v_{+} - v_{-}\right) \tag{4.22a}$$

$$F_{xL} = Z\left(v_{+} e^{-j\kappa L} - v_{-} e^{j\kappa L}\right) \tag{4.22b}$$

Express equations (4.22a) (4.22b) in matrix form, it becomes

$$\begin{Bmatrix} F_{x0} \\ F_{xL} \end{Bmatrix} = \begin{bmatrix} Z & -Z \\ Ze^{-j\kappa L} & -Ze^{j\kappa L} \end{bmatrix} \begin{Bmatrix} v_{+} \\ v_{-} \end{Bmatrix} \tag{4.23}$$

or

$$\{ F_{NP} \} = [\beta] \{ v_{coeff} \} = [\beta][A]^{-1} \{ v_{NP} \} \tag{4.24}$$

Compare equation (4.19b) and (4.24), the mobility matrix regarding to the longitudinal wave propagation in a finite beam can be obtained as:

$$[M_{ij}] = [A][\beta]^{-1} = \begin{bmatrix} 1 & 1 \\ e^{-j\kappa L} & e^{j\kappa L} \end{bmatrix} \begin{bmatrix} Z & -Z \\ Ze^{-j\kappa L} & -Ze^{j\kappa L} \end{bmatrix}^{-1} \tag{4.25}$$

4.1.3 Torsional wave in a Finite Beam

The torsional wave equation of a rectangular bar can be expressed by (Cremer et al,1988):

$$T \frac{\partial^2 w_x}{\partial x^2} = \vartheta' \frac{\partial^2 w_x}{\partial t^2} \tag{4.26}$$

where w_x is the angular velocity about the x-axis, ϑ' represents the mass moment of inertia per unit length of the bar, T is the torsional rigidity. For a rectangular bar of height h and width b,

$$\vartheta' = \frac{1}{12}\rho(bh^3 + hb^3) = \frac{1}{12}\rho S^2(\frac{h}{b} + \frac{b}{h}) \tag{4.27}$$

$$T = G\kappa b^3 h \tag{4.28}$$

where G is the shear modulus. κ is a factor depending on the aspect ratio h/b, as shown in Table 4.1 from theory of elasticity.

Table 4.1 κ value of rectangles with various ratios of h/b

h/b	1.0	1.5	2.0	2.5	3.0	5.0	6.0	10	∞
κ	0.141	0.196	0.229	0.249	0.263	0.291	0.298	0.312	0.333

Analogous to equation (4.15), the solution of equation (4.26) can be obtained by:

$$w_x = w_+ e^{-j\kappa x} + w_- e^{j\kappa x} \tag{4.29}$$

where

$$\kappa = \frac{2\pi}{\lambda} = \frac{\omega}{C_T} = \omega\left[\frac{12\kappa GSb}{\rho(h^2 + b^2)h}\right]^{-\frac{1}{2}} \tag{4.30}$$

$$C_T = (\frac{T}{\vartheta'})^{1/2} = (\frac{12\kappa GSb}{\rho(h^2 + b^2)h})^{1/2} \tag{4.31}$$

By the similar procedure, the mobility matrix for the torsional wave propagation in a finite bar is derived by:

$$[M_{ij}] = \begin{bmatrix} 1 & 1 \\ e^{-j\kappa L} & e^{j\kappa L} \end{bmatrix} \begin{bmatrix} Z & -Z \\ Ze^{-j\kappa L} & -Ze^{j\kappa L} \end{bmatrix}^{-1} \tag{4.32}$$

where

$$Z = \vartheta' C_T \tag{4.33}$$

4.2 Wave Propagation in a Finite Rectangular Plate

4.2.1 Two Dimension Elastic Bending Wave in a Finite Rectangular Plate

The two dimensional bending wave equation of a finite thin plate is (Cremer et al, 1988):

$$\Delta\Delta\eta - \kappa^4\eta = 0 \tag{4.34a}$$

or

$$\Delta\Delta v - \kappa^4 v = 0 \tag{4.34b}$$

where Δ is the Laplace operator, η and v are the lateral displacement and velocity of the plate particle in z direction respectively.

$\Delta = (\frac{\partial^2}{\partial x^2} + \frac{\partial^2}{\partial y^2})$: Laplace operator

$\kappa^4 = \omega^2 m'' / B'$: wave number

$m'' = \rho h$: mass per unit area of plate (kg/m^2)

ρ : density of plate

h : plate thickness (m)

$B' = \frac{Eh^3}{12(1-\mu^2)}$: bending rigidity of plate ($N\text{-}m^2$)

For deriving the mobility function of a plate in a bending wave, it consists of solving the

differential equation (4.34a), subject to the following boundary condition:

1. There is no rotation of the plate particle at the site of excitation about x and y axes, in other words, this implies that the vibration is small and the first derivatives of the particle displacement with respect to x and y are equal to zero.

2. The excitation force is equal to the sum of the shear force Q_r in the plate around the excitation site.

3. Far away from the excitation point, a decayed wave field occurs.

4. The displacements must be axially symmetric.

Equation (4.34a) may then be replaced by two differential equations of second order, namely

$$\Delta\eta + \kappa^2\eta = 0 \tag{4.35a}$$

$$\Delta\eta - \kappa^2\eta = 0 \tag{4.35b}$$

Equation (4.35a) may be recognized as the usual wave equation for nondispersive media (e.q., for sound wave in air); its axially symmetric solution in two dimensions, as is well known, consists of zero-order cylindrical functions. If one takes account of the boundary condition (3), one finds that Hankel function of the second kind is the only type of these functions that can serve as a solution. Thus,

$$\eta_1 = C_1 H_0^{(2)}(\kappa r) \tag{4.36}$$

where r represents the distance from the excitation point. For the remainder of the discussion, one may use the asymptotic expression for the Hankel function,

$$H_0^{(2)}(\kappa r) \approx -\frac{2j}{\pi}\ln\frac{\kappa r}{2} \quad , \quad \text{for} \left|\kappa r\right| << 1 \tag{4.37a}$$

$$H_0^{(2)}(\kappa r) \approx \sqrt{\frac{2}{\pi\kappa r}} e^{-j(\kappa r - \pi/4)} \quad , \quad \text{for} \ \left|\kappa r\right| >> 1 \tag{4.37b}$$

instead of a more exact representation. Detail derivations of equations (4.37a) and (4.37b) are shown in Appendix A.

The solution of equation (4.35b) that satisfies the previously mentioned boundary conditions simply by replacing κr in equation (4.36) by $-j\kappa r$, thus,

$$\eta_2 = C_2 H_0^{(2)}(-j\kappa r) \tag{4.38}$$

Using equation (4.37b) for large values of κr, one finds

$$H_0^{(2)}(-j\kappa r) \approx \sqrt{\frac{2}{-j\pi\kappa r}} e^{j\pi/4} e^{-\kappa r} \tag{4.39}$$

Thus equation (4.38) represents a near exponentially decay field.

The general solution, obtained by combining equations (4.36) and (4.38), may be expressed as:

$$\eta = C_1 H_0^{(2)}(\kappa r) + C_2 H_0^{(2)}(-j\kappa r) \tag{4.40}$$

The boundary condition (1) requires that

$$\frac{\partial \eta}{\partial r} = C_1 \kappa \left[-\frac{2j}{\pi\kappa r} + \cdots \right] - jC_2 \kappa \left[\frac{2}{\pi\kappa r} + \cdots \right] = \frac{2j}{\pi r}(-C_1 - C_2) + \cdots = 0$$

Because the terms in κr and in higher power of κr reduce to zero at $r \to 0$, only the first term remains for consideration. Hence

$$C_1 = -C_2$$

Thus

$$\eta = C_1 \left[H_0^{(2)}(\kappa r) - H_0^{(2)}(-j\kappa r) \right] \tag{4.41}$$

The value of equation (4.41) at $r = 0$ again may be found from the asymptotic expansion of the Hankel functions:

$$\eta(0) = \eta_0 = C_1\left[-\frac{2j}{\pi}\ln\frac{\kappa r}{2} + \cdots + \frac{2j}{\pi}(\ln\frac{\kappa r}{2} + \ln(-j) + \cdots\right]$$

$$= C_1\frac{2j}{\pi}\ln(-j) = C_1$$

The constant C_1 here is equal to the displacement amplitude at the excitation point, thus

$$\eta = \eta_0\left[H_0^{(2)}(\kappa r) - H_0^{(2)}(-j\kappa r)\right] = \eta_0\Pi(\kappa r) \tag{4.42}$$

where the propagation function $\Pi(\kappa r)$ is defined by:

$$\Pi(\kappa r) = H_0^{(2)}(\kappa r) - H_0^{(2)}(-j\kappa r) \tag{4.43}$$

The remaining unknown η_0 may be related to the exciting force on the basis of boundary condition (2). For this purpose, one may consider the excitation point to be at the center of a small circle of radius r_0, and one may take the external exciting force F_0 to act on the area enclosed by that circle. Let the shear force that acts on the circumference of this circle, per unit length, be represented by Q_r. From mechanics of elasticity

$$Q_r = B'\frac{\partial\Delta\eta}{\partial r} \tag{4.44}$$

Substituting equation (4.42) into equation (4.44), it becomes

$$Q_r = -B'\kappa^3\eta_0\left[\frac{dH_0^{(2)}(\kappa r)}{d(\kappa r)} + \frac{dH_0^{(2)}(-j\kappa r)}{d(\kappa r)}\right]$$

For $\kappa r = \kappa r_0$ and by using of the small-argument expansion of the Hankel functions, then

$$Q_{r_0} = Q_r\Big|_{r=r_0} = \frac{4jB'\kappa^2}{\pi r_0}\eta_0 \tag{4.45}$$

Thus

$$F_0 = 2\pi r_0 Q_{r_0} = 8jB'\kappa^2\eta_0 \tag{4.46}$$

The work of Cremer et al (1988) stopped here. The following derivation extends the Cremers' work to an innovative numerical model to cope with the analysis of structure-

borne noise propagation. If F_0 is applied to one corner of a rectangular plate, then F_0 can be considered as applied in a quarter of a small circle of radius r_0 and with center at the corner. In this case,

$$F_0 = 2jB'\kappa^2\eta_0 \tag{4.47}$$

Now, equation (4.42) becomes:

$$\eta = \frac{F_0}{2jB'\kappa^2}\left[H_0^{(2)}(\kappa r) - H_0^{(2)}(-j\kappa r)\right] \tag{4.48}$$

Considering that $v_0 = j\omega\eta_0$, the driving point force impedance Z_{F_0} at one corner of a rectangular plate regarding to the bending wave propagation is :

$$Z_{F_0} = \frac{F_0}{\hat{v}_0} = \frac{2B'k^2}{\omega} = \frac{2\omega m''}{k^2} \tag{4.49}$$

Thus the lateral velocity distribution of the plate particle is:

$$v(x,y) = \frac{F_0\omega}{2B'k^2}[H_0^{(2)}(kr) - H_0^{(2)}(-jkr)] = \frac{F_0}{Z_{F_0}}\Pi(kr) \tag{4.50}$$

The rotational speed w_x and w_y about x and y axis can be expressed as :

$$w_x(x,y) = \frac{\partial v}{\partial x} = \frac{\partial v}{\partial r}\cdot\frac{\partial r}{\partial x} = \frac{F_0\omega}{2B'\kappa^2}\left[\frac{\partial H_0^{(2)}(\kappa r)}{\partial r} - \frac{\partial H_0^{(2)}(-j\kappa r)}{\partial r}\right]\cdot\frac{x}{r} \tag{4.51}$$

$$w_y(x,y) = \frac{\partial v}{\partial y} = \frac{\partial v}{\partial r}\cdot\frac{\partial r}{\partial y} = \frac{F_0\omega}{2B'\kappa^2}\left[\frac{\partial H_0^{(2)}(\kappa r)}{\partial r} - \frac{\partial H_0^{(2)}(-j\kappa r)}{\partial r}\right]\cdot\frac{y}{r} \tag{4.52}$$

For a finite rectangular plate element, as shown in Figure 4.3 with nodal force vector $< F_{z1}\cdots F_{z4}\ M_{x1}\cdots M_{x4}\ M_{y1}\cdots M_{y4} >^T$ and nodal velocity vector $< v_{z1}\cdots v_{z4}\ w_{x1}\cdots w_{x4}\ w_{y1}\cdots w_{y4} >$, the transfer relationships between the nodal parameters can be related by:

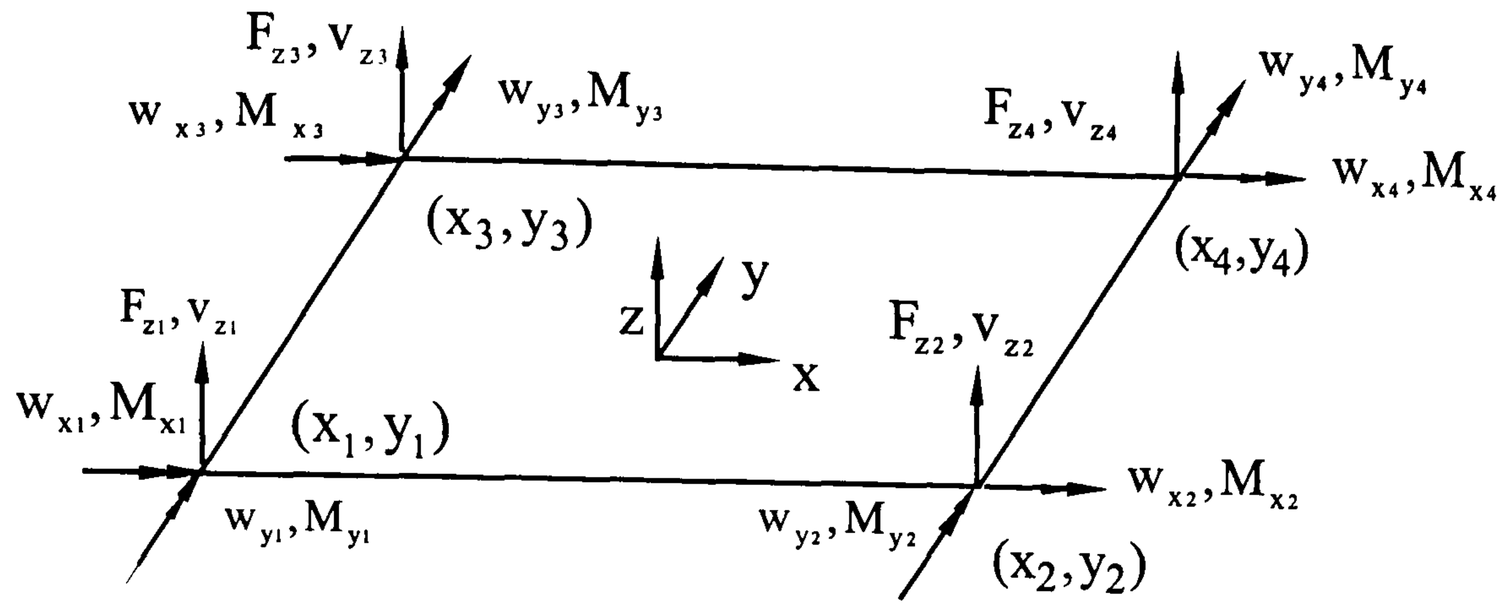

Figure 4.3 State nodal parameters of the bending wave pattern in a rectangular plate element

$$\begin{Bmatrix} v_{z1} \\ \vdots \\ v_{z4} \\ w_{x1} \\ \vdots \\ w_{x4} \\ w_{y1} \\ \vdots \\ w_{y4} \end{Bmatrix} = \begin{bmatrix} M_{1,1} & \cdots & M_{1,4} & M_{1,5} & \cdots & M_{1,8} & M_{1,9} & \cdots & M_{1,12} \\ \vdots & & \vdots & \vdots & & \vdots & \vdots & & \vdots \\ M_{4,1} & \cdots & M_{4,4} & M_{4,5} & \cdots & M_{4,8} & M_{4,9} & \cdots & M_{4,12} \\ M_{5,1} & \cdots & M_{5,4} & M_{5,5} & \cdots & M_{5,8} & M_{5,9} & \cdots & M_{5,12} \\ \vdots & & \vdots & \vdots & & \vdots & \vdots & & \vdots \\ M_{8,1} & \cdots & M_{8,4} & M_{8,5} & \cdots & M_{8,8} & M_{8,9} & \cdots & M_{8,12} \\ M_{9,1} & \cdots & M_{9,4} & M_{9,5} & \cdots & M_{9,8} & M_{9,9} & \cdots & M_{9,12} \\ \vdots & & \vdots & \vdots & & \vdots & \vdots & & \vdots \\ M_{12,1} & \cdots & M_{12,4} & M_{12,5} & \cdots & M_{12,8} & M_{12,9} & \cdots & M_{12,12} \end{bmatrix} \begin{Bmatrix} F_{z1} \\ \vdots \\ F_{z4} \\ M_{x1} \\ \vdots \\ M_{x4} \\ M_{y1} \\ \vdots \\ M_{y4} \end{Bmatrix} \tag{4.53}$$

By use of equations (4.50) , (4.51) and (4.52) and successively setting one nodal force $F_0 = 1$ and all the other nodal forces and moments equal to zero, then M_{ij} (i=1,2,3,4 and j=1,2,…,12) can be obtained by equation (4.53).

For an excitation moment M_0 applied to one given corner, the moment can be replaced by a set of two coupling forces with a small distance 2a apart each other as shown in Figure 4.4.

$$M_0 = 2aF \tag{4.54}$$

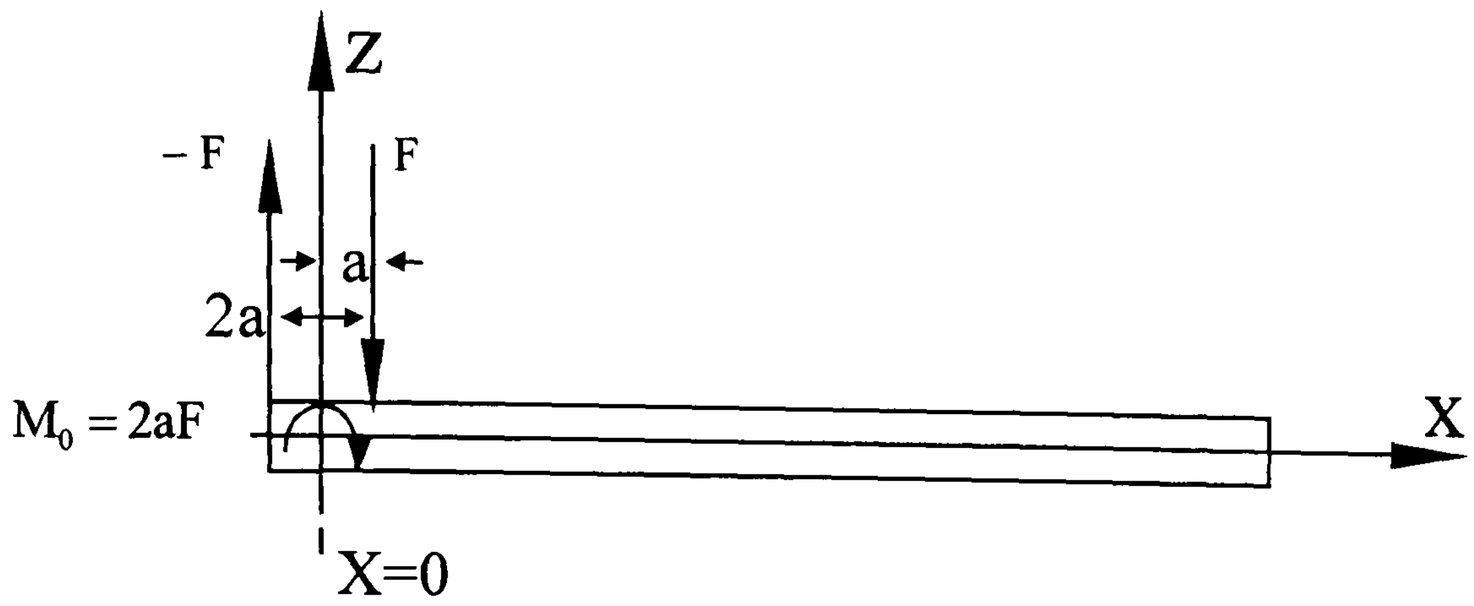

Figure 4.4 Moment excitation at a corner of a rectangular plate

From equation (4.50), it can be seen by superposition principle that the lateral velocity of the plate particle is :

$$v_z(x,y) = \frac{F\omega}{2B'\kappa^2}[\Pi(\kappa r_1) - \Pi(\kappa r_2)] \tag{4.55}$$

where r_1 , r_2 are the distances from the excitation point x = a and x = -a to any point (x,y in the plate respectively.

For the points along x axis, there are:

$$\begin{cases} \Pi(kr_1) = H_0^{(2)}[k(x-a)] - H_0^{(2)}[-jk(x-a)] \\ \Pi(kr_2) = H_0^{(2)}[k(x+a)] - H_0^{(2)}[-jk(x+a)] \end{cases} \tag{4.56}$$

Expanding the Hankel functions with respect to the small quantity of k(x-a) or k(x+a), then

$$\begin{cases} \Pi(kr_1) \approx 1 + 2k^2(y-a)^2\left[\alpha_1 + \alpha_2 \ln\frac{\gamma\, k(y-a)}{2} - \frac{1}{2}\alpha_2 \ln(-j)\right] \\ \Pi(kr_2) \approx 1 + 2k^2(y+a)^2\left[\alpha_1 + \alpha_2 \ln\frac{\gamma\, k(y+a)}{2} - \frac{1}{2}\alpha_2 \ln(-j)\right] \end{cases}$$

where $\alpha_1 = -\frac{1}{4} - \frac{j}{2\pi}$, $\alpha_2 = \frac{j}{2\pi}$, $\gamma = 1.781$.

Thus, for $a \to 0$, the angular velocity at the excitation corner can be obtained from equation (4.55) as:

$$w_y(0) = \left.\frac{\partial v_z}{\partial x}\right|_{a\to 0} = \frac{Fa\omega k^2}{2B'k^2}\left(1 - \frac{4j}{\pi}\ln\frac{\gamma ka}{2}\right) = \frac{M_0\omega}{4B'}\left(1 - \frac{4j}{\pi}\ln\frac{\gamma ka}{2}\right) \tag{4.57}$$

Using equation (4.55) and the relations $w_x = \partial v_z / \partial y$, $w_y = \partial v_z / \partial x$; successively setting $M_0 = 1$ at each node and substituting them by the coordinates of nodal points, then M_{ij}, ($i = 5,6,7,8$; $j = 1,2,\ldots,12$), in equation (4.53) can be obtained.

A similar procedure can be followed to derived the transfer mobility function M_{ij},($i = 9,\ldots,12$; $j = 1,2,\ldots,12$), in equation (4.53) along y axis. Thus a full mobility matrix of a finite rectangular plate element in bending wave is derived as show in Table A.1 of Appendix A.

4.2.2 Longitudinal Wave in a Rectangular Plate

Analogous to the longitudinal wave pattern in a finite rod, the longitudinal wave patterns in both x and y directions of a rectangular plate can be expressed as:

$$v_x(x,y) = v_{x+}e^{-jkx} + v_{x-}e^{jkx}$$

$$v_y(x,y) = v_{y+}e^{-jky} + v_{y-}e^{jky}$$

The transfer matrix between the nodal parameters, which includes the nodal forces and nodal velocities as shown in Figure 4.5, can be followed by:

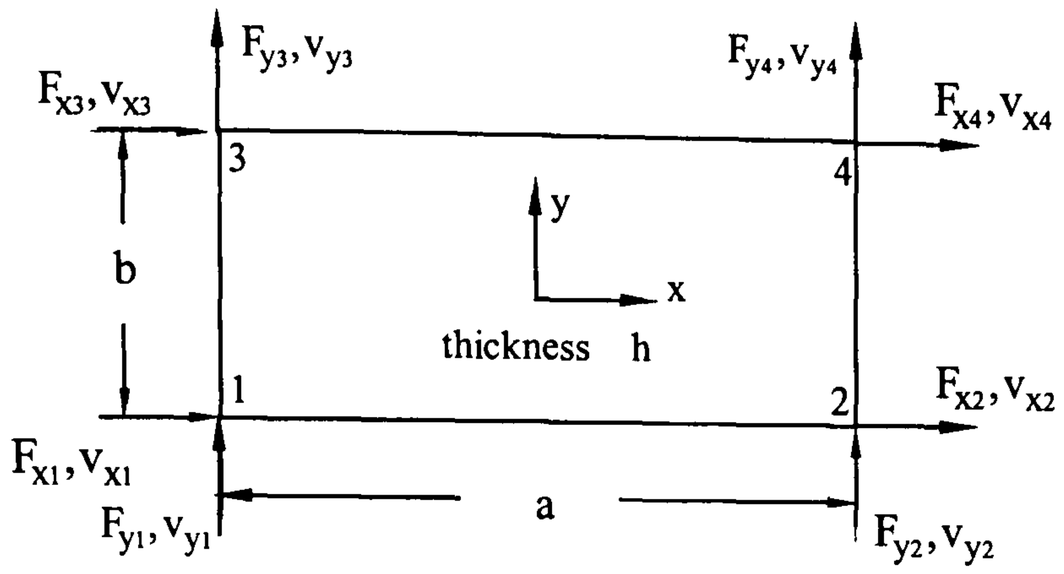

Figure 4.5 State nodal parameters of the longitudinal wave pattern in a rectangular plate element

$$\begin{Bmatrix} v_{x1} \\ v_{x2} \\ v_{x3} \\ v_{x4} \\ v_{x5} \\ v_{x6} \\ v_{x7} \\ v_{x8} \end{Bmatrix} = \begin{bmatrix} M_{11} & M_{12} & M_{13} & M_{14} & M_{15} & M_{16} & M_{17} & M_{18} \\ M_{21} & M_{22} & M_{23} & M_{24} & M_{25} & M_{26} & M_{27} & M_{28} \\ M_{31} & M_{32} & M_{33} & M_{34} & M_{35} & M_{36} & M_{37} & M_{38} \\ M_{41} & M_{42} & M_{43} & M_{44} & M_{45} & M_{46} & M_{47} & M_{48} \\ M_{51} & M_{52} & M_{53} & M_{54} & M_{55} & M_{56} & M_{57} & M_{58} \\ M_{61} & M_{62} & M_{63} & M_{64} & M_{65} & M_{66} & M_{67} & M_{68} \\ M_{71} & M_{72} & M_{73} & M_{74} & M_{75} & M_{76} & M_{77} & M_{78} \\ M_{81} & M_{82} & M_{83} & M_{84} & M_{85} & M_{86} & M_{87} & M_{88} \end{bmatrix} \begin{Bmatrix} F_{x1} \\ F_{x2} \\ F_{x3} \\ F_{x4} \\ F_{x5} \\ F_{x6} \\ F_{x7} \\ F_{x8} \end{Bmatrix} \tag{4.58}$$

where

$$\begin{bmatrix} M_{11} & M_{12} \\ M_{21} & M_{22} \end{bmatrix} = \begin{bmatrix} M_{33} & M_{34} \\ M_{43} & M_{44} \end{bmatrix} = Z_1^{-1} \begin{bmatrix} 1 & 1 \\ e^{-jka} & e^{jka} \end{bmatrix} \begin{bmatrix} 1 & -1 \\ e^{-jka} & -e^{jka} \end{bmatrix}^{-1} \tag{4.58a}$$

$$\begin{bmatrix} M_{55} & M_{57} \\ M_{75} & M_{77} \end{bmatrix} = \begin{bmatrix} M_{66} & M_{68} \\ M_{86} & M_{88} \end{bmatrix} = Z_2^{-1} \begin{bmatrix} 1 & 1 \\ e^{-jkb} & e^{jkb} \end{bmatrix} \begin{bmatrix} 1 & -1 \\ e^{-jkb} & -e^{jkb} \end{bmatrix}^{-1} \tag{4.58b}$$

$M_{ij} = 0$ for all the elements not mentioned in equations (4.58a) and (4.58b). where

$$k = \frac{\omega}{\sqrt{D/\rho}} \quad , \quad D = \frac{E}{1-\mu^2} \quad , \quad Z_1 = \frac{1}{2}\sqrt{D\rho}\, bh \quad , \quad Z_2 = \frac{1}{2}\sqrt{D\rho}\, ah$$

4.3 Modelling Noise Propagation in a Ship Structure

4.3.1 Fluid-Structure Interaction

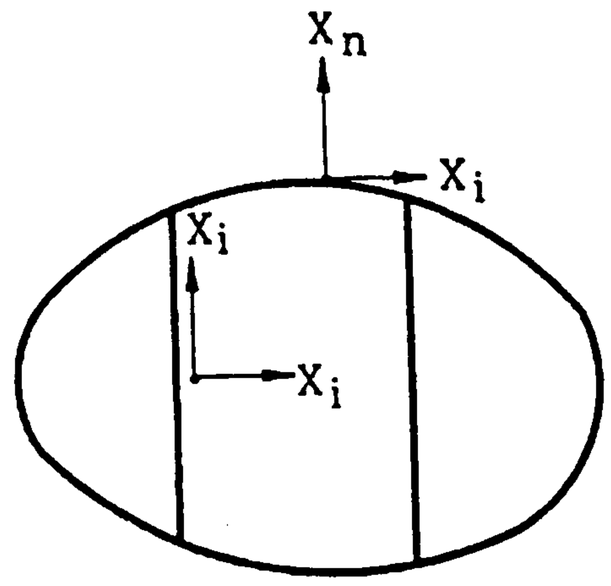

Figure 4.6 Definition of $\{x_n\}$ and $\{x_i\}$

When a ship is floating in water and subjected to machine induced vibrating forces $\{f\}$, then the equations of motion of the ship structure can be expressed in matrix form as:

$$[M]\{\ddot{x}\}+[C]\{\dot{x}\}+[K]\{x\}=\{f\}-\{p\} \tag{4.59}$$

where [M],[C] and [K] represent the mass, damping and stiffness matrices respectively. $\{f\}$ is the acoustic loading transmitted from the machine mountings which is obtained by the mobility theory and charaterising the vibrational sources as velocity sources. While $\{p\}$ represents the hydrodynamic pressure which can be only applied to the surfaces of the structure in contact with the water and shall be analysed by the coupling algorithm which is a combination of finite element (FE) and boundary element (BE) methods.

If the internal structural damping effect can be neglected and the displacement vector $\{x\}$ of the structure is divided into $\{x_n\}$, ie, the normal displacment of the surface contacted with the ambient water, and $\{x_i\}$, ie, the displacement of the interior structure as well as the tangential displacement on the water contacting surface as shown in Figure 4.6, then equation (4.59) becomes :

$$\begin{bmatrix} M_{nn} & M_{ni} \\ M_{in} & M_{ii} \end{bmatrix} \begin{Bmatrix} \ddot{x}_n \\ \ddot{x}_i \end{Bmatrix} + \begin{bmatrix} K_{nn} & K_{ni} \\ K_{in} & K_{ii} \end{bmatrix} \begin{Bmatrix} x_n \\ x_i \end{Bmatrix} = \begin{Bmatrix} f_n \\ f_i \end{Bmatrix} - \begin{Bmatrix} p \\ 0 \end{Bmatrix} \tag{4.60}$$

4.3.2 Coupling of the FE and BE Methods

Consider a linear structure system and put $\{x\} = \{X\}\, e^{i\omega t}$ into equation (4.60) then,

$$\begin{bmatrix} K_{nn} & K_{ni} \\ K_{in} & K_{ii} \end{bmatrix} \begin{Bmatrix} X_n \\ X_i \end{Bmatrix} - \omega^2 \begin{bmatrix} M_{nn} & M_{ni} \\ M_{in} & M_{ii} \end{bmatrix} \begin{Bmatrix} X_n \\ X_i \end{Bmatrix} = \begin{Bmatrix} f_n \\ f_i \end{Bmatrix} - \begin{Bmatrix} p \\ 0_i \end{Bmatrix} \tag{4.61}$$

The second equation in (4.61) is:

$$([K_{in}] - \omega^2 [M_{in}])\{X_n\} + ([K_{ii}] - \omega^2 [M_{ii}])\{X_i\} = \{f_i\} \tag{4.62}$$

and $\{X_i\}$ can be expressed in terms of $\{X_n\}$ from equation (4.62) as :

$$\{X_i\} = ([K_{ii}] - \omega^2 [M_{ii}])^{-1} (\{f_i\} - ([K_{in}] - \omega^2 [M_{in}])\{X_n\}) \tag{4.63}$$

Substituting (4.63) into the first row column expansion of equation (4.61),

$$([K_{nn}] - \omega^2 [M_{nn}])\{X_n\} + ([K_{ni}] - \omega^2 [M_{ni}])\{X_i\} = \{f_n\} - \{p\}$$

or

$$(([K_{nn}] - \omega^2 [M_{nn}]) - ([K_{ni}] - \omega^2 [M_{ni}])([K_{ii}] - \omega^2 [M_{ii}])^{-1} ([K_{in}] - \omega^2 [M_{in}]))\{X_n\}$$

$$= -([K_{ni}] - \omega^2 [M_{ni}])([K_{ii}] - \omega^2 [M_{ii}])^{-1} \{f_i\} + \{f_n\} - \{p\} \tag{4.64}$$

Since the underwater acoustic pressure distribution radiated from a vibrating hull surface is governed by the Helmhotz equation:

$$\nabla^2 p(\vec{r},\omega) + k^2 p(\vec{r},\omega) = 0 \tag{4.65}$$

and $p(\vec{r})$ can be expressed as in Appendix B :

$$P(\vec{r}) = \frac{1}{2\pi} \int_{S_s} [P(\vec{r}_s) \frac{\partial P(\vec{r})}{\partial n(\vec{r})} - G(\vec{r},\vec{r}_s) \frac{\partial P(\vec{r})}{\partial n(\vec{r})}] dS_s \tag{4.67}$$

where

$\vec{r}$ = position vector in water;

$\vec{r}_s$ = position vector on immersed hull surface;

$n(\vec{r}_s)$ = normal direction vector at $\vec{r}_s$;

S_s = immersed hull surface area;

$P(\vec{r})$ = underwater acoustic pressure amplitude at $\vec{r}$;

$G(\vec{r}, \vec{r}_s)$ = Green's function.

The relation between $P(\vec{r})$ and the normal displacement amplitude X_n on the hull surface must satisfy :

$$\frac{\partial P(\vec{r}_s)}{\partial n(\vec{r}_s)} = -i\rho_0 \omega v_n(\vec{r}_s) = \rho_0 \omega^2 X_n \tag{4.68}$$

Utilizing the discretization technique with interpolating shape functions to the water contacting hull surface, equation (4.68) becomes :

$$[A]\{P\} = [G]\{X_n\} \tag{4.69}$$

Substituting equation (4.69) into (4.64), the governing equation for the combined FE and BE methods for the structure-borne noise transmission problem inboard ships can show to be:

$$\left[([K_{nn}] - \omega^2[M_{nn}]) - ([K_{ni}] - \omega^2[M_{ni}])([K_{ii}] - \omega^2[M_{ii}])^{-1}([K_{in}] - \omega^2[M_{in}])\right]\{X_n\}$$

$$+[A]^{-1}[G]\{X_n\} = \{f_n\} - ([K_{ni}] - \omega^2[M_{ni}])([K_{ii}] - \omega^2[M_{ii}])^{-1}\{f_i\} \tag{4.70}$$

4.4 Flow Chart of the Computer Program

Based on the above mentioned formulation of mobility matrix regarding to the stress wave propagation in finite beam and rectangular plate elements,a computer program has been coded in Matlab software and FORTRAN language to analyse the structure-borne sound

propagation in a stiffened-plated structure. In principle , this program developed is somewhat analogous to the general existing finite element analysis program which created mainly for strength and vibration computations. The procedure is :

1. Assembly of element mobility matrix

Combining the mobility matrices of a beam for bending wave (equation (4.14)) , longitudinal wave (equation (4.25)) and torsional wave (equation (4.32)) and allocating each elements of H_{ij} to its corresponding position in the assembly mobility matrix with respect to the numbering of the degrees of freedom of the modal forces and nodal velocity , the complete mobility matrix of a beam element can be formed . Which has a dimension of 12×12 . Similarly , the complete mobility matrix of a rectangular plate element can then be obtained by combining the matrix in equation (4.53), as shown in Table A.1 of Appendix A for bending wave, and the matrix in equation (4.58) for longitudinal wave .

2. Transfer the element mobility matrix to the global mobility matrix

Since the derivation of element mobility matrices is referred to the local coordinate system (x,y,z) , which is depending on the orientation of the element . While the coordinates of the locations of nodal points are referred to the unified global coordinate system (X,Y,Z) . Thus the unit vectors , $\vec{n}_x$, $\vec{n}_y, \vec{n}_z$, along x,y,z –axis are given by :

$$\vec{n}_x = \frac{1}{|\vec{r}_{12}|}\vec{r}_{12} \tag{4.95a}$$

$$\vec{n}_y = \vec{n}_z \times \vec{n}_x \tag{4.95b}$$

$$\vec{n}_z = \frac{\vec{r}_{12} \times \vec{r}_{13}}{|\vec{r}_{12} \times \vec{r}_{13}|} \tag{4.95c}$$

where $\vec{r}_{ij}$ means the vector from nodal point i to nodal point j .

To calculate the direction cosines between the axes (x,y,z) and (X,Y,Z) , the rotation transformation matrix $[T]$ between these two coordinate system can be attained . Thus the global mobility matrix for one element , $[M_G^e]$, can be given by :

$$[M_G^e] = [T]^T [M^e] [T] \tag{4.60}$$

where $[H^e]$ is the assembly element mobility matrix .

3. Form integrated structural mobility matrix

Recurring the process of step 2 for each element in the order of the numbering of the elements . The whole structural mobility matrix $[M_G]$ can be attained .

4. Partition of $[M_G]$ and boundary conditions

For given kinematic boundary conditions at constrained supports and given source excitations the wave propagation equation , such as

$$\{v\} = [M_G]\{F\}$$

can be partitioned to the form as:

$$\begin{Bmatrix} v_k \\ v_u \end{Bmatrix} = \begin{bmatrix} M_{I\,I} & M_{I\,II} \\ M_{II\,I} & M_{II\,II} \end{bmatrix} \begin{Bmatrix} F_u \\ F_k \end{Bmatrix} \tag{4.61}$$

where $\{v_k\}$ and $\{F_k\}$ are the known velocities and forces , $\{v_u\}$ and $\{F_u\}$ are the unknown velocities and force excitations .

5. Solution

Expanding equation (4.61) the solution of the unknown nodal velocities and nodal forces can be expressed in terms of the given velocities and forces as :

$$\begin{Bmatrix} F_u \\ v_u \end{Bmatrix} = \begin{bmatrix} M_{II} - M_{III} M_{IIII} M_{III} & M_{III} M_{IIII}^{-1} \\ -M_{IIII}^{-1} M_{III} & M_{IIII}^{-1} \end{bmatrix}^{-1} \begin{Bmatrix} v_k \\ F_k \end{Bmatrix} \tag{4.62}$$

6. Backward transformation

The solved nodal velocities and nodal forces in global coordinate system should be transformed backward to the local coordinate system .

7. Power flow calculation

Detail of the calculation of the structure-borne sound power transmission in structure will be illustrated in the next section by example .

To follow this procedure, the FORTRAN program listed in Appendix E was written to perform the analysis of structure-borne sound propagation and Figure 4.7 illustrates a simplified flow chart of its development. This program allows the user to cope with the mobility distribution of a structure composed of rectangular plate elements and beam elements and is especially suitable for analysing structure-borne noise within the medium frequency range.

To validate the correctness of this program the comparison of the mobility spectra of simple structures obtained by experiment and conventional FEM solution are made. This will be discussed in the next section.

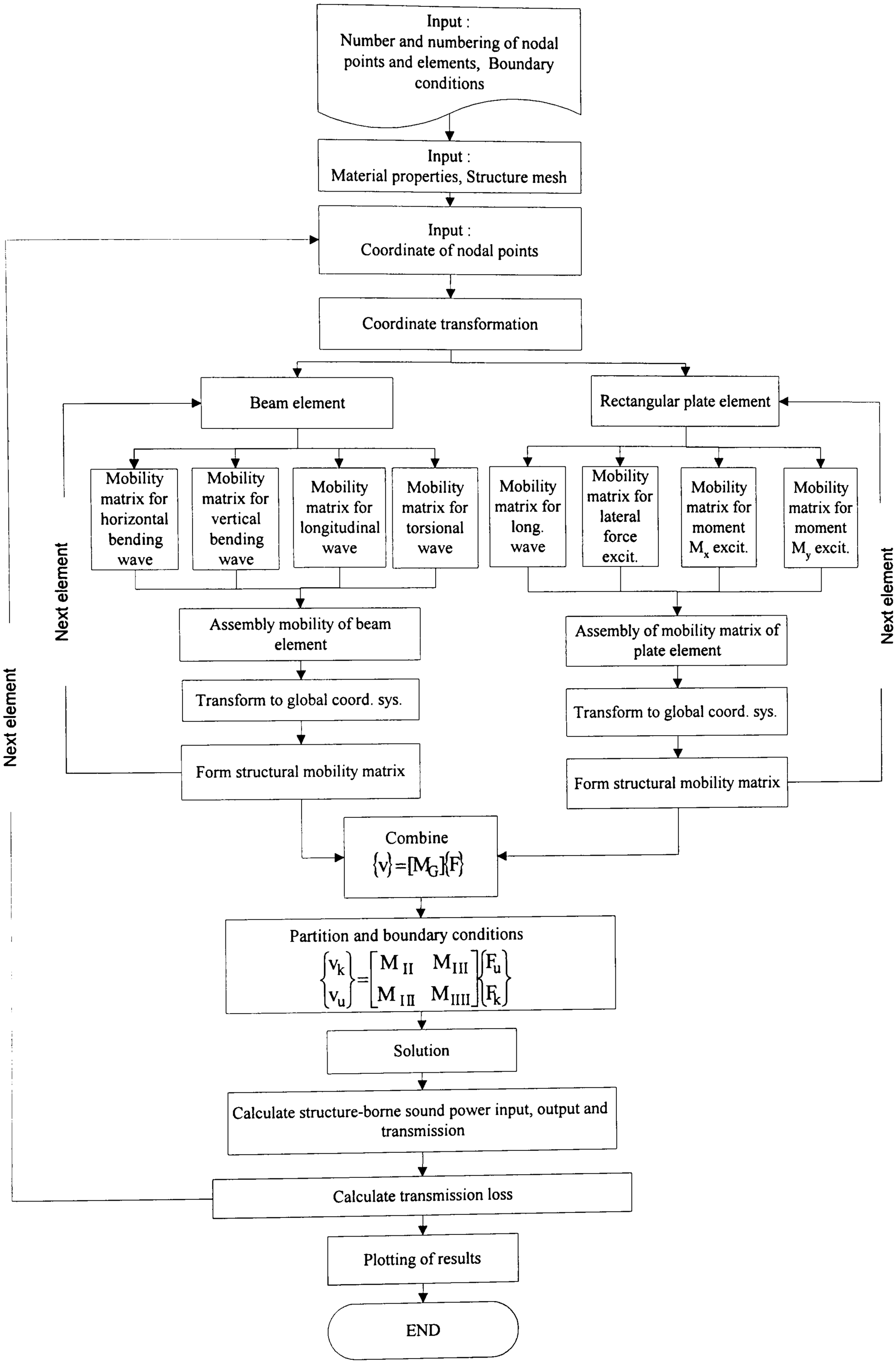

Figure 4.7 Flow chart of the program development for structure-borne sound propagation analysis

4.5 Validation of the Computer Code by Analysing the Structure-Borne Noise Propagation via Simple Structures

To validate the correctness of the developed software, the mobility analysis are carried out for simple structures such as a beam and a rectangular plate. Then compare the results to experiment measurements. Also the results are compared with that by FEM using the software ANSYS (De Salvo and Swanson,1983) for double check.

4.5.1 Validation of Mobility of a Free-Free Beam

Consider a pipe beam of length 1m and diameter 0.0156 m. The beam was bolted to the shaker at midspan, so it acted as a free-free beam. The input data of the beam for FE analysis are:

pipe thickness (t)	:	1.0E-3	m
pipe diameter (d)	:	15.6E-3	m
cross section area (A)	:	4.585E-5	m^2
moment of inertia (I)	:	1.227E-9	m^4
Young's modulus (E)	:	2.1E+11	N/m^2
density (ρ)	:	7850	kg/m^3
Poisson's ratio (μ)	:	0.3	
damping ratio (ξ)	:	0.001	
element length (L)	:	0.01	m
number of elements	:	100	

The beam was divided into 100 equal elements as shown in Figure 4.8. Each beam element has a length 1cm. The origin of the coordinates put on the left end of the beam. Since the beam was rigidly linked to the shaker at midspan, hence the driving point of the beam has only the vertical force applied and without any moment and torque existed for such symmetrical arrangement. In this case only the flexural bending modes can be excited.

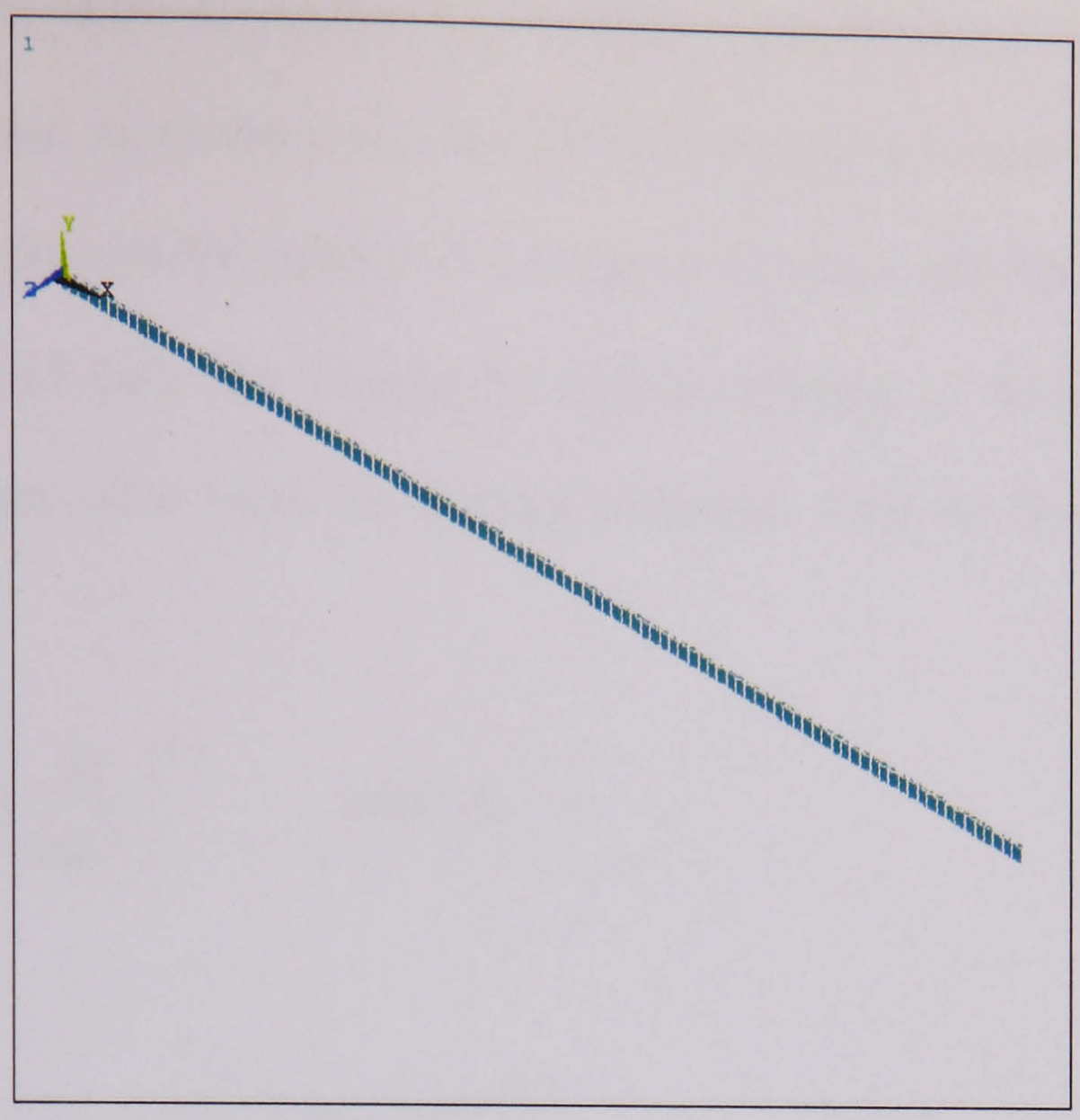

Figure 4.8 FE model of the pipe beam

In addition, experimental measurement of the mobitities at driving point and free end of the beam is conducted by utilizing the experiment instrument layout shown in Figure 4.9. In which an impedance head (B&K 8001) was put at A and an accelerometer (B&K 4374) put at B.

Pipe thickness	1.0E-3(m)	Material density	7850 (Kg/m_3)
Cross section area	4.585E-5 (m_2)	Poisson's ratio	0.3
Moment of inertia	1.227E-9 (m_4)	Damping ratio	0.001
Young's modulus	2.1E+11 (N/m_2)		

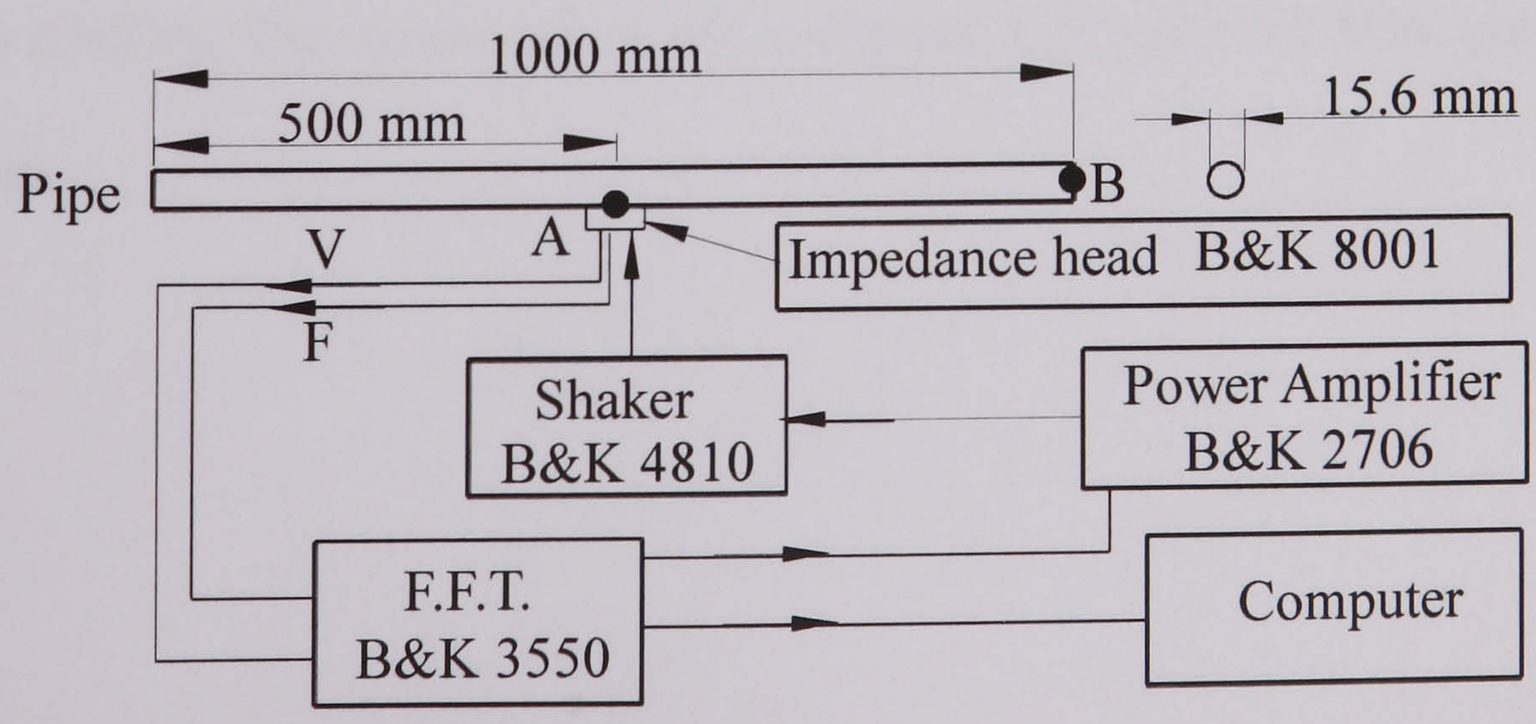

Figure 4.9 Experiment layout for the mobility measurement of the beam

The comparisons of the driving point mobility at A and the transfer mobility at B obtained by FE analysis and the measurement are shown in Figures 4.10 and 4.11 respectively. Good coincidence of the mobility spectra in the frequency below 800 Hz is displayed. To check the correctness of these two Figures by analytic solution of the model frequencies, the natural frequency of a beam in bending vibration, refer to Thomson (1993), can be expressed as:

$$\omega_n = C_n \left(\frac{EI}{mL^2} \right)^{1/2} \qquad \text{(rad / s)} \tag{4.63}$$

Here

$$\omega_n = C_n \left(\frac{2.1\times10^{11} \times 1.22\times10^{-9}}{7850 \times 4.585\times10^{5} \times 1} \right)^{1/2} = 26.68\, C_n$$

Where $C_n = 22.4, 121.0, 298.6, \cdots$ for symmitrical modes. Thus, the natural frequencies of the first two symmitrical modes are 597.6 and 3228.3 rad/sec respectively, i.e., 95.1 Hz and 513.8 Hz. These are coinciding with the peak frequencies shown in Figures 4.10 and 4.11.

Also, the same driving point and transfer mobilities are analyzed by using the developed stress wave model with two equal beam elements only, each of length 0.5m, and compare to that by ANSYS. The results are shown in Figures 4.12 and 4.13. Very good coincidence is obtained.

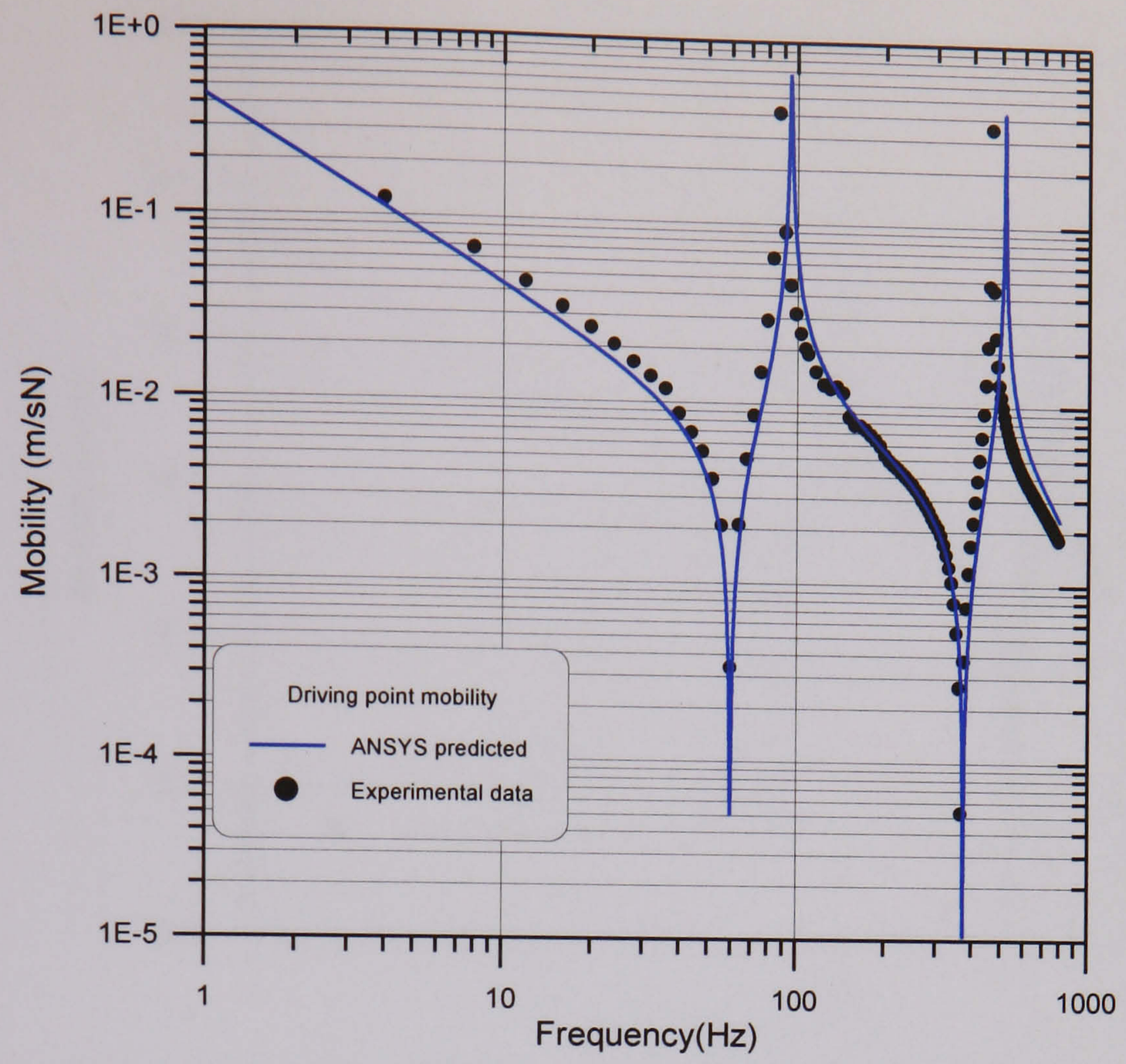

Figure 4.10 Comparison of the driving point mobility spectra of the beam by ANSYS and experiment.

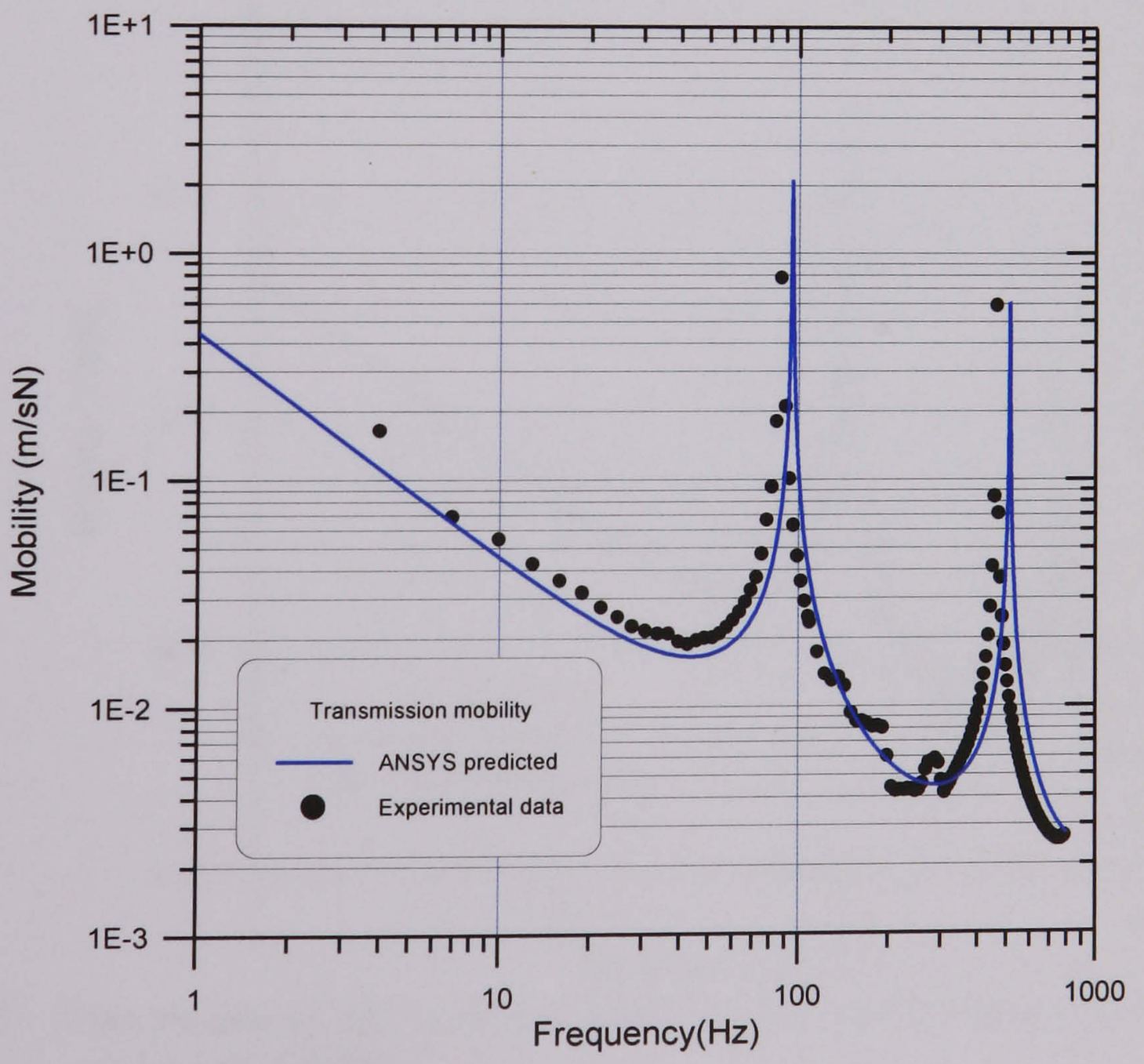

Figure 4.11 Comparison of the transfer mobility spectra of the beam by ANSYS and experiment

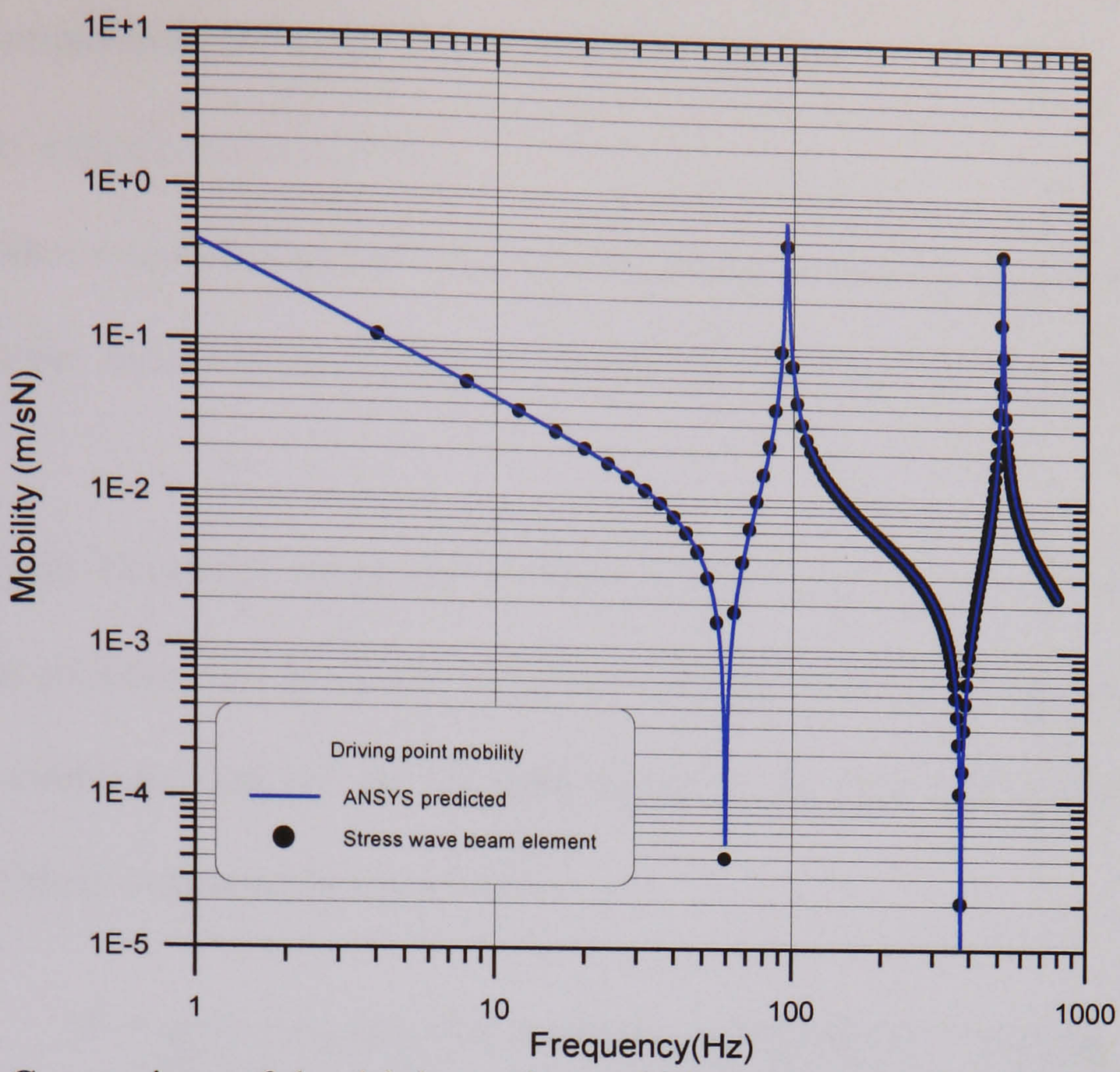

Figure 4.12 Comparison of the driving point mobility spectrum of the beam by stress wave model and ANSYS

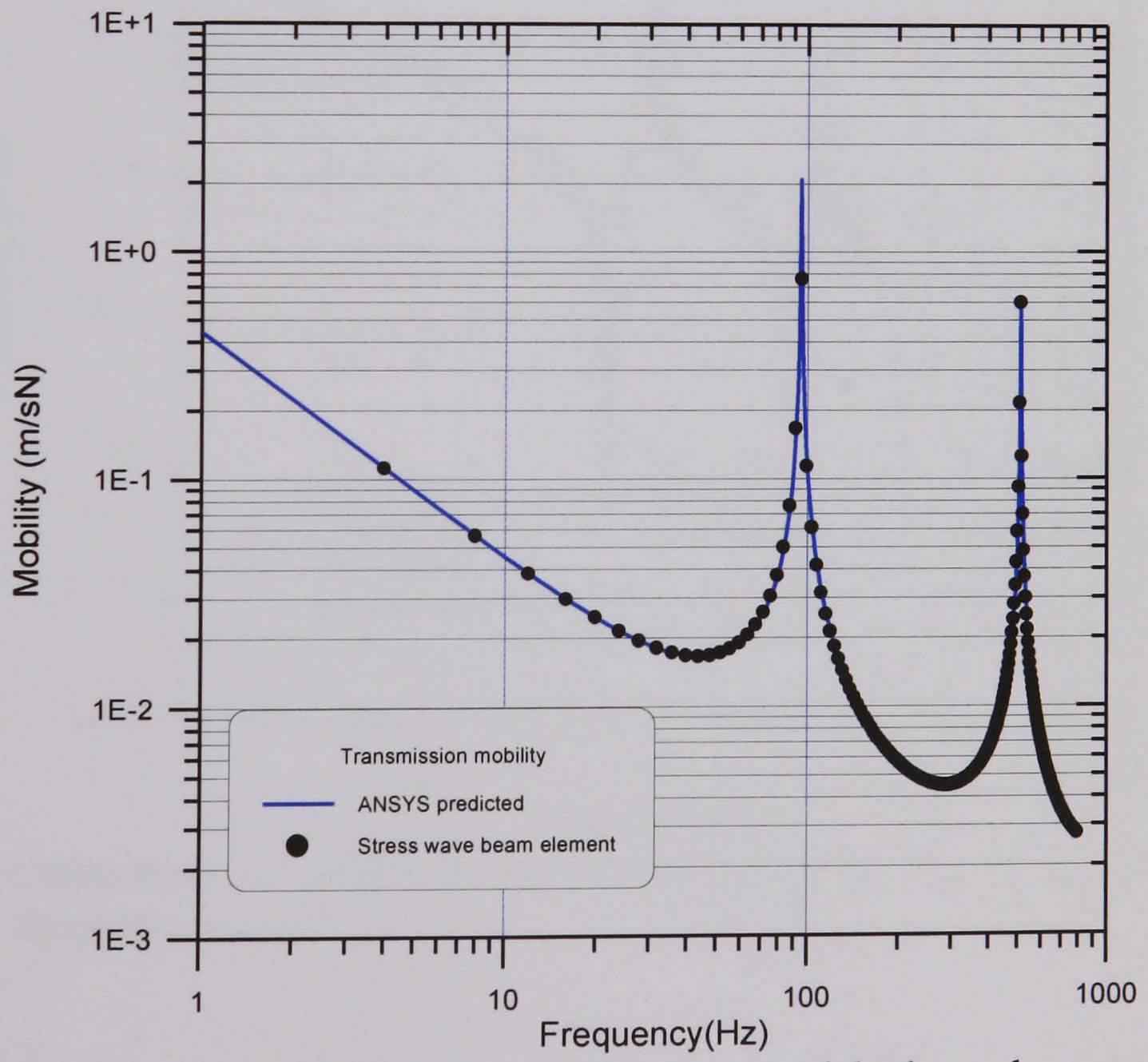

Figure 4.13 Comparison of the transfer mobility spectra of the beam by stress wave model and ANSYS

From these comparisons in Figures 4.10 to 4.13, it illustrates:

1.The mobility experiment is credible.

2.The stress wave model is very efficient in time saving to form the global mobility matrix by using fewer elements and accurate for mobility analysis by using only very few elements.

3.Even in higher frequency range up to 4000 Hz, the stress wave model for mobility analysis can maintain the precision by using very few number of elements, while the number of elements used for the FE analysis has to be increased as the frequency is increased. This is compared in Figure 4.14.

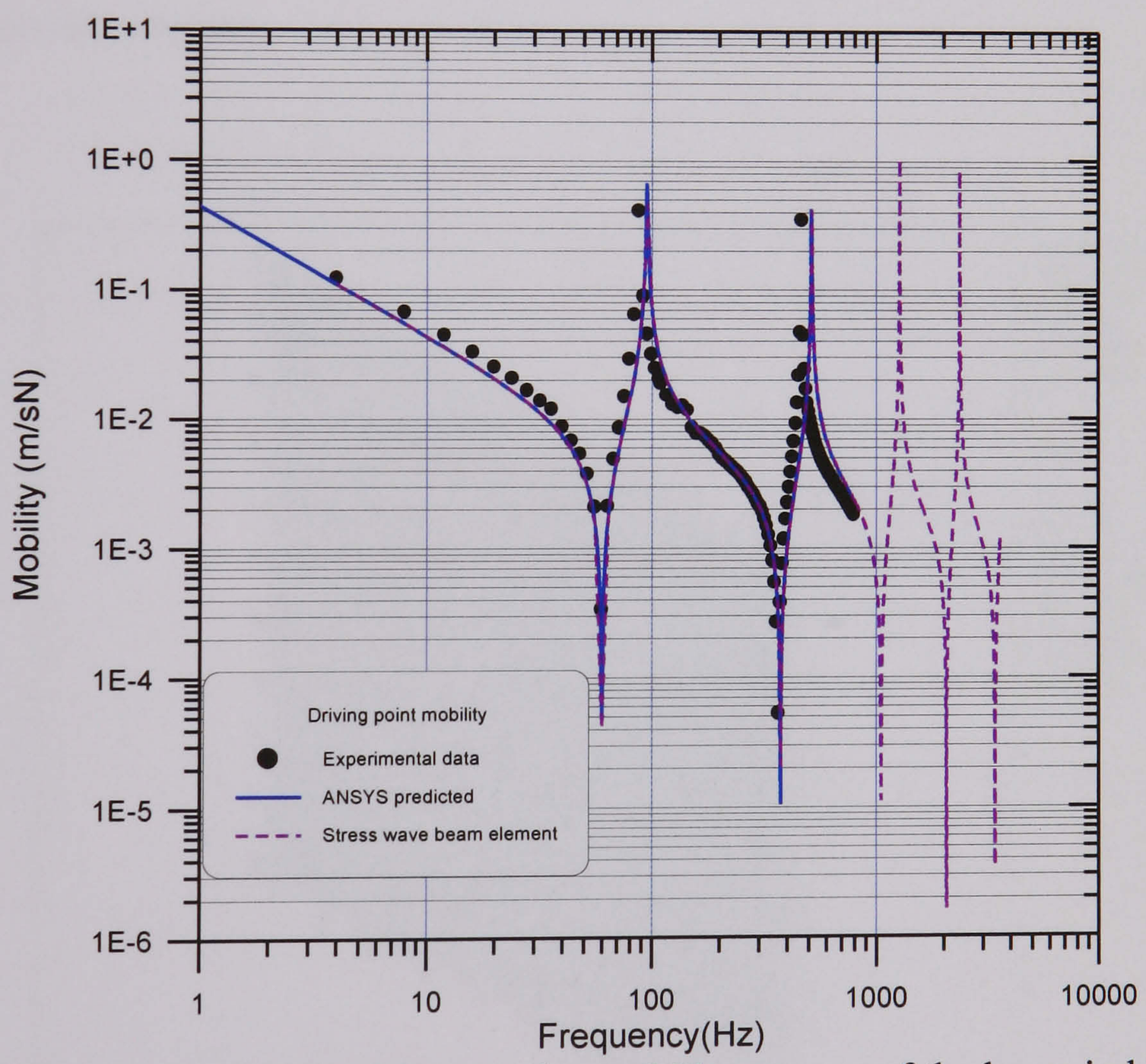

Figure 4.14 Comparison of the driving point mobility spectra of the beam in higher frequency range.

4.5.2 Validation of Mobility of a Square Plate

Consider a square steel plate of dimension 1000mm×1000mm×2mm. All four edges of the plate are simply supported. Driving point of the excitation is located at the center of the

plate. The input data for the driving point mobility analysis by using the stress wave model and ANSYS are:

plate size	: 1000mm×1000mm×2mm	
Young's modulus	: 2.1E+11	N/m^2
density	: 7850	kg/m^3
Poisson's ratio	: 0.25	
damping ratio	: 0.001	
element length	: 0.1m×0.1m for ANSYS and 0.5m×0.5m for stress wave model	
number of elements	: 100 for ANSYS and 4 for stress wave model	

The mesh generation for the FE mobility analysis is shown in Figure 4.15.Where 100 rectangular plate elements are used. While in the stress wave model only 4 stress wave plate elements are adopted.

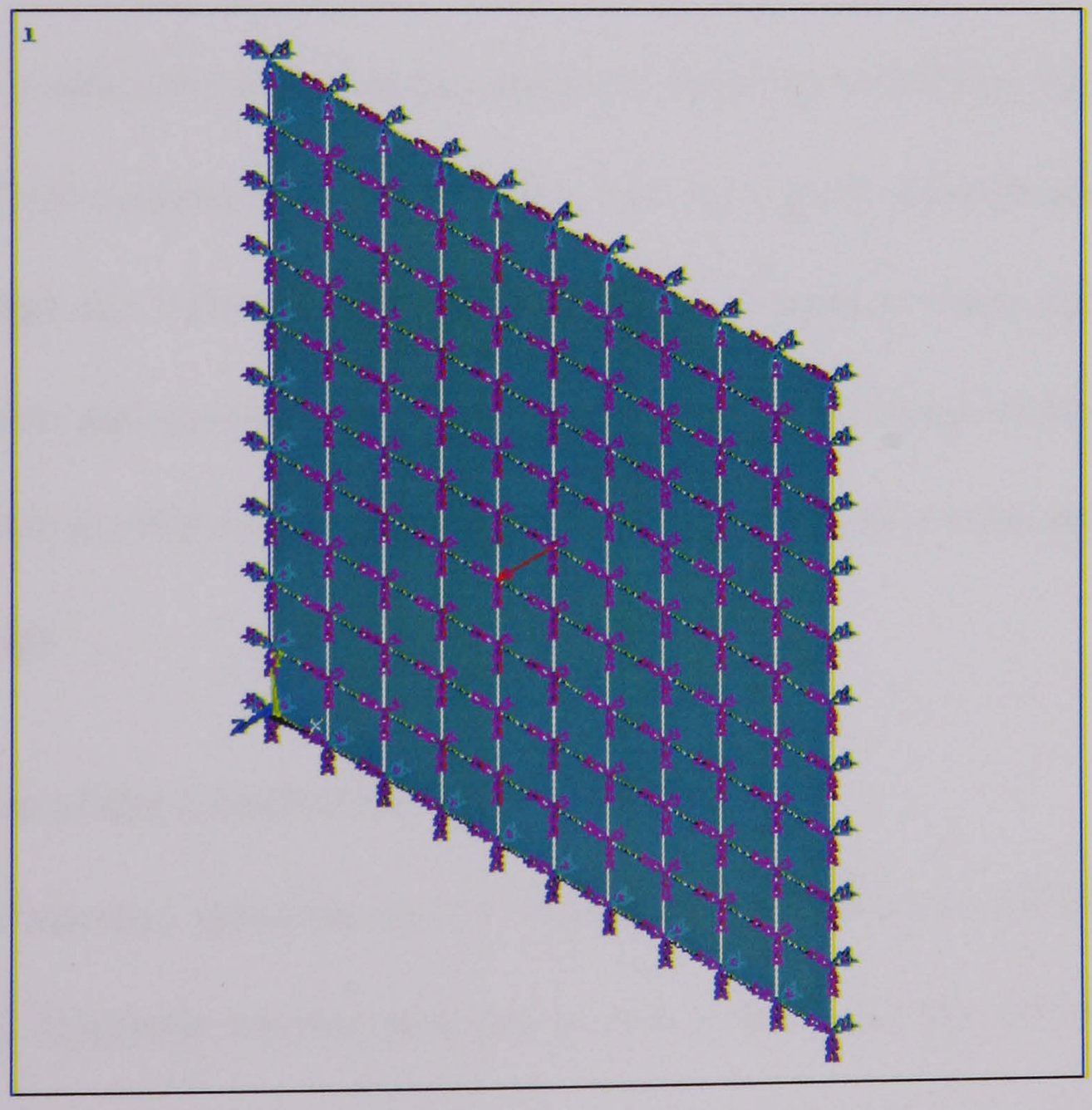

Figure 4.15 Mesh generation of the plate for FE mobility analysis.

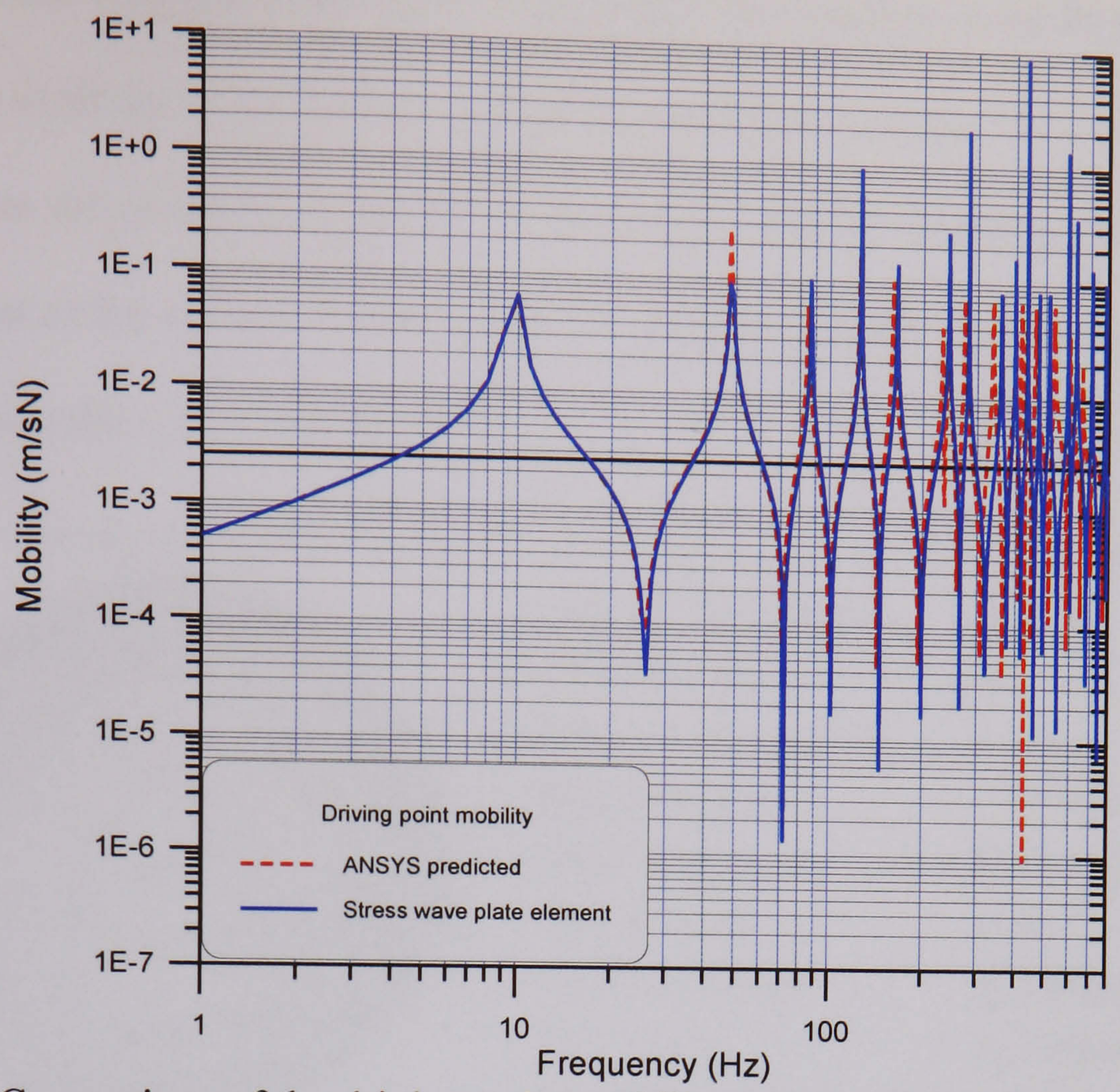

Figure 4.16 Comparison of the driving point mobility spectra of the plate by stress wave model and ANSYS.

The analysis results of the central driving point mobility spectra by the stress wave model and the FEM are compared in Figure 4.16. Also very good coincidence is shown in lower frequency range (to 120Hz) only, while in higer frequency range the deviation of FEM becomes greater and greater. Once again it proves that the stress wave model for mobility analysis in plate is efficient by using fewer elements especially when applying in the higher frequency range.

4.6 Validation of the Coupled FE and BE Model

Consider a submerged spherical shell of radius 1m and thickness 0.03m. When the shell is subjected to a harmonic internal pressure of magnitude 1 Pa, the analytical solution of the sound pressure and normal velocity on the surface of this spherical shell can be found in the studies of Everstine (1991) and Jeans and Mathews (1990). Figure 4.17 shows the coupled FEM/BEM model. Comparisons of the numerical solutions of the spectra of the surface pressure and normal velocity by using equations (4.61) to that by Everstine are

shown in Figures 4.18 and 4.19 respectively. Where the abscissa in the Figures adopts the wave number in air k_a, which is ω/c_a, c_a is the speed of sound in air. The coincidence of the curves validate the coupled FE and BE model being credible. Detail accuracy analysis of the application of the coupled FE/BE model for predicting the underwater sound radiation is discussed in section 7.1.3 of Chapter 7.

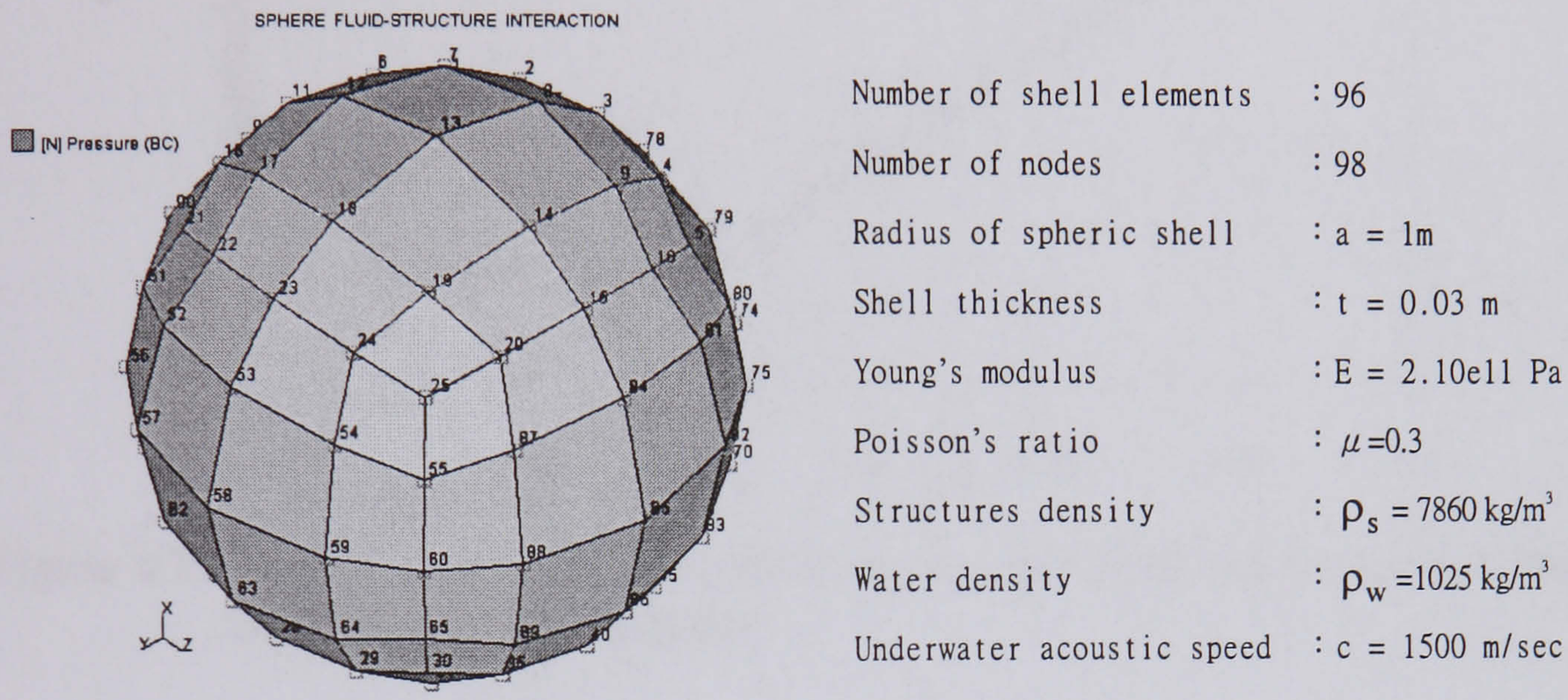

Figure 4.17 Coupled FEM/BEM model of a spherical shell

Figure 4.18 Surface pressure spectrum on a spherical shell under harmonic internal pressure excitation

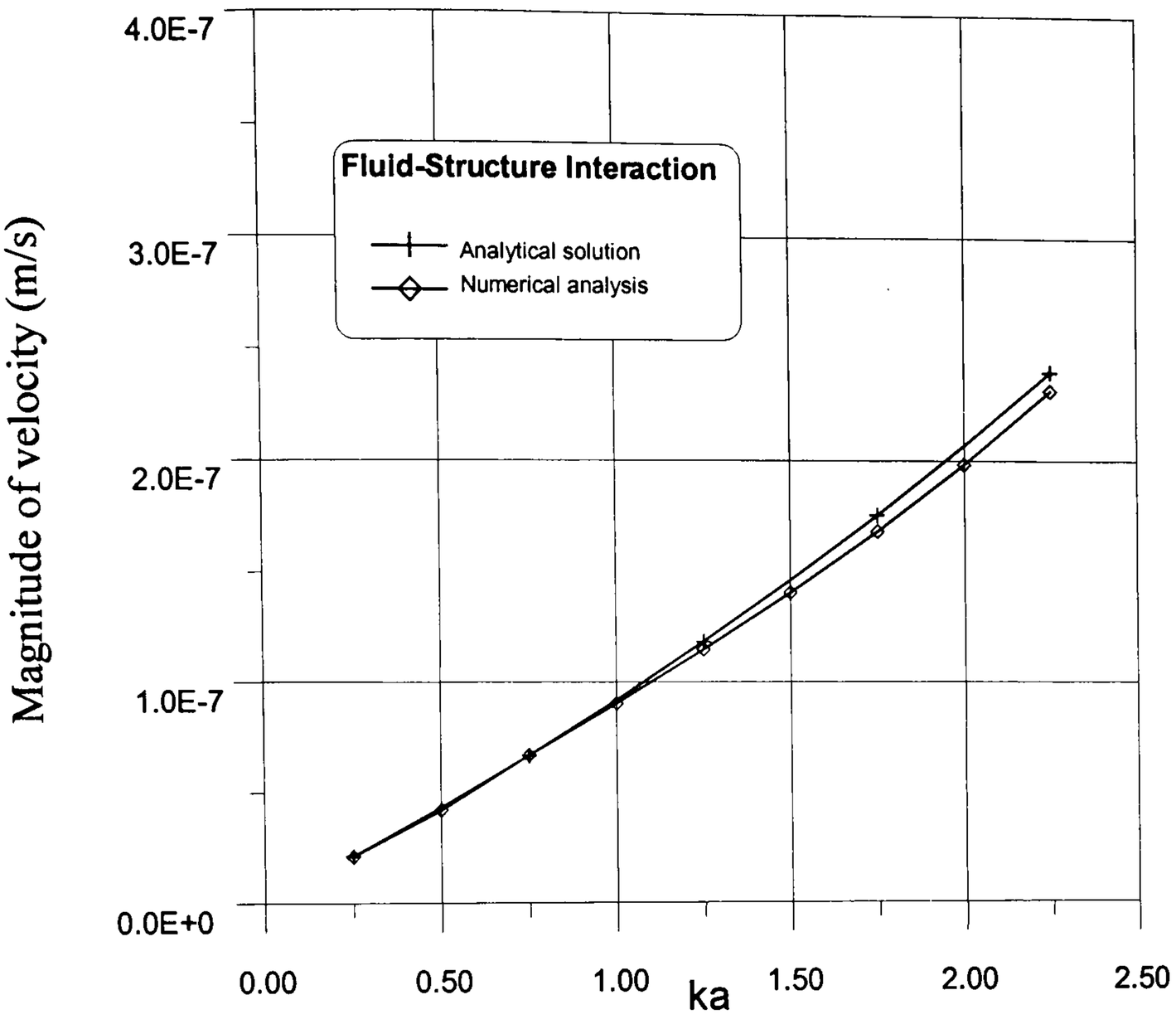

Figure 4.19 Surface normal velocity spectrum on a spherical shell under unit harmonic internal pressure excitation

CHAPTER 5

EXPERIMENTAL MODELS FOR VALIDATING POINT AND TRANSFER MOBILITY OF A MACHINE TO FOUNDATION

To validate the accuracy of applying the mobility analysis model established in Chapter 4 to the machine induced noise and vibration transmission, mobility measurement studies were undertaken on two scale models of engine room structure of two different ships. The larger model is 3m long and the smaller one is 0.585m long . Both models were performed the mobility measurements to validate the correctness of the four-pole parameters method described in Chapter 3 for ascertaining the mechanical vibration and structure-brone noise transmission. In addition, the effectiveness of the transmitted vibrational power reduction via the resilient mounts of a machine has also been characterized during the experiments. A resilient mount usually composed of an elastic element, such as a spring, and a viscoelastic element, such as a rubber piece, to absorb and dissipate the vibrational power. The characterization is performed by the comparison of the transfer mobilities, the vibrational velocity spectra and the transmitted power spectra when the scale model of engine room is installed resilient mounts with and without rubber pad respectively.

Secondly, the smaller model of the engine room structure also used to illustrate the validation of a machine induced underwater acoustic radiation prediction obtained by the coupled FEM/BEM model described in Chapter4 and experiment measurement in a water tank respectively . This part of the study will be described in the next Chapter. The reason for the adoption of a smaller scale model for the underwater acoustic radiation study is

owing to the consideration of reducing the reflection effect of the tank wall as far as possible.

Finally, a patrol vessel study was undertaken by applying the mobility theory and FEA to understand the structure-borne noise transmission from engine. For the purpose of reducing the noise level onboard, the effectiveness of squeeze-film technique was also assessed in the application. A squeeze film is an auxiliary plate attached parallel to the surface of a structure at corners, thereby trapping a thin layer of air. Relative vibration of the plates pump this air at high velocities, resulting in energy loss due to the viscosity of air. Once the loss factor of the squeeze film damping plate is determined, the mobility reduction can be analysed by FEA.

Basically, the measuring system common to the mobility measurements were arranged as shown in the block diagram of Figure 5.1. The specifications were:

- Accelerometer, B&K 4370, weight 54g , suitable for a frequency range of 0-5 kHz, 5% error for a range 0.2-3.5 kHz, and 10% error for a range of 0.1-4.8 kHz, maximum acceleration 20kms^{-2}.
- Hammer-kit , B&K 8202, suitable for a frequency range of 0-7 kHz (which was defined as a 10dB force amplitude drop range) with steel tip, weight 10.3g, force range 500-5000N , exerted duration 0.25-2 ms; attached force transducer, B&K 8200, suitable for a frequency range of 0-10 kHz, weight 21g, force range 1000N (tension) - 5000N (compression) stiffness 5×10^{8} Nm^{-1}, resonant frequency 35 kHz, charge sensitivity 3.79 P C/N.
- Charge amplifier, B&K 2635*8 sets, magnification factor range 0.1-1000 mv/unit.

- Tape recorder, TEAC RD-135T, 16 channels, reliable frequency band 0-5 kHz for 8 channels used simultaneously.
- Spectrum analyser, B&K 3550, 8 channels, highest effective analysis frequency range 26.5 kHz for each channel.
- Impedance head, B&K 8001, weight 31g , 5% error for range 1 Hz -6 kHz and 10% error for 1 Hz -10 kHz.

The accelerometers, charge amplifiers, and force transducer attached to the hammer-kit and the digital tape recorder were utilized together to measure the necessary data related to the mobility.

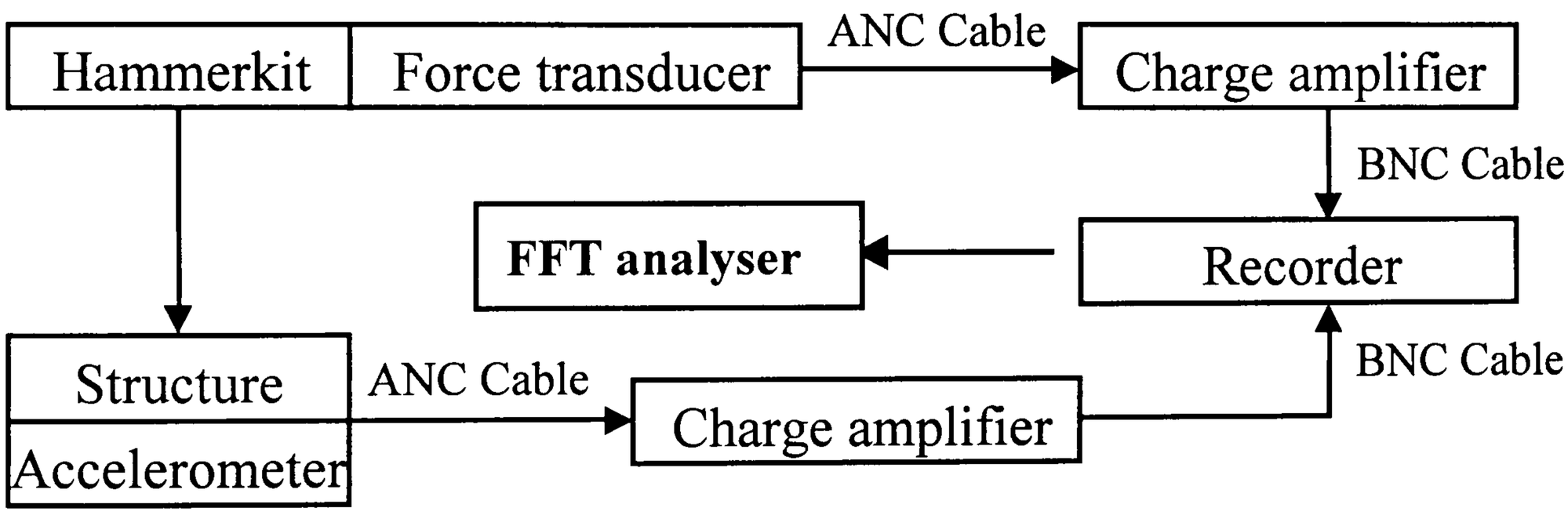

Figure 5.1 Instrument arrangement for mobility measurement

5.1 Mobility Study of Scale Engine Room Model (I)

Consider a scale model of an engine room structure as shown in Figure 5.2. This model with a length 3 m, consists of two equally spaced web frames, two end bulkheads, four girders on the bottom, one stringer on each side shell and two hatchside deck longitudinals. In the middle of the bottom a bedplate, 600mm×300mm, is installed and botted to the bottom girders. On the top of the bedplate four resilient mounts were used to support a

steplees motor. On the shaft of the motor there is attached a deliberately designed eccentric mass to simulate a dynamical unbalance.

In order to recognize the structure-borne sound transmission via the resilient mount of the motor-resilient mount-foundation structure, also shown in Figure 5.2, all mobilities in equation (3.108) are necessary to be measured.

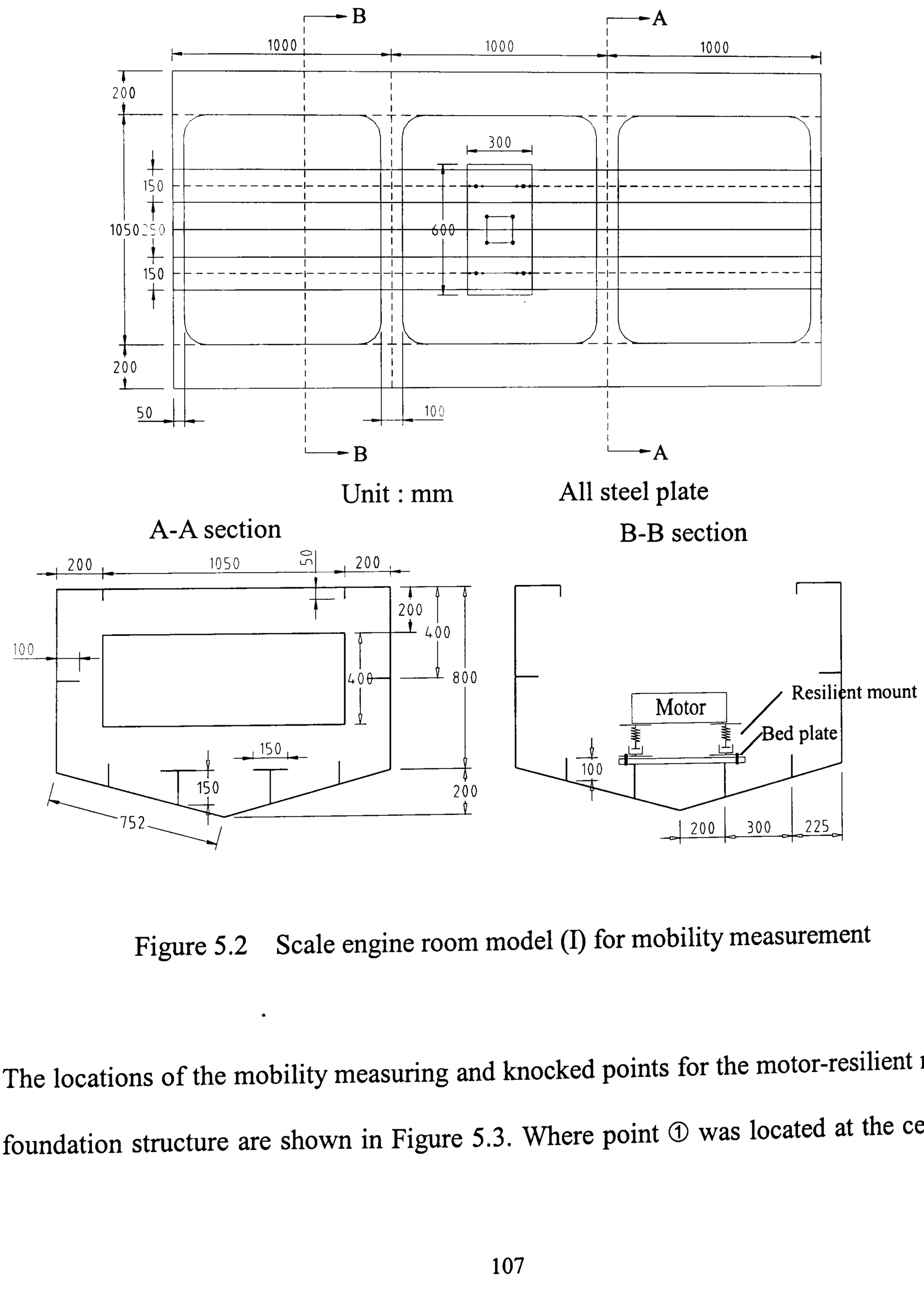

Figure 5.2 Scale engine room model (I) for mobility measurement

The locations of the mobility measuring and knocked points for the motor-resilient mount-foundation structure are shown in Figure 5.3. Where point ① was located at the centre of

gravity of the motor, points ② and ③ were located close to the bolt joint of the motor and the resilient mount while point ④ was close to the bolt joint of the bedplate and the bottom girder. The scale engine room model, had a mass of 500 kg, was hung in air and floating in a water tank respectively during the mobility measurements. The mobility measurements were undertaken by the conditions defined by :

M_{12}: hung and separated the subsystem A, knocked point ② by a hammer and measured the transfer mobility at point ①.

M_{22}: hung and separated the subsystem A, measured the point mobility at point ②.

M_{33}: put subsystem A on subsystem B together but did not fasten, measured the point mobility at point ③.

M_{34}: put subsystem A on subsystem B, knocked point ④ by a hammer and measured the transfer mobility at point ③.

M_{41}: linked and fastened the subsystems A and B, knocked point ① and measured the transfer mobility at point ④.

where subsystems A and B are coupled in series as shown in Figure 5.5.

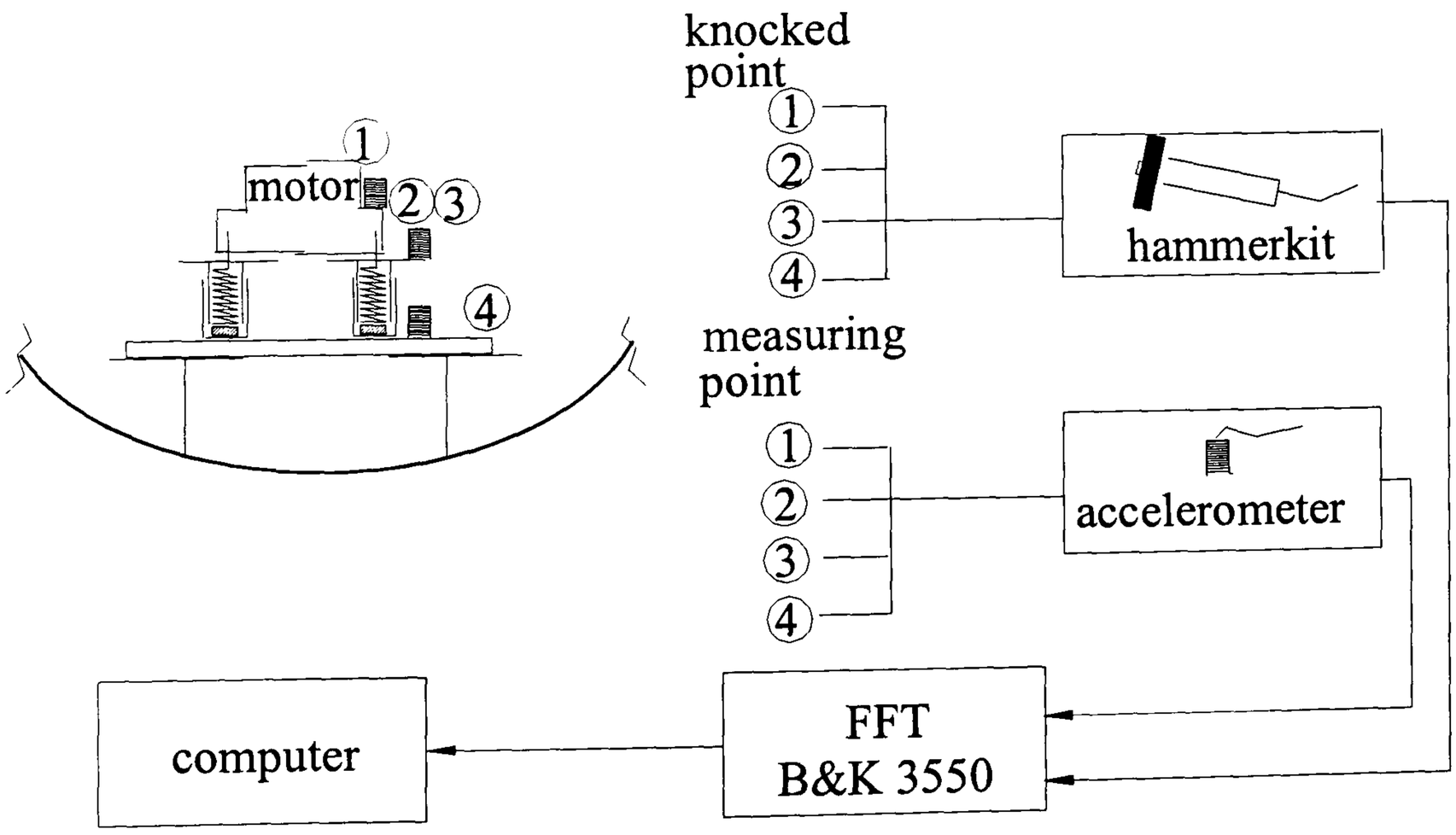

Figure 5.3 Mobility measuring points and experiment setup of the motor-resilient mount-foundation system

For the mobility testing of the mounts, which interposing the bedplate and the girders in

Figure 5.2, a sleeve type of resilient mount as shown in Figure 5.4 was selected to study. In which the spring and rubber piece put in series connection within a sleeve. Where the rubber piece can be replaced. Thus, the selction of this type of resilient mount is capable of studying and comparing the vibration isolation characteristics for different kind and thickness of rubber in a replaceable way.

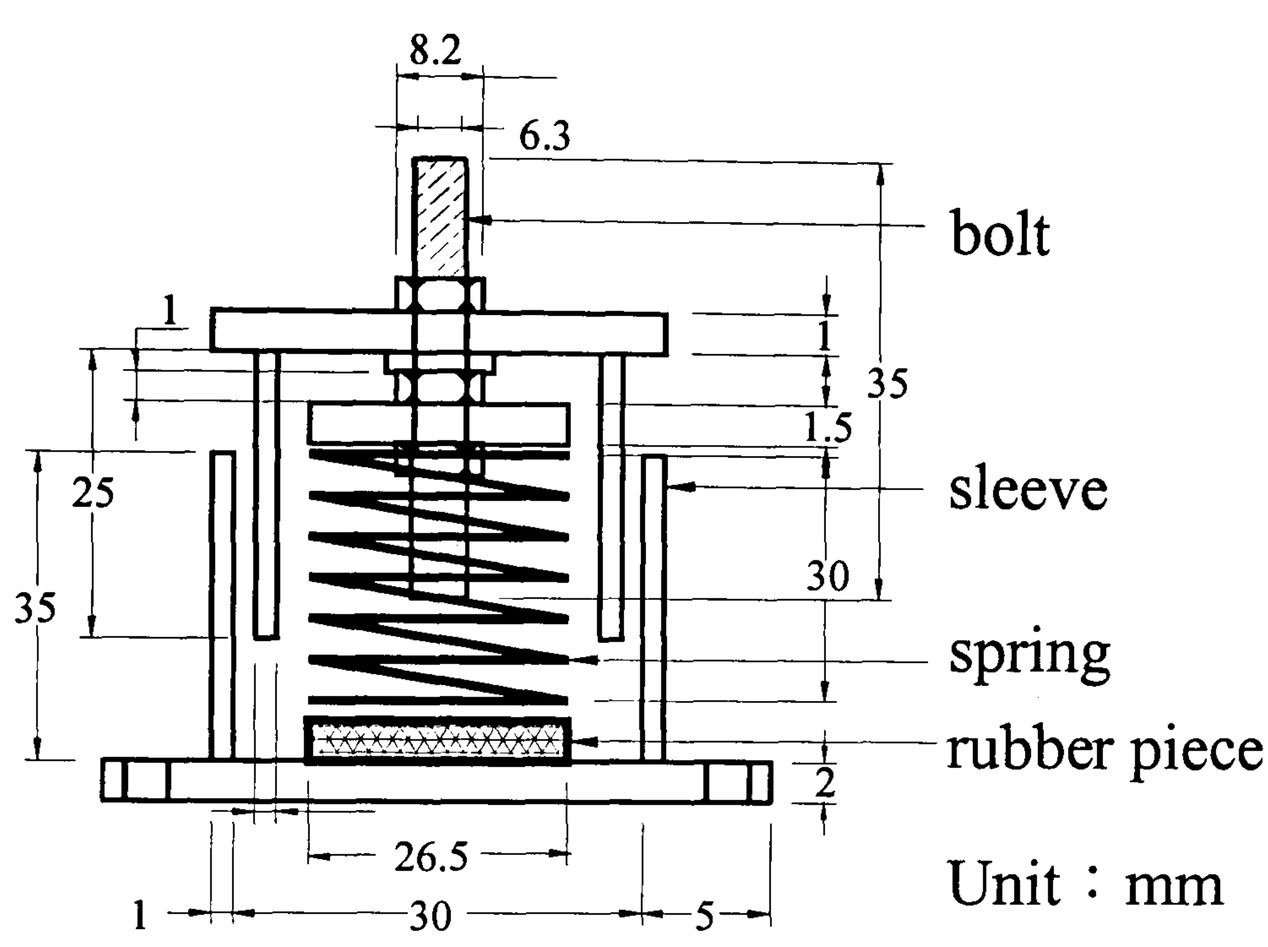

Figure 5.4 Configuration of the sleeve type of resilient mount

5.1.1 Validation of the Four-Pole Parameters Model

Consider the scale model as two subsystems A and B coupled in series as shown in Figure 5.5. Subsystem A consists of the motor and the upper part of the sleeve type mount, while subsystem B consists of the lower part of the sleeve type mount, bedplate and the hull structure. To validate the model of equation (3.108), the comparison of $|M_{41}|$ by direct measurement and by calculation were made. The comparisons have carried out for four cases, i.e., the scale engine room model hung in air as shown in Figure 5.6, and floated in a water tank, of dimension 4.2m long, 3.6m wide and 2.4m deep, with and without inserting a Butyl rubber piece in the resilient mounts.

The comparison results are shown in Figures 5.7 to 5.10. Detail accuracy analysis of the

mobility model for evaluating vibration transmission via mounts is discussed in Section 7.1.1 of Chapter 7.

Figure 5.7 represents the comparison of the predicted and measured mobility spectrum M_{41} when the scale model was hung in air with rubber pieces interposing in the mounts.

Figure 5.8 represents the comparison of the predicted and measured mobility spectrum M_{41} when the scale model was hung in air without rubber pieces interposing in the mounts.

Figure 5.9 represents the comparison of the predicted and measured mobility spectrum M_{41} when the scale model was floating in the tank with rubber pieces interposing in the mounts.

Figure 5.10 represents the comparison of the predicted and measured mobility spectrum M_{41} when the scale model was floating in the tank without rubber pieces interposing in the mounts.

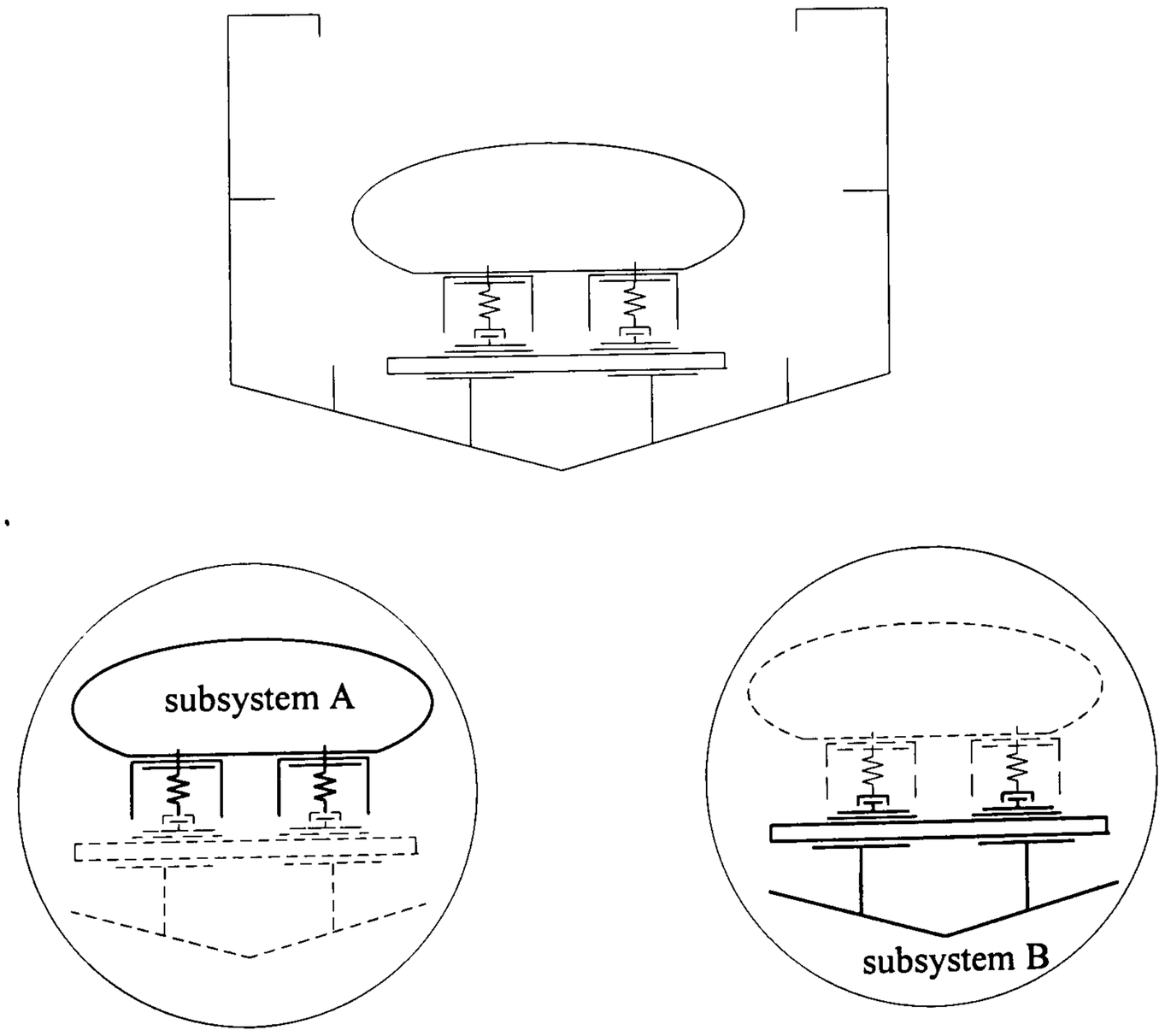

Figure 5.5 Couped subsystems A and B of the scale engine room model (I)

Figure 5.6 The hanging arrangement of the scale engine room model (I)

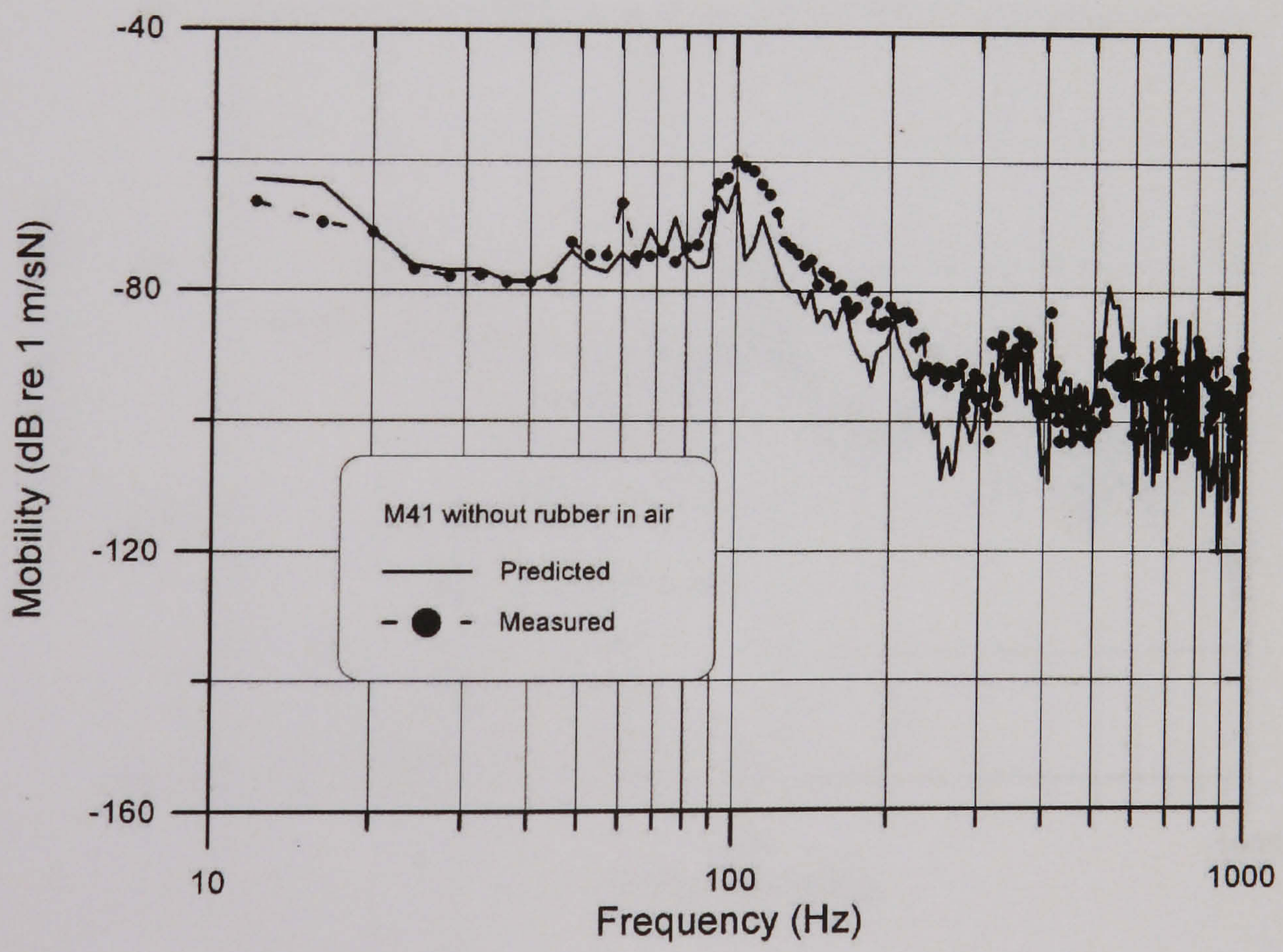

Figure 5.7 Comparison of the predicted and measured mobility spectrum M_{41} when the scale model (I) was hung in air with rubber pieces interposing in the mounts

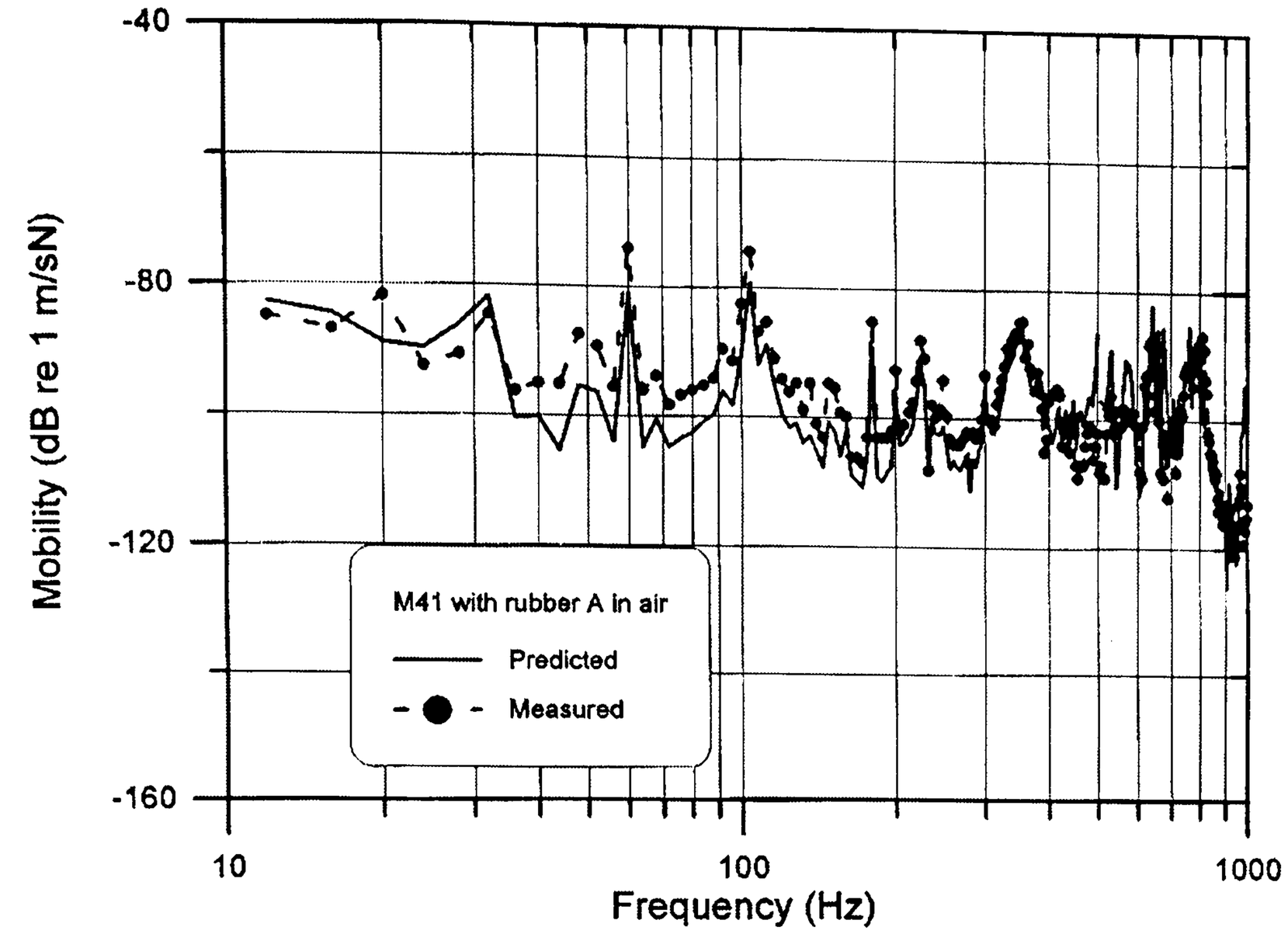

Figure 5.8 Comparison of the predicted and measured mobility spectrum M_{41} when the scale model (I) was hung in air without rubber pieces interposing in the mounts

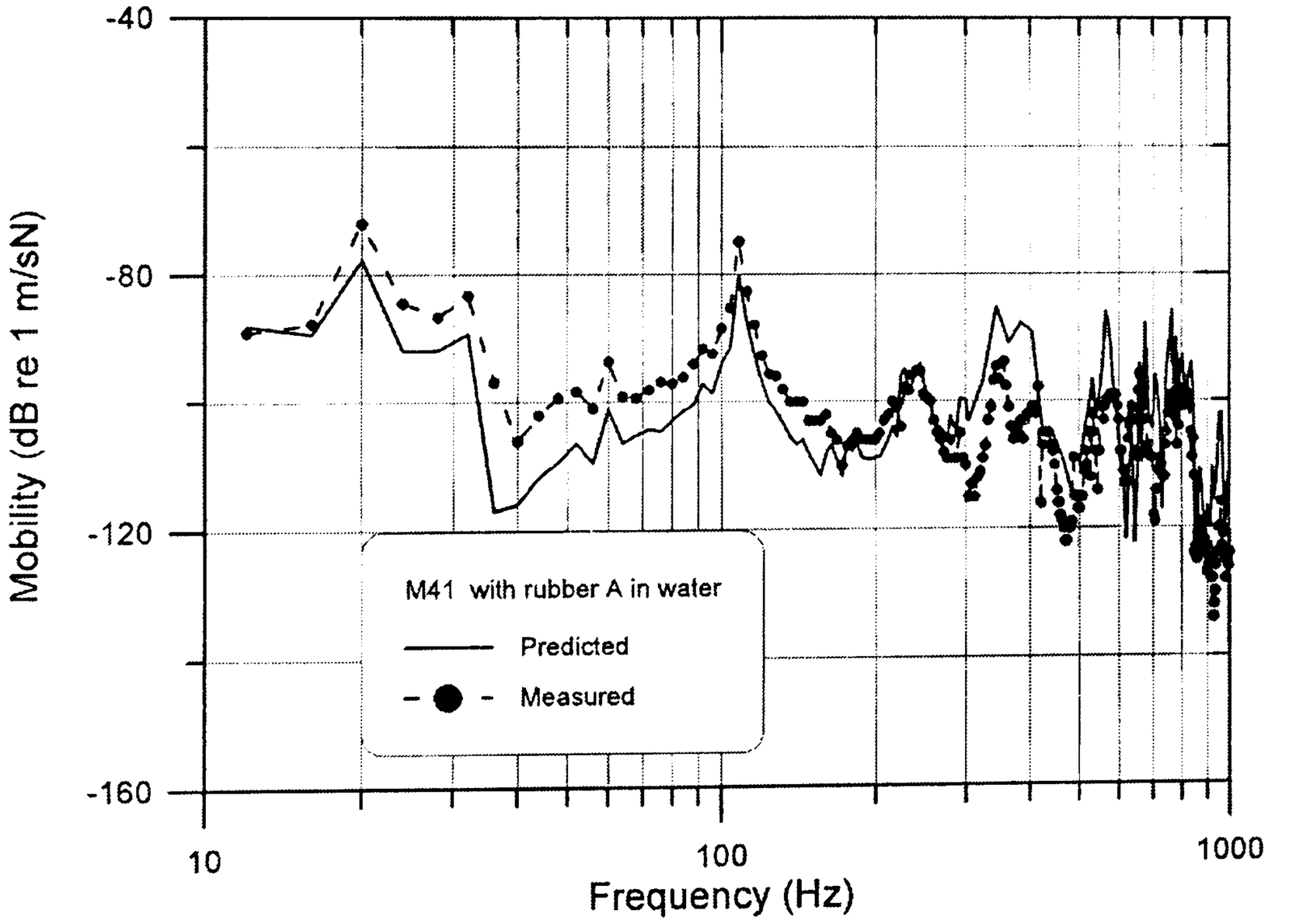

Figure 5.9 Comparison of the predicted and measured mobility spectrum M_{41} when the scale model (I) was floating in the tank with rubber pieces interposing in the mounts

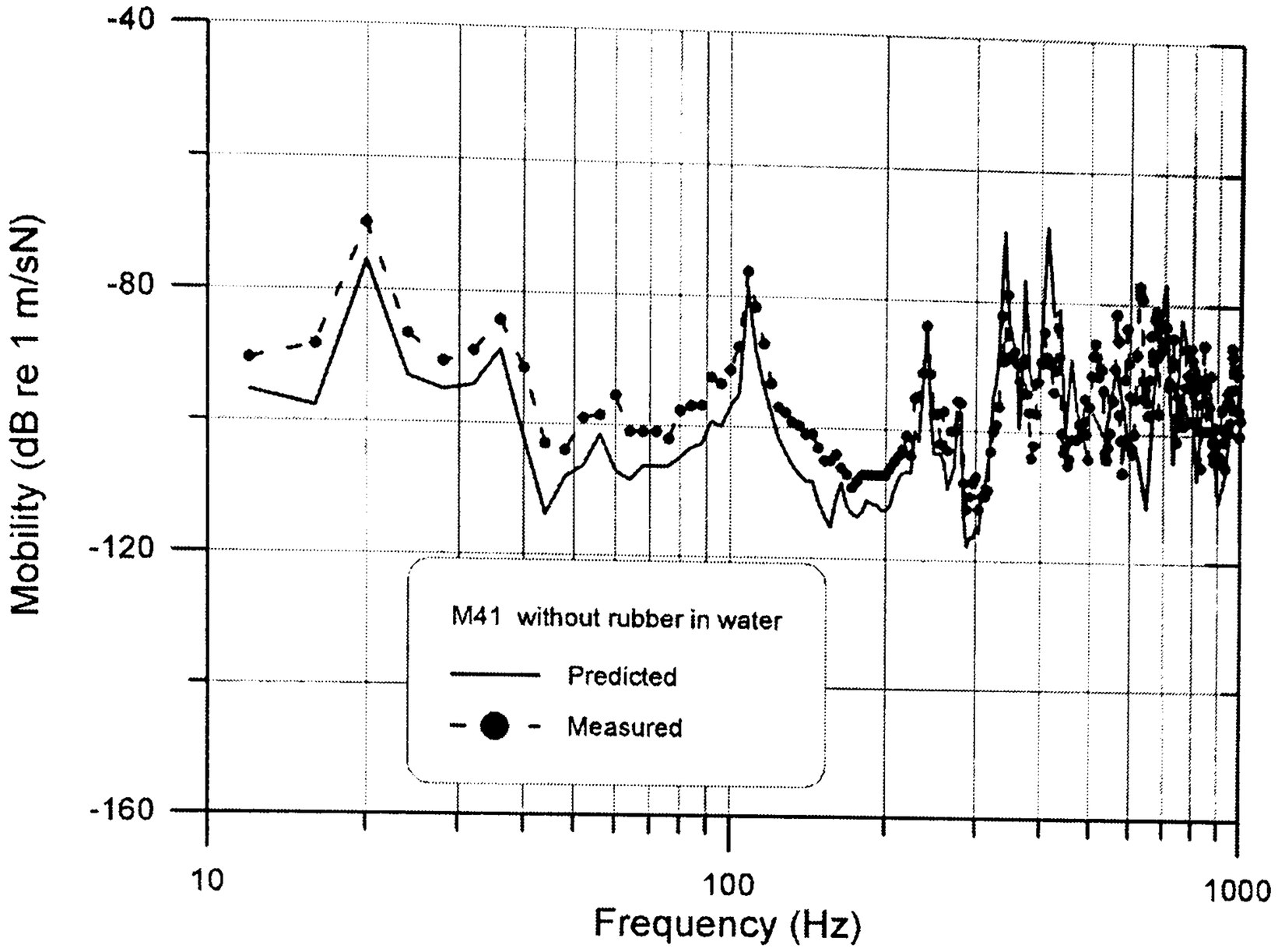

Figure 5.10 Comparison of the predicted and measured mobility spectrum M_{41} when the scale model (I) was floating in the tank without rubber pieces interposing in the mounts

From the measured transfer mobility sprectra M_{41} shown in Figures 5.7 and 5.8, the effect of the rubber pad for the reduction of transfer mobility function from the motor to the bottom structure can be characterized and is shown in Figure 5.11. It can be seen that the rubber pad can reduce M_{41} by an average amount around 12dB at the peak frequencies below 200 Hz, while the reduction in higher frequency is not apparent.

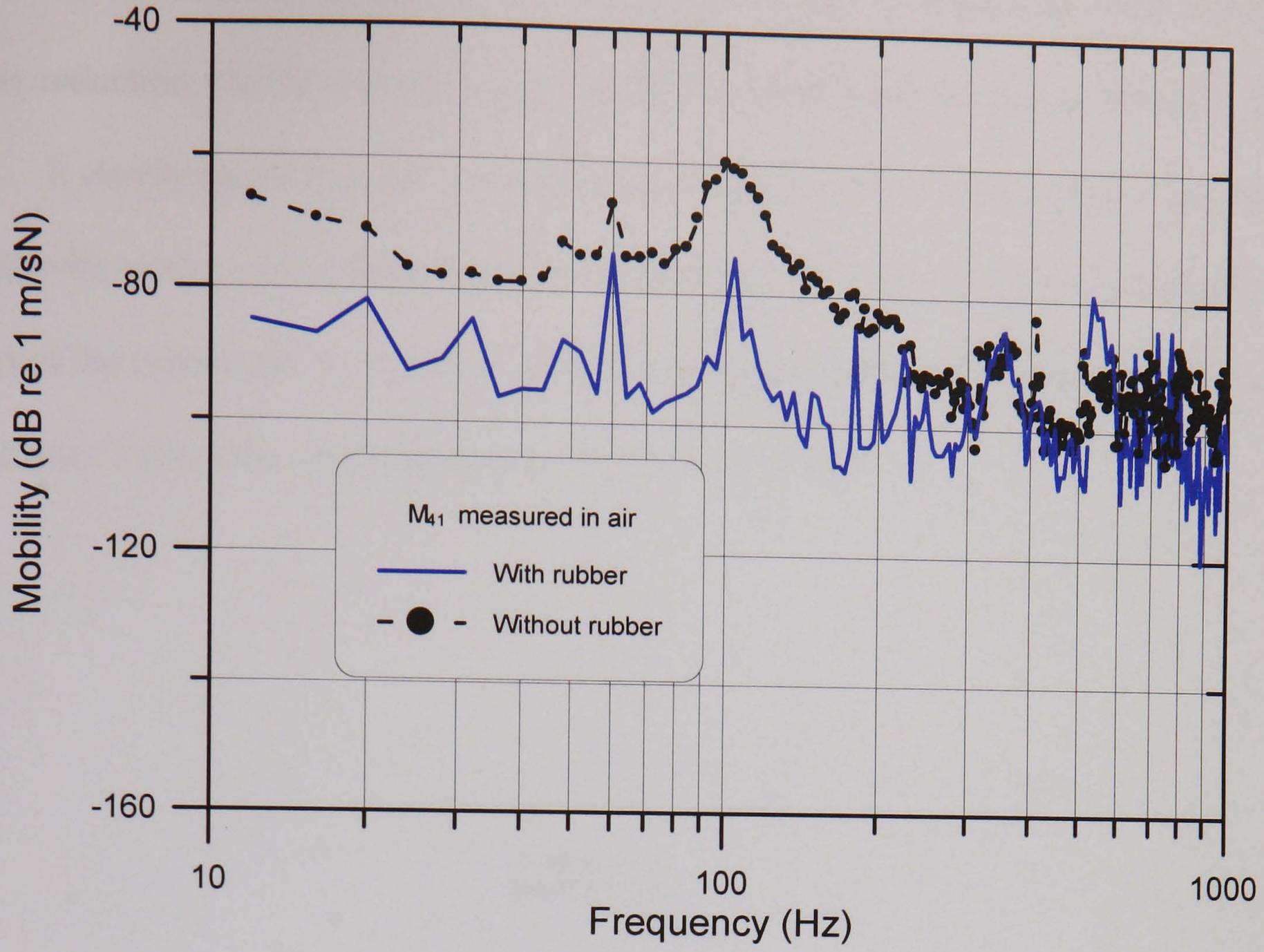

Figure 5.11 Effect of rubber pad in reducing the transfer mobility of the scale engine room model (I) hung in air.

5.1.2 Prediction of Vibrational Power Transmission via Resilient Mount from Motor

When the motor in the scale engine room model was rotating at a constant speed 1140 rpm, there was a vibration caused by the unbalanced mass attached to the shaft. This vibration can transmit to the foundation via the mounts. The vibrational power flow transmission can be predicted by using the velocity and impedance spectra as expressed in equations (3.70a) to (3.70c), in which the impedances are also related to the mobilities by equations (3.69a) to (3.69c). Thus the power flow calculation can be schemed as the flow chart shown in Figure 5.12.

The measured vibrational velocity spectrum density functions at motor side and girder side of the resilient mount with/without rubber pad are compared in Figures 5.13 and 5.14 . Combining the measured mobility spectra, the predicted vibration power at input of the

mount are calculated as shown in Figures 5.15 and 5.16. Comparison of the vibrational power reduction via the resilient mount with and without rubber pad is shown in Figure 5.17. It clearly shows that the Noise Reduction (NR) in power transmission via a resilient mount with rubber pad is better than that without rubber. Detail quantitative analysis of the effect of the rubber pad in reduction of vibration transmission is discussed in Section 7.1.4 of Chapter 7 about the results shown in Figures 5.11 to 5.16.

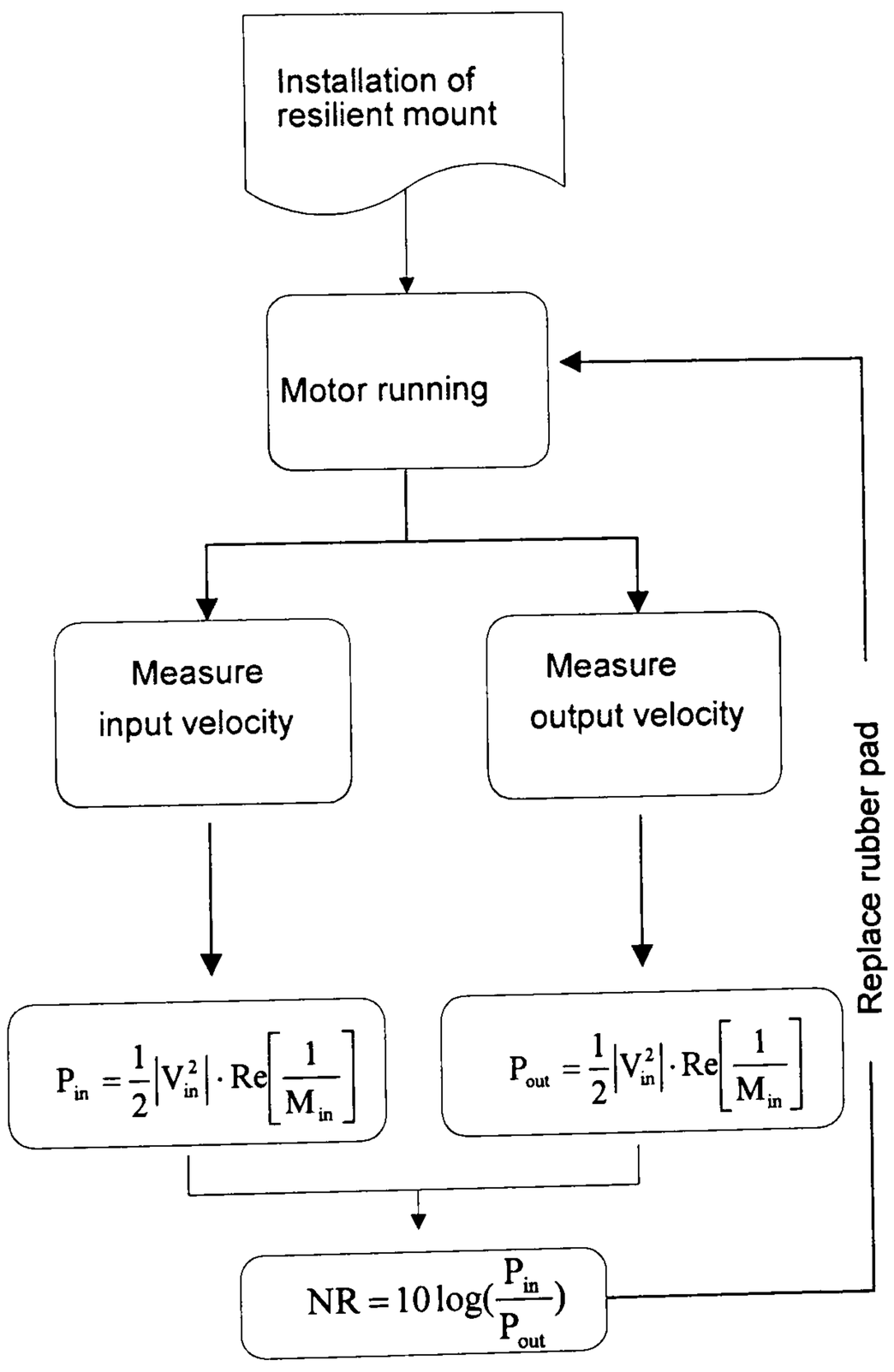

Figure 5.12 Flow chart for calculating the noise reduction in power flow transmission via resilient mount

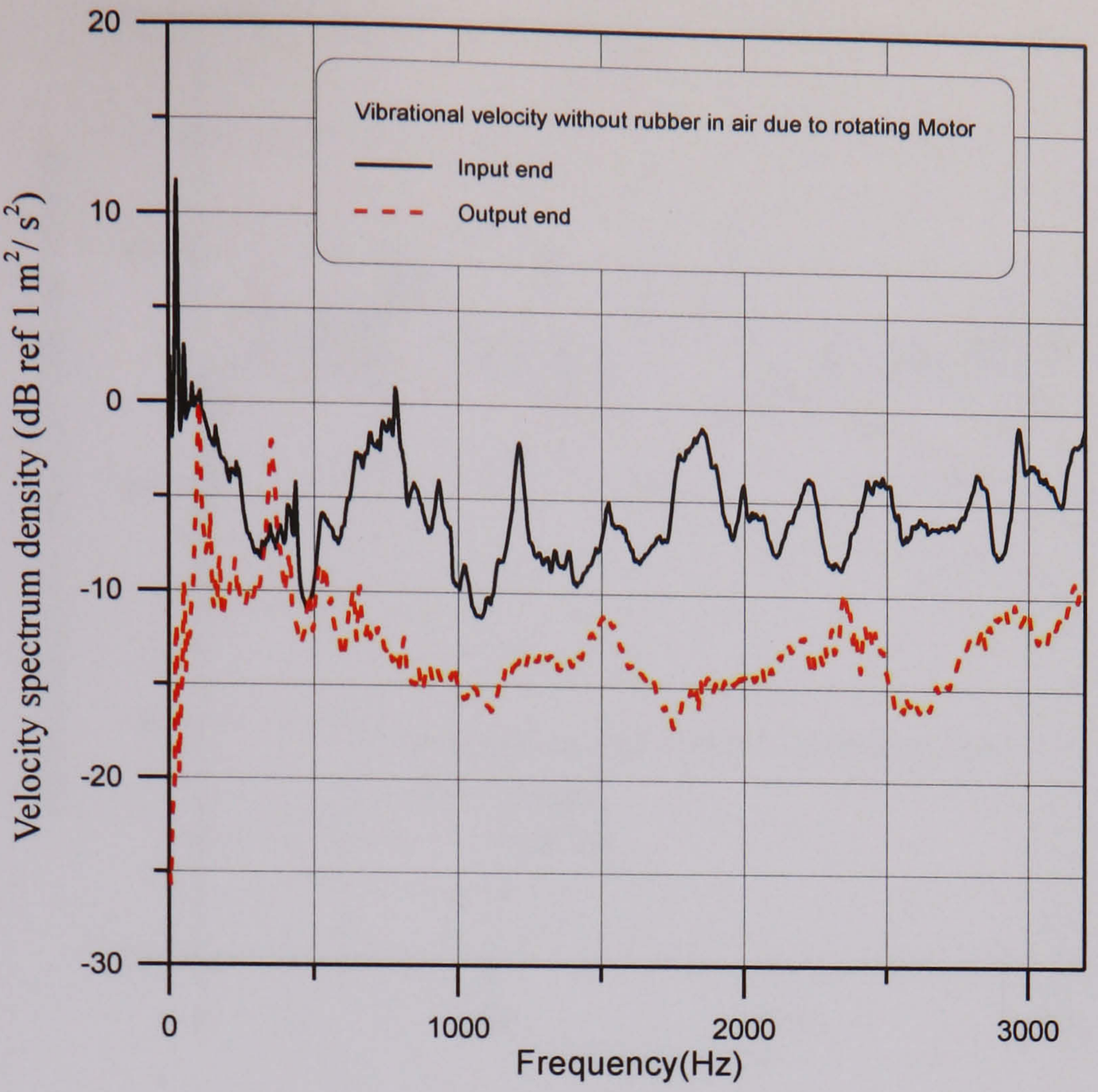

Figure 5.13 Velocity spectra density at input and output sides of the resilient mount without rubber pad.

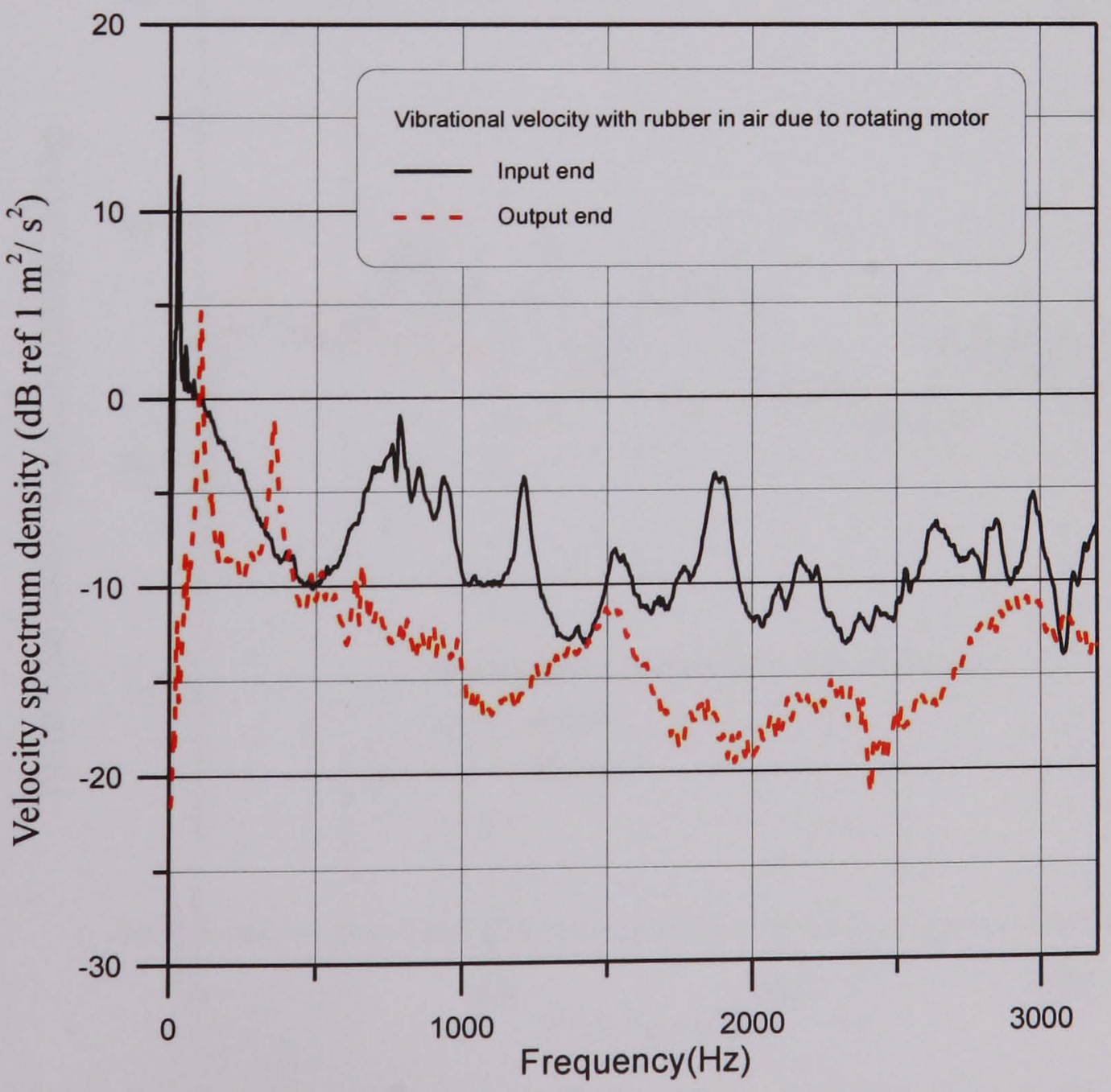

Figure 5.14 Velocity spectra density at input and output sides of the resilient mount with rubber pad.

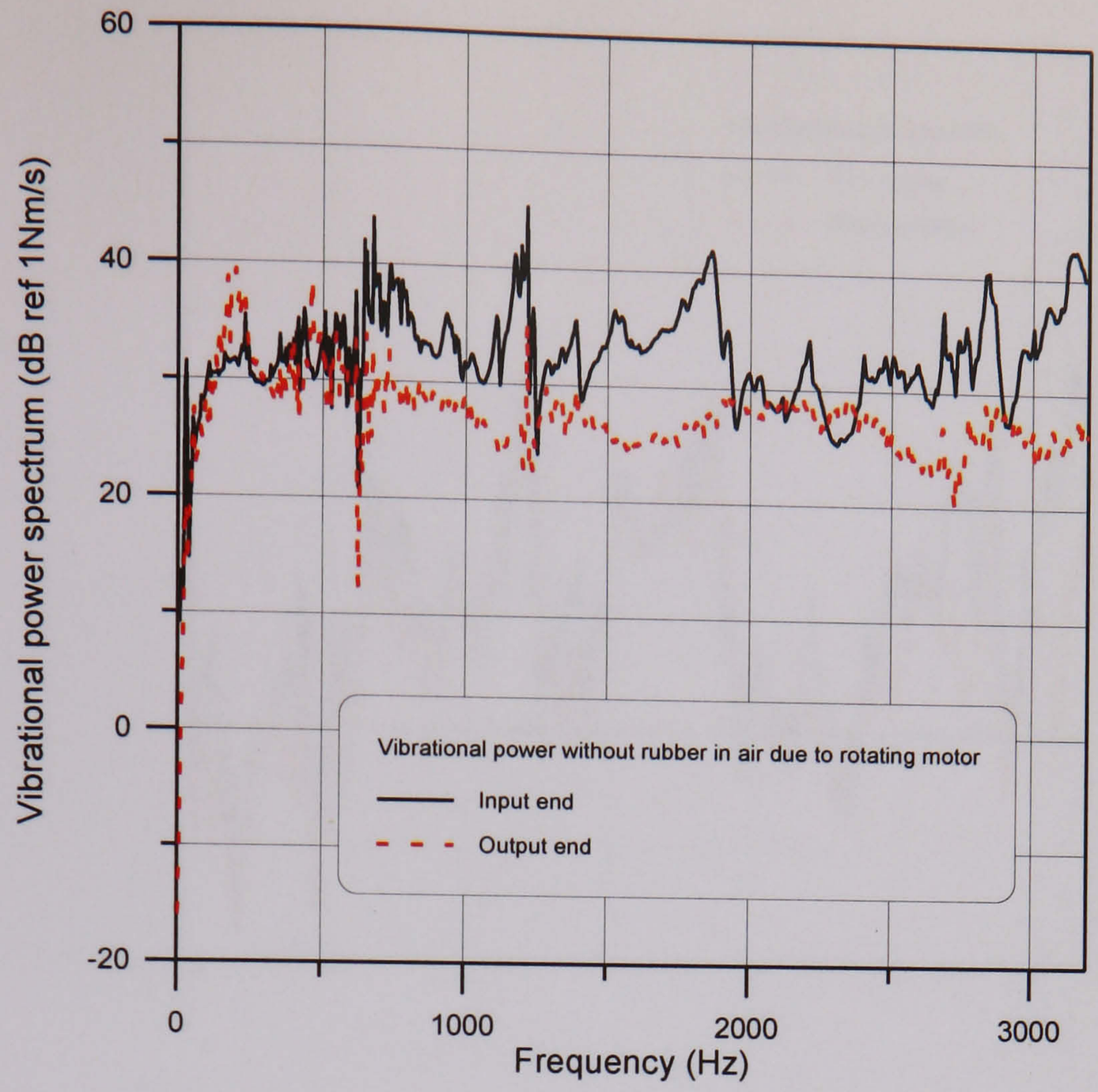

Figure 5.15 Vibrational power spectra at input and output sides of the resilient mount without rubber pad

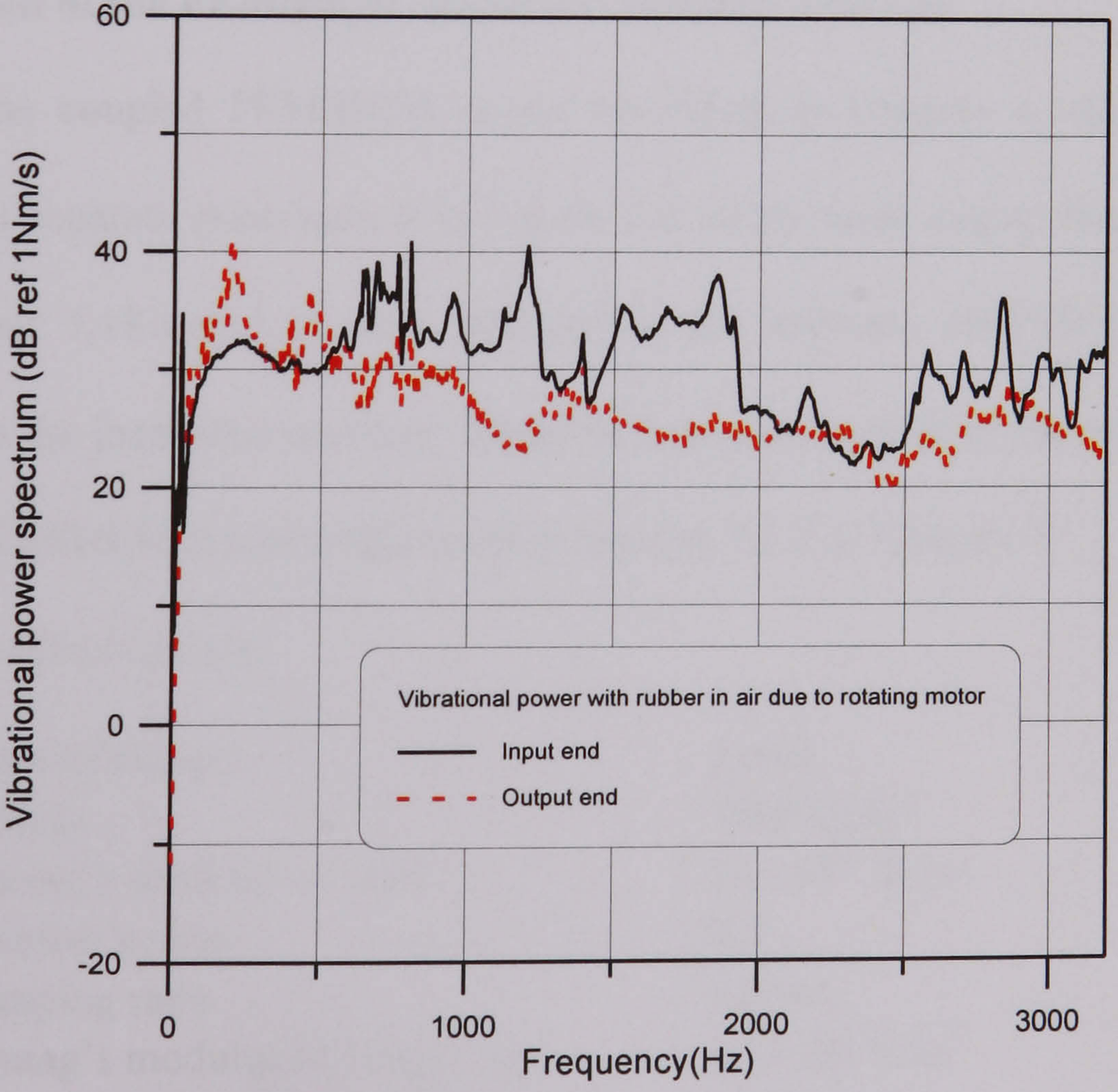

Figure 5.16 Vibrational power spectra at input and output sides of the resilient mount with rubber pad

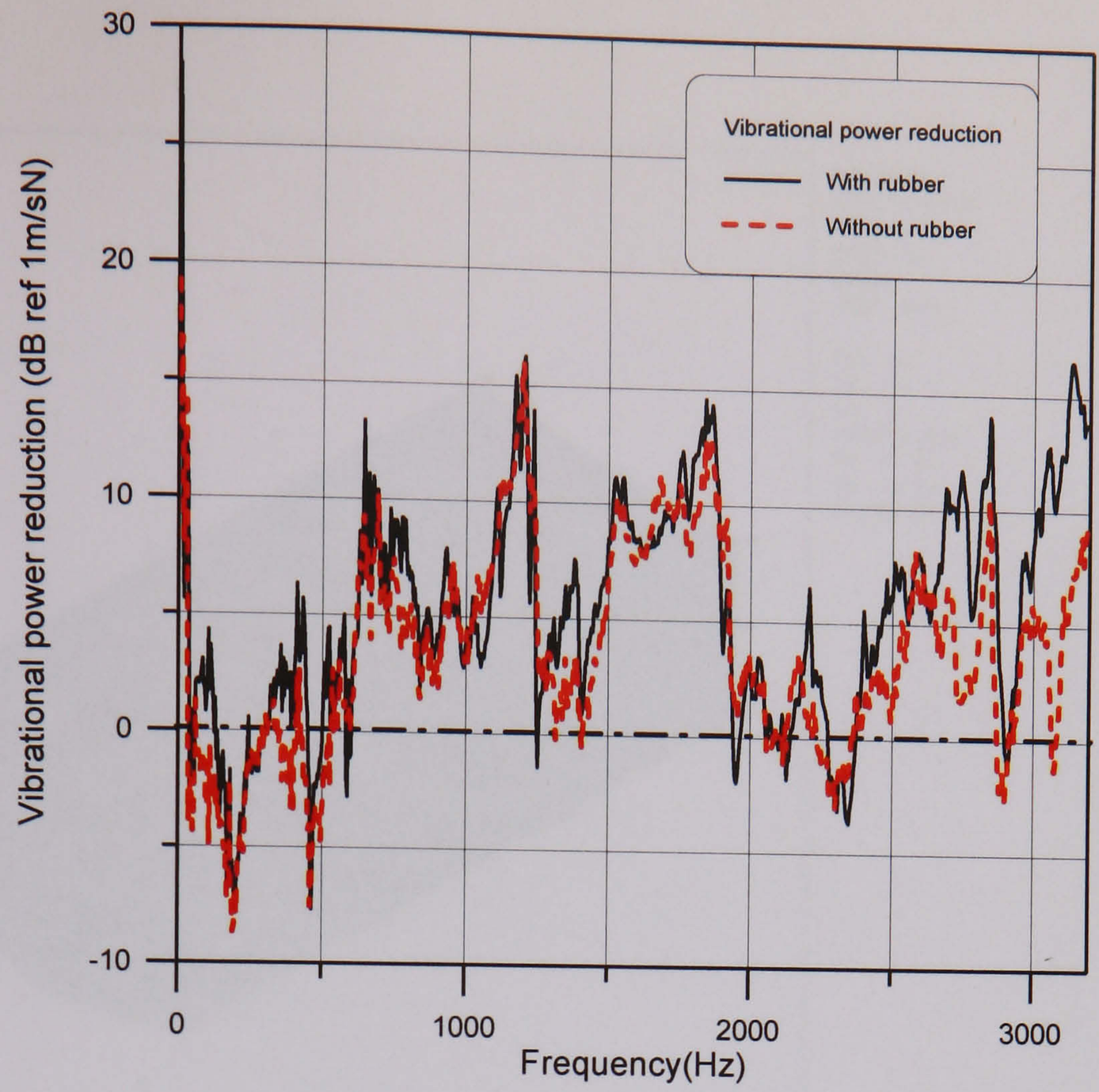

Figure 5.17 Comparison of Vibrational power reduction via mount with and without rubber pad

5.1.3 Validation of the FEM/BEM Model for Mobility Analysis

To validate the coupled FEM/BEM model described in Chapter 4, the driving point mobility of the separate subsystem B in Figure 5.5, of the scale engine room model (I) as shown in Figure 5.18 and 5.19, was analyzed by the software ANSYS/SYSNOISE and compared with the measured mobility. Detail accuracy evatuation of the mobility analysis by using the FEM/BEM model is discussed is Section 7.1.2 of Chapter 7.

Input data to the analysis are:

plate thickness	: 3 mm
density	: 7860 kg/m^3
Young's modulus of steel	: 2.1×10^{11} N/m^2
Poisson's ratio	: 0.3
damping ratio	: 0.0014
Young's modulus of bungie rope	: 4.7×106 N/m^2
linear stiffness of bungie rope	: 8.3 N/m
number of rectangular plate elements	: 8217
number of master degree of freedom	: 670
minimum element size	: 0.05 m

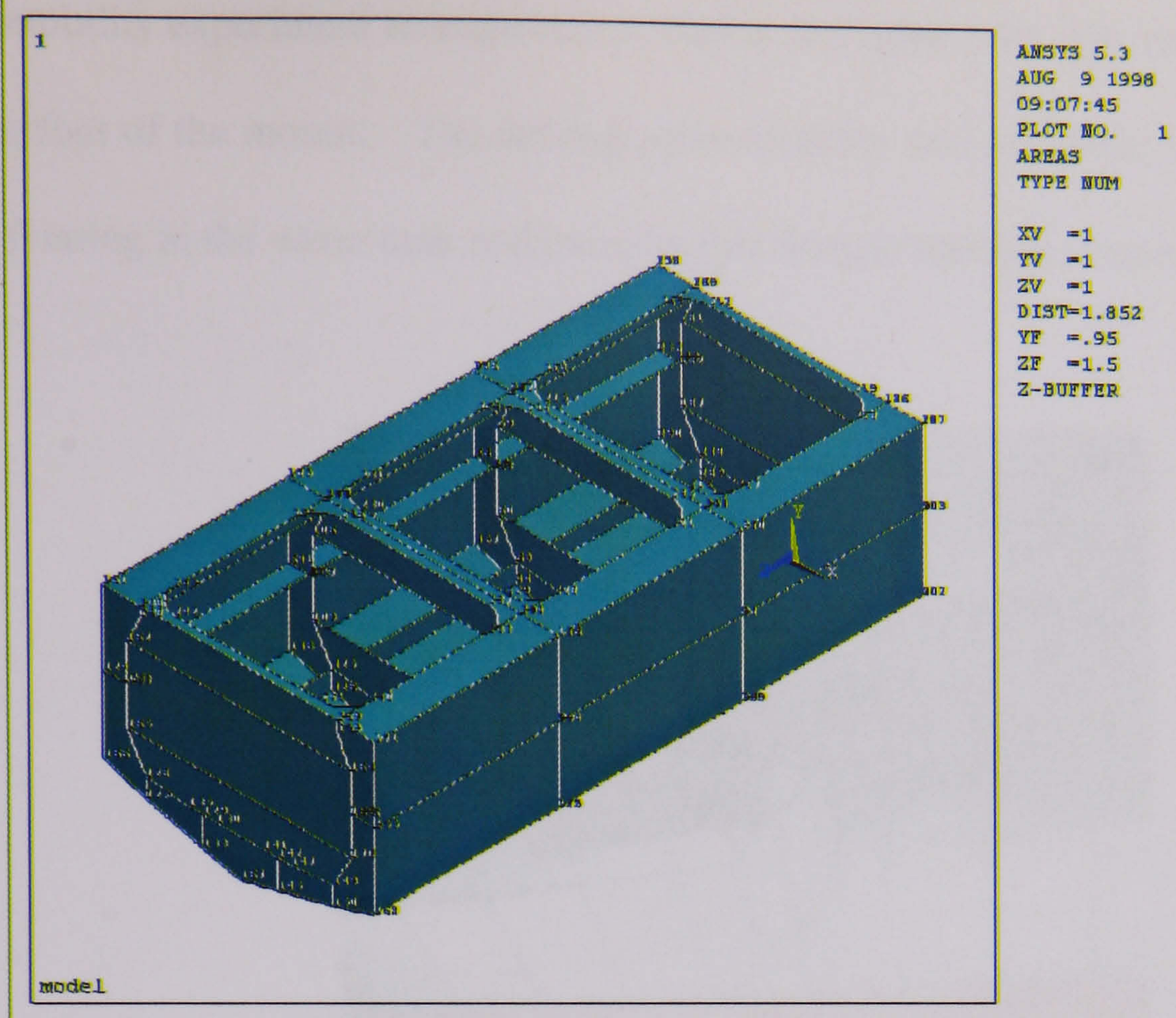

Figure 5.18 Geomentry of the experimental scale engine room model (I)

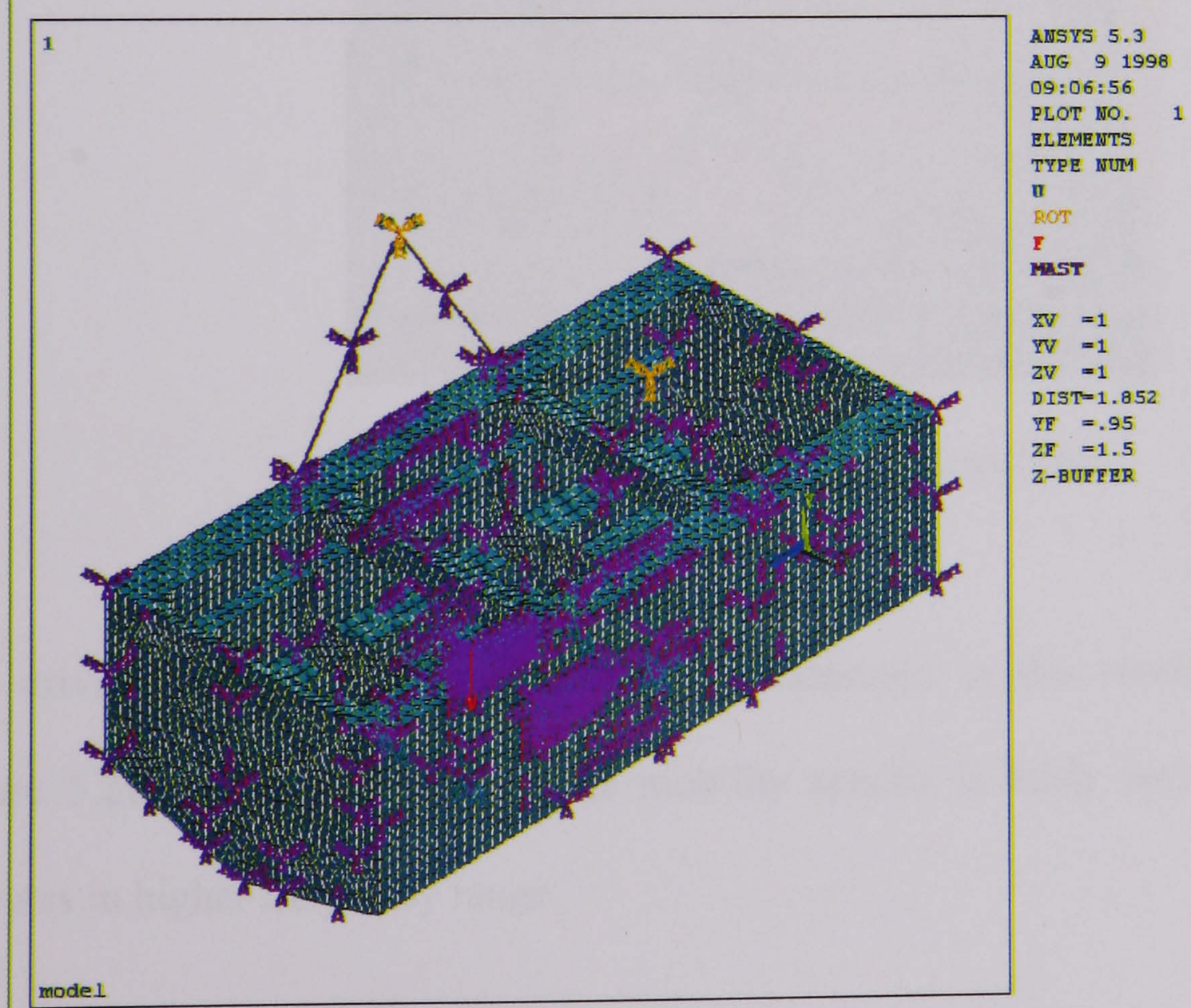

Figure 5.19 Mesh generation of the scale engine room mode (I).

The mobility experiment arrangement is shown in Figure 5.20. The driving point is located at the foot of the mount. The driving point mobility was measured when the scale model was floating in the water tank and hung by four bungie rope simultaneously.

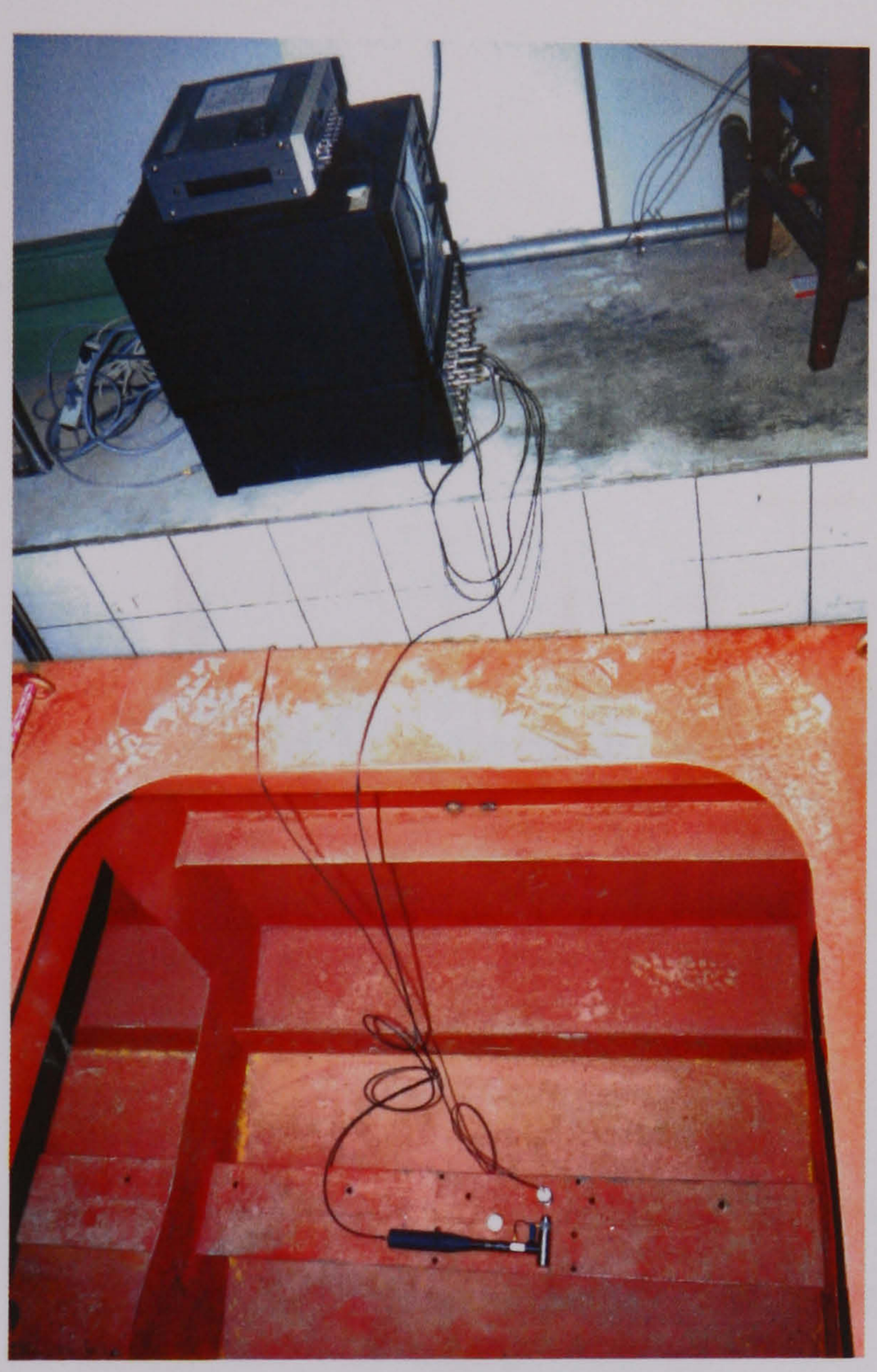

Figure 5.20 Experiment arrangement

The driving point mobilities predicted and measured in this condition is compared in Figure 5.21. The coincidence of the mobility spectra is fairly well below 550 Hz and deviates in higher frequency range.

Even in lower frequency range the measured mobility spectrum existed fluctuations deviated from the predicted spectrum curve. This illustrates the influence of the reflection

effect of the tank wall. Deviations in higher frequency range can be explained as that element size should be less than one tenth of the structure-borne wave length as a common practice, Cabos and Jokat (1998), i.e., the credible frequency range is below 450 Hz for the established FEA mesh model. Thus, it can be concluded that FEA is only suitable for mobility analysis in lower frequency range of the analysis and the one sixth rule is proved to be applicable.

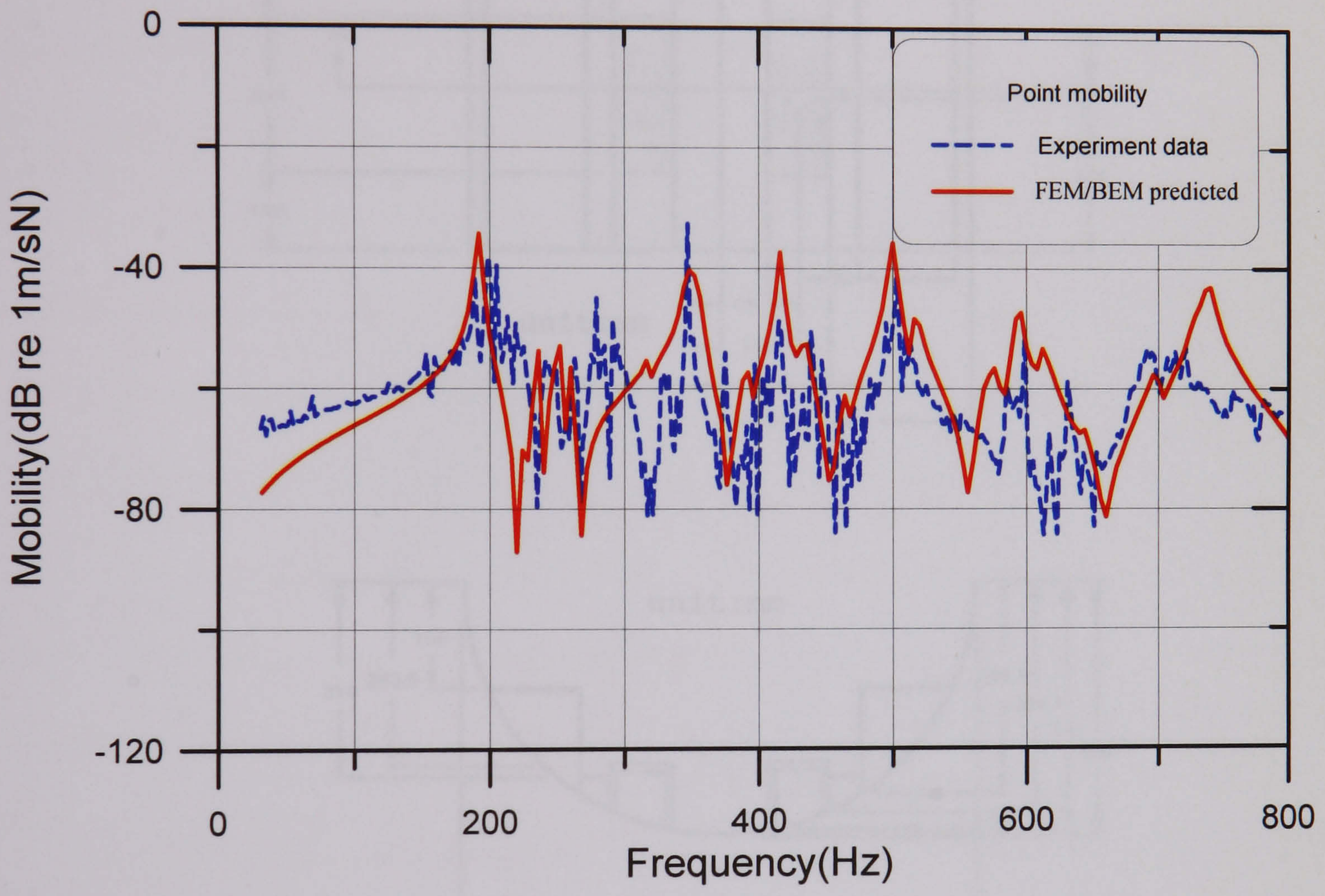

Figure 5.21 Comparison of the driving point mobility

5.2 Mobility Study of Scale Engine Room Model (II)

5.2.1 Description of the Experiment

In order to validate the accuracy of the mobility analysis and the FEM/BEM noise propagation models, experiments were undertaken on a smaller scale model of an engine room structure having a round bilge. This model with a length 808mm, is shown in Figure 5.22, consists of two end bulkheads, four girders on the bottom, one bilge tank on

each side. On the top of the girders there installed a bedplate and a stepless motor supported by four resilient mounts bolted on the bedplate. The motor was also designed with a deliberate eccentric mass on the shaft. The arrangement of mobility measurement is shown in Figure 5.23 and the configuration of the resilient mount used is the same as shown in Figure 5.4.

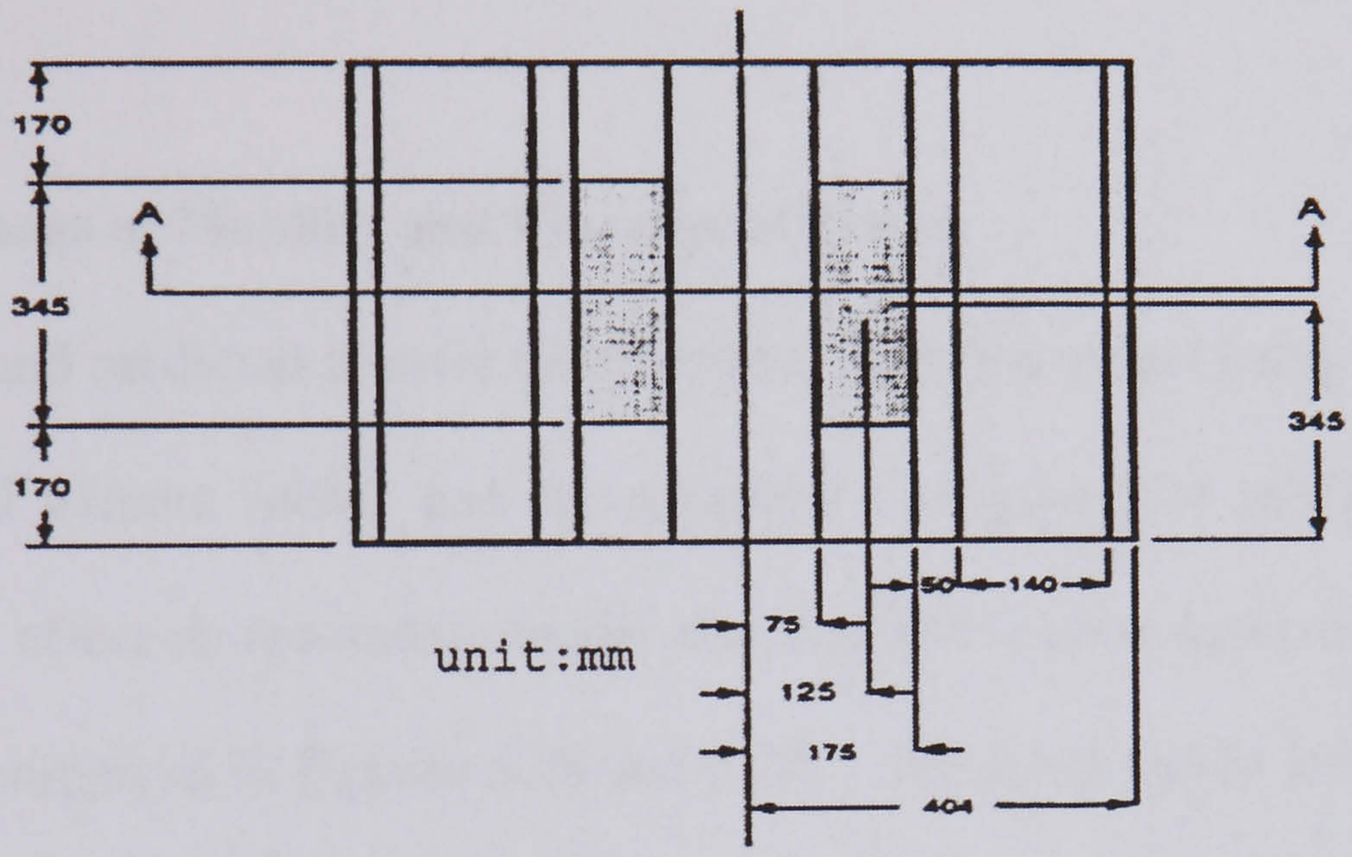

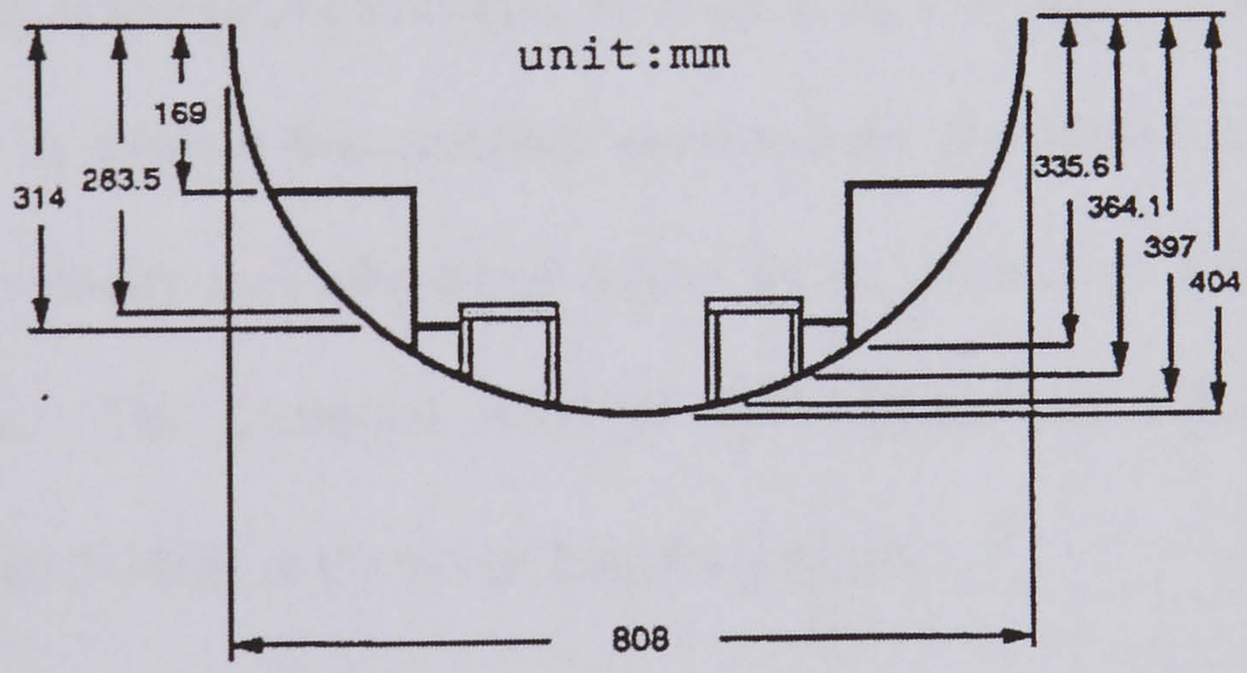

Figure 5.22 Scale engine room mode (II) for mobility measurement.

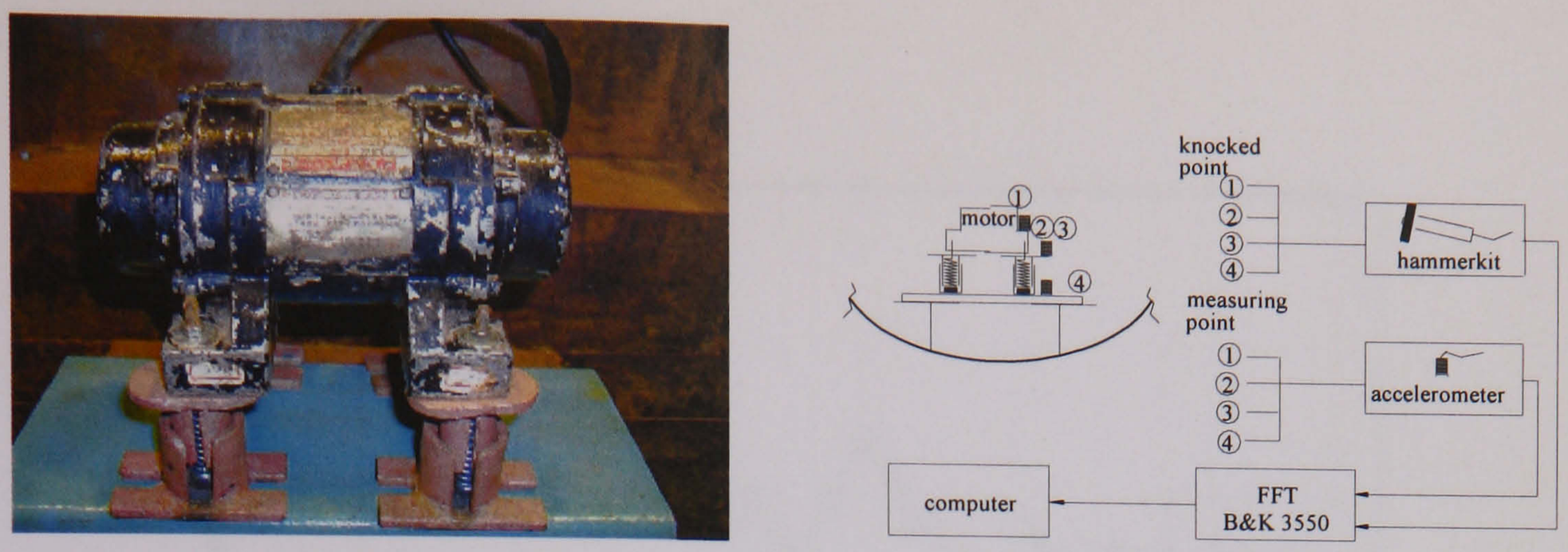

Figure 5.23 Instrument arrangement for mobility measurement

5.2.2 Comparisons of Mobility and Vibrational Power

The measured and predicted transfer mobility M_{41} when the model being put in water and in air with and without rubber pad are compared in Figure 5.24 to Figure 5.27. The resilient mount effect on measured transfer mobility of the same scale model (II) in water and in air are compared in Figures 5.28 and 5.29. When the motor ran at a speed 1800 rpm, the rubber pad effect on the exciting vibration velocity and the transfer power of the same acale model (II) at the input and output ends are shown in Figure 5.30 to Figure 5.37. From the results, it is evident that resilient mounts have the effects to reduce transfer mobility, vibratory velocity and vibrational power by an amount of 5-20dB, 2-5dB and 10-40% respectively. The entrained mass of water apparently reduced the transfer mobility by an amount 5-10dB in the lower frequency range.

Detail discussions regarding the accuracy analysis of the mobility model applying to the scale model (II) and the quantitative analysis of the effect of the fluid-structure interaction on the structure-borne vibration propagation are given in Sections 7.1.1 and 7.1.5 of Chapter 7 respectively.

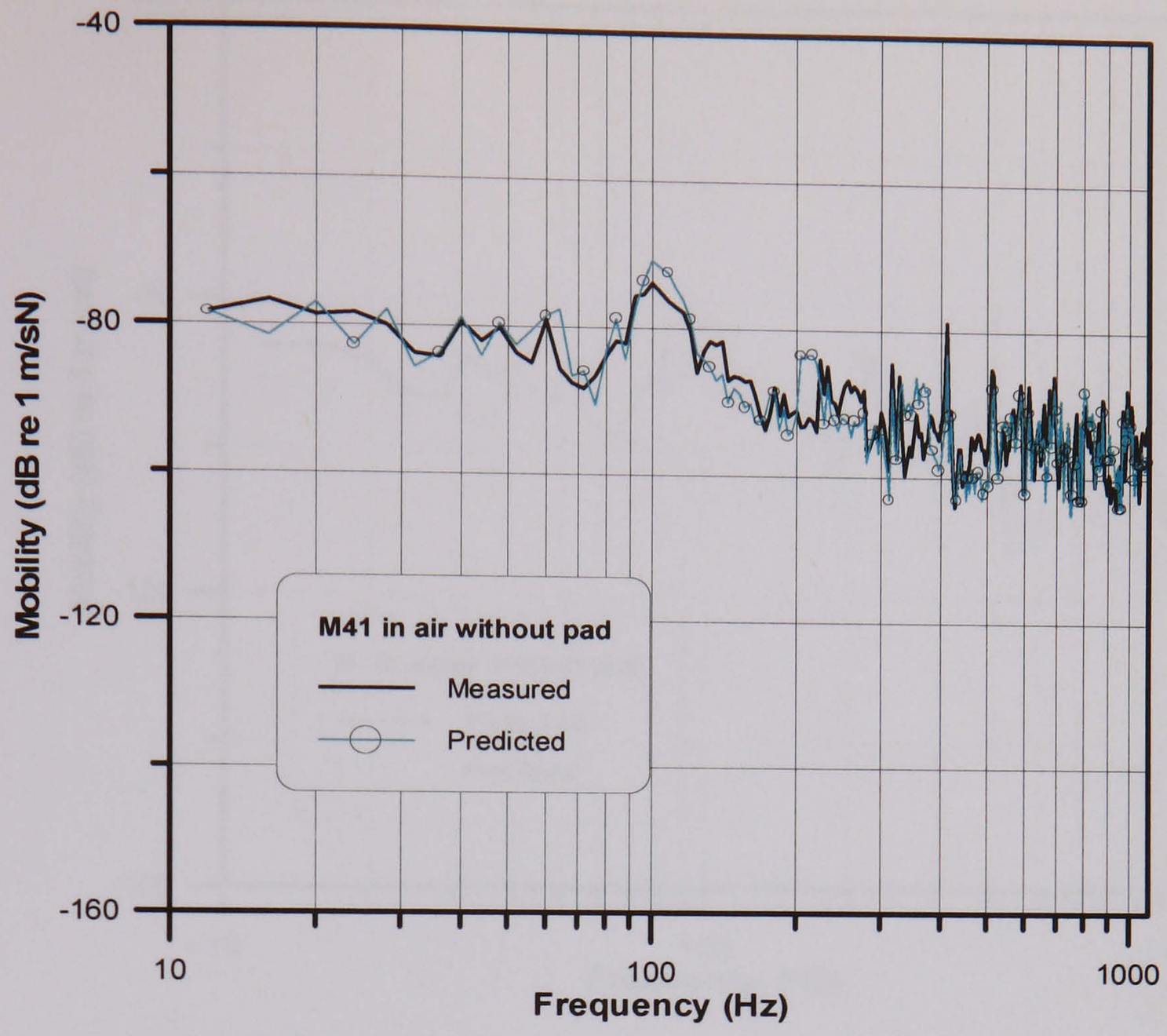

Figure 5.24 Comparison of transfer mobility M_{41} in air without rubber pad in resilient mount

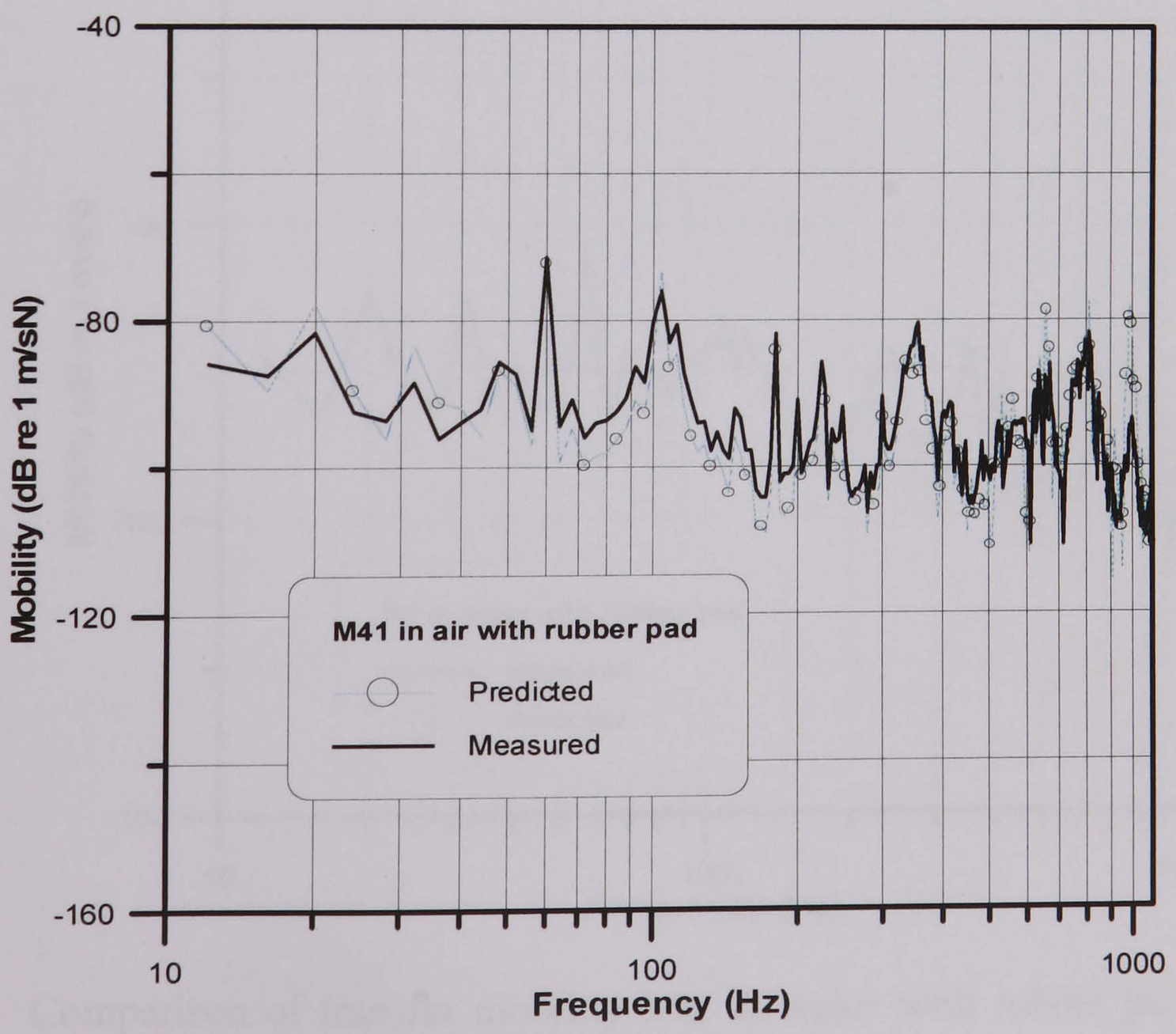

Figure 5.25 Comparison of transfer mobility M_{41} in air with rubber pad in resilient mount

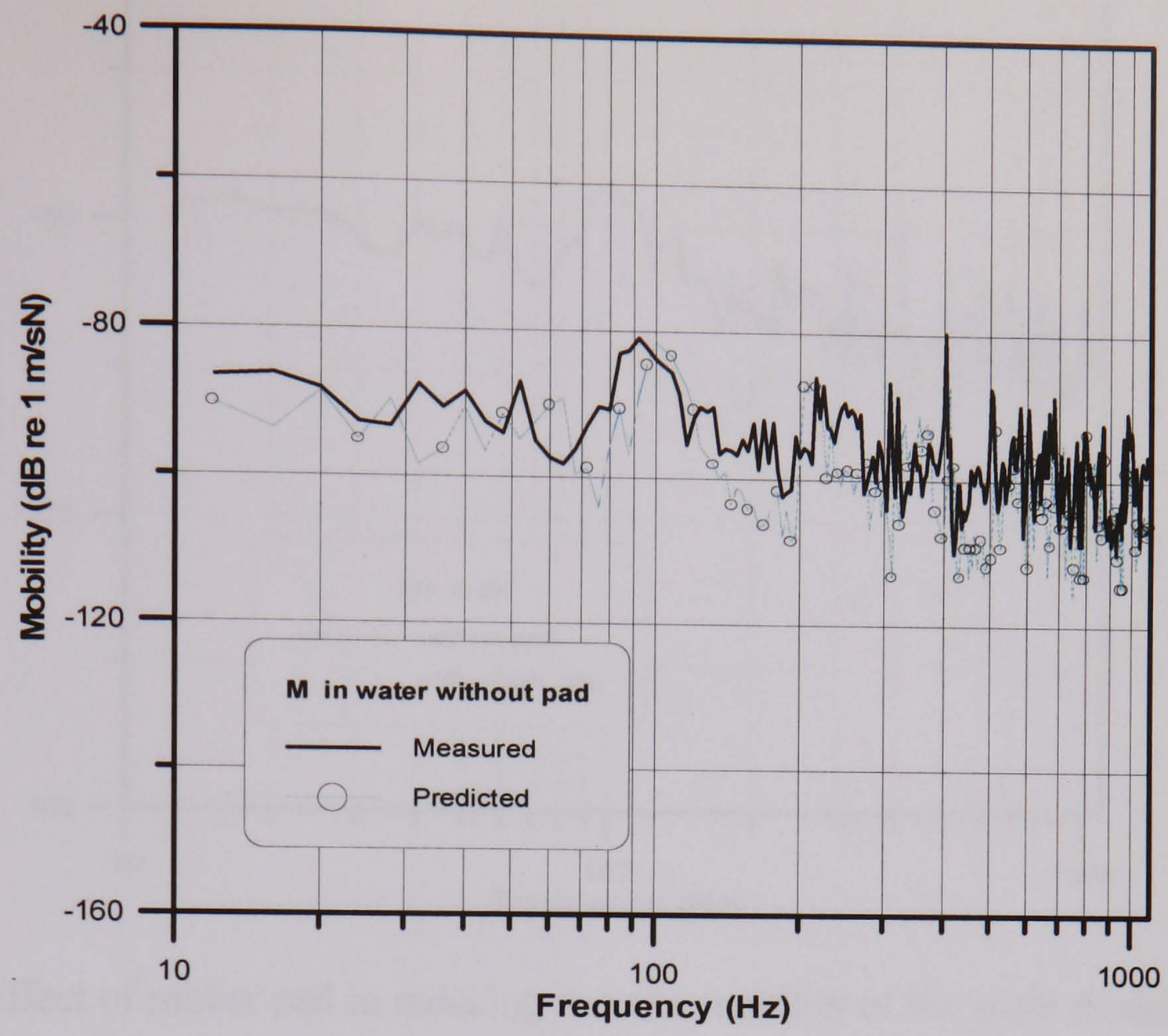

Figure 5.26 Comparison of transfer mobility M_{41} in water without rubber pad in resilient mount

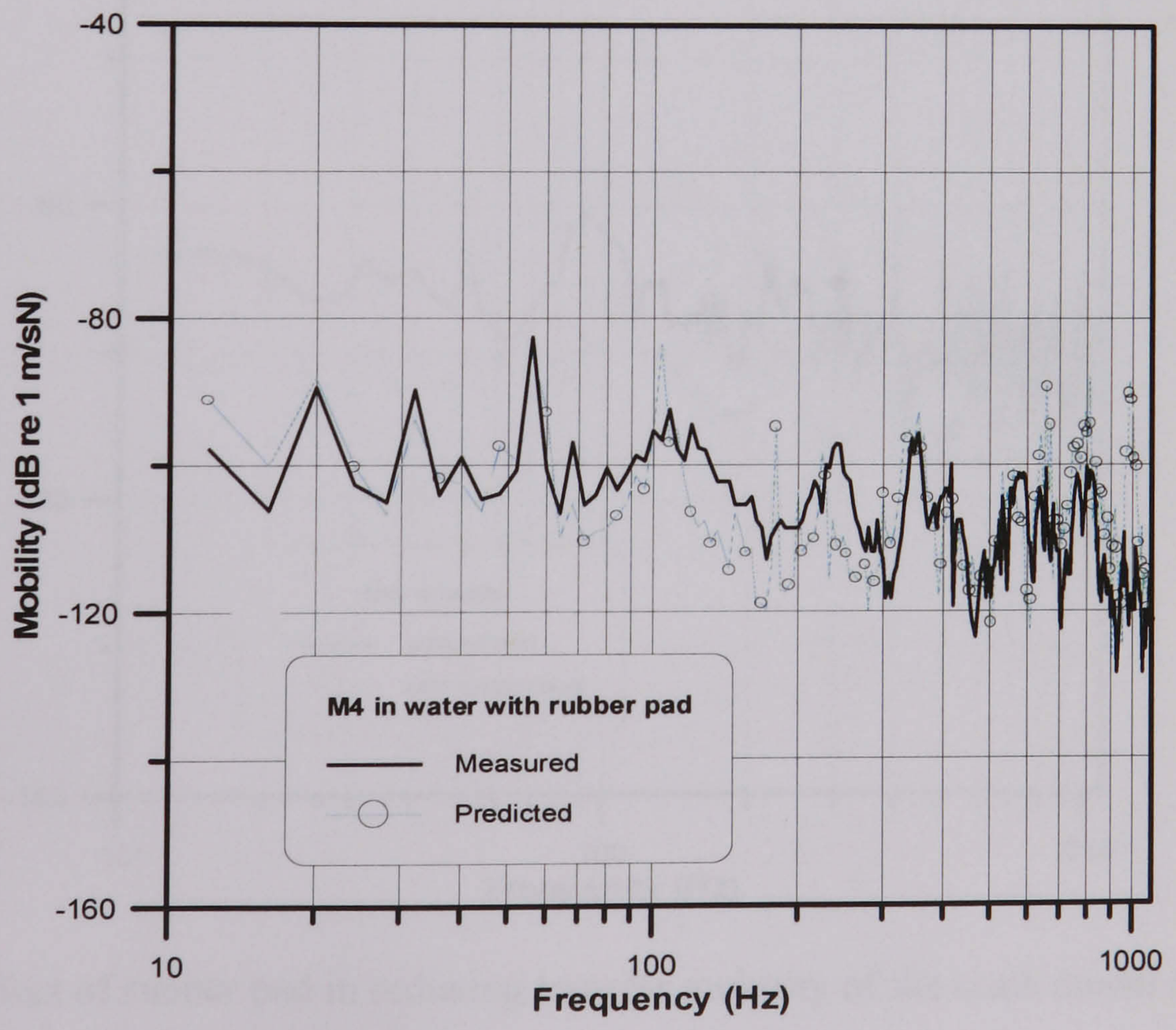

Figure 5.27 Comparison of transfer mobility M_{41} in water with rubber pad in resilient mount

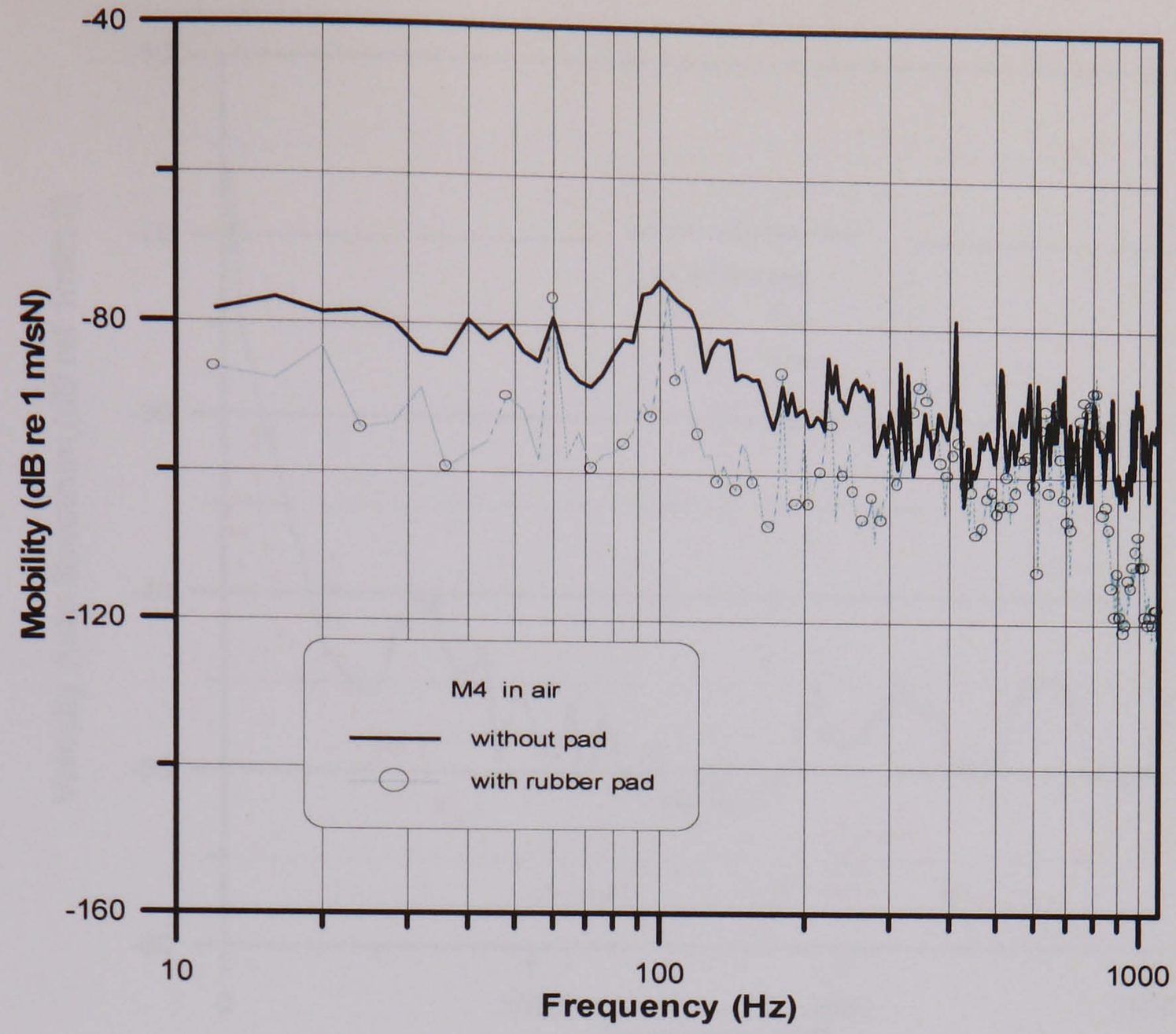

Figure 5.28 Effect of rubber pad in reducing transfer mobility of the scale model (II) hung in air.

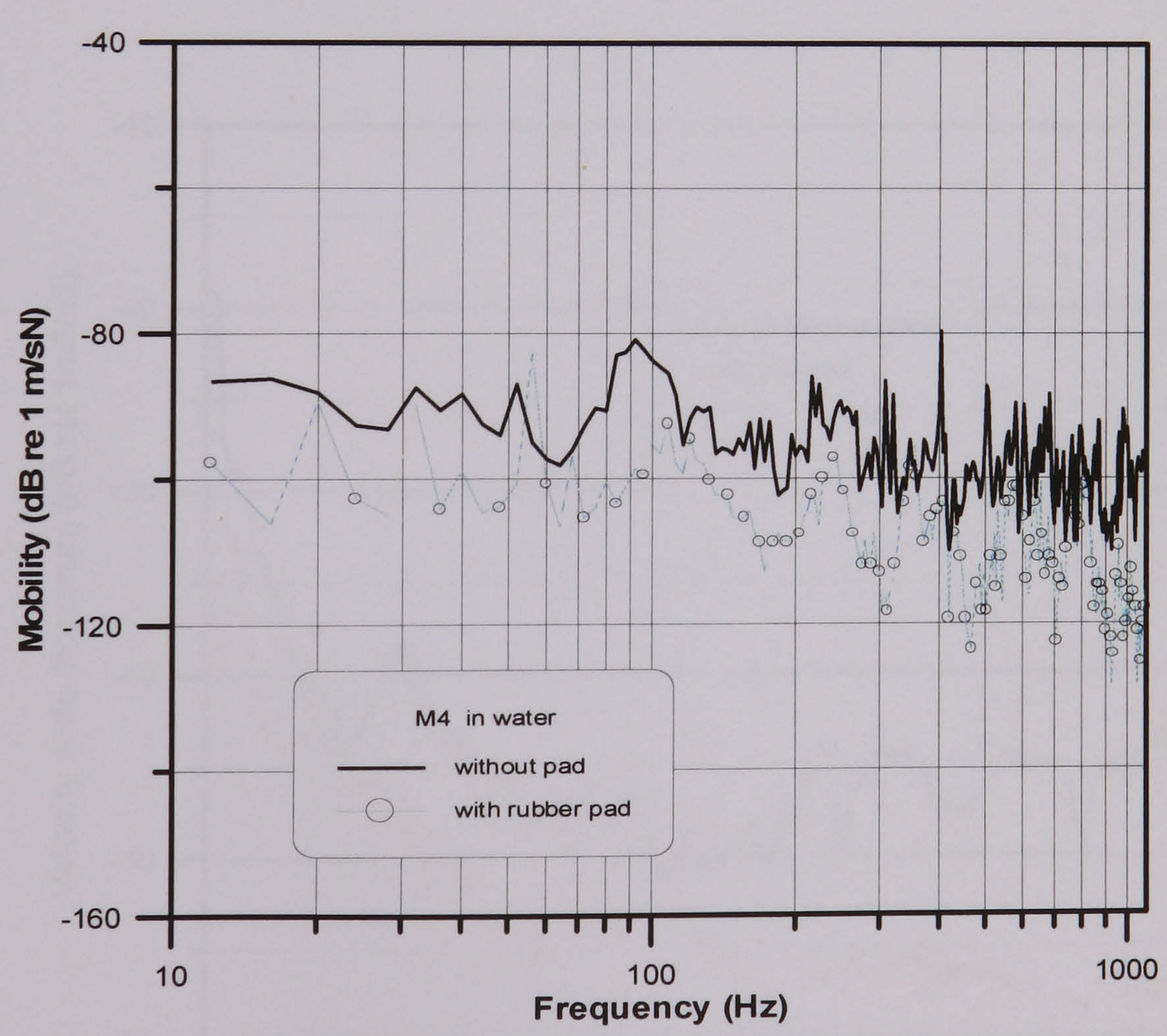

Figure 5.29 Efect of rubber pad in reducing transfer mobility of the scale model (II) floated in water tank

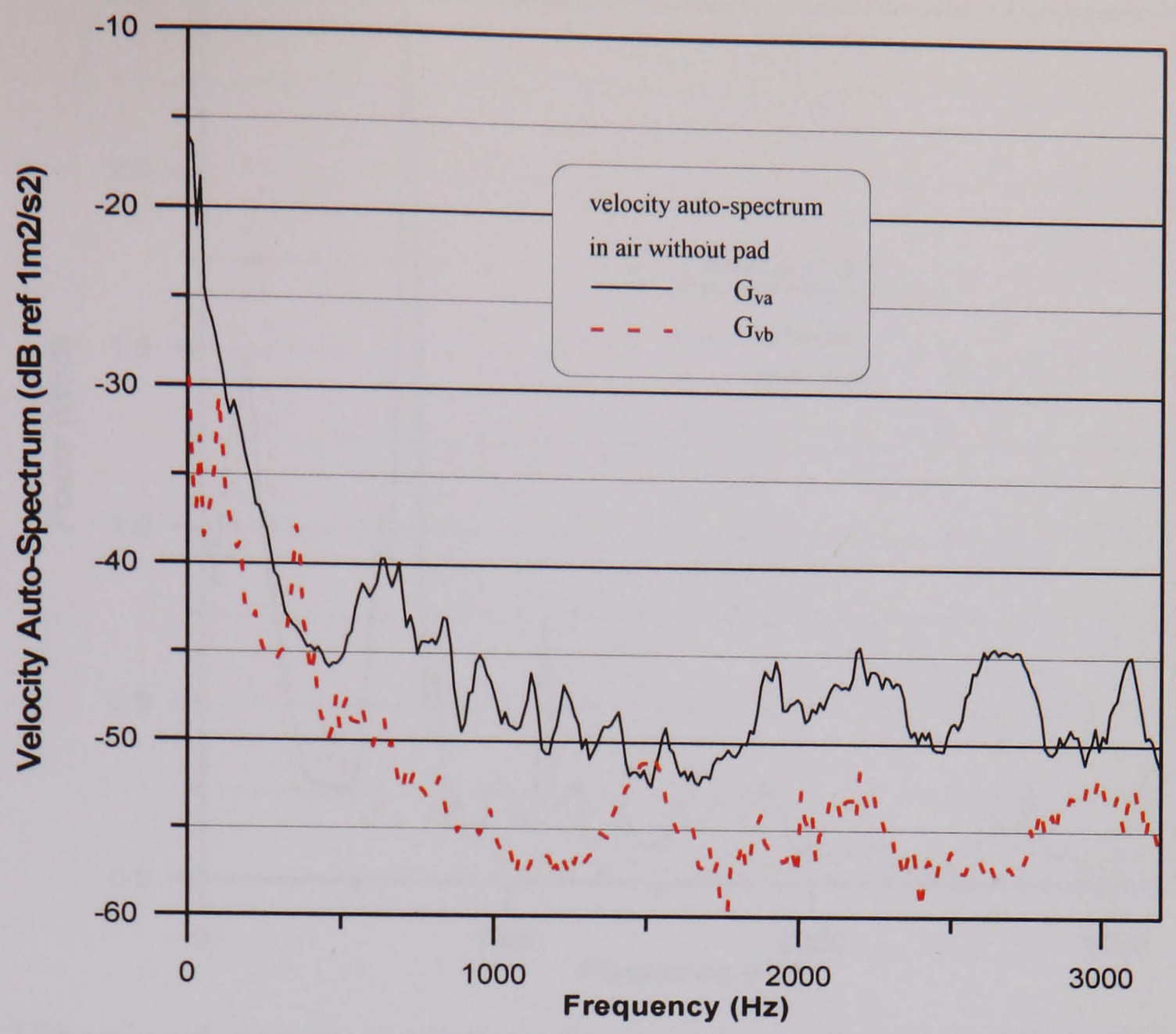

Figure 5.30 Velocity auto-spectra in air at input and out sides of the resilient mount without rubber pad

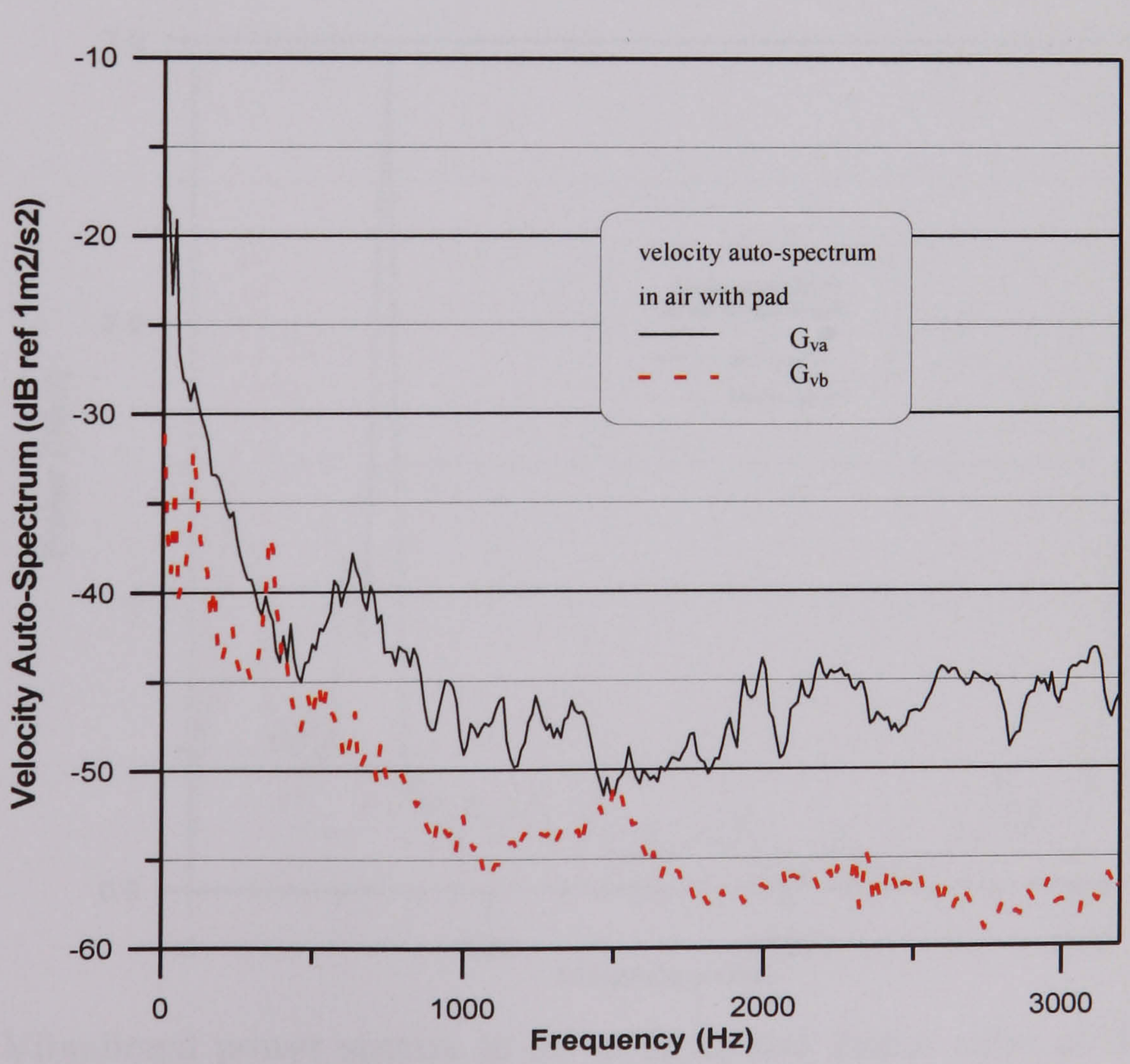

Figure 5.31 Velocity auto-spectra in air at input and out sites of the resilient mount with rubber pad

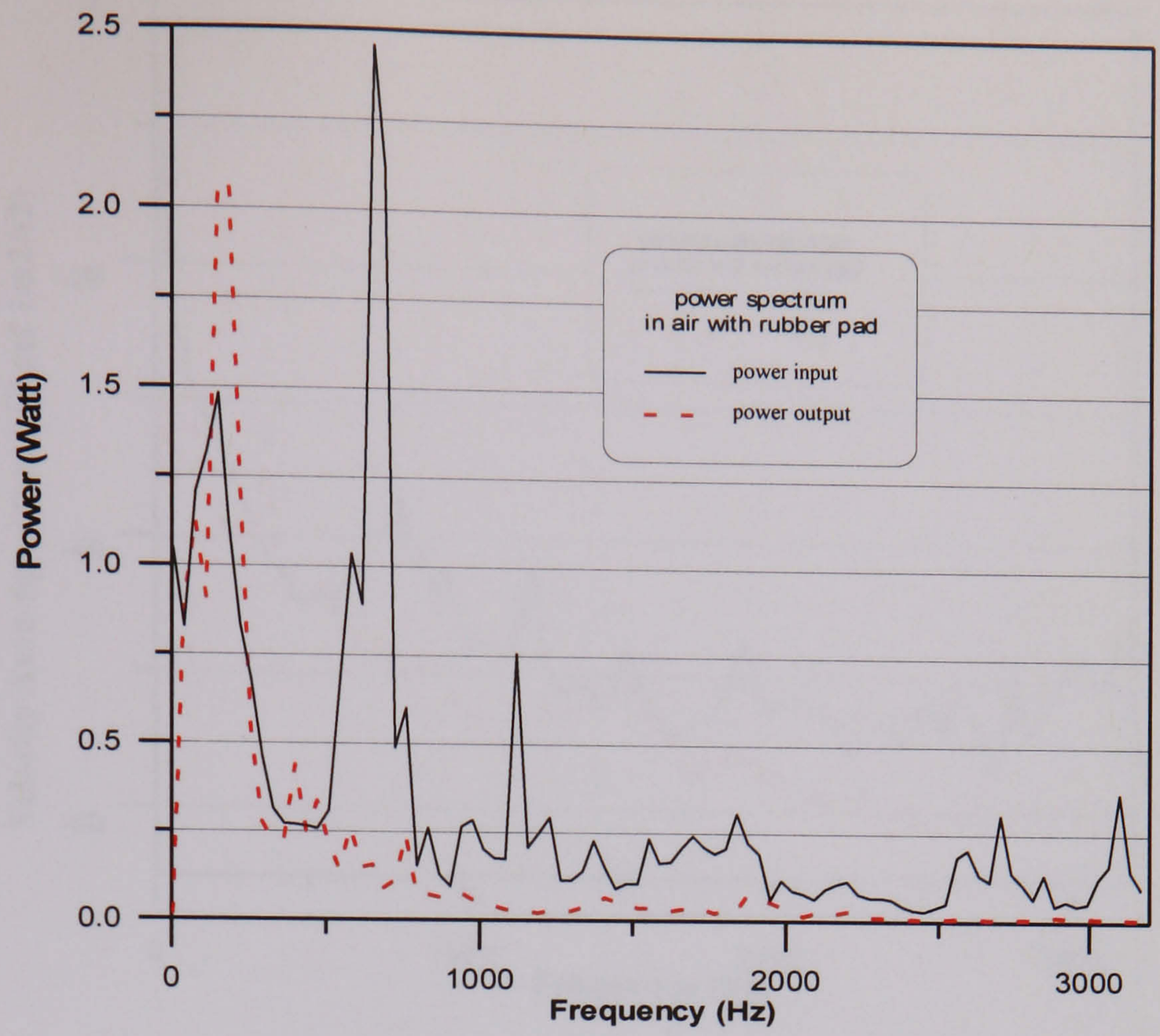

Figure 5.32 Vibrational power spectra in air at input and output sides of the resilient mount with rubber pad.

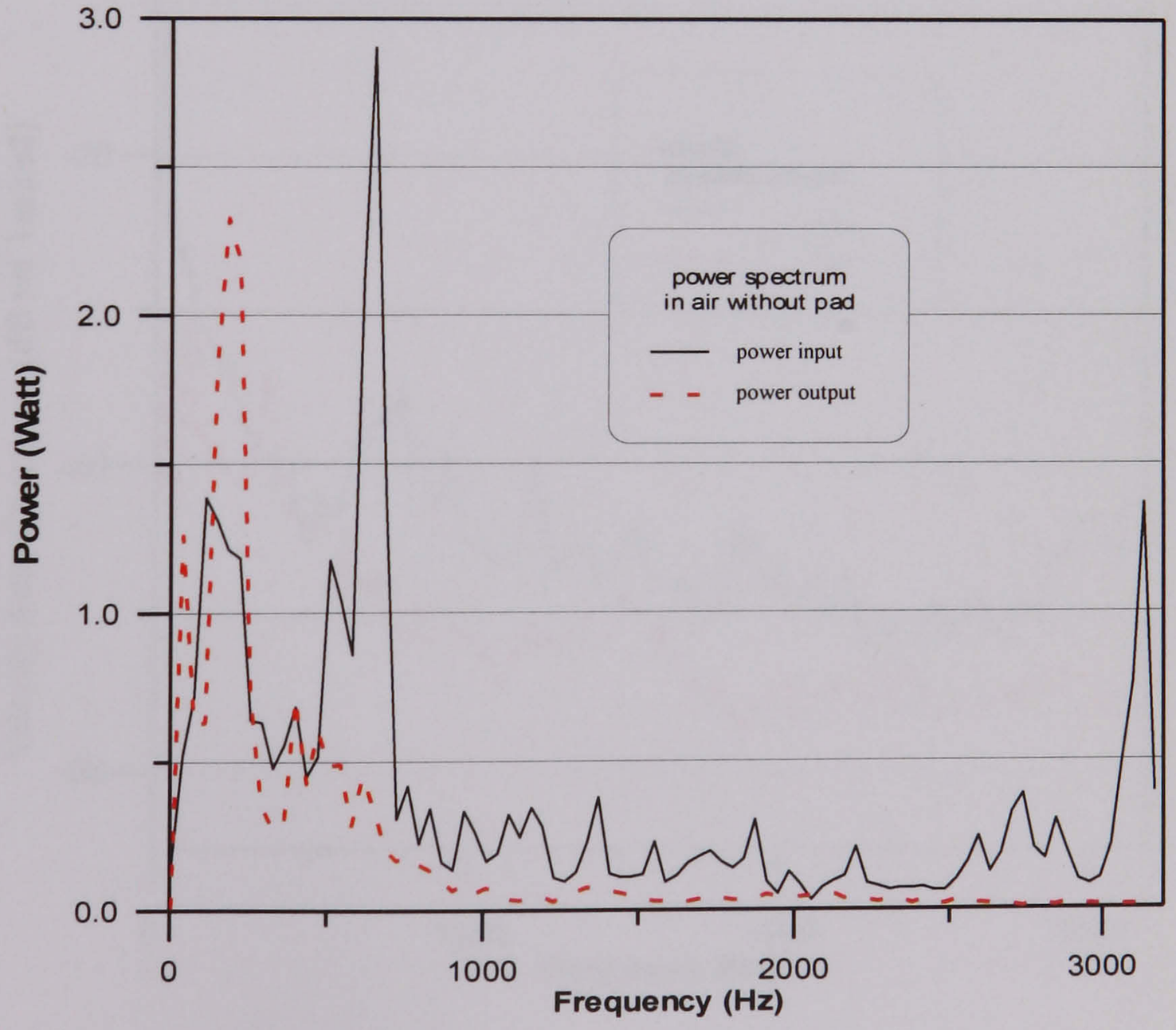

Figure 5.33 Vibrational power spectra in air at input and output sides of the resilient mount without rubber pad.

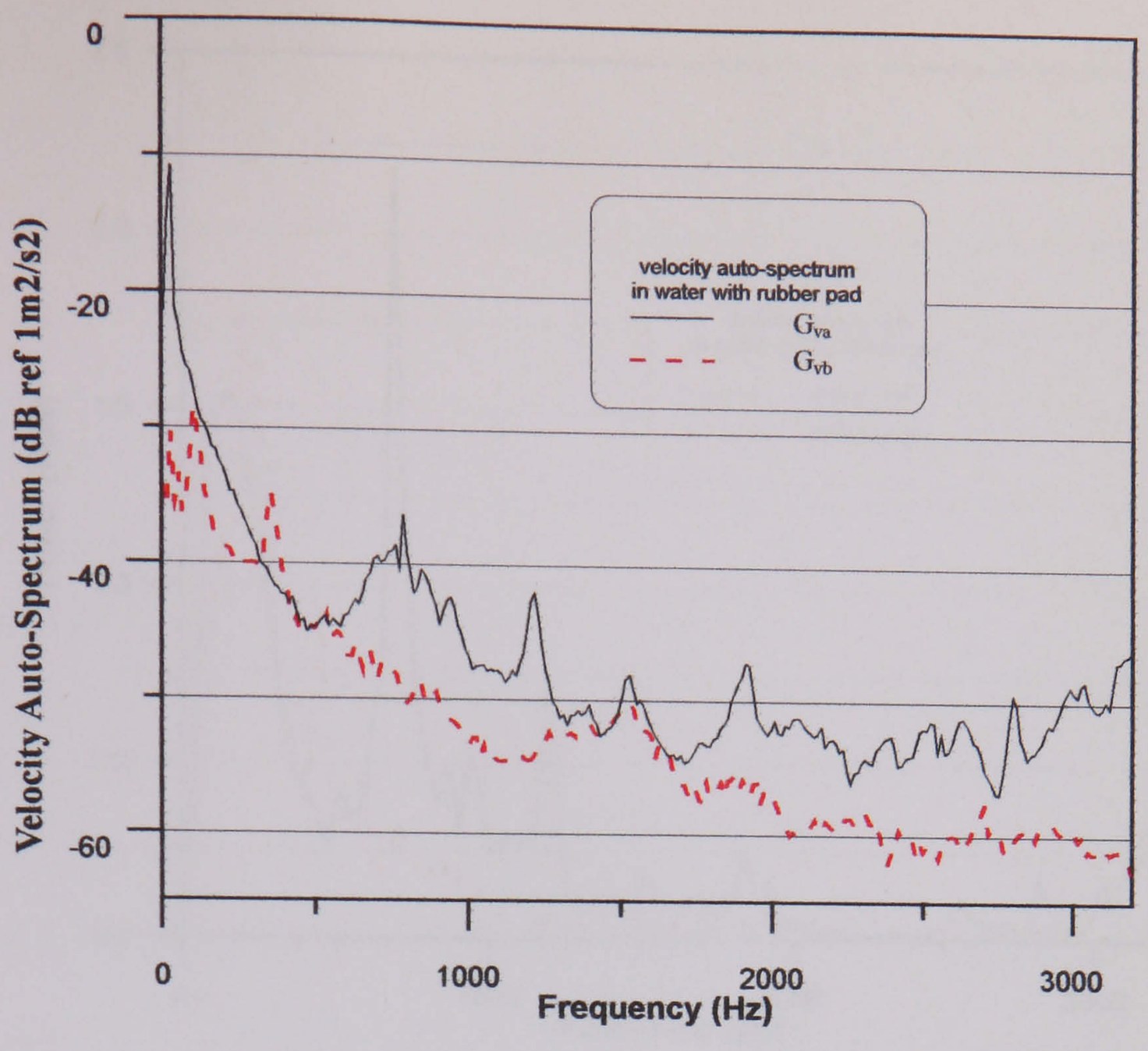

Figure 5.34 Velocity auto-spectra in water at input and output sides of the resilient mount with rubber pad

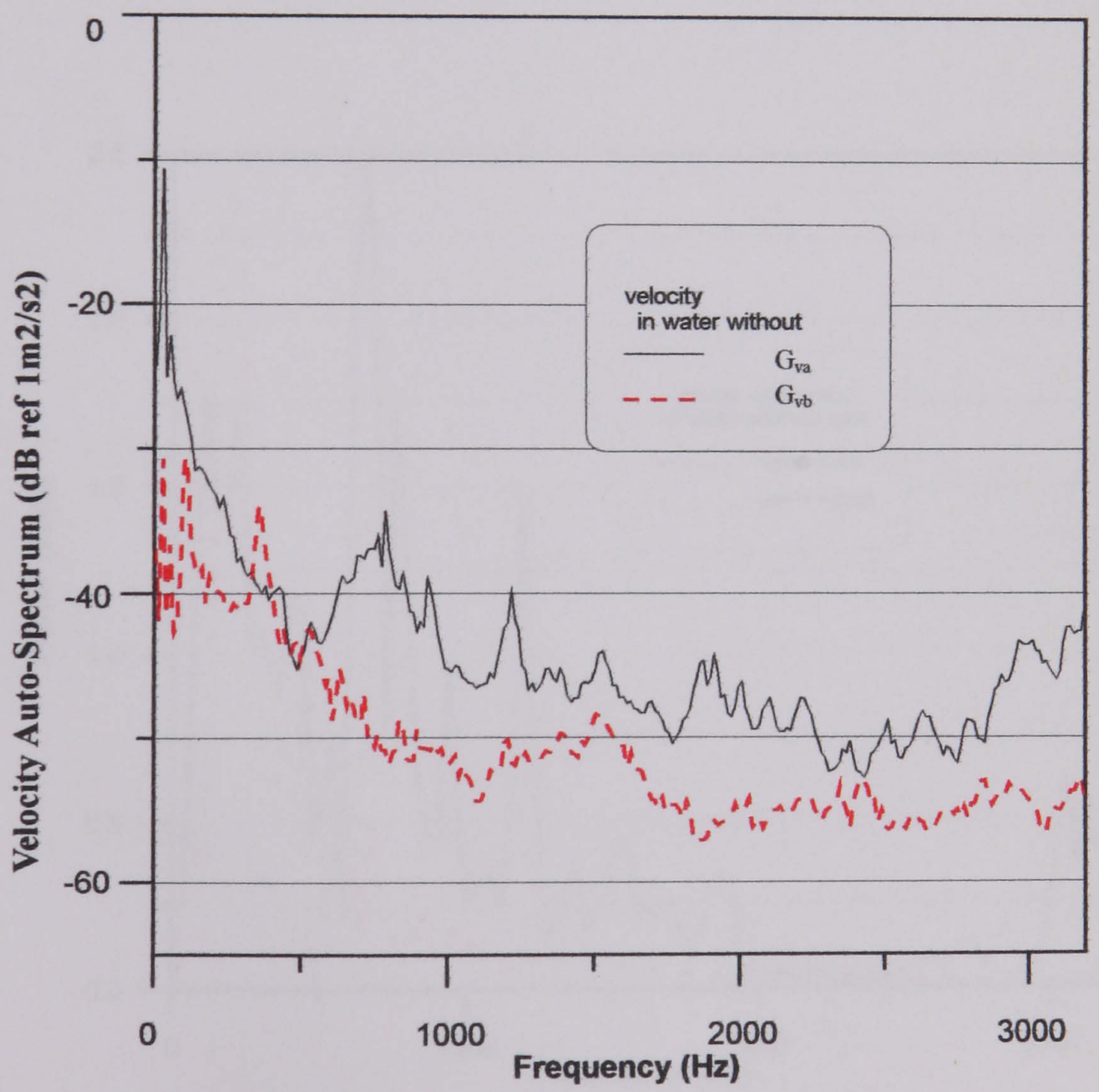

Figure 5.35 Velocity auto-spectra in water at input and output sides of the resilient mount without rubber pad

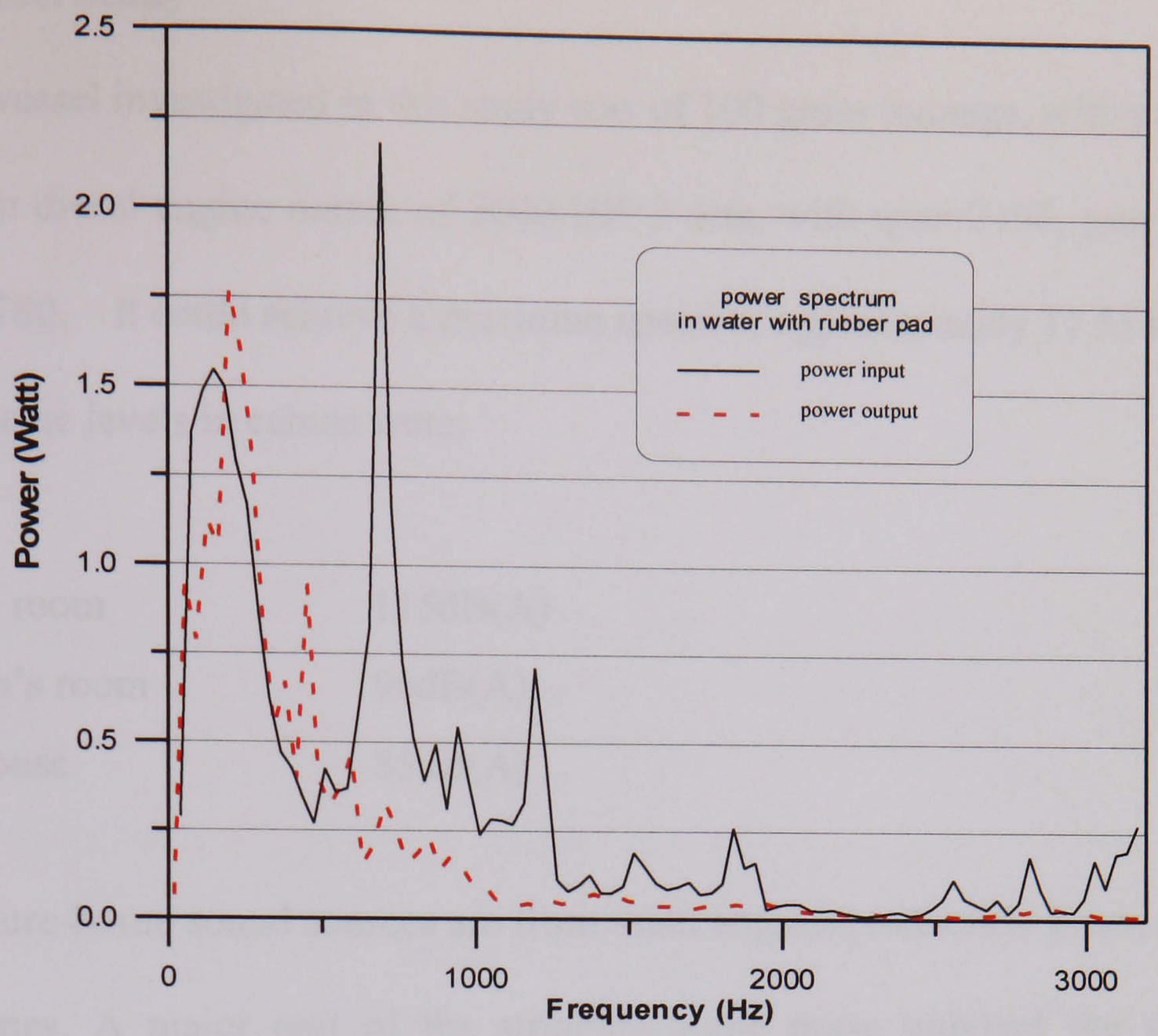

Figure 5.36 Vibrational power spectra in water at input and output sides of the resilient mount with rubber pad.

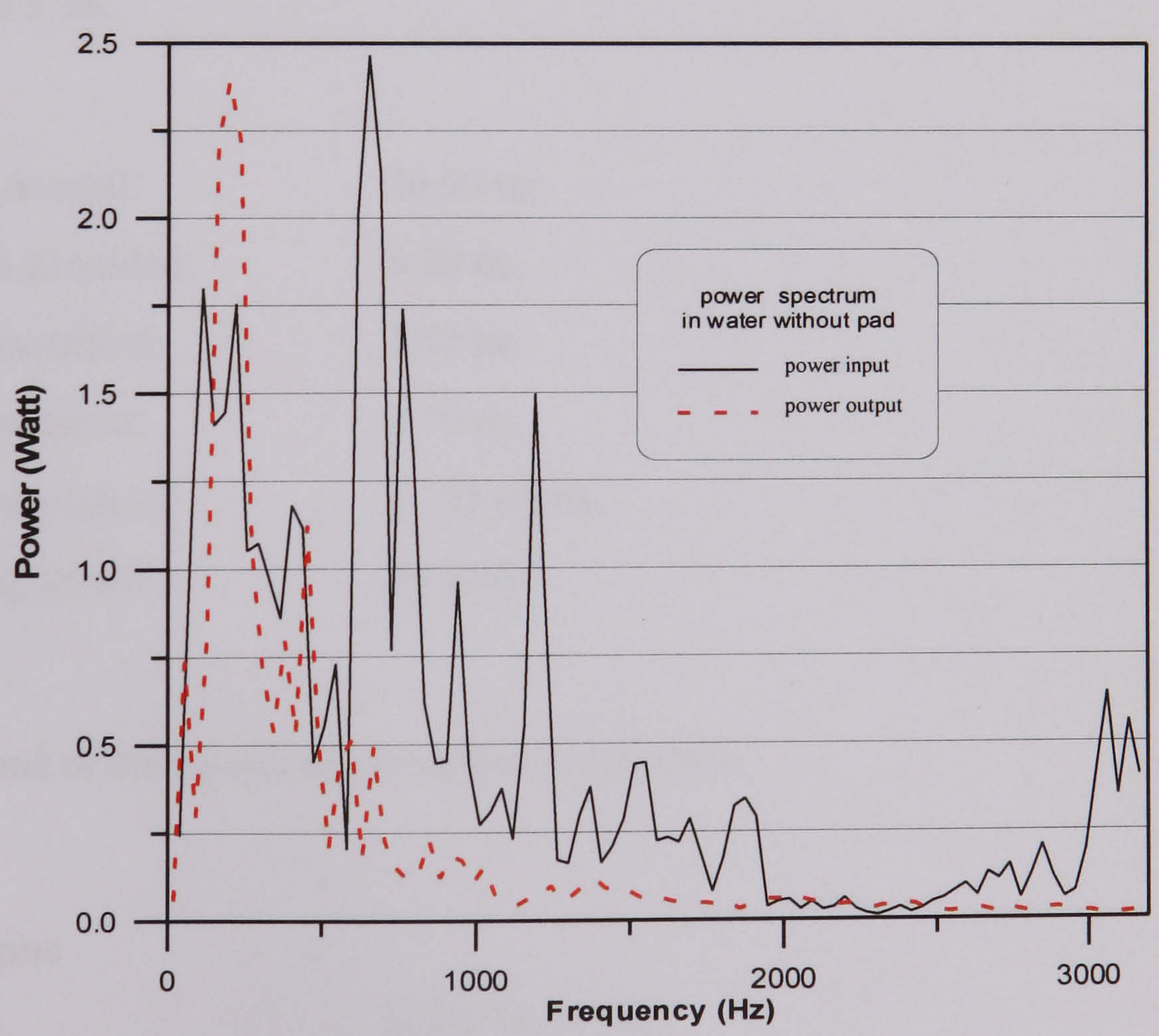

Figure 5.37 Vibrational power spectra in water at input and output sides of the resilient mount without rubber pad.

5.3 Patrol Vessel Study

The fast patrol vessel investigated in this study was of 100 gross tonnage, with a maximum continuous main diesel engine output of 3000 HP*2 sets, with rpm=2100, gear ratio=2.7, and shaft rpm=780. It could achieve a maximun speed of approximately 31.55 knots. The measured noise levels in cabins were:

engine room	115dB(A)
captain's room	90dB(A)
pilothouse	85dB(A)

The main structure-borne sound sources are from main engines, reduction gears, generators and exhaust pipes. A major part of the structure-borne noise onboard the vessel was identified to be the main engine vibration transmitted via the mounts (Wang, 1996). The principal particulars of the vessel are listed and the general arrangement of the vessel is shown as Figure 5.38.

length overall:	30.50 m;
breadth moulded:	6.80 m;
depth moulded:	3.55 m;
draft moulded:	1.70 m;
maximun speed:	31.55 knots;
cruising speed:	28 knots.

The specifications of the machinery in engine room were:

Main diesel engine

model:	MTU 16 V 396;
revolution speed:	2100 rpm
continuous rating:	3000 HP * 2 sets;
weight:	7.5 tons × 2 sets.

Generator

revolution speed:	1900 rpm
output:	23 kW*2 sets.

Reduction gear

reduction gear ratio:	2.7;
shaft speed:	780rpm;
type:	V drive.

In order to attenuate the noise level in the cabins of the vessel, one of the measures adopted to reduce the structure-borne noise transmission from the main diesel engines was to install squeeze plates to the web of the engine girders. The squeeze-film damping technique and the prediction of its loss factor were developed by Chow and Pinnington (1982 and 1985). Each squeeze plate used is a rectangular steel plate of dimensions 300 mm long, 200 mm wide and 1 mm thick and tack welded to the web, at its corners, beneath the engine mounts. Figure 5.39 shows the locations of these squeeze plates. When the squeeze plate and the web vibrate out-of-phase with each other or in different wave length, then it forms a air pumping effect, with the alternative action to squeeze the air in between the plates out and attract the outer air in, so as to dissipate the vibrational energy.

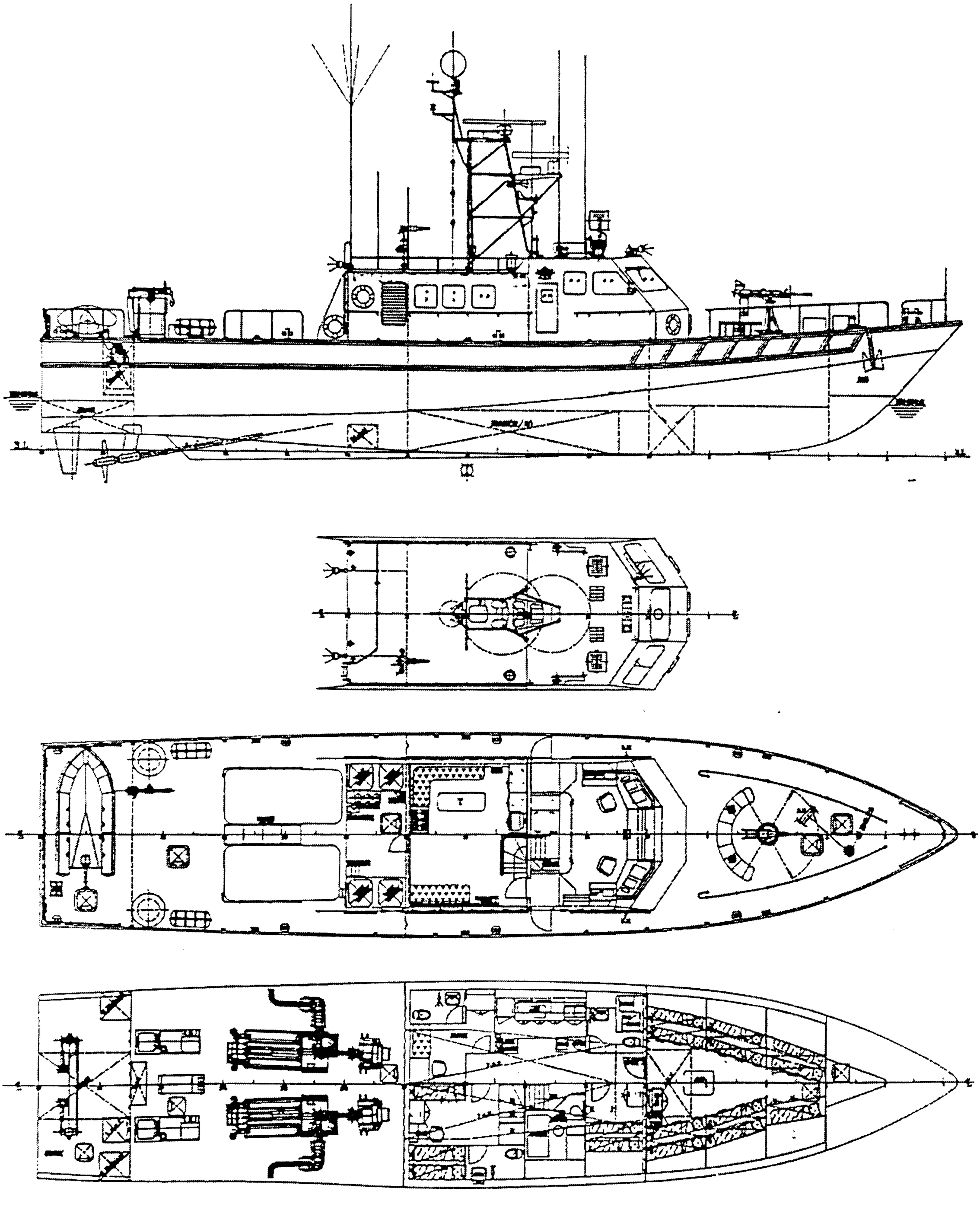

Figure 5.38 General arrangement if a fast vessel

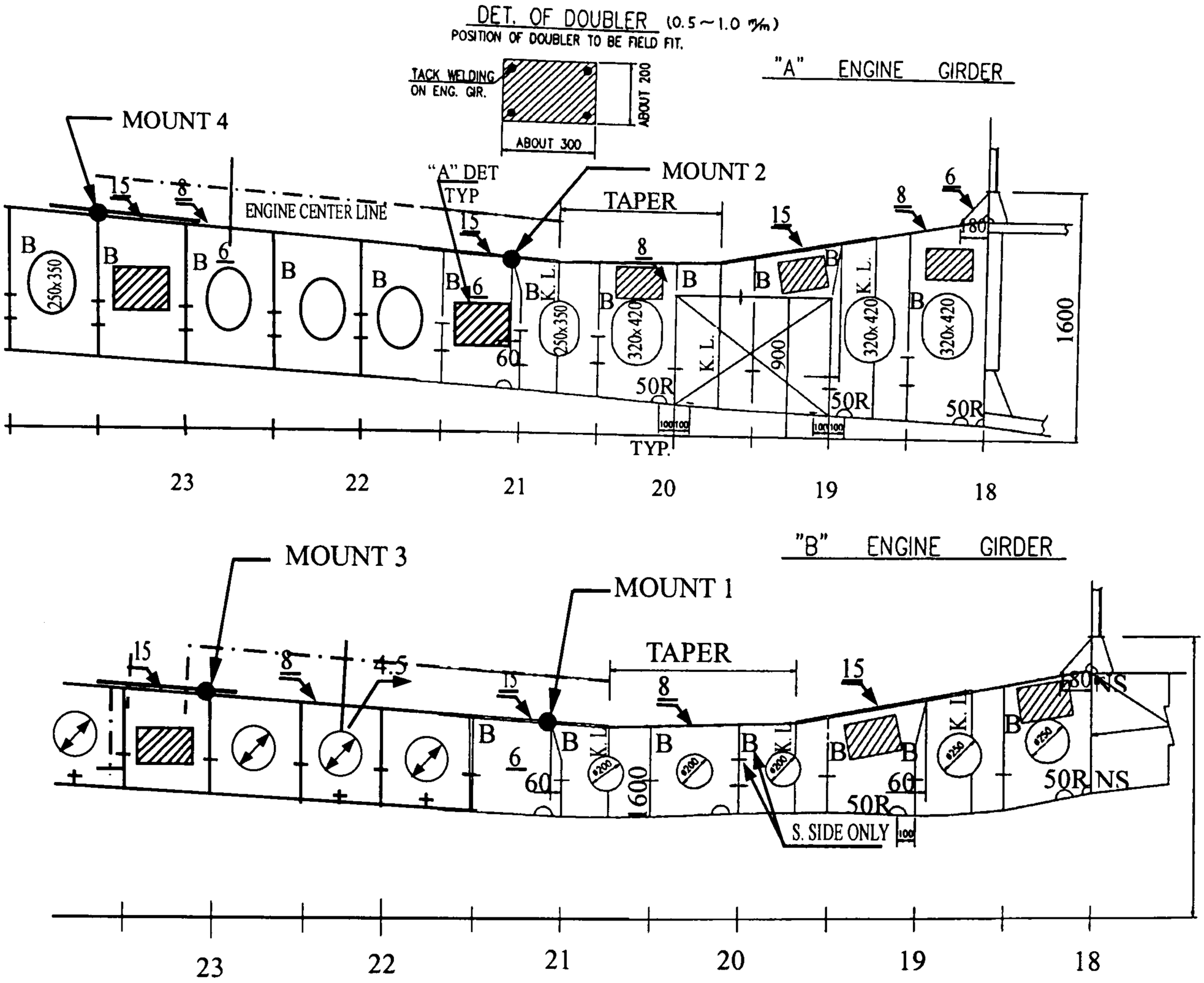

Figure 5.39 Locations of the spot welded squeeze plates to engine girders.

To perform the mobility reduction analysis, concentration is put on the bottom of engine room, as shown in Figure 5.40, since it is the structure part, close to the excitation source of the main desiel engines. The FE mesh generation including shell elements and beam elements is shown in Figure 5.41.

The inuput data fed to ANSYS were:

thickness of plate elements	: 1.5, 3, 4.5, 5, 6, 8, 10, 15 mm
density of material	: 7850 kg/m^3
Young's modulus	: 2.1×1011 N/m^3
Poisson's ratio	: 0.3
number of nodes	: 5281
number of shell elements	: 7260
number of beam elements	: 1249
number of master degrees of freedom	: 500

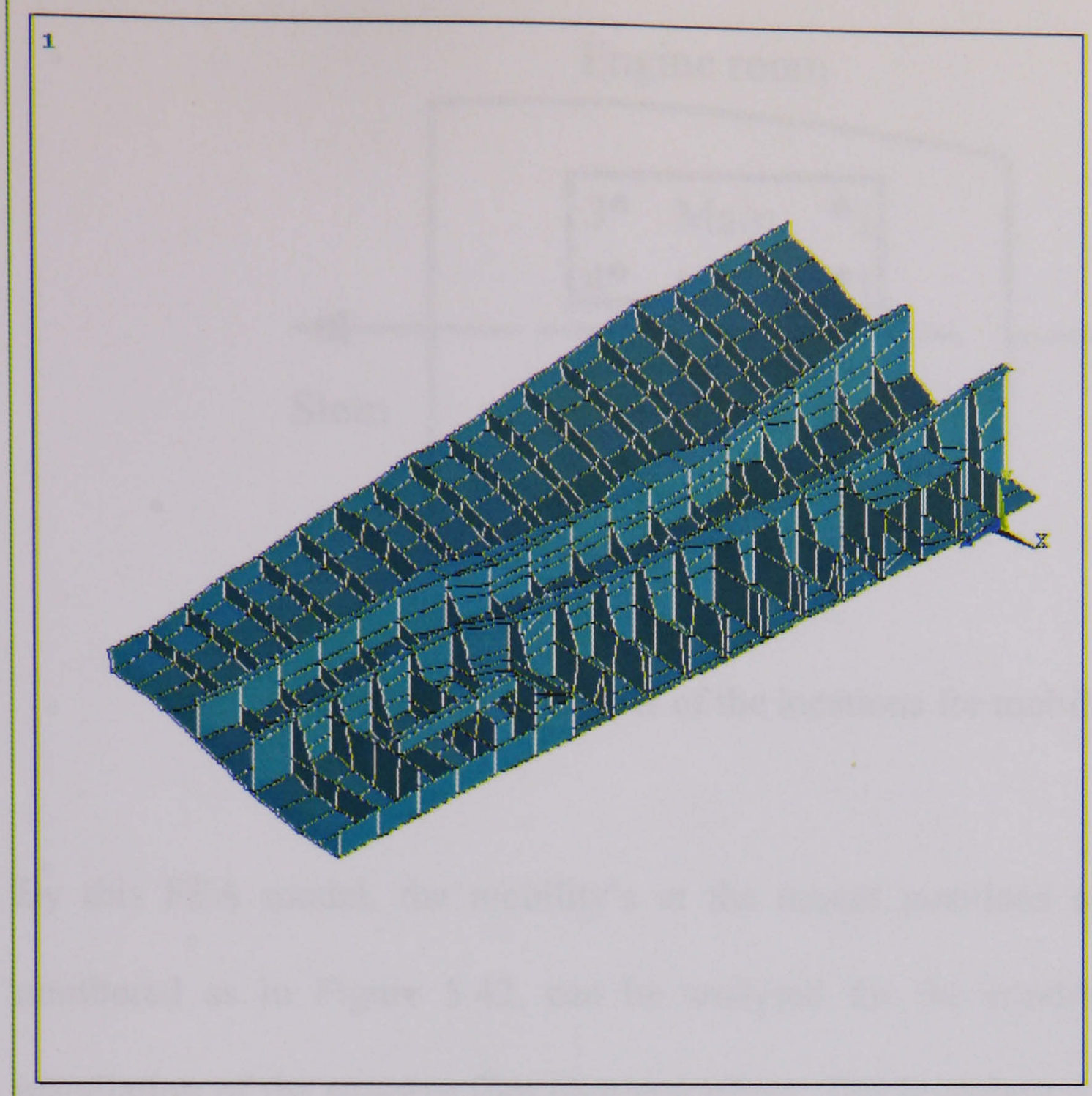

Figure 5.40 Bottom structure of the engine room of the patrol vessel

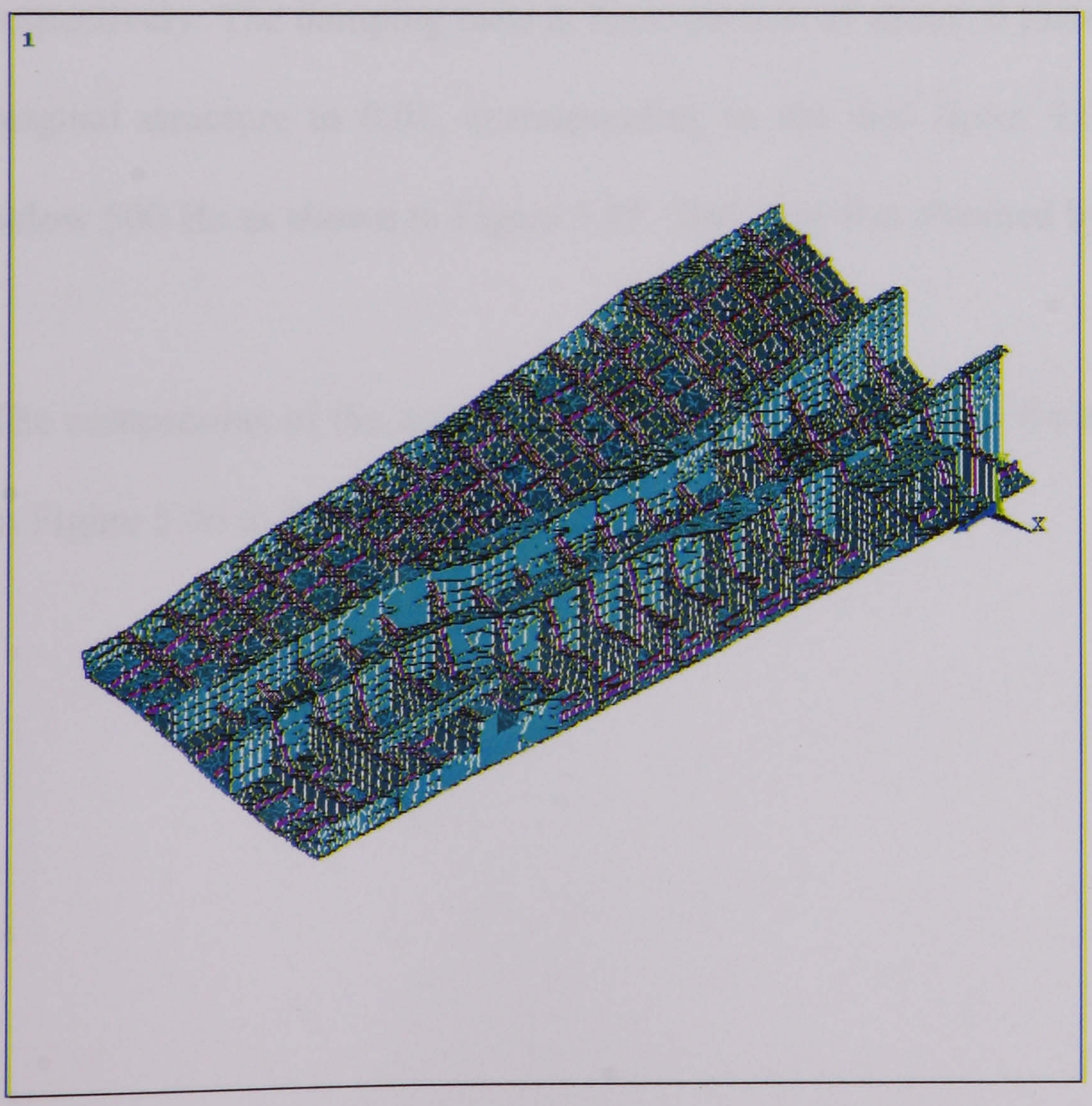

Figure 5.41 FEA model of the engine room bottom of the patrol vessel

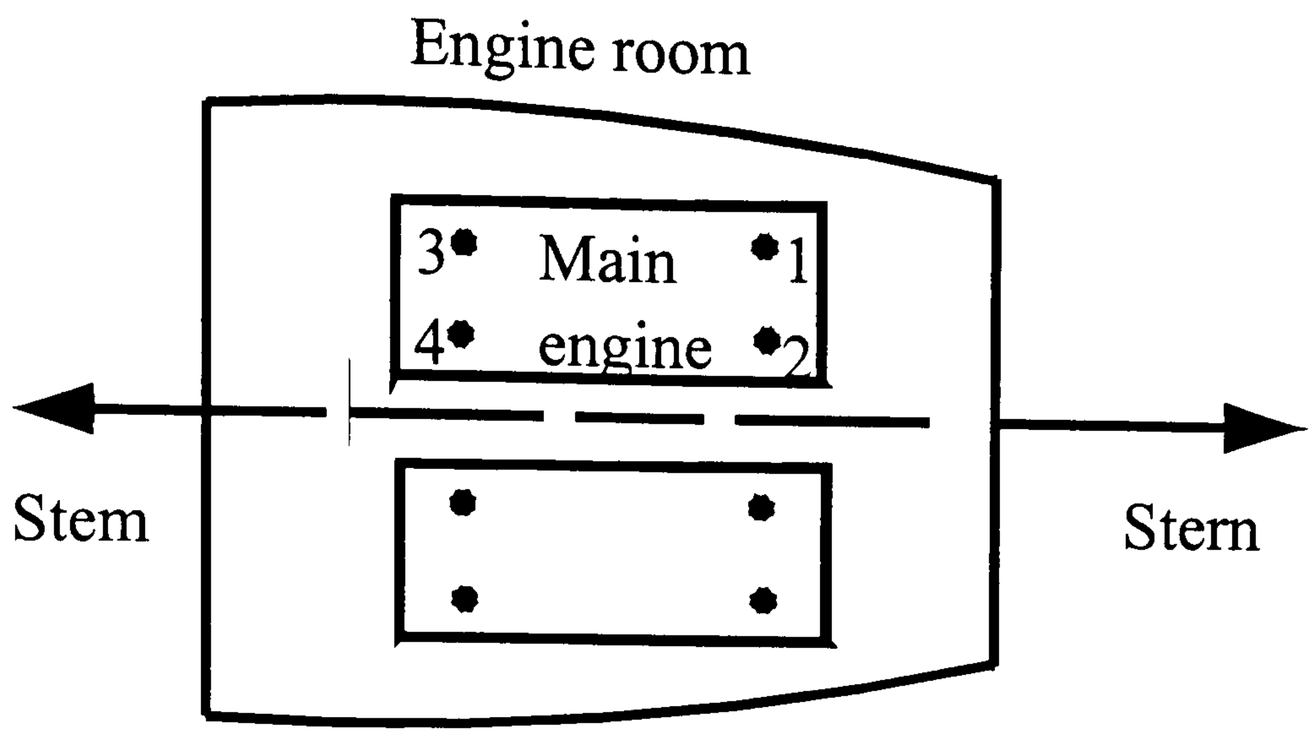

Figure 5.42 Number of the locations for mobility analyis

By this FEA model, the mobility's at the mount positions on the girder, which were numbered as in Figure 5.42, can be analysed for the conditions before and after the installation of the squeeze film damping plates. The boundary conditions and the locations of master degree of freedom of the FEA model are shown in Figures 5.43 and 5.44 respectively. The damping ratio at these portion of attached plates raised from 0.001 of the original structure to 0.01, corresponding to the loss factor 0.02 in the frequency range below 500 Hz as shown in Figure 5.45. This data was obtained by Wang and Yang (1999).

The comparsons of the analysed driving point mobilities at the mount positions are shown in Figure 5.46 to Figure 5.49.

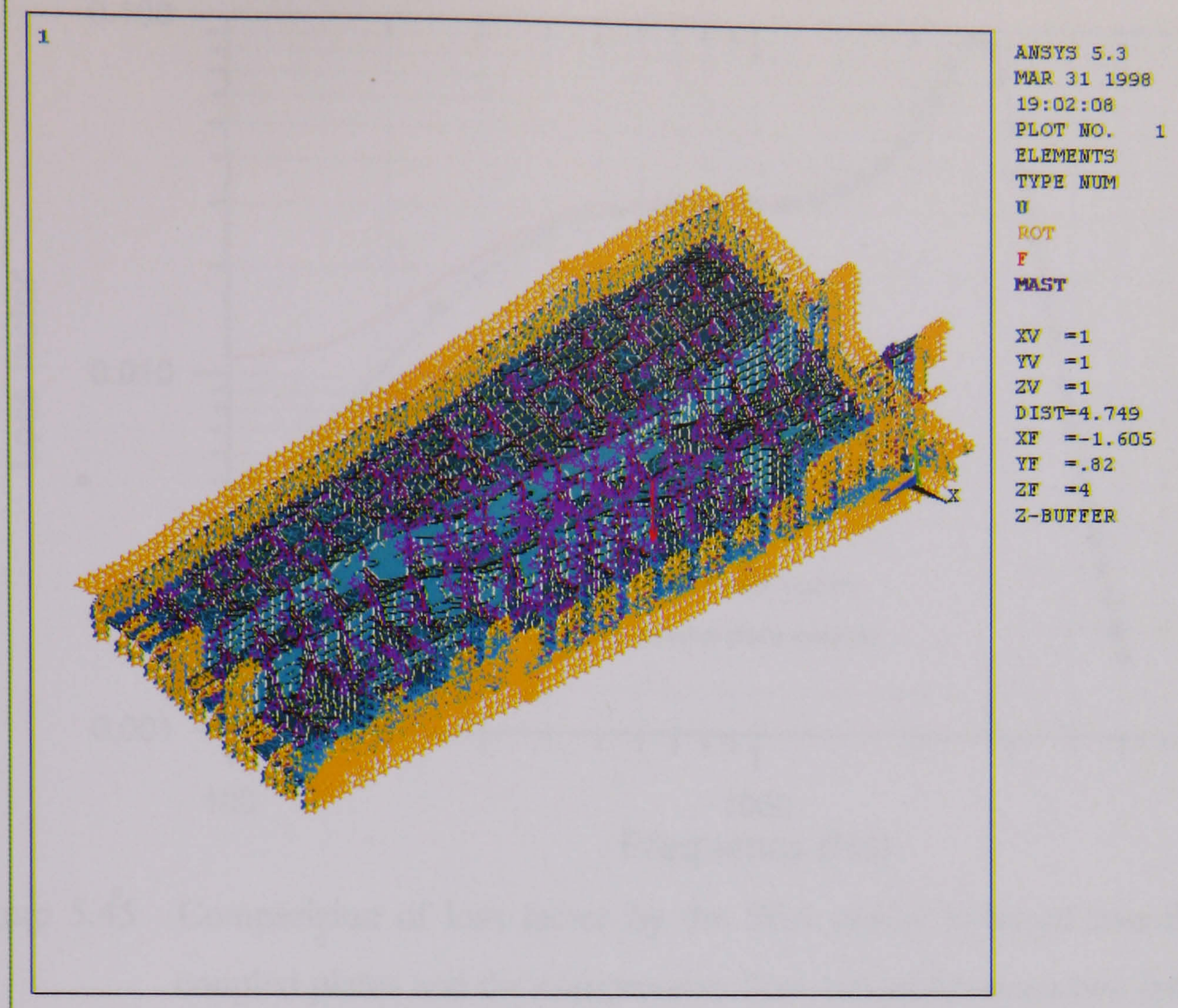

Figure 5.43 Boundary condition of the FEA model

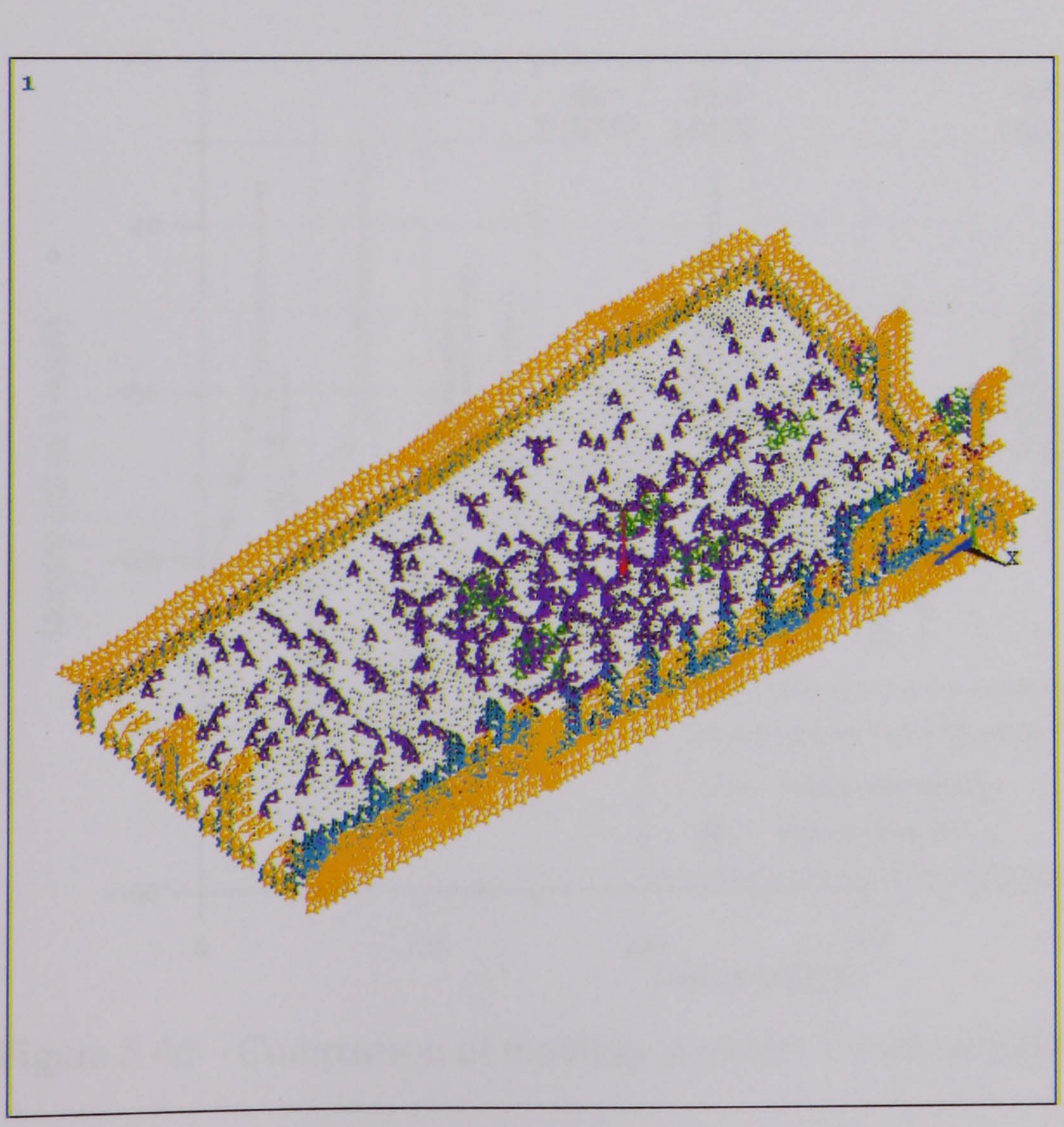

Figure 5.44 Locations of the master degree of freedom

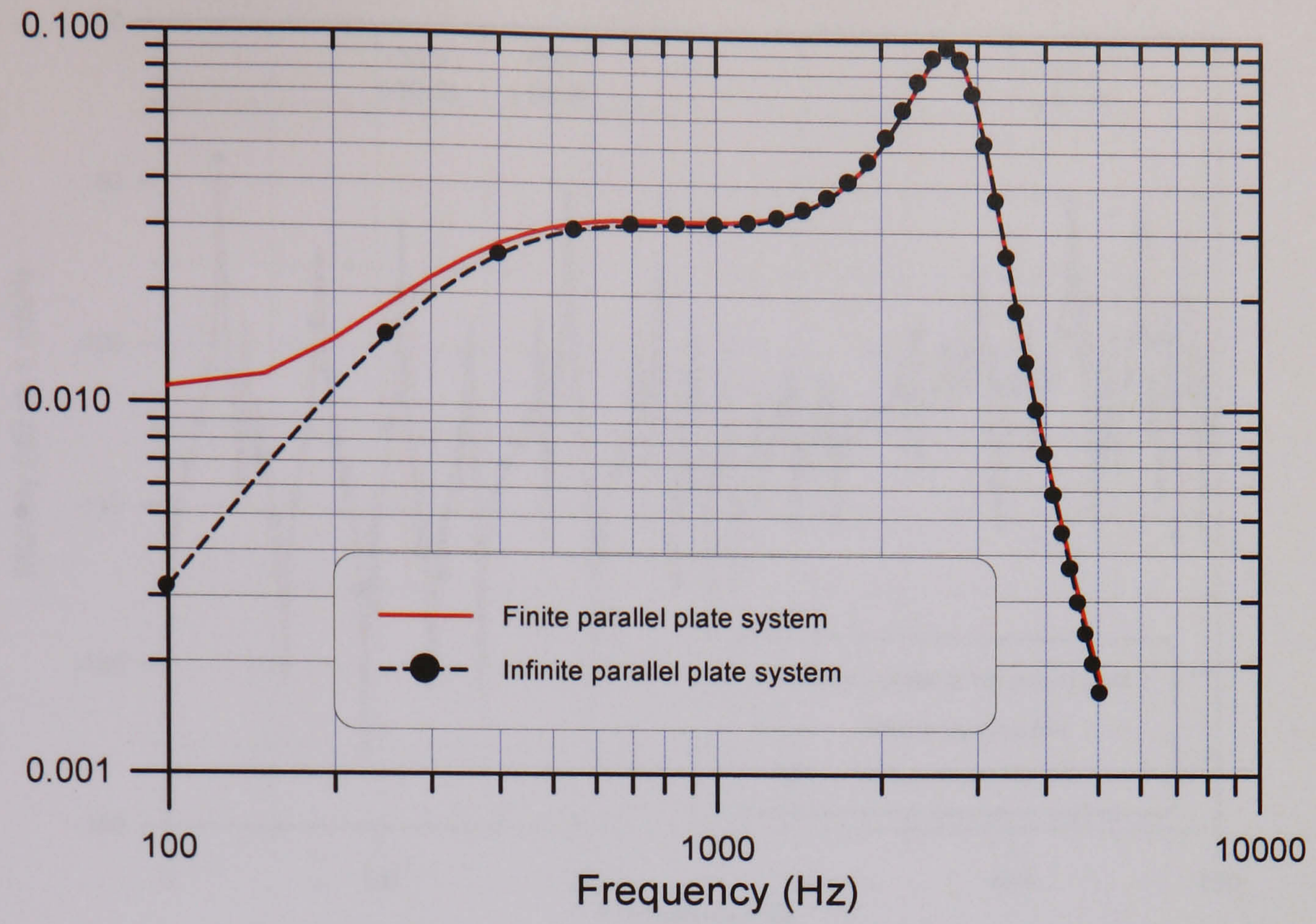

Figure 5.45 Comparision of loss factor by the SEA model between two finite parallel coupled plates and the compressive flow model between two infinite parallel coupled plates (Wang and Yang, 1998)

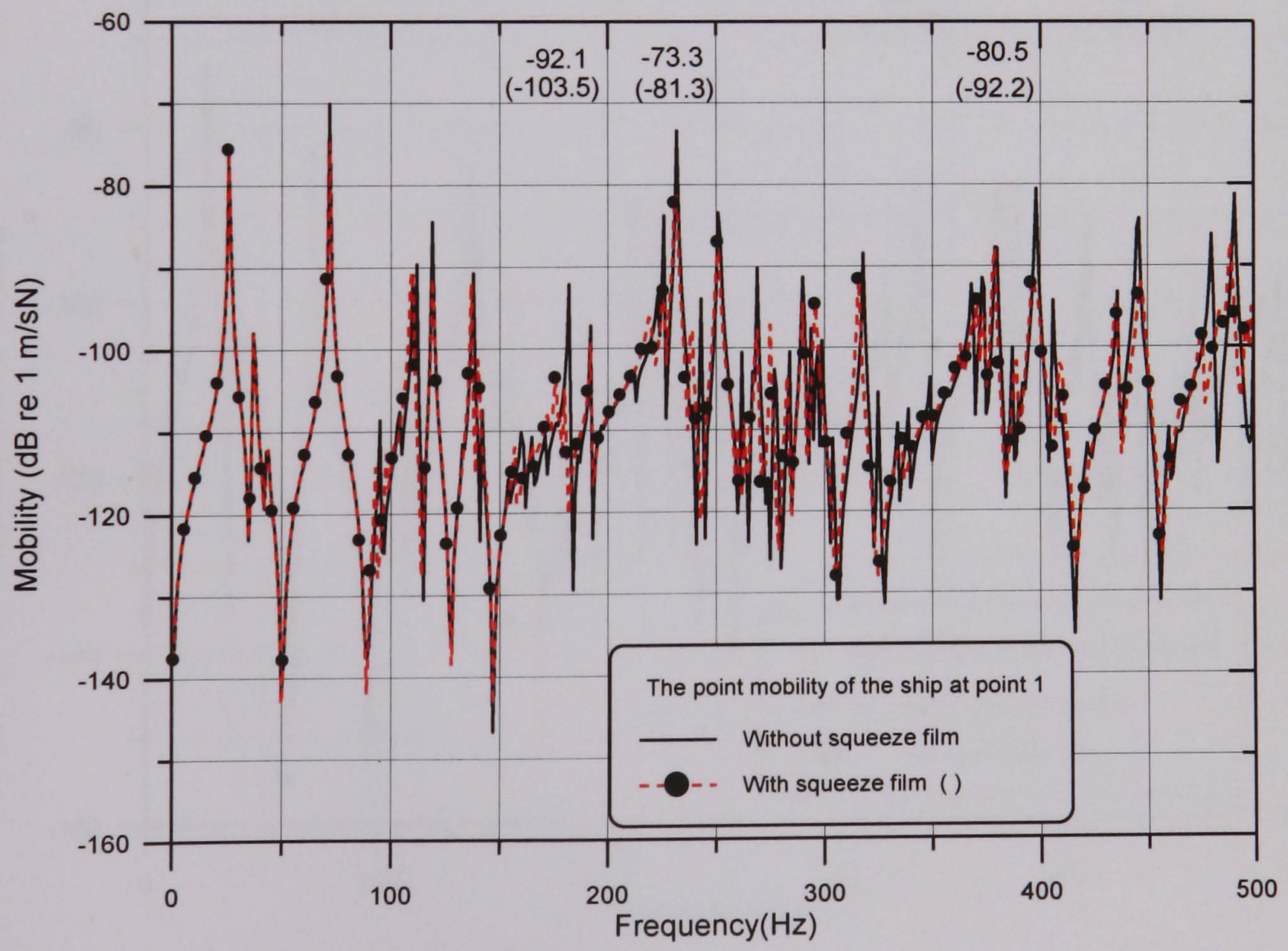

Figure 5.46 Comparison of mobility at mount 1 with and without squeeze film

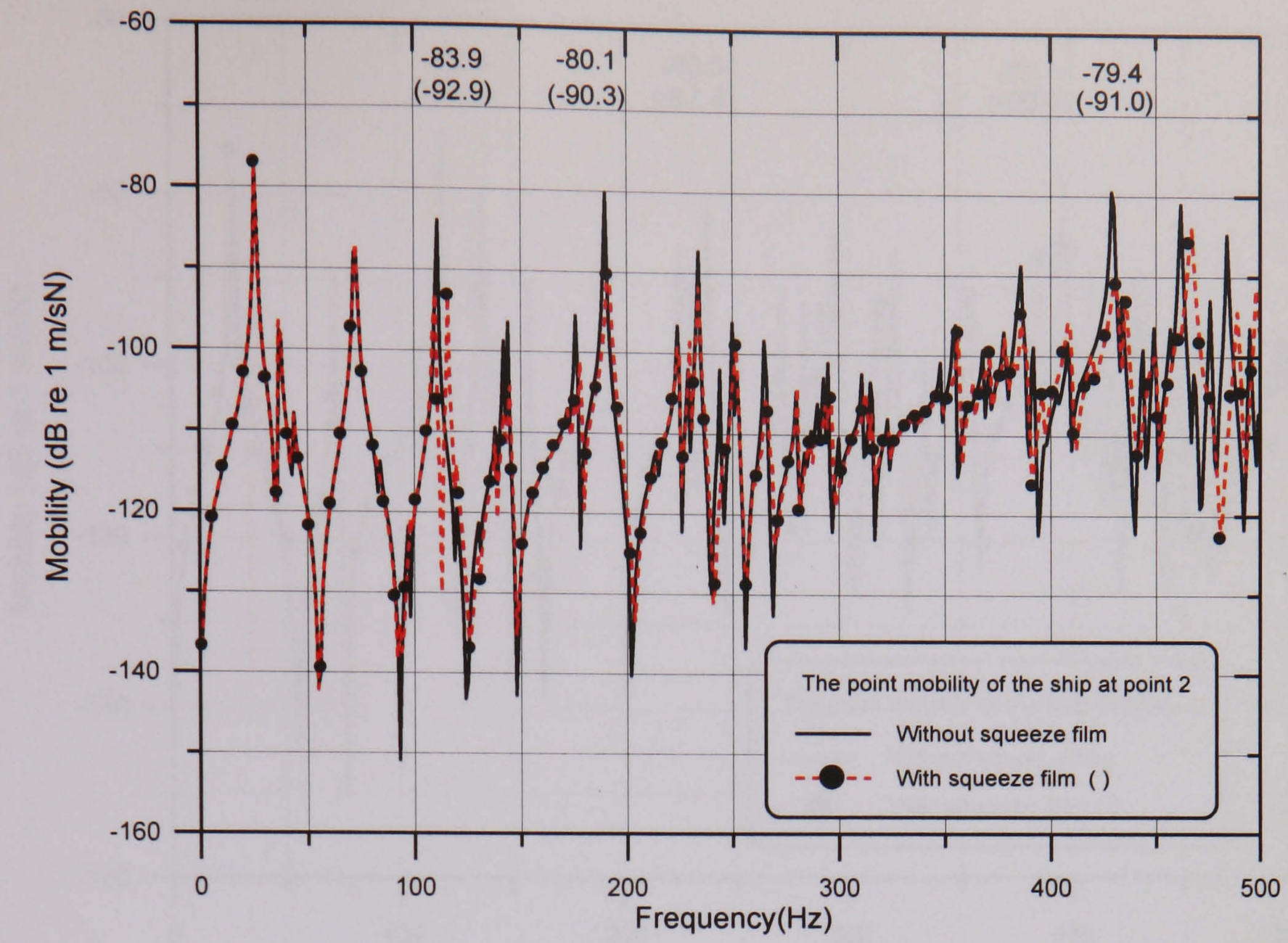

Figure 5.47 Comparison of mobility at mount 2 with and without squeeze film

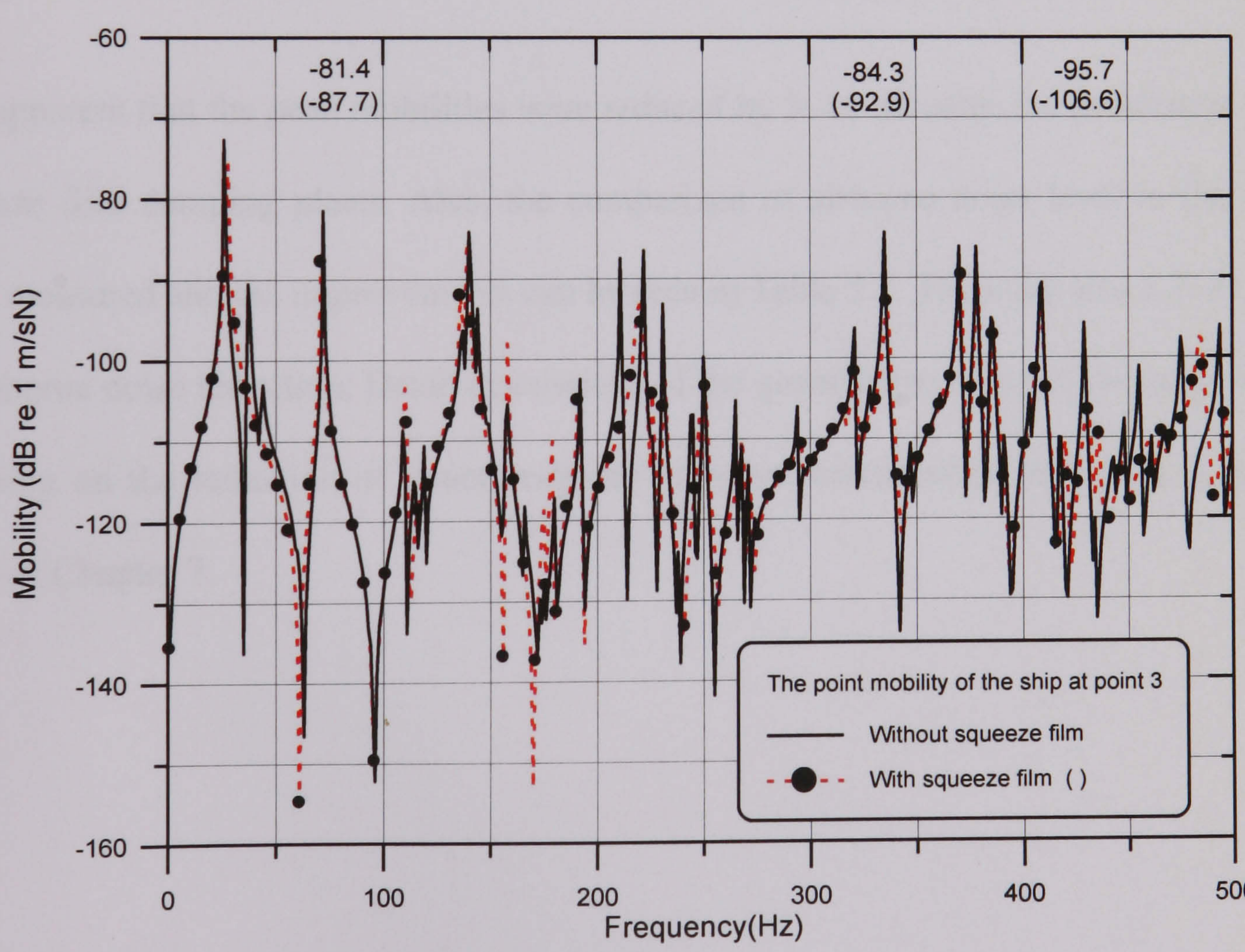

Figure 5.48 Comparison of mobility at mount 3 with and without squeeze film

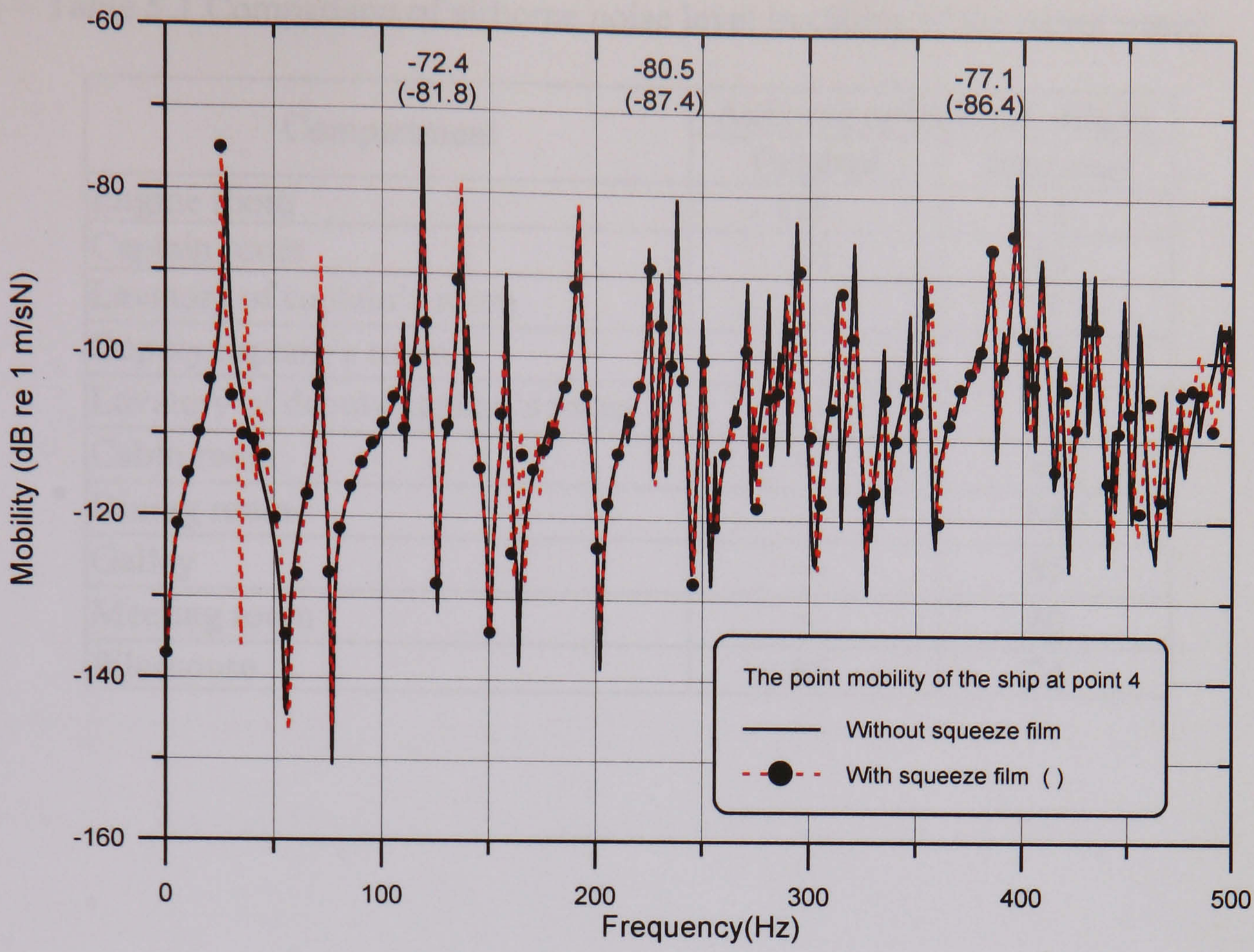

Figure 5.49 Comparison of mobility at mount 4 with and without squeeze film

It is apparent that the peak mobilities were reduced by 5~10 dB after the installation of the squeeze film damping plates. Also, the comparison of airborne noise level in the cabins were measured and the improvements can be seen in Table 5.1. There are also a 3~11 dB(A) in airborne noise reduction. Detail discussions of the quantitative effect of the squeeze-film damping on the reduction of structure-borne vibration transmission are given in Section 7.1.6 of Chapter 7.

Table 5.1 Comparison of airborne noise level in cabins of the patrol vessel

Compartment	Airborne noise level, dB(A)	
	Original	Improved
Engine room	115	112
Captain room	90	86
Lavatory of captain's room	—	91
Deputy captain's room	—	89
Lavatory of deputy captain's room	—	93
Cabin room	—	82
Dining room	—	84.5
Galley	—	85
Meeting room	—	80
Pilothouse	85	74

CHAPTER 6

APPLICATION OF THE COUPLED FEM/BEM MODEL TO PREDICT MACHINE INDUCED UNDERWATER ACOUSTIC RADIATION

The coupled FEM/BEM model can be applied for solving the fluid-structure interaction problem in structure-borne noise propagation and underwater acoustic radiation of ships. Accordingly, the estimation of the structure-borne noise characteristics of a ship is important in the design of a quiter ship structure. The hull vibration response and the pressure distribution on the wetted surface of a ship subjected to the excitation from the source like a machine can be analysed by utilizing the developed method. For this part of application and validation of the numerical model can be illustrated by taking the scale engine room model (II) into account.

6.1 Numerical Analysis Model of the Underwater Sound Radiation for Scale Engine Room Model (II)

The FEM and BEM meshes of the scale engine room model (II), as described in section 5.2, were established in Figures 6.1 and 6.2. Input data fed to the FEA are :

number of shell elements	: 711
number of nodes	: 654
plate thickness	: 0.0024 m
Young's modulus	: 2.1×10^{11} Pa
Poisson's modulus	: 0.3
material density	: 7860 kg/m^3

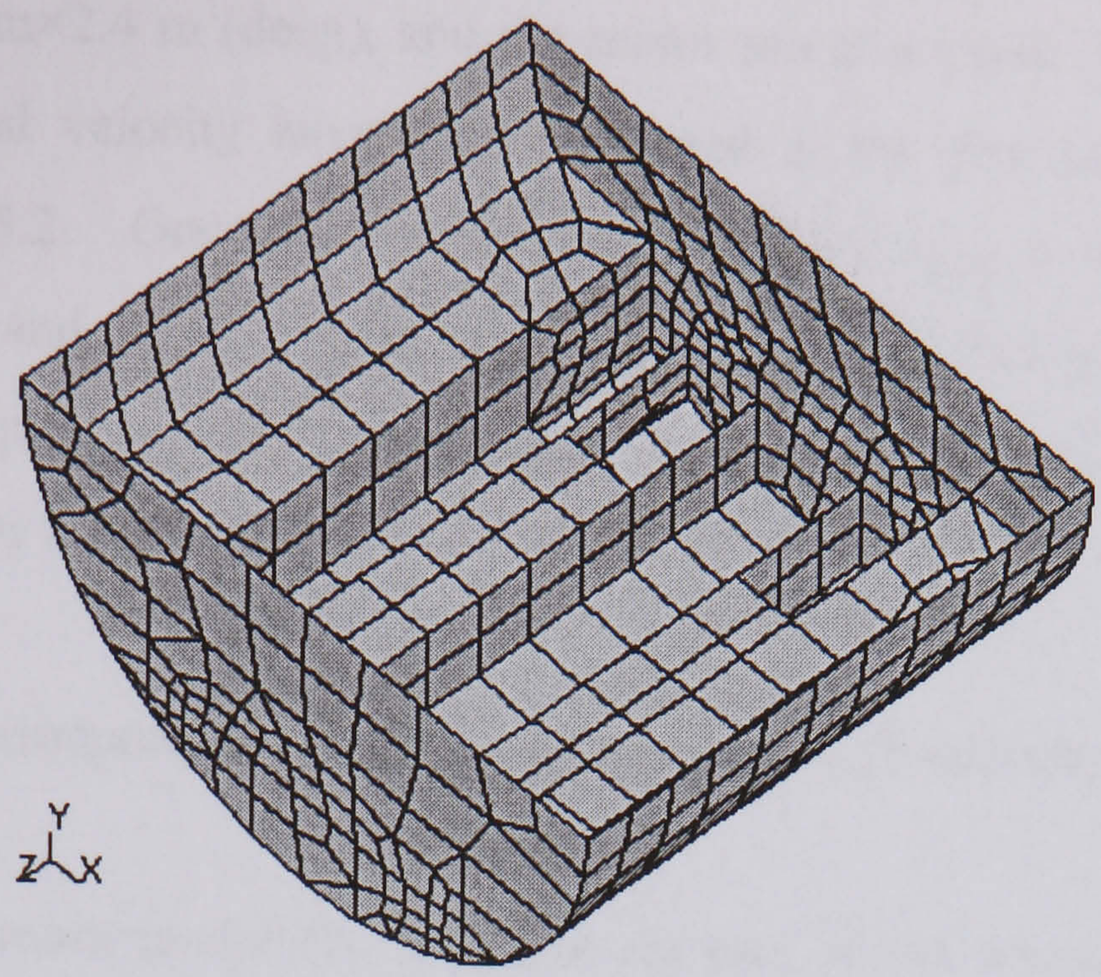

Figure 6.1 FEM mesh generation of the scale engine room model (II)

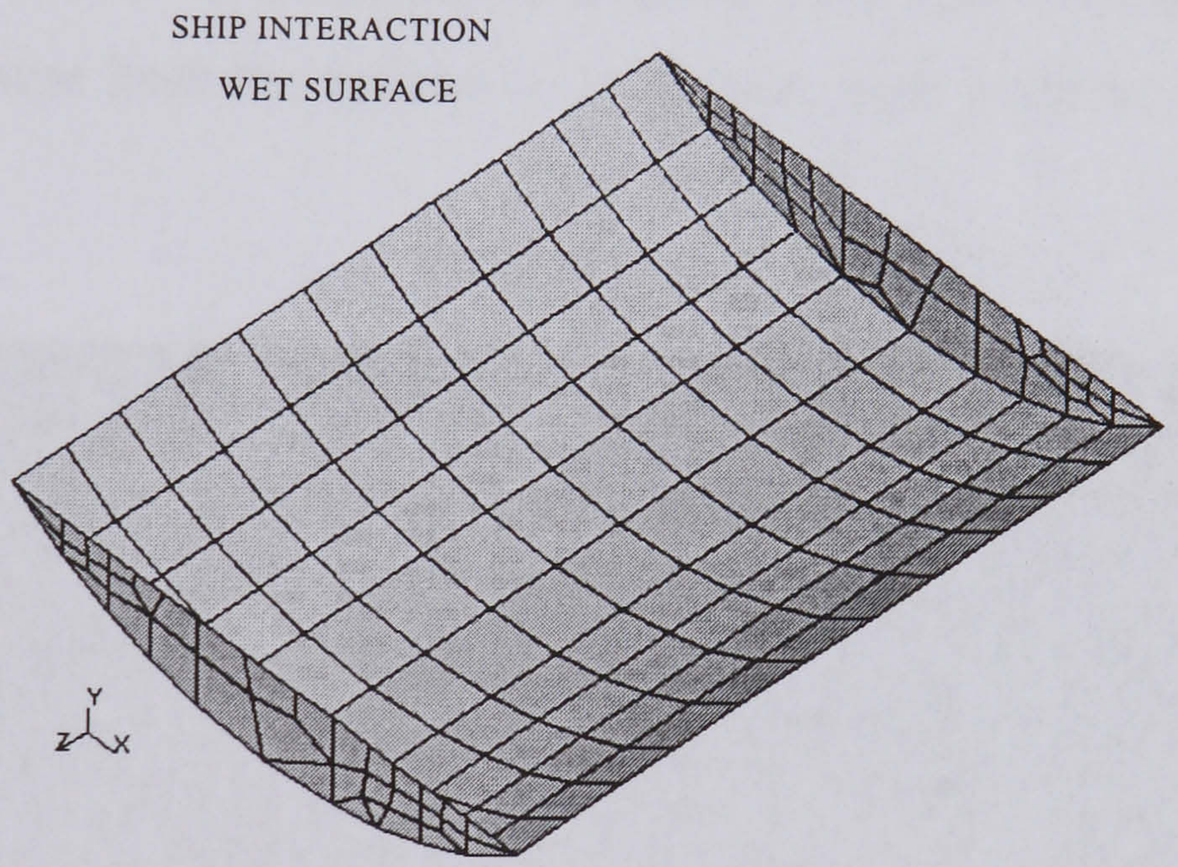

Figure 6.2 BEM grid generation of the wetted surface of the scale engine room model (II)

Input data fed to BEM are :

number of boundary elements	: 180
number of nodes	: 201
sound speed	: 1500 m/s
fluid density	: 998 kg/m^3

When the scale model was floating at the center part of the free surface of the water tank,

with size 4.2 m×3.6 m×2.4 m (deep), and the motor ran at a speed 1800 rpm, the output power and vibrational velocity have been measured at the feet of reslient mounts as described in Section 5.2. Once these measured excitations input to the numerical model, the vibration velocity and pressure distribution on the wetted surface of the scale model (II) can be analysed by equations (4.62) and (4.63). The underwater radiated sound pressure can also be obtained by equation (4.67).

6.2 Experimental Arrangement for Underwater Acoustic Radiation Measurement

Put the scale engine room model (II) at the center part of the water surface and let the model floating freely but keeping it in the doubly symmetrical position relative to the tank with four bungee rope hung in assistance, as shown in Figure 6.3. Arrange four hydrophones also in the doubly symmetrical positions as shown in Figure 6.4. During the motor in the engine room was running at a speed 1800 rpm (30 Hz), the underwater radiated sound pressure from the surface of the bottom plate could be measured by these hydrophones.

Figure 6.3 Experimental arrangement for underwater acoustic radiation measurement

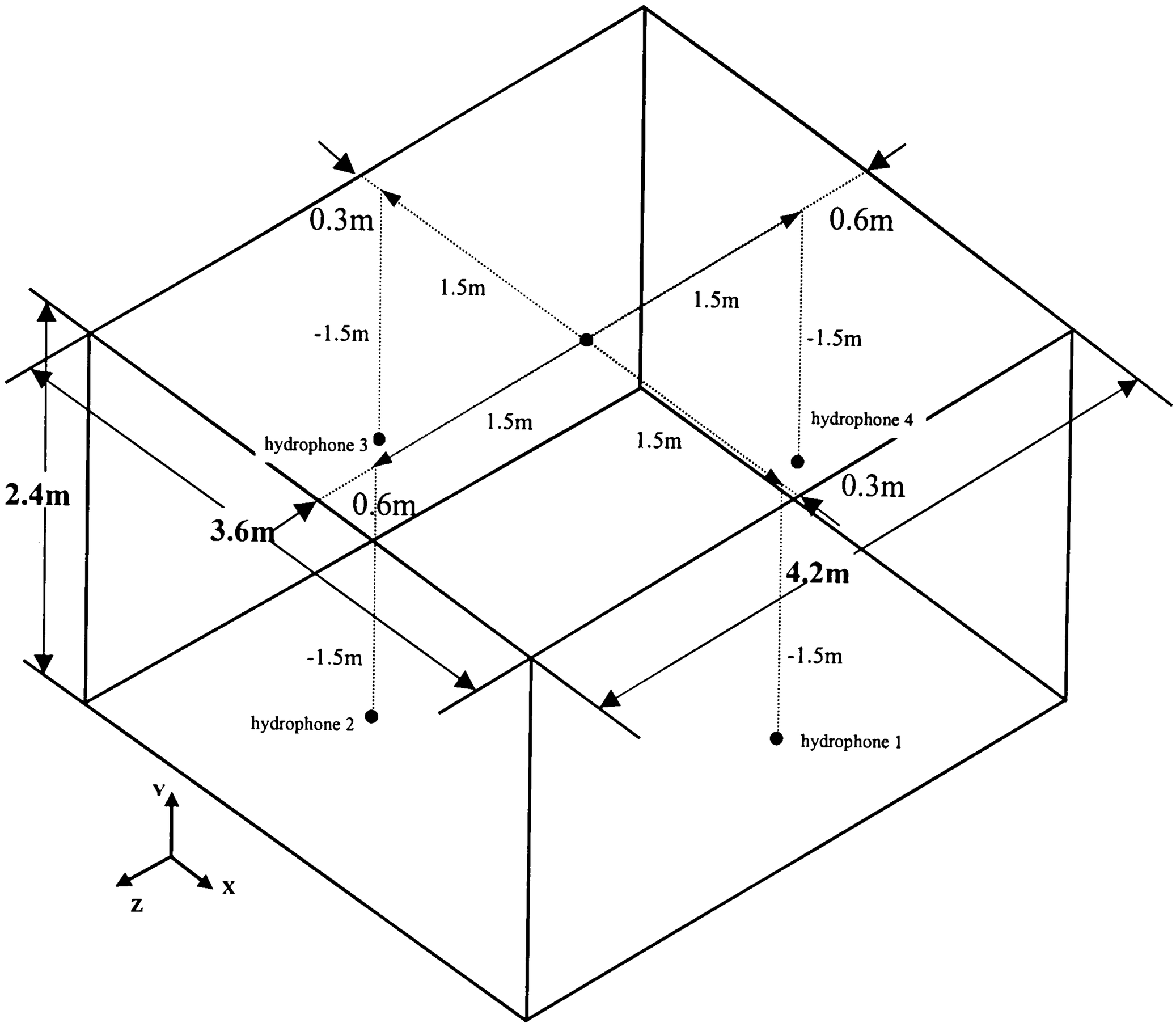

Figure 6.4 Locations of the hydrophones

6.3 Predicted and Measured Underwater Sound Pattern

When the scale model (II) was floating at the surface center of a rectangular water tank of length 4.2m, breadth 3.6m and water depth 2.4m, the motor ran at 1800 rpm. The distributions of sound pressure, normal velocity, and sound intensity on the wetted surface are predicted as shown in Figure 6.5 to Figure 6.7. The predicted underwater sound pressure on two symmetrical planes in the fluid domain, apart from the wall of a distance 0.3m for the location of hydrophones 1 and 3 and 0.6m for hydrophones 2 and 4, and a horizontal plane at a depth 1.5m are compared with the measured sound pressure level (SPL) by the four hydrophones in Figure 6.8 to Figure 6.10.

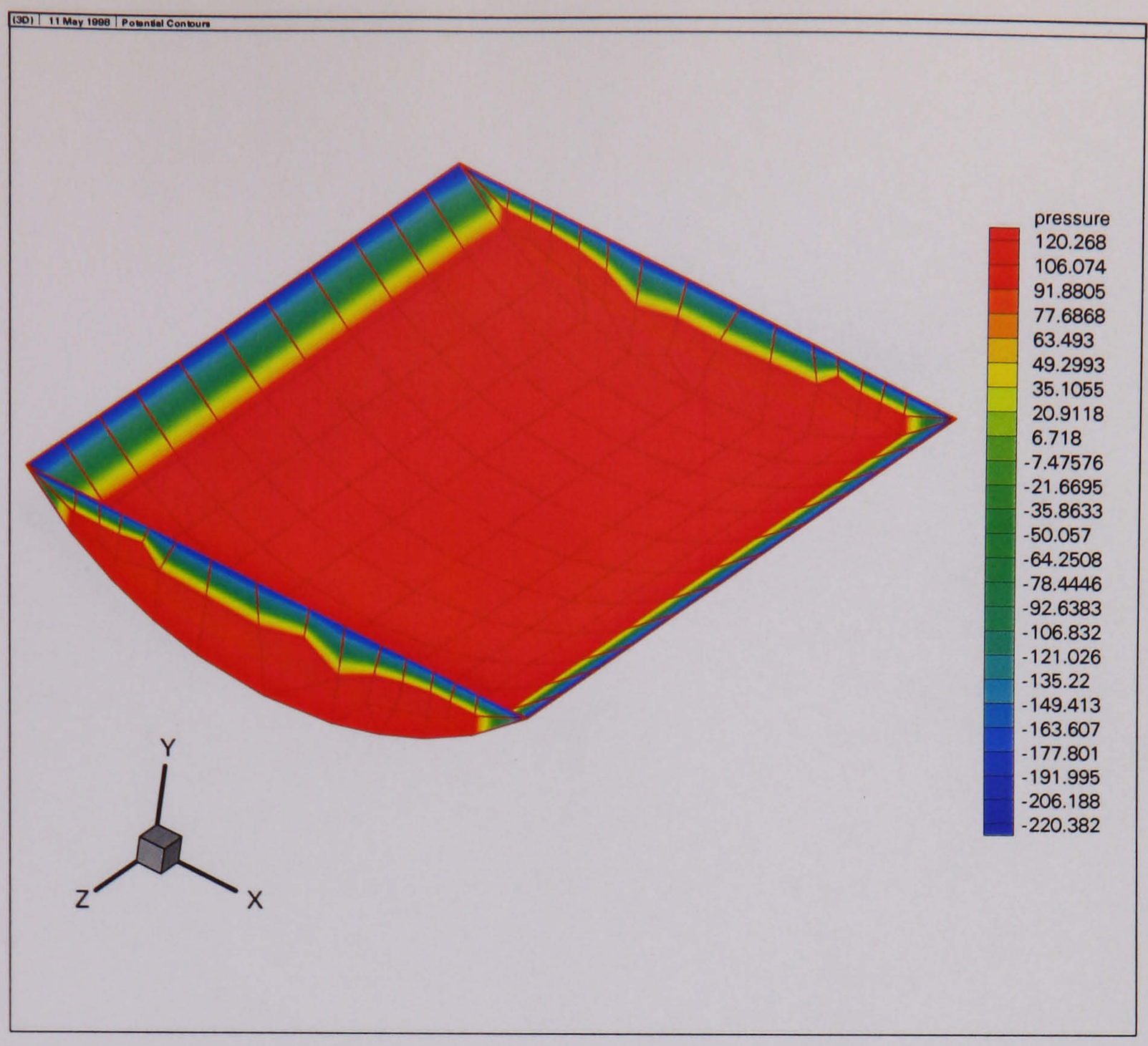

Figure 6.5 Predicted sound pressure distribution on the wetted surface

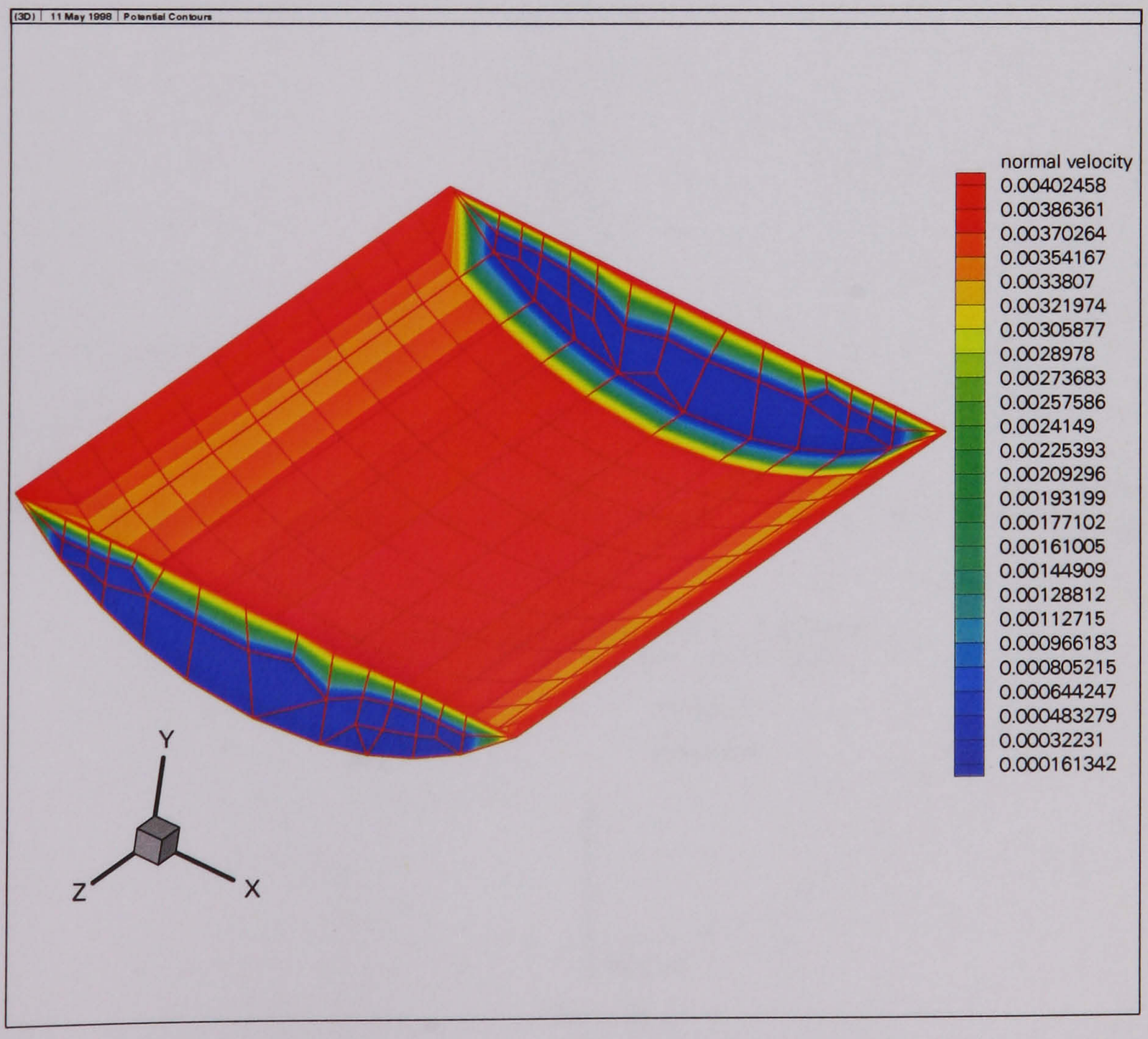

Figure 6.6 Predicted normal velocity distribution on the wetted surface

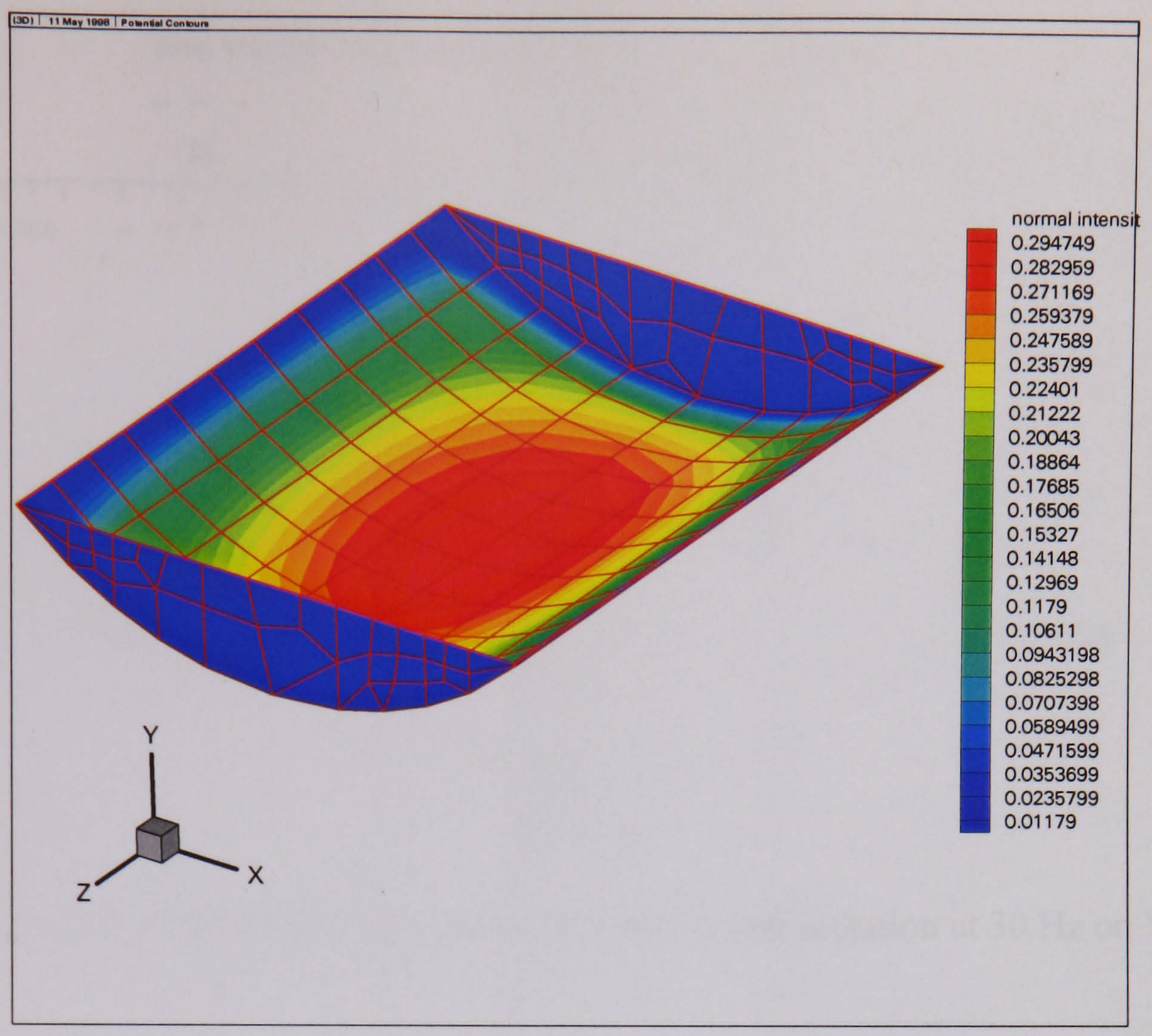

Figure 6.7 Predicted sound intensity distribution on the wetted surface

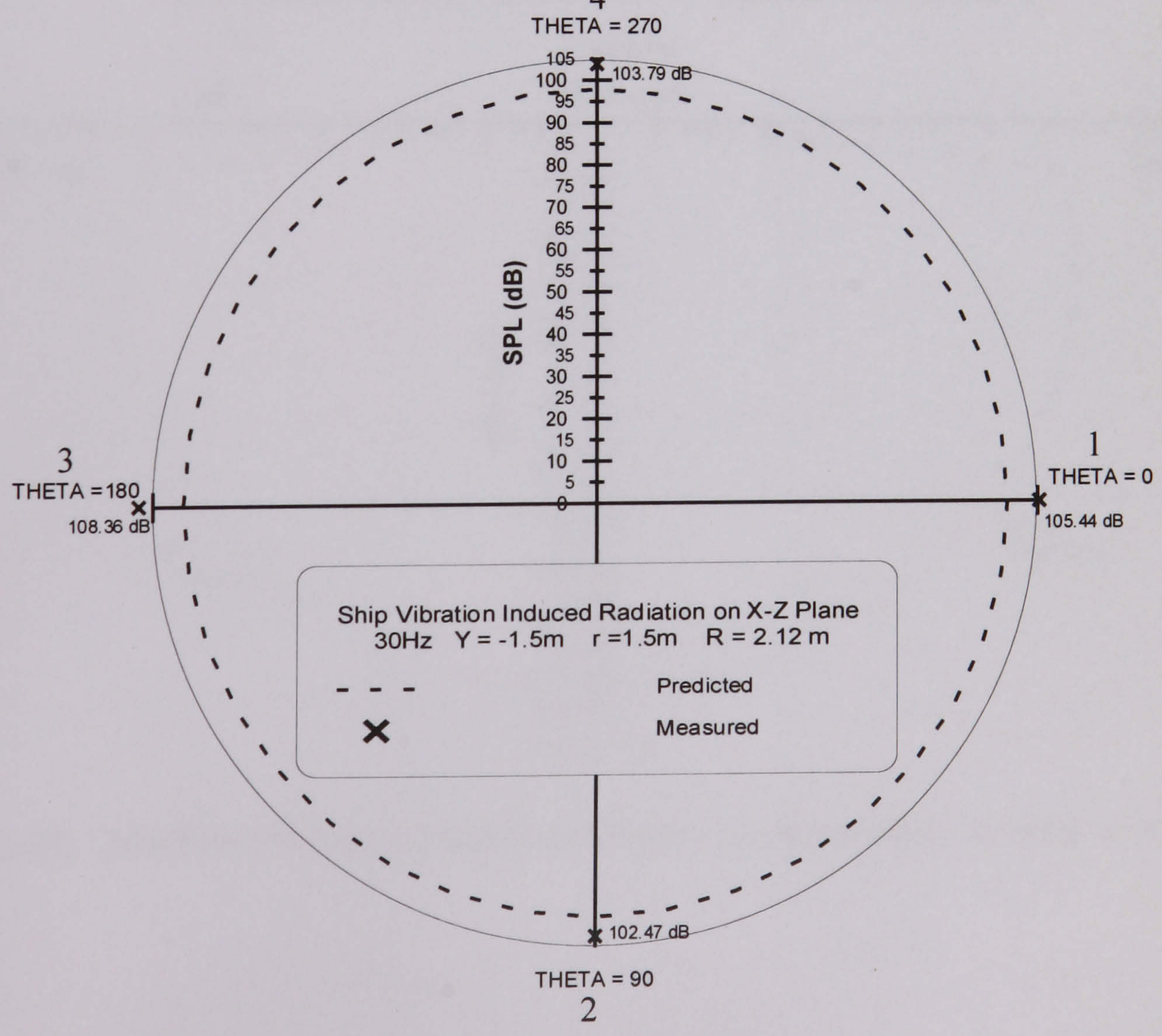

Figure 6.8 · Machine vibration induced underwater sound radiation at 30Hz on X-Z plane

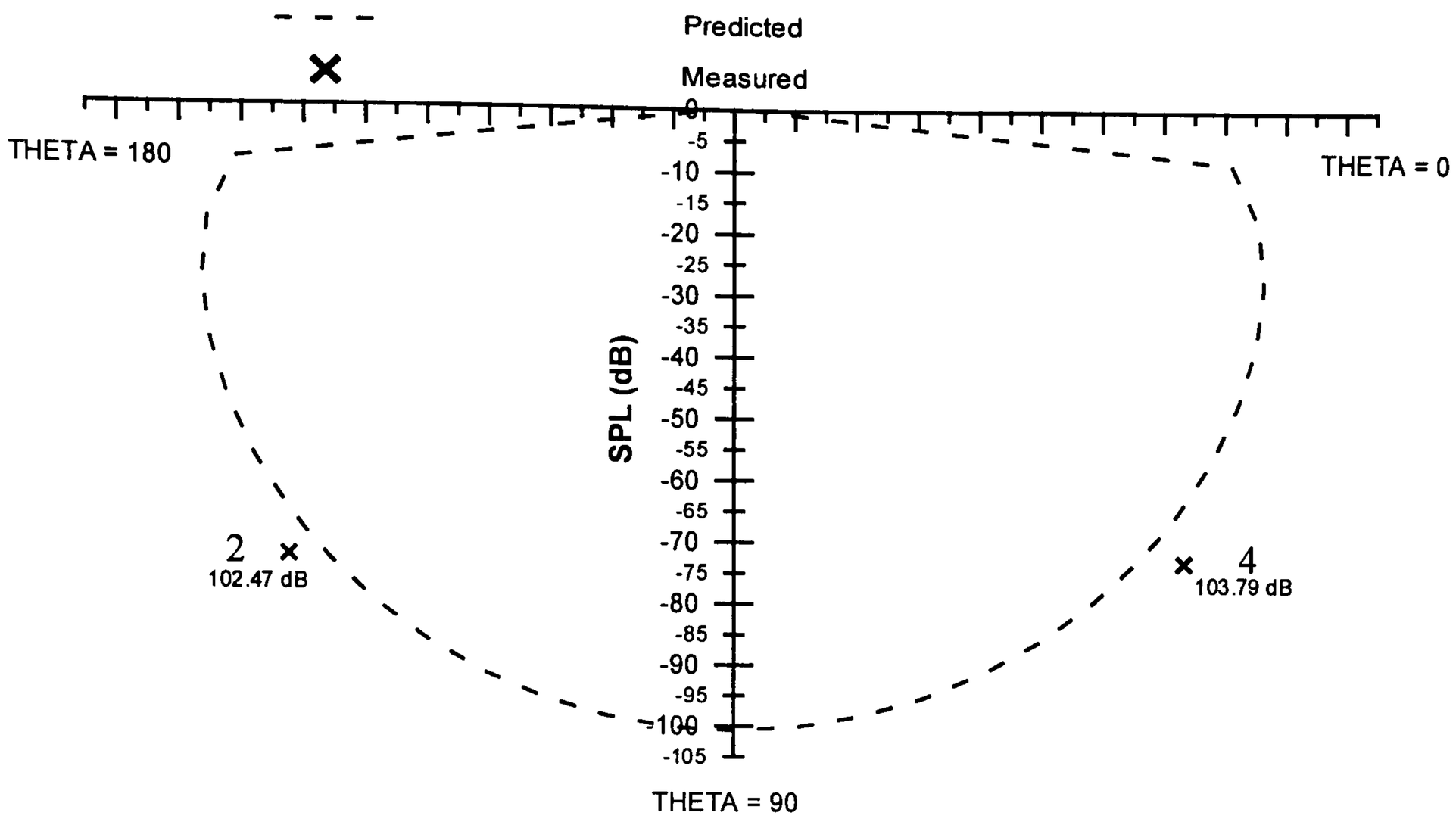

Figure 6.9 Machine vibration induced underwater sound radiation at 30 Hz on Y-Z plane

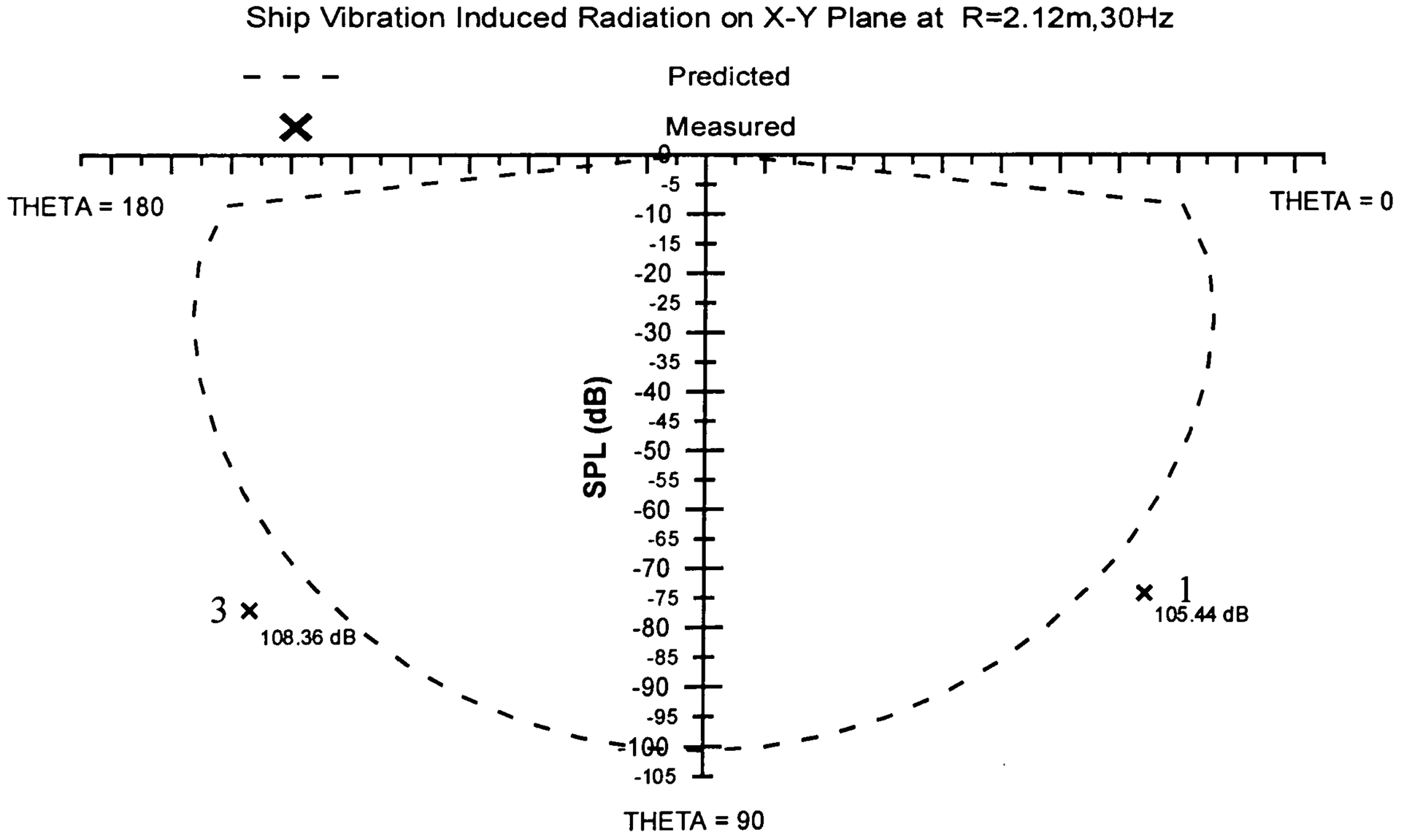

Figure 6.10 Machine vibration induced underwater sound radiation at 30Hz at X-Y plane

From the comparisons of the radiated SPL shown in Figure 6.8 to Figure 6.10, it can be found some deviations. By the error comparison shown in Table 6.1, points 1 and 3 have larger errors than points 2 and 4. This is owing to that the locations of points 1 and 3 are closer to the tank wall than points 2 and 4. Thus the influence of the sound reflection effect at points 1 and 3 is bigger than that at points 2 and 4. While the predicted model by using the FEM/BEM software only consider the free-field sound radiation. Indeed, the validation of the FEM/BEM model needs an underwater anechoic chamber to constitute a free field environment for underwater sound radiation measurement.

Table 6.1 Error analysis between the predicted and measured SPL

Measuring point	1	2	3	4
Predicted SPL (dB)	98.35	98.35	98.35	98.35
Measured SPL (dB)	105.44	102.47	108.36	103.79
Error (dB)	+7.09	+4.12	+10.01	+5.44

CHAPTER 7

CONCLUDING REMARKS

7.1 Discussion and Conclusions

In this study the machine (e.g. a motor or a diesel engine) induced structure-borne sound propagation in the engine room model structures or the underwater acoustic sound radiation was analysed and measured. Basically the structure-borne sound power is predominantly transmitted through a sound carrying structure from a source via a number of contact points. In turn, the noise and vibrations are propagated in the structure possibly causing sensitive equipment to vibrate or to cause undesired radiated noise. In principle, this may be avoided by measures at sources, in transmission, during propagation or at radiation.

To this point, the resilient mounts were characterised as an effective countermeasure to reduce noise and vibrational power transmitted from the source to the sound receiver as discussed in Chapter 5. In addition, the effectiveness of the squeeze-film damping plate has also been evaluated in this study, shown in Figure 5.46 to Figure 5.49, as a measure for the attenuation of structure-borne noise propagation at the positions close to the excitation source of the receiving structure.

The quantitative evaluation of these countermeasures for attenuating the structure-borne noise and vibrations and the error analyses of the prediction models established in this study are discussed as follows.

7.1.1 Accuracy of the Mobility Model for Evaluating Vibration Transmission via Mounts

The mobility theory discussed in Chapter 3 for the prediction of power flow transmission via a mount has been validated by a number of experimental measurement results on the scale engine room models (I) and (II) as shown in Chapter 5. The error analyses between the predicted and measured transfer mobilities, shown in Figure 5.7 to Figure 5.10, of the scale engine room model (I) are listed in Table 7.1. While that for the scale engine room model (II), shown in Figure 5.24 to Figure 5.27, are also analysed as appeared in Table 7.2. From Table 7.1, the mobility prediction model only has the average errors 2.8% and 4.0% different from that measured on the scale mode (I) in dry condition, with and without the rubber pad inserted in the resilient mounts, respectively. Whilst the mobility predictions of the scale model (I) have the corresponding errors 4.8% and 3.6% in water respectively. The greater errors are owing to the wave reflection effect of the tank wall in the measurements. This reflection effect does not have taken into consideration in the prediction model.

From Table 7.2, it is evident that the average mobility prediction errors in the case of the smaller scale engine room model (II) are obviously reduced, to 1.4% and 3.6% in air, and – 3.5% and 4.6% in water respectively. Since the smaller scale model subjected to less influence from the tank wall reflections.

Thus, it can be concluded that a credible mobility model for predicting the transfer mobility of engine vibrations via resilient mounts has been established with a considerable precision at least over 95% both in dry and wetted hull conditions.

Table 7.1 Mobility error analysis between prediction and measurement on the scale engine room model (I)

Condition		Frequency (Hz)																	Average error $\frac{1}{n}\sum_{i=1}^{n}\|e_i\|$,(%)
		20	30	40	50	60	70	80	90	100	200	300	400	500	600	700	800	900	1000	
in air with rubber pad	predicted (dB)	-61	-78	-79	-72	-74	-73	-75	-64	-62	-83	-96	-105	-99	-100	-90	-92	-104	-92	2.8
	measured (dB)	-61	-79	-79	-74	-68	-75	-74	-62	-60	-82	-94	-99	-101	-102	-87	-93	-98	-90	
	prediction error e_i (%)	0	+1.3	0	+2.7	-8.8	+2.7	-1.4	-3.2	-3.3	-1.2	-2.1	-6.1	+2.0	+2.0	-3.4	+1.1	-6.1	-2.2	
in air without rubber pad	predicted (dB)	-88	-82	-100	-95	-80	-102	-102	-99	-85	-97	-93	-101	-96	-112	-108	-95	-124	-102	4.0
	measured (dB)	-82	-84	-96	-89	-75	-98	-98	-93	-82	-92	-93	-102	-102	-110	-110	-96	-122	-110	
	prediction error e_i (%)	-7.3	+2.4	-4.2	-6.7	-6.7	-4.1	-4.1	-6.5	-3.7	-5.4	0	+1.0	+5.9	-1.8	+1.9	+1.0	-1.4	+7.3	
in water with rubber pad	predicted (dB)	-79	-90	-115	-107	-101	-105	-102	-99	-107	-110	-102	-90	-117	-99	-102	-99	-120	-121	4.8
	measured (dB)	-73	-85	-106	-99	-94	-99	-98	-94	-105	-107	-110	-98	-116	-99	-108	-98	-123	-124	
	prediction error e_i (%)	-8.2	-5.9	-8.5	-8.1	-7.4	-6.1	-4.1	-5.3	-1.9	-2.8	-7.3	-8.2	+0.9	0	+5.6	-1.0	+2.4	+2.4	
in water without rubber pad	predicted (dB)	-77	-95	-101	-105	-105	-104	-103	-100	-98	-112	-117	-92	-98	-102	-78	-90	-110	-97	3.6
	measured (dB)	-71	-92	-93	-102	-98	-101	-99	-98	-93	-107	-115	-92	-98	-101	-82	-88	-105	-98	
	prediction error e_i (%)	-8.5	-3.3	-8.6	-2.9	-7.1	-3.0	-4.0	-2.0	-5.4	-4.7	-1.7	0	0	-1.0	+4.9	-2.3	-4.8	+1.0	

Table 7.2 Mobility error analysis between prediction and measurement on the scale engine room model (II)

Condition		Frequency (Hz)																	Average error $\frac{1}{n}\sum_{i=1}^{n}\|e_i\|$,(%)
		20	30	40	50	60	70	80	90	100	200	300	400	500	600	700	800	900	1000	
in air without rubber pad	predicted (dB)	-78	-82	-79	-82	-79	-86	-83	-80	-72	-96	-94	-92	-100	-102	-98	-101	-98	-90	1.4
	measured (dB)	-79	-82	-79	-83	-79	-87	-83	-80	-75	-96	-92	-90	-96	-102	-101	-101	-102	-92	
	prediction error e_i (%)	+1.3	0	0	+1.2	0	+1.1	0	0	+4.0	0	-2.2	-2.2	-4.2	0	+3.0	0	+3.9	+2.2	
in air with rubber pad	predicted (dB)	-79	-90	-91	-87	-73	-98	-99	-96	-82	-92	-92	-104	-111	-110	-102	-117	-80	-110	3.6
	measured (dB)	-81	-91	-92	-86	-73	-96	-96	-94	-80	-100	-90	-102	-110	-102	-110	-110	-94	-110	
	prediction error e_i (%)	+2.5	+1.1	+1.1	-1.2	0	-2.1	-3.1	-2.1	-2.5	+8.0	-2.2	-2.0	-0.9	-7.8	+7.3	-6.4	+14.9	0	
in water without rubber pad	predicted (dB)	-90	-94	-90	-91	-90	-99	-95	-92	-81	-98	-103	-85	-92	-112	-106	-114	-105	-99	3.5
	measured (dB)	-90	-90	-88	-90	-98	-95	-90	-82	-82	-98	-103	-80	-86	-108	-106	-110	-103	-100	
	prediction error e_i (%)	0	-4.4	-2.3	-1.1	+8.2	-4.2	-5.6	-12.2	+1.2	0	0	-6.3	-7.0	-3.7	0	-3.6	-1.9	+1	
in water with rubber pad	predicted (dB)	-89	-100	-102	-99	-92	-107	-106	-102	-98	-107	-103	-110	-121	-119	-111	-95	-118	-110	4.6
	measured (dB)	-90	-98	-99	-102	-100	-102	-101	-100	-98	-109	-112	-103	-117	-110	-122	-100	-119	-120	
	prediction error e_i (%)	+1.1	-2.0	-3.0	+2.9	+8.0	-4.9	-5.0	-2.0	0	+1.8	+8.0	-6.8	-3.4	-8.2	+9.0	-5.0	+0.8	+8.3	

7.1.2 Accuracy of the Coupled FE and BE Model for Mobility Prediction

When the machine induced vibrations fed into the bottom structure of a engine room via the contact points of mounts, this vibrations can propagate in the structure domain and radiate noise to ambient environment. To evaluate the vibration mobility spectral function of the structures, the coupled FE and BE model has been used to take the fluid-structure interaction effect into consideration. Applying this model the driving point mobility analysis of the engine scale room scale model (I) has been analysed and been compared with the measurements as described in Figure 5.21. Error analysis of the predicted mobility and the mean line of the fluctuating measured mobility spectrum is shown in Table 7.3. The mean error is exhibited to be only 4.0%. The fluctuations existing in the measured mobility spectral curve has been demonstrated to be the reflection effect of the tank wall.

Table 7.3 Error analysis of the mobility predicted by the coupled FE/BE model on scale engine room model (I) in water

Condition	Frequency (Hz)								Mean error $\frac{1}{n}\sum_{i=1}^{n}\|e_i\|$, (%)
	100	200	300	400	500	600	700	800	
predicted (dB)	-65	-52	-60	-59	-38	-55	-60	-66	4.0
measured (dB)	-62	-50	-61	-62	-40	-53	-58	-63	
Error e_i (%)	-4.8	-4.0	+1.7	+4.8	+5.0	-3.8	-3.4	-4.8	

As described in Chapter 5, this FEM/BEM model is only suitable for mobility analysis of structure-borne propagation of vibrations in a lower frequency range, i.e., below 450 Hz. The mesh sizes of numerical model is limited by one-tenth of the structure-borne wave length, which is dependent on the frequency range to be considered, and can be considered as a common rule.

7.1.3 Accuracy of the Coupled FE/BE Model for Predicting Underwater Sound Radiation

The established coupled FEM and BEM model can also be applied to the underwater sound radiated from the vibrations of the wetted hull. In Chapter 4, a fully submerged spherical shell in infinite fluid domain has been studied. By using this numerical model the predicted pressure and velocity spectrum due to unit harmonic internal pressure has been compared with the analytical solutions by Everstine (1991) and Jeans and Mathews (1990) as shown in Figures 4.18 and 4.19. From the error analyses in Table 7.4 and 7.5, it can be seen that both mean errors within the range below the wave number under k_a=2.25 are less than 3%. So this model can be concluded to be credible.

Again, application of this combined FE/BE model to predict the radiated underwater sound of the scale engine room model (II) in fluid domain has been described when it was excited by the operating motor. By the error analysis of the SPL shown in Table 6.1, there is a mean error of –6.3% compared to the SPL measured at two pairs symmetrical positions. The greater error occurs owing to the developed FE/BE model was only considered the infinite and semi-infinite fluid domain conditions, thereby the error enlarged in the tank measurement.

Table 7.4 Error of the pressure spectrum on the shell surface by FEM/BEM prediction with respect to analytical solution

Condition	Wave number in air, k_a									Mean error $\frac{1}{n}\sum_{i=1}^{n}\|e_i\|$, (%)
	0.25	0.50	0.75	1.00	1.25	1.50	1.75	2.00	2.25	
Analytical (Pa)	0.01	0.03	0.05	0.087	0.13	0.17	0.23	0.27	0.33	2.93
FEM/BEM (Pa)	0.01	0.03	0.05	0.082	0.125	0.18	0.24	0.28	0.34	
Error e_i (%)	0	0	0	-6.1	-4.0	-5.6	-4.2	-3.6	-2.9	

Table 7.5 Error of the velocity spectrum on the shell surface by FEM/BEM prediction with respect to analytical solution

Condition	Wave number in air, k_a									Mean error $\frac{1}{n}\sum_{i=1}^{n}\|e_i\|$, (%)
	0.25	0.50	0.75	1.0	1.25	1.50	1.75	2.00	2.25	
Analytical ($x10^{-7}$ m/s)	0.20	0.40	0.65	0.80	1.20	1.30	1.76	2.00	2.30	2.63
FEM/BEM ($x10^{-7}$ m/s)	0.20	0.40	0.65	0.82	1.19	1.40	1.70	2.10	2.40	
Error e_i (%)	0	0	0	-2.4	-1.7	-7.1	-3.5	-4.8	-4.2	

7.1.4 Quantitative Effect of Rubber Pad in the Reduction of Vibration Transmission

The mobility analyses and measurements have been discussed in Chapter 5. To quantify the effect of a rubber pad in the resilient mount to reduce the machine induced vibration transmission into the bottom structure, two scale engine room models (I) and (II) has been considered by interposing in the resilient mounts with or without rubber pads respectively during the motor was running.

In the case of the scale model (I) hung in air, the peaks of the transfer mobility spectrum were reduced by the amount summarized in Table 7.6 and the mean reduction of the effect of the rubber pad on the transfer mobility attained to be 6.42 dB. The comparisons of the vibrational velocity auto-spectra at the input and output sides of the resilient mount with or without rubber pad at spectral peaks are detailed in Table 7.7 and 7.8 respectively.

Table 7.6 Effect of the rubber pad on the transfer mobility reduction at the peak frequencies of the scale engine room model (I) hung in air

Mobility (dB)	Peak frequency (Hz)											
	20	32	48	60	101	140	160	180	200	360	420	540
with rubber	-81	-84	-87	-73	-77	-95	-95	-83	-92	-84	-96	-79
without rubber	-71	-78	-63	-65	-50	-78	-78	-79	-82	-84	-82	-90
reduction	10	6	14	8	14	17	17	4	10	0	-14	-11
mean reduction	6.42 (dB)											

Table 7.7 Effect of the rubber pad on the reduction of the vibrational velocity auto-spectrum reduction at the peak frequencies of the dry scale engine room model (I)

Velocity auto-spectrum (dB)		Peak frequency (kHz)															Mean (dB)
		0.10	0.35	0.52	0.75	0.80	0.90	1.20	1.55	1.78	2.00	2.25	2.40	2.60	2.75	2.95	3.20	
without rubber in mount	input side (A)	0.1	-2.5	-6.0	1.0	-4.0	-4.0	-2.5	-5.5	-1.0	-4.0	-3.5	-4.0	-6.0	-3.5	-1.0	-1.0	-2.96
	output side (B)	0.1	-7.0	-9.0	-15.0	-15.0	-14.5	-14.0	-12.0	-15.0	-14.5	-14.0	-12.0	-16.0	-12.0	-11.0	-10.0	-21.03
	reduction (C)=(A)-(B)	0	4.5	3.0	16.0	11.0	10.5	11.5	6.5	14.0	10.5	10.5	8.0	10.0	8.5	10.0	9.0	18.07
with rubber in mount	input side (D)	4.5	-2.0	-11.0	-1.0	-4.0	-4.5	-4.5	-8.0	-4.0	-12.0	-10.5	-12.0	-7.0	-7.0	-5.5	-7.0	-5.97
	output side (E)	0	-8.5	-10.0	-12.0	-13.5	-13.0	-15.0	-12.0	-17.0	-19.0	-17.5	-21.0	-16.5	-12.5	-11.0	-13.5	-13.25
	reduction (F)=(D)-(E)	0.1	6.5	-1.0	11.0	9.5	8.5	10.5	4.0	13.0	7.0	7.0	9.0	9.5	5.5	5.5	6.5	19.20
reduction effect of rubber	reduction in input side (G)=(A)-(D)	-4.5	-0.5	5.0	2.0	0	0.5	2.0	2.5	3.0	8.0	7.0	8.0	1.0	3.5	4.5	6.0	2.69
	reduction in output side (H)=(B)-(E)	-0.1	1.5	1.0	-3.0	-1.5	-1.5	1.0	0	5.0	4.5	3.5	9.0	0.5	0.5	0	3.5	1.49

Table 7.8 Effect of the rubber pad on the vibration power reduction at the peak frequencies of the dry scale engine room model (I) hung in air

Power spectrum (dB)		Peak frequency (kHz)																			Mean (dB)
		0.10	0.20	0.40	0.60	0.70	0.75	0.80	0.90	1.15	1.25	1.40	1.55	1.70	1.80	2.20	2.40	2.60	2.70	2.80	3.20	
Without rubber in mount	input side (A)	31	39.5	38	36	44	40	33	37.5	32	45	35	36	34	41	34	32	32	38	40.5	42	36.9
	output side (B)	26	37	37	31	32	29	29	28	28	25	29	25	25	29	29	28	24	24	29	28	28.6
	reduction (C)=(A)-(B)	5	2.5	1	5	12	11	4	9.5	4	20	16	11	9	12	5	4	8	14	11.5	14	8.3
with rubber in mount	input side (D)	34	40	30	33	39	40	33	36	31.5	40.5	32	35	35	34	28	23	32	32	37	31	33.8
	output side (E)	29	33	36	31	30	29	29.5	30	27	22.5	28	25	24	25	25	20	22	25	28	22	27.1
	reduction (F)=(D)-(E)	5	7	-6	2	9	11	4.5	6	4.5	18	4	10	11	9	3	3	10	7	9	9	6.7
reduction effect of rubber	reduction in input side (G)=(A)-(D)	-3	-0.5	8	3	5	0	0	1.5	0.5	4.5	3	1	-1	7	6	9	0	6	3.5	11	3.2
	reduction in output side (H)=(B)-(E)	-3	4	1	0	2	0	-0.5	-2	1	2.5	1	0	1	4	4	8	2	-1	1	6	1.6

From the quantitative analyses, it is found that the rubber pad in the resilient mount has the effect to reduce the vibration power flow transmission in three ways, i.e., (1) the reduction of the transfer mobility level at the peak frequencies in a wide band as summarized in Table 7.6, (2) the reduction of the input velocity auto-spectrum level at the peak frequencies in wide band as indicated in Table 7.7, and (3) the reduction of the output velocity auto-spectrum level at the peak frequencies also in wide band. While the velocity differences at input and output sides in both conditions of the resilient mount with or without rubber do not change apparently.

7.1.5 Quantitative Effect of the Fluid-Structure Interaction on Structure-Borne Vibration Propagation

To quantify the effect of the fluid–structure interaction on the structure-borne vibration propagation, the study of the scale engine room model (II) described in Chapter 5 can be illustrated as an example. Comparisons of the changes in the transfer mobilities of the model both in dry and wetted conditions are shown in Figures 5.28 and 5.29, the changes in the velocity auto-spectra are shown in Figures 5.30 and 5.34 and the changes in the vibrational power spectra are shown in Figures 5.32 and 5.36, respectively. Tables 7.9, 7.10 and 7.11 exhibit the individual comparison results for the condition concentrating on that the resilient mount interposed with rubber pad.

Table 7.9 Effect of the fluid-structure interaction on the transfer mobility of the scale engine room model (II)

Mobility spectrum (dB)	Peak frequency range (Hz)									
	20	32	40 | 50	55 | 60	105	180	230	350	600 | 650	700 | 800
Dry model	-83	-90	-91	-78	-78	-83	-90	-90	-90	-88
Wetted model	-90	-90	-100	-102	-92	-110	-97	-96	-103	-100
Reduction	7	0	9	24	14	27	7	6	13	12
Mean reduction	11.9 (dB)									

Table 7.10 Effect of the fluid-structure interaction on the velocity auto-spectrum of the scale model (II) at both input and output sides of mount

Velocity auto-spectrum (dB)		Peak frequency range (kHz)														Mean (dB)
		0.01 | 0.10	0.30 | 0.40	0.60 | 0.80	0.90 | 1.00	1.00 | 1.15	1.20 | 1.30	1.35 | 1.40	1.50 | 1.55	1.75 | 1.90	2.00 | 2.10	2.15 | 2.55	2.60 | 2.80	2.90 | 3.05	3.10 | 3.20	
in air with rubber in mount	input side (A)	-19	-40	-38	-45	-46	-46	-46.5	-48.5	-48	-44	-44	-44.5	-45.5	-43	-39.3
	output side (B)	-33	-37.5	-47	-52.5	-55	-53.5	-53.5	-52.5	-57	-56.5	-56.5	-57	-56	-55.5	-51.6
in water with rubber in mount	input side (C)	-11	-35	-36	-42	-44	-42	-50	-48	-48	-52	-54	-50	-48	-46	43.3
	output side (D)	-29	-42	-50	-51	-52	-54	-54	-51	-56	-60	-61	-60	-61	-63	-60.8
Reduction	input side (E)=(A)-(C)	-8	-5	-2	-3	-2	-4	3.5	-0.5	0	8	10	5.5	2.5	3	0.6
	output side (F)=(B)-(D)	-4	4.5	3	-1.5	-3	0.5	0.5	-1.5	-1	3.5	4.5	3	5	7.5	1.5

Table 7.11 Effect of the fluid-structure interaction on the vibrational power of the scale model (II) at both input and output sides of the mount

Vibrational power (Watt)		Peak frequency range (kHz)															Mean (Watt)
		0.15 0.25	0.45 0.55	0.55 0.70	0.75 0.88	0.80 0.95	0.95 1.05	1.10 1.18	1.20 1.35	1.38 1.50	1.50 1.65	1.70 1.80	1.85 1.90	2.50 3.00	2.70 2.85	3.00 3.15	
in air with rubber in mount	input side (A)	1.47	1.02	2.45	0.62	0.26	0.30	0.75	0.30	0.24	0.24	0.25	0.3	0.23	0.16	0.35	0.596
	output side (B)	1.10	0.40	0.30	0.24	0.10	0.10	0.05	0.02	0.10	0.05	0.05	0.08	0.01	0.01	0.01	0.181
in water with rubber in mount	input side (C)	1.55	0.40	2.20	0.50	0.55	0.30	0.70	0.15	0.20	0.10	0.25	0.15	0.15	0.12	0.2	0.489
	output side (D)	1.10	0.60	0.30	0.24	0.20	0.10	0.05	0.05	0.08	0.04	0.05	0.02	0.01	0.01	0.01	0.191
Reduction	input side (E)=(A)-(C)	-0.37	0.62	0.25	0.12	-0.19	0	0.05	0.15	0.04	0.14	0	0.15	0.08	0.04	0.15	0.082
	output side (F)=(B)-(D)	0	-0.2	0	0	-0.1	0	0	-0.03	0.02	0.01	0	0.06	0	0	0	-0.016

It is found that the mean reduction of the peak transfer mobilities with an amount 11.9 dB, as shown in Table 7.9, due to the fluid radiation impedance effect. When the motor on board was running, the mean velocity auto-spectrum level was reduced by 0.6 dB and 1.5 dB at input and output sides of the mount respectively by the fluid-structure interaction effect, as shown in Table 7.10. A special phenomenom has been found in Table 7.11 that the mean peak vibrational power at the output side of the mount was enhanced by 0.016 Watt due to the fluid-structure interactions. While in a usual condition the power at the input side of the mount should be reduced. This phenomenom could be explained by the reason that the vibrational power spectra at both sides of the mount changed hugely within the range between 450~550 Hz, as shown in Figures 5.32 and 5.36. Since the bigger the area between the power spectral curves the more the power flow was transmitted. Thus, in the wetted hull case, the input side of the mount absorbed more vibrational power from the output side owing to the change of vibration pattern within this frequency range compared with the dry hull condition.

Thereby, it can be concluded that the fluid-structure interaction affects the structure-borne vibration propagation in many aspects. Normally, this interaction can reduce not only the mobilities and vibrational velocity levels, but also change the vibration pattern of the structure.

7.1.6 Quantitative Effect of the Squeeze-Film Damping on the Reduction of Vibration Transmission

By Figures 5.46 to 5.49, the driving mobilities at the four engine mounts supported by the bottom girders, which was improved by attaching the squeeze-film damping plates, have a mean reduction at the top twelve peak frequencies 6.3 dB at mount 1, 6.2 dB at mount 3; 5.3 dB at mount 2 and 5.6 dB at mount 4; as displayed in Table 7.12. It is seen that the reductions at mounts 1 and 3; and that at mounts 2 and 4 are analogical respectively. This is owing to the mounts 1 and 3; and the mounts 2 and 4 were respectively supported by the same individual girder as shown in Figure 5.39. The girders linked to the engine via the

Table 7.12 Effect of the squeeze-film damping in the reduction of the driving point mobility of the patrol vessel

Mount 1	Mobility (dB)	Top 12 peak frequencies (Hz)											Mean reduction (dB)
		25	72	125	140	232	255	320	380	398	445	480	490	
	without squeeze-film	-75	-70	-85	-90	-73	-83	-89	-88	-80	-85	-87	-80	6.3
	with squeeze-film	-83	-83	-92	-92	-81	-87	-91	-89	-92	-93	-97	-88	
	reduction	8	7	7	2	8	4	2	1	11	8	10	8	
Mount 2	Mobility (dB)	Top 12 peak frequencies (Hz)											Mean reduction (dB)
		25	38	72	115	178	190	232	380	428	460	470	480	
	without squeeze-film	-78	-96	-88	-84	-96	-80	-88	-89	-80	-81	-93	-85	5.3
	with squeeze-film	-80	-98	-91	-93	-101	-90	-99	-95	-90	-84	-94	-92	
	reduction	2	2	3	4	5	10	11	6	10	3	1	7	
Mount 3	Mobility (dB)	Top 12 peak frequencies (Hz)											Mean reduction (dB)
		25	38	72	190	210	220	232	330	370	385	410	445	
	without squeeze-film	-73	-90	-81	-84	-88	-87	-93	-85	-87	-87	-91	-96	6.2
	with squeeze-film	-76	-105	-88	-91	-93	-93	-106	-92	-90	-89	-92	-111	
	reduction	3	15	7	7	5	6	13	7	3	2	1	5	
Mount 4	Mobility (dB)	Top 12 peak frequencies (Hz)											Mean reduction (dB)
		25	72	115	140	190	232	240	292	320	380	398	410	
	without squeeze-film	-75	-89	-73	-79	-81	-87	-80	-83	-86	-86	-78	-88	5.6
	with squeeze-film	-79	-94	-85	-82	-85	-90	-85	-89	-98	-89	-85	-92	
	reduction	4	5	12	3	4	3	5	6	12	3	7	4	

mounts disperse vibrations. Thus, once the driving point mobilities were reduced, the cabins' noise levels were attenuated accordingly.

7.1.7 Conclusions

From the work of the study, it is concluded that the developed models for predicting the machine induced noise and vibration in a ship structure have been ascertained to be credible with an error less than 5%. These models were established in order to solve the transmission, propagation and radiation of noise and vibration problems starting from a machine source to the receiver in a logical and realistic ways.

Besides, the characterisation method of the resilient mount of a machine and the squeeze film damping plate used as the countermeasures for the structure-borne noise and vibration control has been preformed.

7.2 Recommendations for Further Work

Based on the stress wave model of beam element and the rectangular plate element derived in Chapter 4, the stress wave shell element is necessary to derive for more diverse applications. Further, the interface program of the stress wave model should be edited to combine the BEM software to predict the structure-borne noise and vibration propagation in the intermediate and higher frequency range.

The optimization algorithm for determining the size, quantity and locations to apply the squeeze-film damping plates needs to be realized for practical use.

Once the underwater anechoic chamber at the author's Institution, the National Taiwan Ocean University, being completed, the underwater sound radiation experiment performed in this study shall be repeated by virtue of the free field environment and comparisons made.

REFERENCES

Bert, C.W. (1973) "Material Damping: An Introductory Review of Mathematical Models, Measures and Experimental Techniques", Journal of Sound and Vibration, Vol. 29 (2), pp. 129-153.

Besio, G. and V. Loredan (1993) "Structure-B orne Noise Control on Cruise Ships", Paper 18, ICMES 93, Marine System Design and Operation.pp. 18.1-18.9.

Bishop, R.E.D. and S. Mahalingam (1981) " An Elementary Investigation of Local Vibration", Journal of Sound and Vibration, Vol. 77, pp.149-163.

Buiten, J. (1976) "Ex periences with Structure-Borne Sound Transmission in Sea-going Ships", Proceedings of International Symposium on Shipboard Acoustics, Janssen ed., Elsevier, 1977, pp. 319-340.

Cabos, C. and J. Jokat (1998) "Computation of Structure-Borne Noise Propagation in Ship Structures Using Noise-FEM", Proceedings of the Seventh International Symposium on Practical Design of Ships and Mobile Units, Hague, Elsevier, pp. 927-934.

Chen, P.T. and J.H. Ginsberg (1988) "Conventional and Variational Formulation of Fluid-Structure Interaction for an Elastic Plate in a Baffle", Proceedings of NOISE-CON 88, Purdure University, Indiana, pp. 293-298.

Chen, P.T. and J.H. Ginsberg (1993) "Variational Formulation of Acoustic Radiation from Submerged Spherical Shells", Journal of Acoustic Society of American, Vol.94, pp.221-233.

Chow, L.C. and R.J. Pinnington (1982) "Practical Industrial Method of Increasing Structural Damping in Machinery, I: Squeeze-Film Damping with Air", Journal of Sound and Vibration, Vol.118 (1), pp. 123-139.

Chow, L.C. and R.J. Pinnington (1985) "On the Prediction of Loss Factors due to Squeeze-Film Damping Mechanisms", ISVR Report 130, University of Southanpton.

Crandall, S.H. (1970) "The Role of Damping in Vibration Theory", Journal of Sound Vibration, Vol. 11 (1), pp. 3-18.

Cremer, l., M.Heckl and E.Ungar (1988) "Structure-B orne Sound", Springer Verlag, Berlin.

De Salvo, G. J., J. A. Swanson (1983) "ANSYS-Eng ineering Analysis System User's Manual", Swanson Analysis Systems, Inc. Revision 4.1, Houston, PA.

Dobson, B.J., R.J. Pinnington and R.G. White (1993) "Vibrational Power Transmission Analysis of Machinery Installations in Ships with the Objective of Noise Reduction", ISVR Report 216, University of Southampton.

Everstine, R.A. (1991) "Prediction of Low Frequency Vibrational Response of Submerged Structures", Journal of Vibration and Acoustics, Vol.113, pp187-191.

Ewins, D.J. (1980) "On Predicting Point Mobility Plots from Measurements of Other Mobility Parameters", Journal of Sound and Vibration, Vol. 70, p69.

Ewins, D.J. and J. Griffin (1981) "A State-of-the-Art Assessment of Mobility Measurement Techniques-Results for the Mid-Range Structures (30-300Hz)", Journal of Sound and Vibration, Vol. 78, p197.

Fahy, F. (1989) "Sound and Structure Vibration, Radiation, Transmission and Response", 2nd ed., Academic Press.

Gibbs, B.M. and J.D. Tattersall (1987) "Vibrational Energy Transmission and Mode Conversion at a Corner Junction of Square Section Rods", Transactions of the ASME, Vol. 109, p348.

Gingsberg, J.H. and C.E. Rosenkilde (1986) "DAA Modal Analysis for Parametric Investigations of Fluid-Structure Interaction in Underwater Shock", Shock and Vibration Digest, Vol.55, Suppl.3, pp. 25-35.

Gophey, L.G. (1967) "Integral Equation Method for Radiation from Vibrating Bodies", Journal of the Acoustical Society of America, Vol. 41, No. 4, pp. 807-816.

Goyder, H.G.D. and R.G. White (1980a) "Vibrational Power Flow from Machines into Built-Up structure, Part I: Introduction and Approximate Analyses of Beam and Plate-Like Foundations", Journal of Sound and Vibration, Vol. 68 (1), pp. 59-75.

Goyder, H.G.D. and R.G. White (1980b) "Vibrational Power Flow from Machines into Built-Up Structure, Part II: Wave Propagation and Power Flow in Beam-Stiffened Plates", Journal of Sound and Vibration, Vol. 68 (1), pp. 77-96.

Goyder, H.G.D. and R.G. White (1980c) "Vibrational Power Flow from Machines into Built-up Structure, Part III: Power Flow through Isolation System", Journal of Sound and Vibration, Vol. 68 (1), pp. 97-119.

Goyder, H.G.D. (1980) "Methods and Application of Structural Modelling from Measured Structural Frequency Response Data", Journal of Sound and Vibration, Vol. 68, p209.

Hale, A.L. and L. Meirovitch (1980) "A General Substructure Synthesis Method for the Dynamic Simulation of Complex Structures", Journal of Sound and Vibration, Vol. 69, p309.

Heckl, M. (1976) "The Different Ways of Sound Transmission in and around Resilient Mounts", Proceedings of International Symposium on Shipboard Acoustics, Janssen ed., Elsevier, 1977.

Horner, J.L. (1990) "Vibrational Power Transmission through Beam-Like Structures", PhD Theses, University of Southampton.

Horner, J.L. and R.G. White (1990) "Prediction of Vibrational Power Transmission through Jointed Beams", International Journal of Mechanical Science, Vol. 32 (3),

pp. 215-223.

Horner, J.L. and R.G. White (1991) "Prediction of Vibrational Power Transmission through Bends and Joints in Beam-Like Structures", Journal of Sound and Vibration, Vol. 147 (1), pp. 87-103.

Irie, T. and S. Takagi (1978) "Structure-B orne Noise Transmission in Steel Structure Like a Ship", Proceedings INTER-NOISE 78, San Francisco, pp. 789-794.

Janssen, J.H. and J. Buiten (1973) "On Acoustical Designing in Naval Architecture", Proceedings INTER-NOISE 79, pp. 344-356.

Jeans, R.A. and I. C. Mathews (1990) "Solution of Fluid-Structure Interaction Problem Using a Coupled Finite Element and Variational Boundary Element Technique", Journal of Acoustical Society of America, Vol.88(5), pp. 2459-2466.

Jensen, J. O. (1976) "Calculation of Structure-Borne Noise Transmission in Ships, Using the " Statistical Energy Analysis " Approach", Proceedings of International Symposium on Ship Acoustics, Janssen ed., Elsevier, 1977, pp. 281-295.

Kihlman, T. and J. Plunt (1976) "Prediction of Noise Levels in Ships", Proceedings of International Symposium on Ship Acoustics, Janssen ed., Elsevier, 1977.pp. 297-318.

Kihlman, T. (1978) "Urg ent Need for Structure-Borne Sound Source Data", Proceedings INTER-NOISE 78, San Francisco, pp. 343-348.

Kihlman, T. (1982) "Prediction of Structure-Borne Sound from Source and Foundation Data", Proceedings INTER-NOISE 82, pp. 437-444.

Koh, Y.K. (1992) "Prediction and Control of Vibration Power Transmission between Coupled Structural Systems", PhD Thesis, ISVR, University of Southampton.

Looser, W. (1982) "Accuracy of Modal Parameters from Modal Testing", Proceedings of 1st International Modal Analysis Conference, Orlando, Florida, PP. 201-207.

Lyon, R.H. (1975) "Statistical Energ y Analysis of Dynamical Systems", MIT Press.

Middleton, A.H. (1976) "Source of Strength of Marine Machinery", Proceedings of International Symposium on Shipboard Acoustics, Janssen ed., Elsevier, 1977, pp. 121-125.

Nashif, A.D., D.I.G. Jones and J.P. Henderson (1985) "Vibration Damping", John Wiley & Sons.

Nilsson, A.C. (1976) "Wave Propagation in Simple Hull-Frame Structures of Ships", Journal of Sound and Vibration, Vol. 44, p393.

Nilsson, A.C. (1977) "Attenuation of Structure-Borne Sound in Superstructures on Ships", Journal of Sound and Vibration, Vol. 55, pp. 71-91.

Nilsson, A.C. (1978a) "Noise Prediction and Prevention in Ships", Proceedings of Ship Vibration Symposium, SNAME, Arlington, pp. N1-N8.

Nilsson, A.C. (1978b) "Reduction of Structureborne Sound Propagating in Simple Ship Structures, Results of Model Tests", Journal of Sound and Vibration, Vol. 61 (1), pp. 45-60.

Nilsson, A.C. (1980) "Propeller Induced Hull Plate Vibration", Journal of Sound and Vibration, Vol. 69 (4), pp. 539-557.

Nilsson, A.C. (1981) "Propag ation of Low Frequency Noise in Ships", INTER-NOISE 81, Amsterdam, pp. 693-696.

O'hara, G. J. (1967) "Mechanical Impedance and Mobility Concepts", Journal of the Acoustical Society of America, Vol. 41, pp. 1180-1184.

Ohlrich, M. (1979) "Response of Bedplates and the Transmission of Structure-Borne Sound in the Bottom Structure of Ships", Proceedings INTER-NOISE 79, PP. 635-639.

Ohlrich, M. (1980) "On the Transmission of Audio Frequency Vibration from Multipoint Mounted Engines to Ship Bottom Structures", International Conference on Recent Advances in Structural Dynamics, ISVR, University of Southampton. pp. 225-235.

Pavic, G. (1976) "Techniques for the Determination of Vibration Transmission Mechanisms in Structures", PhD Thesis, ISVR, University of Southampton.

Petersson, B. (1980) "Effective Mobilities for the Description of Vibration Transmission between Machinery and Foundations", Proceedings INTER-NOISE 80, Miami, pp. 719-722

Petersson, B. and J. Plunt (1980) "Structure-B orne Sound Transmission from Machinery to Foundation", Report 80-09, Department of Building Acoustics, Chalmers University of Technology, Sweden.

Petersson, B. and J. Plunt (1981) "Approx imate Effective Point Mobilities for Foundations and Machinery Footings", Proceedings INTER-NOISE 81, Amsterdam, pp. 209-212.

Petersson, B. and J. Plunt (1982a) "On Effective Mobilities in the Prediction of Structure-Borne Sound Transmission between a Source Structure and a Receiving Structure, Part I: Theoretical Background and Basic Experimental Studies", Journal of Sound and Vibration, Vol. 82, pp. 517-529.

Petersson, B. and J. Plunt (1982b) "On Effective Mobilities in the Prediction of Structure-Borne Sound Transmission between a Source Structure and a Receiving Structure, Part II: Procedure for the Estimation of Mobilities", Journal of Sound and Vibration, Vol. 82, pp. 531-540.

Petersson, B. (1983) "Studies of Ordinary and Effective Mobilities for the Determination of Structureborne Sound Power Transmission", Report F83-05 and PhD Thesis,

Department of Building Acoustics, Chalmers University of Technology.

Pinnington, R.J. (1980) "Power Transmission from Rigid and Resonant Source via Isolator to Resonant and Non-Resonant Structures", ISVR Report 114, University of Southampton.

Pinnington, R.J. and R.G. White (1981) "Power Flow through Machine Isolators to Resonant and Non-Resonant Beams", Journal of Sound and Vibration, Vol. 75, pp. 179-197.

Pinnington, R.J. (1987) "Vibration Power Transmission to a Seating of a Vibration Isolated Motor", Journal of Sound and Vibration, Vol. 118 (3), pp. 515-530.

Pinnington, R.J. (1988) "Approx imate Mobilities of Build-Up Structures", ISVR Technical Report 162, University of Southampton.

Pinnington R.J. and D.C.R. Pearce (1990) "Multipole Expansion of the Vibration Transmission between a Source and a Receiver", Journal of Sound and Vibration, Vol. 142 (3), pp. 461-479.

Plunt, J. (1980) "Methods for Predicting Noise Levels in Ships, Part I", Report 80-06, Department of Building Acoustics, Chalmers University of Technology, Sweden.

Plunt, J. (1982) "The Use of Experimental Structureborne Sound Source Data for Prediction", Proceedings INTER-NOISE 82, pp. 445-448.

Plunt, J. (1983) "Summary of a Nordic Cooperative Project, Structure-Borne Sound in Ships from Diesel Engines", Proceedings INTER-NOISE 83, Edinburgh, pp. 511-514.

Plunt, J. and J. O. Jensen (1983) "Nordic Sources in Ships, II: Diesel Engines, Final Report from a Nordic Cooperative Project: Structure-Borne Sound in Ships from Propellers and Diesel Engines", Nordforsk.

Sawley, R. (1969) "The Evaluation of a Shipboard Noise and Vibration Problem Using Statistical Energy Analysis, Contribution to Stochastic Process in Dynamical Problems", ASME, New York.

Skudrzyk, E. (1980) "The Mean-Value Method of Predicting the Dynamic Response of Complex Vibrators", Journal of Acoustical Society of America, Vol. 67, pp.1105-1135.

Steenhoek, H.F. (1976) "Insertion Loss of Resilient Mounting Systems in Ships", Proceedings of International Symposium on Shipboard Acoustics, Janssen ed., Elsevier, 1977, pp. 167-182.

Snowdon, J.C. (1968) "Vibration and Shock in Damped Mechanical Systems", John Wiley & Sons, New York.

Snowdon, J.C. (1971) "Mechanical Four-Pole Parameters and Their Application", Journal of Sound and Vibration, Vol. 15 (3), pp. 307-323.

Sun, C.T. and Y.P.Lu (1995) "Vibration Damping of Structureal Elements", Prentice Hall PTR.

Timoshenko, S.P. and D.H. Young (1955) "Vibration Problems in Engineering", D.van Nostrand Company Inc., Princetown.

Tomson, T. W. (1993) "Theory of Vibration with Applications", 4th ed., Prentice-Hall International Editions.

Verheij, J.W. (1976) "Acoustic Modelling of Machinery Excitation", Proceedings of International Symposium on Shipboard Acoustics, Janssen ed., 1977, pp. 127-154.

Verheij, J.W. (1986) "Multi-Path Sound Transfer from Resiliently Mounted Shipboard Machinery", Institute of Applied Physics, TNO-TH 2nd ed., Delft.

Verheij, J.W. (1995) "Transmission of Structure-Borne Noise", International Course on Systematic Low Noise Design, SAVOIR, Berlin, pp.6.1~6.53.

Volcy, G.C., M. Bandin and C. Guinard (1988) "The Building and Operation of Vibration-Free and Trouble-Free Propulsion Plants and Ships", Transactions SNAME, Vol. 96, pp. 157-191.

Wang, W.H. (1996) "Integrated Study on the Inboard Sources of Structure-Borne Noise", Proceedings of the National Science Council-Part A: Physical Science and Engineering, Vol. 20, No. 4, pp. 397-417.

Wang, W.H, and T.C. Yang (1999) "Mobility Analysis of the Imprvoved Bottom Structure by Squeeze Film for Structure-Borne Noise Reduction", Proceedings of Third International Students' Congress of the Asia-Pacific Region Countries, Part II, pp.7.1-7.18.

Unger, E.E. (1973) "The Status of Engineering Knowledge Concerning the Damping of Built-Up Structures", Journal of Sound and Vibration, Vol. 26 (1), pp. 141-154.

Appendix A

Derivation of the Transfer Function Matrix of Finite Rectangular Plate For the Two Dimensinal Elastic Bending Wave

Appendix A

Derivation of the Transfer Function Matrix of Finite Rectangular Plate for the Two Dimensional Elastic Bending Wave

Wave equation of a plate in flexure(Cremer et al, 1988):

$$\Delta\Delta\eta - k^4\eta = 0 \tag{A-1}$$

The solution of equation (A.1) can be expressed as:

$$\hat{\eta} = C_1 H_0^{(2)}(kr) + C_2 H_0^{(2)}(-jkr) \tag{A-2}$$

where $H_0^2(kr)$ and $H_0^{(2)}(-jkr)$ are the Hankel functions of the second kind, The expanded form of $H_0^{(2)}(kr)$ is:

$$H_0^{(2)}(kr) = J_0(kr) - jY_0(kr) \tag{A-3}$$

where $J_0(kr)$ is the Bessel function of the first kind of order zero and $Y_0(kr)$ is the Bessel function of the second kind of order zero. They are :

$$J_0(kr) = 1 - \frac{(kr)^2}{2^2(1!)^2} + \frac{(kr)^4}{2^4(2!)^2} - \frac{(kr)^6}{2^6(3!)^2} + - \cdots \tag{A-4}$$

$$Y_0(kr) = \frac{2}{\pi}\left[J_0(kr)(\ln\frac{kr}{2} + \gamma) + \sum_{m=1}^{\infty} \frac{(-1)^{m-1} h_m}{2^{2m}(m!)^2}(kr)^{2m} \right] \tag{A-5}$$

where

$\gamma \approx 0.5772$ is the Euler constant

$$h_m = 1 + \frac{1}{2} + \frac{1}{3} + \cdots + \frac{1}{m} \tag{A-6}$$

Using an asymptotic expansion, $H_0^2(kr)$ and $H_0^{(2)}(-jkr)$ have the following characteristics :

$$H_0^{(2)}(kr) \approx \begin{cases} -\frac{2j}{\pi}\ln\frac{kr}{2} & \text{for } |kr| << 1 \\ \sqrt{\frac{2}{\pi kr}} e^{-j(kr-\frac{\pi}{4})} & \text{for } |kr| >> 1 \end{cases} \tag{A-7}$$

By using the boundary conditions explained in section 5.4, the solution of equation (A.1) has the form as:

$$\hat{\eta} = \frac{\hat{F}_0}{2jB'k^2}[H_0^{(2)}(kr) - H_0^{(2)}(-jkr)] \qquad \text{(A-8)}$$

for the force excitation F_{z1} acting at a corner, as shown in Figure A.1. Thus the lateral velocity and angular velocity distribution of the plate can be obtained by:

$$v_z(x,y) = j\omega\eta = \frac{F_z\omega}{2B'k^2}[H_0^{(2)}(kr) - H_0^{(2)}(-jkr)] = \frac{F_{z_1}}{Z_{F_0}}\Pi(kr) \qquad \text{(A-9)}$$

$$W_x(x,y) = \frac{\partial v_z}{\partial y} = \frac{\partial v_z}{\partial r}\frac{\partial r}{\partial y} = \frac{F_z\omega}{2B'\kappa^2}\left[\frac{\partial H_0^{(2)}(\kappa r)}{\partial r} - \frac{\partial H_0^{(2)}(-j\kappa r)}{\partial r}\right]\frac{y}{r} \qquad \text{(A.10)}$$

$$W_y(x,y) = \frac{\partial v_z}{\partial y} = \frac{\partial v_z}{\partial r}\frac{\partial r}{\partial x} = \frac{F_z\omega}{2B'\kappa^2}\left[\frac{\partial H_0^{(2)}(\kappa r)}{\partial r} - \frac{\partial H_0^{(2)}(-j\kappa r)}{\partial r}\right]\frac{x}{r} \qquad \text{(A.11)}$$

where $r = (x^2 + y^2)^{1/2}$

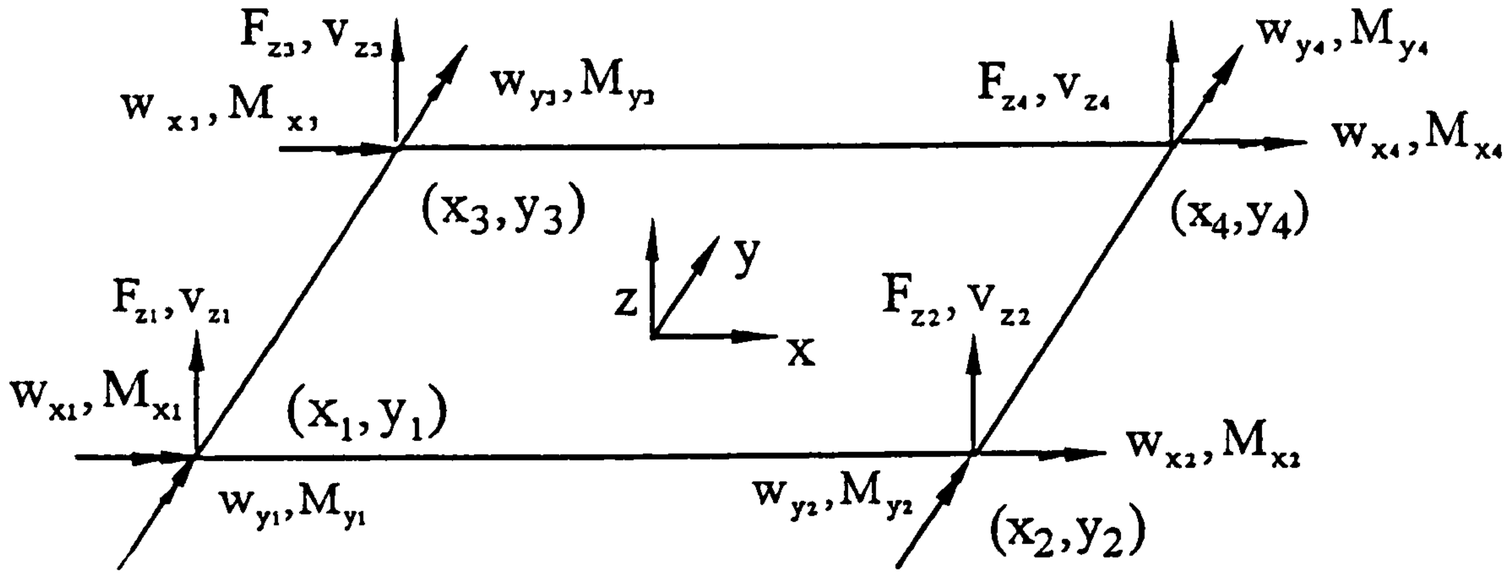

Figure A.1 Nodal forces and nodal velocities of a rectangular in bending waves

For the mobility transfer relations between nodal forces and nodal velocities, it can be written as:

$$\langle v_{z1} \cdots v_{z4} w_{x1} \cdots w_{x4} w_{y1} \cdots w_{y4} \rangle^T = [H_{ij}]\langle F_{z1} \cdots F_{z4} M_{x1} \cdots M_{x4} M_{y1} \cdots M_{y4} \rangle^T \qquad \text{(A-12)}$$

From equation (A.9) ~ (A.11), the relations between F_z and v_z, w_x or w_y can be established respectively.

Setting $F_{zj} = 1$ in equation (A.9) at node j, then

$$H_{ij} = v_{z1} = \frac{\kappa^2}{2\omega m''} = \frac{\omega}{2B'\kappa^2} \qquad \text{for } i = j$$

$$H_{ij} = V_{z2} = \frac{\omega}{2B'\kappa^2}\left[H_0^{(2)}(\kappa r_{ij}) - H_0^{(2)}(-j\kappa r_{ij})\right] \qquad \text{for } i \neq j$$

where r_{ij} is the distance between nodes i and j. Then H_{ij}, $i, j = 1,2,3,4$ can be obtained.

By equations (A.10) and (A.11), the derivatives of Hankel functions with respect to kr are:

$$\frac{\partial H_0^{(2)}(kr)}{\partial r} = -\frac{2k(kr)}{2^2(1!)^2} + \frac{4k(kr)^3}{2^4(2!)^2} - \frac{6k(kr)^5}{2^6(3!)^2} + \cdots\cdots - \frac{2j}{\pi}J_0(kr)\frac{1}{r} - \frac{2j}{\pi}[(\ln\frac{kr}{2} + r)$$

$$(-\frac{2k(kr)}{2^2(1!)^2} + \frac{4k(kr)^3}{2^4(2!)^2} + \frac{4k(kr)^5}{2^6(3!)^2} + \cdots\cdots) + \sum_{m=1}^{\infty}\frac{(-1)^{m-1}h_m}{2^{2m}(m!)^2}2mk(kr)^{2m-1}] \qquad \text{(A.13)}$$

and

$$\frac{\partial \dot{H}_0^{(2)}(kr)}{\partial r} = -\frac{2k(kr)}{2^2(1!)^2} + \frac{-4jk(-jkr)^3}{2^4(2!)^2} + \frac{-6jk(-jkr)^5}{2^6(3!)^2} + \cdots\cdots$$

$$-\frac{2j}{\pi}J_0(-jkr)\frac{1}{r} - \frac{2j}{\pi}[(\ln\frac{-jkr}{2} + r)(-\frac{-2jk(-jkr)}{2^2(1!)^2} + \frac{-4jk(-jkr)^3}{2^6(2!)^2}$$

$$-\frac{-6jk(-jkr)^5}{2^6(3!)^2} + \cdots) + \sum_{m=1}^{\infty}\frac{(-1)^m h_m}{2^{2m}(m!)^2}2mjk(-jkr)^{2m-1} \qquad \text{(A.14)}$$

Substituting the distance $r = r_{ij}$ (i, j =1, 2,3,4), and the relative y distance $y = y_{ij}$ for the mode i to the node j of force excitation F_{zj} into equations (A10), then H_{ij}(i = 5,...,8; j=1,...4) can be found. Similarly, substituting the distance r_{ij} (i, j =1, 2,3,4) and the relative x distance x_{ij} for the node i to the force applied node j into equation (A.11), H_{ij}(i = 9,...,12; j=1,...4) can be found.

For the excitation couple M_{xy} applied at node j of a relative small arm 2a, as shown in figure A2, the total velocity can be obtained as:

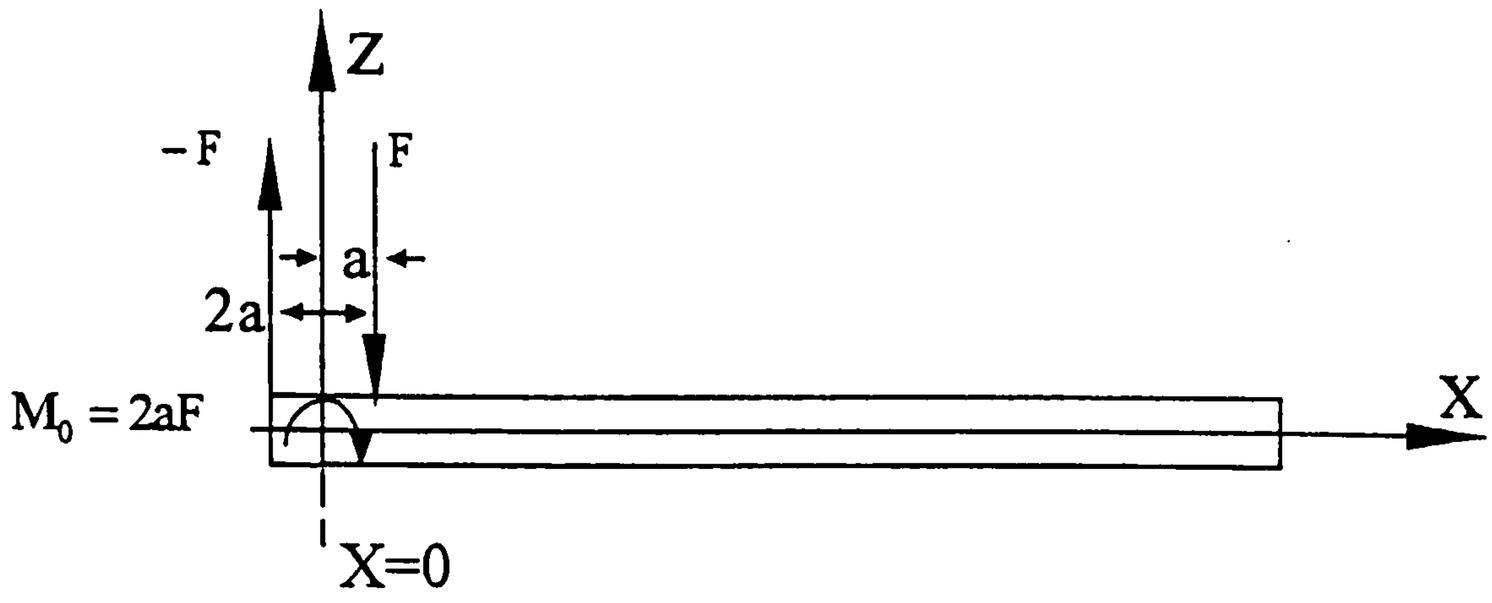

Figure A2 A couple applied at node j of a rectangular plate

$$V_2(x,y) = \frac{F_z w}{2B'k^2}\{[H_0^{(2)}(kr_1) - H_0^{(2)}(-jkr_1)] - [H_0^{(2)}(kr_2) - H_0^{(2)}(-jkr_2)]\} \qquad (A.16)$$

where

$$r_1 = [(y-a)^2 + x^2]^{\frac{1}{2}}$$

$$r_2 = [(y+a)^2 + x^2]^{\frac{1}{2}}$$

The angular velocities w_x and w_y are:

$$W_x(x,y) = \frac{\partial V_z}{\partial y} = \frac{\partial V_z}{\partial r}\frac{\partial r}{\partial y}$$

$$= \frac{M_{xj}\omega}{2B'k^2a}\{[\frac{\partial H_0^{(2)}(kr_1)}{\partial r_1} - \frac{\partial H_0^{(2)}(-jkr_1)}{\partial r_1}]\frac{y-a}{r_1}$$

$$-[\frac{\partial H_0^{(2)}(kr_2)}{\partial r_2} - \frac{\partial H_0^{(2)}(-jkr_2)}{\partial r_2}]\frac{y+q}{r_2}\} \qquad (A.17)$$

$$W_x(x,y) = \frac{\partial \hat{V}}{\partial y} = \frac{\partial \hat{V}}{\partial r}\frac{\partial r}{\partial y}$$

$$= \frac{M_{xj}\omega}{2B'k^2a}\{[\frac{\partial H_0^{(2)}(kr_1)}{\partial r_1} - \frac{\partial H_0^{(2)}(-jkr_1)}{\partial r_1}]\frac{x}{r_1}$$

$$-[\frac{\partial H_0^{(2)}(kr_2)}{\partial r_2} - \frac{\partial H_0^{(2)}(-jkr_2)}{\partial r_2}]\frac{x}{r_2}\} \qquad (A.18)$$

where " a " is set to be a small distance, namely $a = 10^{-5}$ m. Expanding the Hankel functions $H_0^{(2)}(kr_1)$ and $H_0^{(2)}(kr_2)$ with respect to k(y+a) respectively then the propagation functions become:

$$\prod(kr_1) \approx 1 + 2k^2(y-a)^2[\alpha_1 + \alpha_2 \ln\frac{\gamma k(y-a)}{2} - \frac{1}{2}\alpha_2 \ln(-j) \qquad \text{(A.19a)}$$

$$\prod(kr_2) \approx 1 + 2k^2(y+a)^2[\alpha_1 + \alpha_2 \ln\frac{\gamma k(y+a)}{2} - \frac{1}{2}\alpha_2 \ln(-j) \qquad \text{(A.19b)}$$

where $\alpha_1 = -\frac{1}{4} - \frac{j}{2\pi}$, $\alpha_2 = \frac{j}{2\pi}$, $\gamma = 1.781$.

For

$$\frac{\partial r}{\partial y} = \frac{1}{2}\frac{2(y-a)}{r_1} = \frac{y-a}{r_1}, \qquad \frac{\partial r_1}{\partial r_x} = \frac{x}{r_1}$$

$$\frac{\partial r_2}{\partial y} = \frac{y+a}{r_2}, \qquad \frac{\partial r_2}{\partial r_x} = \frac{x}{r_2}$$

Successively substituting the x distance $x = x_i$ ($i = 1,\ldots,4$) and $r_1 = (r_1)_{ij}$ of the distance from the concer node i to the moment excitaion corner j into equations (A.16) to (A.18) respectively, then H_{ij} ($i = 1,\ldots 12$; j=5,...8) can be attained.

Similar procedure can be utilized to derive the mobility transfer functions H_{ij} ($i = 1,\ldots 12$; j=9,...,12) for the moment excitations M_{yj} ($j = 1,\ldots 4$) applied at corner j via the velocity propagation distributions as:

$$v_z(x,y) = \frac{M_{yj}\omega}{2B'k^2}\{[H_0^{(2)}(kr_1) - H_0^{(2)}(-jkr_1)] - [H_0^{(2)}(kr_2) - H_0^{(2)}(-jkr_2)]\}$$

$$W_x = \frac{\partial V_z}{\partial y} = \frac{\partial \hat{V}}{\partial r}\frac{\partial r}{\partial y} = \frac{M_{xj}\omega}{2B'k^2a}\{[\frac{\partial H_0^{(2)}(kr_1)}{\partial r_1} - \frac{\partial H_0^{(2)}(-jkr_1)}{\partial r_1}]\frac{x}{r_1}$$

$$-[\frac{\partial H_0^{(2)}(kr_2)}{\partial r_2} - \frac{\partial H_0^{(2)}(-jkr_2)}{\partial r_2}]\frac{x}{r_2}\}$$

$$W_y(x,y) = \frac{\partial V_z}{\partial x} = \frac{\partial V}{\partial r}\frac{\partial r}{\partial y} = \frac{M_{xj}\omega}{2B'k^2a}\{[\frac{\partial H_0^{(2)}(kr_1)}{\partial r_1} - \frac{\partial H_0^{(2)}(-jkr_1)}{\partial r_1}]\frac{x-a}{r_1}$$

$$-[\frac{\partial H_0^{(2)}(kr_2)}{\partial r_2} - \frac{\partial H_0^{(2)}(-jkr_2)}{\partial r_2}]\frac{x+a}{r_2}\}$$

Thus, to summarize the results of H_{ij} i, j = 1, 2, ...,12 and take a $=10^{-5}$ m, the full mobility matrix of a rectangular plate for bending wave propagation can be listed as table A1. Clearly, $[H_{ij}]$ is symmetrical.

Table A.1 Full mobility matrix of finite rectangular plate in bending wave

	j=1	j=2	j=3	j=4
i=1	$\frac{k^2}{2\omega m''}=\frac{\omega}{2B'k^2}$	$\frac{\omega}{2B'k^2}\left[H_0^{(2)}(kr_{12})-H_0^{(2)}(-jkr_{12})\right]$	$\frac{\omega}{2B'k^2}\left[H_0^{(2)}(kr_{13})-H_0^{(2)}(-jkr_{13})\right]$	$\frac{\omega}{2B'k^2}\left[H_0^{(2)}(kr_{14})-H_0^{(2)}(-jkr_{14})\right]$
i=2	$\frac{\omega}{2B'k^2}\left[H_0^{(2)}(kr_{21})-H_0^{(2)}(-jkr_{21})\right]$	$\frac{k^2}{2\omega m''}=\frac{\omega}{2B'k^2}$	$\frac{\omega}{2B'k^2}\left[H_0^{(2)}(kr_{23})-H_0^{(2)}(-jkr_{23})\right]$	$\frac{\omega}{2B'k^2}\left[H_0^{(2)}(kr_{24})-H_0^{(2)}(-jkr_{24})\right]$
i=3	$\frac{\omega}{2B'k^2}\left[H_0^{(2)}(kr_{31})-H_0^{(2)}(-jkr_{31})\right]$	$\frac{\omega}{2B'k^2}\left[H_0^{(2)}(kr_{32})-H_0^{(2)}(-jkr_{32})\right]$	$\frac{k^2}{2\omega m''}=\frac{\omega}{2B'k^2}$	$\frac{\omega}{2B'k^2}\left[H_0^{(2)}(kr_{34})-H_0^{(2)}(-jkr_{34})\right]$
i=4	$\frac{\omega}{2B'k^2}\left[H_0^{(2)}(kr_{41})-H_0^{(2)}(-jkr_{41})\right]$	$\frac{\omega}{2B'k^2}\left[H_0^{(2)}(kr_{42})-H_0^{(2)}(-jkr_{42})\right]$	$\frac{\omega}{2B'k^2}\left[H_0^{(2)}(kr_{43})-H_0^{(2)}(-jkr_{43})\right]$	$\frac{k^2}{2\omega m''}=\frac{\omega}{2B'k^2}$
i=5	0	$\frac{\omega}{2B'\kappa^2}\left[\frac{\partial H_0^{(2)}(\kappa r_{12})}{\partial r}-\frac{\partial H_0^{(2)}(-j\kappa r_{12})}{\partial r}\right]\cdot\frac{y_{12}}{r_{12}}$	$\frac{\omega}{2B'\kappa^2}\left[\frac{\partial H_0^{(2)}(\kappa r_{13})}{\partial r}-\frac{\partial H_0^{(2)}(-j\kappa r_{13})}{\partial r}\right]\cdot\frac{y_{13}}{r_{13}}$	$\frac{\omega}{2B'\kappa^2}\left[\frac{\partial H_0^{(2)}(\kappa r_{14})}{\partial r}-\frac{\partial H_0^{(2)}(-j\kappa r_{14})}{\partial r}\right]\cdot\frac{y_{14}}{r_{14}}$
i=6	$\frac{\omega}{2B'k^2}\left[\frac{\partial H_0^{(2)}(kr_{21})}{\partial r}-\frac{\partial H_0^{(2)}(-jkr_{21})}{\partial r}\right]\cdot\frac{y_{21}}{r_{21}}$	0	$\frac{\omega}{2B'\kappa^2}\left[\frac{\partial H_0^{(2)}(\kappa r_{23})}{\partial r}-\frac{\partial H_0^{(2)}(-j\kappa r_{23})}{\partial r}\right]\cdot\frac{y_{23}}{r_{23}}$	$\frac{\omega}{2B'\kappa^2}\left[\frac{\partial H_0^{(2)}(\kappa r_{24})}{\partial r}-\frac{\partial H_0^{(2)}(-j\kappa r_{24})}{\partial r}\right]\cdot\frac{y_{24}}{r_{24}}$
i=7	$\frac{\omega}{2B'k^2}\left[\frac{\partial H_0^{(2)}(kr_{31})}{\partial r}-\frac{\partial H_0^{(2)}(-jkr_{31})}{\partial r}\right]\cdot\frac{y_{31}}{r_{31}}$	$\frac{\omega}{2B'\kappa^2}\left[\frac{\partial H_0^{(2)}(\kappa r_{32})}{\partial r}-\frac{\partial H_0^{(2)}(-j\kappa r_{32})}{\partial r}\right]\cdot\frac{y_{3}}{r_{32}}$	0	$\frac{\omega}{2B'\kappa^2}\left[\frac{\partial H_0^{(2)}(\kappa r_{34})}{\partial r}-\frac{\partial H_0^{(2)}(-j\kappa r_{34})}{\partial r}\right]\cdot\frac{y_{34}}{r_{34}}$
i=8	$\frac{\omega}{2B'\kappa^2}\left[\frac{\partial H_0^{(2)}(\kappa r_{41})}{\partial r}-\frac{\partial H_0^{(2)}(-j\kappa r_{41})}{\partial r}\right]\cdot\frac{y_{41}}{r_{41}}$	$\frac{\omega}{2B'\kappa^2}\left[\frac{\partial H_0^{(2)}(\kappa r_{42})}{\partial r}-\frac{\partial H_0^{(2)}(-j\kappa r_{42})}{\partial r}\right]\cdot\frac{y_{43}}{r_{42}}$	$\frac{\omega}{2B'\kappa^2}\left[\frac{\partial H_0^{(2)}(\kappa r_{43})}{\partial r}-\frac{\partial H_0^{(2)}(-j\kappa r_{43})}{\partial r}\right]\cdot\frac{y_{43}}{r_{43}}$	0

Table A.1 Full mobility matrix of finite rectangular plate in bending wave (continued)

	j=1	j=2	j=3	j=4
I=9	0	$\frac{\omega}{2B'\kappa^2}\left[\frac{\partial H_0^{(2)}(\kappa r_{12})}{\partial r}-\frac{\partial H_0^{(2)}(-j\kappa r_{12})}{\partial r}\right]\cdot\frac{x_{12}}{r_{12}}$	$\frac{\omega}{2B'\kappa^2}\left[\frac{\partial H_0^{(2)}(\kappa r_{13})}{\partial r}-\frac{\partial H_0^{(2)}(-j\kappa r_{13})}{\partial r}\right]\cdot\frac{x_{13}}{r_{13}}$	$\frac{\omega}{2B'\kappa^2}\left[\frac{\partial H_0^{(2)}(\kappa r_{14})}{\partial r}-\frac{\partial H_0^{(2)}(-j\kappa r_{14})}{\partial r}\right]\cdot\frac{x_{14}}{r_{14}}$
I=10	$\frac{\omega}{2B'\kappa^2}\left[\frac{\partial H_0^{(2)}(\kappa r_{21})}{\partial r}-\frac{\partial H_0^{(2)}(-j\kappa r_{21})}{\partial r}\right]\cdot\frac{x_{21}}{r_{21}}$	0	$\frac{\omega}{2B'\kappa^2}\left[\frac{\partial H_0^{(2)}(\kappa r_{23})}{\partial r}-\frac{\partial H_0^{(2)}(-j\kappa r_{23})}{\partial r}\right]\cdot\frac{x_{2}}{r_{23}}$	$\frac{\omega}{2B'\kappa^2}\left[\frac{\partial H_0^{(2)}(\kappa r_{24})}{\partial r}-\frac{\partial H_0^{(2)}(-j\kappa r_{24})}{\partial r}\right]\cdot\frac{x_{24}}{r_{24}}$
I=11	$\frac{\omega}{2B'\kappa^2}\left[\frac{\partial H_0^{(2)}(\kappa r_{31})}{\partial r}-\frac{\partial H_0^{(2)}(-j\kappa r_{31})}{\partial r}\right]\cdot\frac{x_{31}}{r_{31}}$	$\frac{\omega}{2B'\kappa^2}\left[\frac{\partial H_0^{(2)}(\kappa r_{32})}{\partial r}-\frac{\partial H_0^{(2)}(-j\kappa r_{32})}{\partial r}\right]\cdot\frac{x_{34}}{r_{32}}$	0	$\frac{\omega}{2B'\kappa^2}\left[\frac{\partial H_0^{(2)}(\kappa r_{34})}{\partial r}-\frac{\partial H_0^{(2)}(-j\kappa r_{34})}{\partial r}\right]\cdot\frac{x_{34}}{r_{34}}$
i=12	$\frac{\omega}{2B'\kappa^2}\left[\frac{\partial H_0^{(2)}(\kappa r_{41})}{\partial r}-\frac{\partial H_0^{(2)}(-j\kappa r_{41})}{\partial r}\right]\cdot\frac{x_{41}}{r_{41}}$	$\frac{\omega}{2B'\kappa^2}\left[\frac{\partial H_0^{(2)}(\kappa r_{42})}{\partial r}-\frac{\partial H_0^{(2)}(-j\kappa r_{42})}{\partial r}\right]\cdot\frac{x_{4}}{r_{42}}$	$\frac{\omega}{2B'\kappa^2}\left[\frac{\partial H_0^{(2)}(\kappa r_{43})}{\partial r}-\frac{\partial H_0^{(2)}(-j\kappa r_{43})}{\partial r}\right]\cdot\frac{x_{4}}{r_{43}}$	0

	j=5	j=6	j=7	j=8
i=1	0	$\frac{0.5*10^5\omega}{2B'\kappa^2}\left\{\begin{array}{l}[H_0^{(2)}(\kappa r_1)-H_0^{(2)}(-j\kappa r_1)]\\-[H_0^{(2)}(\kappa r_2)-H_0^{(2)}(-j\kappa r_2)]\end{array}\right\}$	$\frac{0.5*10^5\omega}{2B'\kappa^2}\left\{\begin{array}{l}[H_0^{(2)}(\kappa r_1)-H_0^{(2)}(-j\kappa r_1)]\\-[H_0^{(2)}(\kappa r_2)-H_0^{(2)}(-j\kappa r_2)]\end{array}\right\}$	$\frac{0.5*10^5\omega}{2B'\kappa^2}\left\{\begin{array}{l}[H_0^{(2)}(\kappa r_1)-H_0^{(2)}(-j\kappa r_1)]\\-[H_0^{(2)}(\kappa r_2)-H_0^{(2)}(-j\kappa r_2)]\end{array}\right\}$
i=2	$\frac{0.5*10^5\omega}{2B'\kappa^2}\left\{\begin{array}{l}[H_0^{(2)}(\kappa r_1)-H_0^{(2)}(-j\kappa r_1)]\\-[H_0^{(2)}(\kappa r_2)-H_0^{(2)}(-j\kappa r_2)]\end{array}\right\}$	0	$\frac{0.5*10^5\omega}{2B'\kappa^2}\left\{\begin{array}{l}[H_0^{(2)}(\kappa r_1)-H_0^{(2)}(-j\kappa r_1)]\\-[H_0^{(2)}(\kappa r_2)-H_0^{(2)}(-j\kappa r_2)]\end{array}\right\}$	$\frac{0.5*10^5\omega}{2B'\kappa^2}\left\{\begin{array}{l}[H_0^{(2)}(\kappa r_1)-H_0^{(2)}(-j\kappa r_1)]\\-[H_0^{(2)}(\kappa r_2)-H_0^{(2)}(-j\kappa r_2)]\end{array}\right\}$
i=3	$\frac{0.5*10^5\omega}{2B'\kappa^2}\left\{\begin{array}{l}[H_0^{(2)}(\kappa r_1)-H_0^{(2)}(-j\kappa r_1)]\\-[H_0^{(2)}(\kappa r_2)-H_0^{(2)}(-j\kappa r_2)]\end{array}\right\}$	$\frac{0.5*10^5\omega}{2B'\kappa^2}\left\{\begin{array}{l}[H_0^{(2)}(\kappa r_1)-H_0^{(2)}(-j\kappa r_1)]\\-[H_0^{(2)}(\kappa r_2)-H_0^{(2)}(-j\kappa r_2)]\end{array}\right\}$	0	$\frac{0.5*10^5\omega}{2B'\kappa^2}\left\{\begin{array}{l}[H_0^{(2)}(\kappa r_1)-H_0^{(2)}(-j\kappa r_1)]\\-[H_0^{(2)}(\kappa r_2)-H_0^{(2)}(-j\kappa r_2)]\end{array}\right\}$
i=4	$\frac{0.5*10^5\omega}{2B'\kappa^2}\left\{\begin{array}{l}[H_0^{(2)}(\kappa r_1)-H_0^{(2)}(-j\kappa r_1)]\\-[H_0^{(2)}(\kappa r_2)-H_0^{(2)}(-j\kappa r_2)]\end{array}\right\}$	$\frac{0.5*10^5\omega}{2B'\kappa^2}\left\{\begin{array}{l}[H_0^{(2)}(\kappa r_1)-H_0^{(2)}(-j\kappa r_1)]\\-[H_0^{(2)}(\kappa r_2)-H_0^{(2)}(-j\kappa r_2)]\end{array}\right\}$	$\frac{0.5*10^5\omega}{2B'\kappa^2}\left\{\begin{array}{l}[H_0^{(2)}(\kappa r_1)-H_0^{(2)}(-j\kappa r_1)]\\-[H_0^{(2)}(\kappa r_2)-H_0^{(2)}(-j\kappa r_2)]\end{array}\right\}$	0

Table A.1 Full mobility matrix of finite rectangular plate in bending wave (continued)

	j=5	j=6	j=7	j=8
i=5	$\frac{\omega}{4B'}(1-\frac{4j}{\pi}\ln\frac{\gamma\kappa a}{2})$	$\frac{0.5*10^5\omega}{2B'\kappa^2}\left\{\left[\frac{\partial H_o^{(2)}(\kappa r_1)}{\partial r_1}-\frac{\partial H_o^{(2)}(-j\kappa r_1)}{\partial r_1}\right]\frac{y_1-a}{r_1}-\left[\frac{\partial H_o^{(2)}(\kappa r_2)}{\partial r_2}-\frac{\partial H_o^{(2)}(-j\kappa r_2)}{\partial r_2}\right]\frac{y_1+a}{r_2}\right\}$	$\frac{0.5*10^5\omega}{2B'\kappa^2}\left\{\left[\frac{\partial H_o^{(2)}(\kappa r_1)}{\partial r_1}-\frac{\partial H_o^{(2)}(-j\kappa r_1)}{\partial r_1}\right]\frac{y_1-a}{r_1}-\left[\frac{\partial H_o^{(2)}(\kappa r_2)}{\partial r_2}-\frac{\partial H_o^{(2)}(-j\kappa r_2)}{\partial r_2}\right]\frac{y_1+a}{r_2}\right\}$	$\frac{0.5*10^5\omega}{2B'\kappa^2}\left\{\left[\frac{\partial H_o^{(2)}(\kappa r_1)}{\partial r_1}-\frac{\partial H_o^{(2)}(-j\kappa r_1)}{\partial r_1}\right]\frac{y_1-a}{r_1}-\left[\frac{\partial H_o^{(2)}(\kappa r_2)}{\partial r_2}-\frac{\partial H_o^{(2)}(-j\kappa r_2)}{\partial r_2}\right]\frac{y_1+a}{r_2}\right\}$
i=6	$\frac{0.5*10^5\omega}{2B'\kappa^2}\left\{\left[\frac{\partial H_o^{(2)}(\kappa r_1)}{\partial r_1}-\frac{\partial H_o^{(2)}(-j\kappa r_1)}{\partial r_1}\right]\frac{y_2-a}{r_1}-\left[\frac{\partial H_o^{(2)}(\kappa r_2)}{\partial r_2}-\frac{\partial H_o^{(2)}(-j\kappa r_2)}{\partial r_2}\right]\frac{y_2+a}{r_2}\right\}$	$\frac{\omega}{4B'}(1-\frac{4j}{\pi}\ln\frac{\gamma\kappa a}{2})$	$\frac{0.5*10^5\omega}{2B'\kappa^2}\left\{\left[\frac{\partial H_o^{(2)}(\kappa r_1)}{\partial r_1}-\frac{\partial H_o^{(2)}(-j\kappa r_1)}{\partial r_1}\right]\frac{y_2-a}{r_1}-\left[\frac{\partial H_o^{(2)}(\kappa r_2)}{\partial r_2}-\frac{\partial H_o^{(2)}(-j\kappa r_2)}{\partial r_2}\right]\frac{y_2+a}{r_2}\right\}$	$\frac{0.5*10^5\omega}{2B'\kappa^2}\left\{\left[\frac{\partial H_o^{(2)}(\kappa r_1)}{\partial r_1}-\frac{\partial H_o^{(2)}(-j\kappa r_1)}{\partial r_1}\right]\frac{y_2-a}{r_1}-\left[\frac{\partial H_o^{(2)}(\kappa r_2)}{\partial r_2}-\frac{\partial H_o^{(2)}(-j\kappa r_2)}{\partial r_2}\right]\frac{y_2+a}{r_2}\right\}$
i=7	$\frac{0.5*10^5\omega}{2B'\kappa^2}\left\{\left[\frac{\partial H_o^{(2)}(\kappa r_1)}{\partial r_1}-\frac{\partial H_o^{(2)}(-j\kappa r_1)}{\partial r_1}\right]\frac{y_3-a}{r_1}-\left[\frac{\partial H_o^{(2)}(\kappa r_2)}{\partial r_2}-\frac{\partial H_o^{(2)}(-j\kappa r_2)}{\partial r_2}\right]\frac{y_3+a}{r_2}\right\}$	$\frac{0.5*10^5\omega}{2B'\kappa^2}\left\{\left[\frac{\partial H_o^{(2)}(\kappa r_1)}{\partial r_1}-\frac{\partial H_o^{(2)}(-j\kappa r_1)}{\partial r_1}\right]\frac{y_3-a}{r_1}-\left[\frac{\partial H_o^{(2)}(\kappa r_2)}{\partial r_2}-\frac{\partial H_o^{(2)}(-j\kappa r_2)}{\partial r_2}\right]\frac{y_3+a}{r_2}\right\}$	$\frac{\omega}{4B'}(1-\frac{4j}{\pi}\ln\frac{\gamma\kappa a}{2})$	$\frac{0.5*10^5\omega}{2B'\kappa^2}\left\{\left[\frac{\partial H_o^{(2)}(\kappa r_1)}{\partial r_1}-\frac{\partial H_o^{(2)}(-j\kappa r_1)}{\partial r_1}\right]\frac{y_3-a}{r_1}-\left[\frac{\partial H_o^{(2)}(\kappa r_2)}{\partial r_2}-\frac{\partial H_o^{(2)}(-j\kappa r_2)}{\partial r_2}\right]\frac{y_3+a}{r_2}\right\}$
i=8	$\frac{0.5*10^5\omega}{2B'\kappa^2}\left\{\left[\frac{\partial H_o^{(2)}(\kappa r_1)}{\partial r_1}-\frac{\partial H_o^{(2)}(-j\kappa r_1)}{\partial r_1}\right]\frac{y_4-a}{r_1}-\left[\frac{\partial H_o^{(2)}(\kappa r_2)}{\partial r_2}-\frac{\partial H_o^{(2)}(-j\kappa r_2)}{\partial r_2}\right]\frac{y_4+a}{r_2}\right\}$	$\frac{0.5*10^5\omega}{2B'\kappa^2}\left\{\left[\frac{\partial H_o^{(2)}(\kappa r_1)}{\partial r_1}-\frac{\partial H_o^{(2)}(-j\kappa r_1)}{\partial r_1}\right]\frac{y_4-a}{r_1}-\left[\frac{\partial H_o^{(2)}(\kappa r_2)}{\partial r_2}-\frac{\partial H_o^{(2)}(-j\kappa r_2)}{\partial r_2}\right]\frac{y_4+a}{r_2}\right\}$	$\frac{0.5*10^5\omega}{2B'\kappa^2}\left\{\left[\frac{\partial H_o^{(2)}(\kappa r_1)}{\partial r_1}-\frac{\partial H_o^{(2)}(-j\kappa r_1)}{\partial r_1}\right]\frac{y_4-a}{r_1}-\left[\frac{\partial H_o^{(2)}(\kappa r_2)}{\partial r_2}-\frac{\partial H_o^{(2)}(-j\kappa r_2)}{\partial r_2}\right]\frac{y_4+a}{r_2}\right\}$	$\frac{\omega}{4B'}(1-\frac{4j}{\pi}\ln\frac{\gamma\kappa a}{2})$
i=9	0	$\frac{0.5*10^5\omega}{2B'\kappa^2}\left\{\left[\frac{\partial H_o^{(2)}(\kappa r_1)}{\partial r_1}-\frac{\partial H_o^{(2)}(-j\kappa r_1)}{\partial r_1}\right]\frac{x_1}{r_1}-\left[\frac{\partial H_o^{(2)}(\kappa r_2)}{\partial r_2}-\frac{\partial H_o^{(2)}(-j\kappa r_2)}{\partial r_2}\right]\frac{x_1}{r_2}\right\}$	$\frac{0.5*10^5\omega}{2B'\kappa^2}\left\{\left[\frac{\partial H_o^{(2)}(\kappa r_1)}{\partial r_1}-\frac{\partial H_o^{(2)}(-j\kappa r_1)}{\partial r_1}\right]\frac{x_1}{r_1}-\left[\frac{\partial H_o^{(2)}(\kappa r_2)}{\partial r_2}-\frac{\partial H_o^{(2)}(-j\kappa r_2)}{\partial r_2}\right]\frac{x_1}{r_2}\right\}$	$\frac{0.5*10^5\omega}{2B'\kappa^2}\left\{\left[\frac{\partial H_o^{(2)}(\kappa r_1)}{\partial r_1}-\frac{\partial H_o^{(2)}(-j\kappa r_1)}{\partial r_1}\right]\frac{x_1}{r_1}-\left[\frac{\partial H_o^{(2)}(\kappa r_2)}{\partial r_2}-\frac{\partial H_o^{(2)}(-j\kappa r_2)}{\partial r_2}\right]\frac{x_1}{r_2}\right\}$
i=10	$\frac{0.5*10^5\omega}{2B'\kappa^2}\left\{\left[\frac{\partial H_o^{(2)}(\kappa r_1)}{\partial r_1}-\frac{\partial H_o^{(2)}(-j\kappa r_1)}{\partial r_1}\right]\frac{x_2}{r_1}-\left[\frac{\partial H_o^{(2)}(\kappa r_2)}{\partial r_2}-\frac{\partial H_o^{(2)}(-j\kappa r_2)}{\partial r_2}\right]\frac{x_2}{r_2}\right\}$	0	$\frac{0.5*10^5\omega}{2B'\kappa^2}\left\{\left[\frac{\partial H_o^{(2)}(\kappa r_1)}{\partial r_1}-\frac{\partial H_o^{(2)}(-j\kappa r_1)}{\partial r_1}\right]\frac{x_2}{r_1}-\left[\frac{\partial H_o^{(2)}(\kappa r_2)}{\partial r_2}-\frac{\partial H_o^{(2)}(-j\kappa r_2)}{\partial r_2}\right]\frac{x_2}{r_2}\right\}$	$\frac{0.5*10^5\omega}{2B'\kappa^2}\left\{\left[\frac{\partial H_o^{(2)}(\kappa r_1)}{\partial r_1}-\frac{\partial H_o^{(2)}(-j\kappa r_1)}{\partial r_1}\right]\frac{x_2}{r_1}-\left[\frac{\partial H_o^{(2)}(\kappa r_2)}{\partial r_2}-\frac{\partial H_o^{(2)}(-j\kappa r_2)}{\partial r_2}\right]\frac{x_2}{r_2}\right\}$
i=11	$\frac{0.5*10^5\omega}{2B'\kappa^2}\left\{\left[\frac{\partial H_o^{(2)}(\kappa r_1)}{\partial r_1}-\frac{\partial H_o^{(2)}(-j\kappa r_1)}{\partial r_1}\right]\frac{x_3}{r_1}-\left[\frac{\partial H_o^{(2)}(\kappa r_2)}{\partial r_2}-\frac{\partial H_o^{(2)}(-j\kappa r_2)}{\partial r_2}\right]\frac{x_3}{r_2}\right\}$	$\frac{0.5*10^5\omega}{2B'\kappa^2}\left\{\left[\frac{\partial H_o^{(2)}(\kappa r_1)}{\partial r_1}-\frac{\partial H_o^{(2)}(-j\kappa r_1)}{\partial r_1}\right]\frac{x_3}{r_1}-\left[\frac{\partial H_o^{(2)}(\kappa r_2)}{\partial r_2}-\frac{\partial H_o^{(2)}(-j\kappa r_2)}{\partial r_2}\right]\frac{x_3}{r_2}\right\}$	0	$\frac{0.5*10^5\omega}{2B'\kappa^2}\left\{\left[\frac{\partial H_o^{(2)}(\kappa r_1)}{\partial r_1}-\frac{\partial H_o^{(2)}(-j\kappa r_1)}{\partial r_1}\right]\frac{x_3}{r_1}-\left[\frac{\partial H_o^{(2)}(\kappa r_2)}{\partial r_2}-\frac{\partial H_o^{(2)}(-j\kappa r_2)}{\partial r_2}\right]\frac{x_3}{r_2}\right\}$
i=12	$\frac{0.5*10^5\omega}{2B'\kappa^2}\left\{\left[\frac{\partial H_o^{(2)}(\kappa r_1)}{\partial r_1}-\frac{\partial H_o^{(2)}(-j\kappa r_1)}{\partial r_1}\right]\frac{x_4}{r_1}-\left[\frac{\partial H_o^{(2)}(\kappa r_2)}{\partial r_2}-\frac{\partial H_o^{(2)}(-j\kappa r_2)}{\partial r_2}\right]\frac{x_4}{r_2}\right\}$	$\frac{0.5*10^5\omega}{2B'\kappa^2}\left\{\left[\frac{\partial H_o^{(2)}(\kappa r_1)}{\partial r_1}-\frac{\partial H_o^{(2)}(-j\kappa r_1)}{\partial r_1}\right]\frac{x_4}{r_1}-\left[\frac{\partial H_o^{(2)}(\kappa r_2)}{\partial r_2}-\frac{\partial H_o^{(2)}(-j\kappa r_2)}{\partial r_2}\right]\frac{x_4}{r_2}\right\}$	$\frac{0.5*10^5\omega}{2B'\kappa^2}\left\{\left[\frac{\partial H_o^{(2)}(\kappa r_1)}{\partial r_1}-\frac{\partial H_o^{(2)}(-j\kappa r_1)}{\partial r_1}\right]\frac{x_4}{r_1}-\left[\frac{\partial H_o^{(2)}(\kappa r_2)}{\partial r_2}-\frac{\partial H_o^{(2)}(-j\kappa r_2)}{\partial r_2}\right]\frac{x_4}{r_2}\right\}$	0

Table A.1 Full mobility matrix of finite rectangular plate in bending wave (continued)

	j=9	j=10	j=11	j=12
i=1	0	$\frac{0.5*10^5\omega}{2B'\kappa^2}\left\{\left[H_0^{(2)}(\kappa r_1)-H_0^{(2)}(-j\kappa r_1)\right]-\left[H_0^{(2)}(\kappa r_2)-H_0^{(2)}(-j\kappa r_2)\right]\right\}$	$\frac{0.5*10^5\omega}{2B'\kappa^2}\left\{\left[H_0^{(2)}(\kappa r_1)-H_0^{(2)}(-j\kappa r_1)\right]-\left[H_0^{(2)}(\kappa r_2)-H_0^{(2)}(-j\kappa r_2)\right]\right\}$	$\frac{0.5*10^5\omega}{2B'\kappa^2}\left\{\left[H_0^{(2)}(\kappa r_1)-H_0^{(2)}(-j\kappa r_1)\right]-\left[H_0^{(2)}(\kappa r_2)-H_0^{(2)}(-j\kappa r_2)\right]\right\}$
i=2	$\frac{0.5*10^5\omega}{2B'\kappa^2}\left\{\left[H_0^{(2)}(\kappa r_1)-H_0^{(2)}(-j\kappa r_1)\right]-\left[H_0^{(2)}(\kappa r_2)-H_0^{(2)}(-j\kappa r_2)\right]\right\}$	0	$\frac{0.5*10^5\omega}{2B'\kappa^2}\left\{\left[H_0^{(2)}(\kappa r_1)-H_0^{(2)}(-j\kappa r_1)\right]-\left[H_0^{(2)}(\kappa r_2)-H_0^{(2)}(-j\kappa r_2)\right]\right\}$	$\frac{0.5*10^5\omega}{2B'\kappa^2}\left\{\left[H_0^{(2)}(\kappa r_1)-H_0^{(2)}(-j\kappa r_1)\right]-\left[H_0^{(2)}(\kappa r_2)-H_0^{(2)}(-j\kappa r_2)\right]\right\}$
i=3	$\frac{0.5*10^5\omega}{2B'\kappa^2}\left\{\left[H_0^{(2)}(\kappa r_1)-H_0^{(2)}(-j\kappa r_1)\right]-\left[H_0^{(2)}(\kappa r_2)-H_0^{(2)}(-j\kappa r_2)\right]\right\}$	$\frac{0.5*10^5\omega}{2B'\kappa^2}\left\{\left[H_0^{(2)}(\kappa r_1)-H_0^{(2)}(-j\kappa r_1)\right]-\left[H_0^{(2)}(\kappa r_2)-H_0^{(2)}(-j\kappa r_2)\right]\right\}$	0	$\frac{0.5*10^5\omega}{2B'\kappa^2}\left\{\left[H_0^{(2)}(\kappa r_1)-H_0^{(2)}(-j\kappa r_1)\right]-\left[H_0^{(2)}(\kappa r_2)-H_0^{(2)}(-j\kappa r_2)\right]\right\}$
i=4	$\frac{0.5*10^5\omega}{2B'\kappa^2}\left\{\left[H_0^{(2)}(\kappa r_1)-H_0^{(2)}(-j\kappa r_1)\right]-\left[H_0^{(2)}(\kappa r_2)-H_0^{(2)}(-j\kappa r_2)\right]\right\}$	$\frac{0.5*10^5\omega}{2B'\kappa^2}\left\{\left[H_0^{(2)}(\kappa r_1)-H_0^{(2)}(-j\kappa r_1)\right]-\left[H_0^{(2)}(\kappa r_2)-H_0^{(2)}(-j\kappa r_2)\right]\right\}$	$\frac{0.5*10^5\omega}{2B'\kappa^2}\left\{\left[H_0^{(2)}(\kappa r_1)-H_0^{(2)}(-j\kappa r_1)\right]-\left[H_0^{(2)}(\kappa r_2)-H_0^{(2)}(-j\kappa r_2)\right]\right\}$	0
i=5	0	$\frac{0.5*10^5\omega}{2B'\kappa^2}\left\{\left[\frac{\partial H_0^{(2)}(\kappa r_1)}{\partial r_1}-\frac{\partial H_0^{(2)}(-j\kappa r_1)}{\partial r_1}\right]\frac{y_1}{r_1}-\left[\frac{\partial H_0^{(2)}(\kappa r_2)}{\partial r_2}-\frac{\partial H_0^{(2)}(-j\kappa r_2)}{\partial r_2}\right]\frac{y_1}{r_2}\right\}$	$\frac{0.5*10^5\omega}{2B'\kappa^2}\left\{\left[\frac{\partial H_0^{(2)}(\kappa r_1)}{\partial r_1}-\frac{\partial H_0^{(2)}(-j\kappa r_1)}{\partial r_1}\right]\frac{y_1}{r_1}-\left[\frac{\partial H_0^{(2)}(\kappa r_2)}{\partial r_2}-\frac{\partial H_0^{(2)}(-j\kappa r_2)}{\partial r_2}\right]\frac{y_1}{r_2}\right\}$	$\frac{0.5*10^5\omega}{2B'\kappa^2}\left\{\left[\frac{\partial H_0^{(2)}(\kappa r_1)}{\partial r_1}-\frac{\partial H_0^{(2)}(-j\kappa r_1)}{\partial r_1}\right]\frac{y_1}{r_1}-\left[\frac{\partial H_0^{(2)}(\kappa r_2)}{\partial r_2}-\frac{\partial H_0^{(2)}(-j\kappa r_2)}{\partial r_2}\right]\frac{y_1}{r_2}\right\}$
i=6	$\frac{0.5*10^5\omega}{2B'\kappa^2}\left\{\left[\frac{\partial H_0^{(2)}(\kappa r_1)}{\partial r_1}-\frac{\partial H_0^{(2)}(-j\kappa r_1)}{\partial r_1}\right]\frac{y_2}{r_1}-\left[\frac{\partial H_0^{(2)}(\kappa r_2)}{\partial r_2}-\frac{\partial H_0^{(2)}(-j\kappa r_2)}{\partial r_2}\right]\frac{y_2}{r_2}\right\}$	0	$\frac{0.5*10^5\omega}{2B'\kappa^2}\left\{\left[\frac{\partial H_0^{(2)}(\kappa r_1)}{\partial r_1}-\frac{\partial H_0^{(2)}(-j\kappa r_1)}{\partial r_1}\right]\frac{y_2}{r_1}-\left[\frac{\partial H_0^{(2)}(\kappa r_2)}{\partial r_2}-\frac{\partial H_0^{(2)}(-j\kappa r_2)}{\partial r_2}\right]\frac{y_2}{r_2}\right\}$	$\frac{0.5*10^5\omega}{2B'\kappa^2}\left\{\left[\frac{\partial H_0^{(2)}(\kappa r_1)}{\partial r_1}-\frac{\partial H_0^{(2)}(-j\kappa r_1)}{\partial r_1}\right]\frac{y_2}{r_1}-\left[\frac{\partial H_0^{(2)}(\kappa r_2)}{\partial r_2}-\frac{\partial H_0^{(2)}(-j\kappa r_2)}{\partial r_2}\right]\frac{y_2}{r_2}\right\}$
i=7	$\frac{0.5*10^5\omega}{2B'\kappa^2}\left\{\left[\frac{\partial H_0^{(2)}(\kappa r_1)}{\partial r_1}-\frac{\partial H_0^{(2)}(-j\kappa r_1)}{\partial r_1}\right]\frac{y_3}{r_1}-\left[\frac{\partial H_0^{(2)}(\kappa r_2)}{\partial r_2}-\frac{\partial H_0^{(2)}(-j\kappa r_2)}{\partial r_2}\right]\frac{y_3}{r_2}\right\}$	$\frac{0.5*10^5\omega}{2B'\kappa^2}\left\{\left[\frac{\partial H_0^{(2)}(\kappa r_1)}{\partial r_1}-\frac{\partial H_0^{(2)}(-j\kappa r_1)}{\partial r_1}\right]\frac{y_3}{r_1}-\left[\frac{\partial H_0^{(2)}(\kappa r_2)}{\partial r_2}-\frac{\partial H_0^{(2)}(-j\kappa r_2)}{\partial r_2}\right]\frac{y_3}{r_2}\right\}$	0	$\frac{0.5*10^5\omega}{2B'\kappa^2}\left\{\left[\frac{\partial H_0^{(2)}(\kappa r_1)}{\partial r_1}-\frac{\partial H_0^{(2)}(-j\kappa r_1)}{\partial r_1}\right]\frac{y_3}{r_1}-\left[\frac{\partial H_0^{(2)}(\kappa r_2)}{\partial r_2}-\frac{\partial H_0^{(2)}(-j\kappa r_2)}{\partial r_2}\right]\frac{y_3}{r_2}\right\}$
i=8	$\frac{0.5*10^5\omega}{2B'\kappa^2}\left\{\left[\frac{\partial H_0^{(2)}(\kappa r_1)}{\partial r_1}-\frac{\partial H_0^{(2)}(-j\kappa r_1)}{\partial r_1}\right]\frac{y_4}{r_1}-\left[\frac{\partial H_0^{(2)}(\kappa r_2)}{\partial r_2}-\frac{\partial H_0^{(2)}(-j\kappa r_2)}{\partial r_2}\right]\frac{y_4}{r_2}\right\}$	$\frac{0.5*10^5\omega}{2B'\kappa^2}\left\{\left[\frac{\partial H_0^{(2)}(\kappa r_1)}{\partial r_1}-\frac{\partial H_0^{(2)}(-j\kappa r_1)}{\partial r_1}\right]\frac{y_4}{r_1}-\left[\frac{\partial H_0^{(2)}(\kappa r_2)}{\partial r_2}-\frac{\partial H_0^{(2)}(-j\kappa r_2)}{\partial r_2}\right]\frac{y_4}{r_2}\right\}$	$\frac{0.5*10^5\omega}{2B'\kappa^2}\left\{\left[\frac{\partial H_0^{(2)}(\kappa r_1)}{\partial r_1}-\frac{\partial H_0^{(2)}(-j\kappa r_1)}{\partial r_1}\right]\frac{y_4}{r_1}-\left[\frac{\partial H_0^{(2)}(\kappa r_2)}{\partial r_2}-\frac{\partial H_0^{(2)}(-j\kappa r_2)}{\partial r_2}\right]\frac{y_4}{r_2}\right\}$	0

	j=9	j=10	j=11	j=12
i=9	$\frac{\omega}{4B'}(1-\frac{4j}{\pi}\ln\frac{\gamma\kappa a}{2})$	$\frac{0.5*10^5\omega}{2B'\kappa^2}\left\{\left[\frac{\partial H_o^{(2)}(\kappa r_1)}{\partial r_1}-\frac{\partial H_o^{(2)}(-j\kappa r_1)}{\partial r_1}\right]\frac{x_1-a}{r_1}-\left[\frac{\partial H_o^{(2)}(\kappa r_2)}{\partial r_2}-\frac{\partial H_o^{(2)}(-j\kappa r_2)}{\partial r_2}\right]\frac{x_1+a}{r_2}\right\}$	$\frac{0.5*10^5\omega}{2B'\kappa^2}\left\{\left[\frac{\partial H_o^{(2)}(\kappa r_1)}{\partial r_1}-\frac{\partial H_o^{(2)}(-j\kappa r_1)}{\partial r_1}\right]\frac{x_1-a}{r_1}-\left[\frac{\partial H_o^{(2)}(\kappa r_2)}{\partial r_2}-\frac{\partial H_o^{(2)}(-j\kappa r_2)}{\partial r_2}\right]\frac{x_1+a}{r_2}\right\}$	$\frac{0.5*10^5\omega}{2B'\kappa^2}\left\{\left[\frac{\partial H_o^{(2)}(\kappa r_1)}{\partial r_1}-\frac{\partial H_o^{(2)}(-j\kappa r_1)}{\partial r_1}\right]\frac{x_1-a}{r_1}-\left[\frac{\partial H_o^{(2)}(\kappa r_2)}{\partial r_2}-\frac{\partial H_o^{(2)}(-j\kappa r_2)}{\partial r_2}\right]\frac{x_1+a}{r_2}\right\}$
i=10	$\frac{0.5*10^5\omega}{2B'\kappa^2}\left\{\left[\frac{\partial H_o^{(2)}(\kappa r_1)}{\partial r_1}-\frac{\partial H_o^{(2)}(-j\kappa r_1)}{\partial r_1}\right]\frac{x_2-a}{r_1}-\left[\frac{\partial H_o^{(2)}(\kappa r_2)}{\partial r_2}-\frac{\partial H_o^{(2)}(-j\kappa r_2)}{\partial r_2}\right]\frac{x_2+a}{r_2}\right\}$	$\frac{\omega}{4B'}(1-\frac{4j}{\pi}\ln\frac{\gamma\kappa a}{2})$	$\frac{0.5*10^5\omega}{2B'\kappa^2}\left\{\left[\frac{\partial H_o^{(2)}(\kappa r_1)}{\partial r_1}-\frac{\partial H_o^{(2)}(-j\kappa r_1)}{\partial r_1}\right]\frac{x_2-a}{r_1}-\left[\frac{\partial H_o^{(2)}(\kappa r_2)}{\partial r_2}-\frac{\partial H_o^{(2)}(-j\kappa r_2)}{\partial r_2}\right]\frac{x_2+a}{r_2}\right\}$	$\frac{0.5*10^5\omega}{2B'\kappa^2}\left\{\left[\frac{\partial H_o^{(2)}(\kappa r_1)}{\partial r_1}-\frac{\partial H_o^{(2)}(-j\kappa r_1)}{\partial r_1}\right]\frac{x_2-a}{r_1}-\left[\frac{\partial H_o^{(2)}(\kappa r_2)}{\partial r_2}-\frac{\partial H_o^{(2)}(-j\kappa r_2)}{\partial r_2}\right]\frac{x_2+a}{r_2}\right\}$
i=11	$\frac{0.5*10^5\omega}{2B'\kappa^2}\left\{\left[\frac{\partial H_o^{(2)}(\kappa r_1)}{\partial r_1}-\frac{\partial H_o^{(2)}(-j\kappa r_1)}{\partial r_1}\right]\frac{x_3-a}{r_1}-\left[\frac{\partial H_o^{(2)}(\kappa r_2)}{\partial r_2}-\frac{\partial H_o^{(2)}(-j\kappa r_2)}{\partial r_2}\right]\frac{x_3+a}{r_2}\right\}$	$\frac{0.5*10^5\omega}{2B'\kappa^2}\left\{\left[\frac{\partial H_o^{(2)}(\kappa r_1)}{\partial r_1}-\frac{\partial H_o^{(2)}(-j\kappa r_1)}{\partial r_1}\right]\frac{x_3-a}{r_1}-\left[\frac{\partial H_o^{(2)}(\kappa r_2)}{\partial r_2}-\frac{\partial H_o^{(2)}(-j\kappa r_2)}{\partial r_2}\right]\frac{x_3+a}{r_2}\right\}$	$\frac{\omega}{4B'}(1-\frac{4j}{\pi}\ln\frac{\gamma\kappa a}{2})$	$\frac{0.5*10^5\omega}{2B'\kappa^2}\left\{\left[\frac{\partial H_o^{(2)}(\kappa r_1)}{\partial r_1}-\frac{\partial H_o^{(2)}(-j\kappa r_1)}{\partial r_1}\right]\frac{x_3-a}{r_1}-\left[\frac{\partial H_o^{(2)}(\kappa r_2)}{\partial r_2}-\frac{\partial H_o^{(2)}(-j\kappa r_2)}{\partial r_2}\right]\frac{x_3+a}{r_2}\right\}$
i=12	$\frac{0.5*10^5\omega}{2B'\kappa^2}\left\{\left[\frac{\partial H_o^{(2)}(\kappa r_1)}{\partial r_1}-\frac{\partial H_o^{(2)}(-j\kappa r_1)}{\partial r_1}\right]\frac{x_4-a}{r_1}-\left[\frac{\partial H_o^{(2)}(\kappa r_2)}{\partial r_2}-\frac{\partial H_o^{(2)}(-j\kappa r_2)}{\partial r_2}\right]\frac{x_4+a}{r_2}\right\}$	$\frac{0.5*10^5\omega}{2B'\kappa^2}\left\{\left[\frac{\partial H_o^{(2)}(\kappa r_1)}{\partial r_1}-\frac{\partial H_o^{(2)}(-j\kappa r_1)}{\partial r_1}\right]\frac{x_4-a}{r_1}-\left[\frac{\partial H_o^{(2)}(\kappa r_2)}{\partial r_2}-\frac{\partial H_o^{(2)}(-j\kappa r_2)}{\partial r_2}\right]\frac{x_4+a}{r_2}\right\}$	$\frac{0.5*10^5\omega}{2B'\kappa^2}\left\{\left[\frac{\partial H_o^{(2)}(\kappa r_1)}{\partial r_1}-\frac{\partial H_o^{(2)}(-j\kappa r_1)}{\partial r_1}\right]\frac{x_4-a}{r_1}-\left[\frac{\partial H_o^{(2)}(\kappa r_2)}{\partial r_2}-\frac{\partial H_o^{(2)}(-j\kappa r_2)}{\partial r_2}\right]\frac{x_4+a}{r_2}\right\}$	$\frac{\omega}{4B'}(1-\frac{4j}{\pi}\ln\frac{\gamma\kappa a}{2})$

Appendix B

Helmhotz Equation and Boundary Integral Method

Appendix B.

Helmhotz Equation and Boundary Integral Method

B.1 Helmhotz Equation

If the underwater acoustic pressure can be expressed as a harmonic function of time with frequency ω, then

$$p(\vec{r},t) = P(\vec{r})e^{i\omega t} \tag{B.1}$$

The governing wave equation for underwater sound propagation is,

$$\nabla^2 p(\vec{r},t) = \frac{1}{c^2}\partial_{tt} p(\vec{r}) \tag{B.2}$$

where c is the sound propagation speed in water and $\partial_{tt} = \frac{\partial^2}{\partial t^2}$. Take Fourier transform on both sides of equation (B.2).

$$\int_{-\infty}^{\infty} [\nabla^2 p(\vec{r},t) - \frac{1}{c^2}\partial_{tt} p(\vec{r},t)]e^{-i\omega t} dt = 0$$

or

$$\nabla^2 (\int_{-\infty}^{\infty} p(\vec{r},t)e^{-i\omega t} dt) + \frac{\omega^2}{c^2}(\int_{-\infty}^{\infty} p(\vec{r},t)e^{-i\omega t} dt) = 0 \tag{B.3}$$

Define $P(\vec{r},\omega) = \int_{-\infty}^{\infty} p(\vec{r},t)e^{-i\omega t} dt$ and the wave number $k = \omega / c$,then equation (B.3) becomes

$$\nabla^2 P(\vec{r},\omega) + k^2 P(\vec{r},\omega) = 0 \tag{B.4}$$

Equation (B.4) is known as the Helmhotz equation.

The time domain pressure distribution can then be obtained by the inverse Fourier transform

$$p(\vec{r},t) = \frac{1}{2\pi}\int_{-\infty}^{\infty} P(\vec{r},\omega)e^{i\omega t} d\omega \tag{B.5}$$

B.2 Boundary Integral Method

B.2.1 Basic Boundary Integral Theorem

Suppose there are two functions Φ and λ which have continuous first and second order derivatives, then the following relation can be obtained from the Green's Second Identity :

$$\int_V (\Phi\nabla^2\lambda - \lambda\nabla^2\Phi)dV = \int_V (\Phi\frac{\partial\lambda}{\partial n} - \lambda\frac{\partial\Phi}{\partial n})ds \qquad (B.6)$$

where $\frac{\partial}{\partial n}$ means the outward divergence on the surface of the control volume.

Consider the field point $\vec{r} = \vec{r}(x,y,z)$ and the source point $\vec{r}_s = \vec{r}_s(x_s, y_s, z_s)$ in the control volume, set r to be the distance between these two points, then the free space Green's function can be expressed as :

$$G = \frac{e^{ikr}}{r} \qquad (B.7)$$

where

$$r = \sqrt{(x_s - x)^2 + (y_s - y)^2 + (z_s - z)^2}$$

If P represents the pressure function in V, then from the Green's theorem

$$\int_V (P\nabla^2 G - G\nabla^2 P)dV = \int_V (P\frac{\partial G}{\partial n} - G\frac{\partial P}{\partial n})dS \qquad (B.8)$$

Substituting the Helmholtz equation (B.4) and the Green's function (B.7) into equation (A.8), then it becomes

$$\nabla^2 G + k^2 G = 0 \qquad (B.9)$$

From equations (B.4) and (B.9), it can be shown that within the control volume but excluding the points within the infinitesimal sphere around the field point there exists the relation :

$$\nabla(P\nabla G - G\nabla P) = 0 \tag{B.10}$$

or

$$P\nabla G - G\nabla P = 0 \tag{B.11}$$

B.2.2 Boundary Integral Equation

As in the right side of equation (B.8) the boundary integral should consider the normal direction of the boundary surface. The propagation direction of sound can be characterised by the relative position of the source point and the field point. If within the control volume the sound field point is outside the sound source body, then it is an exterior propagation problem as shown in Figure B1. Otherwise, it is an interior propagation problem, shown in Figure B2.

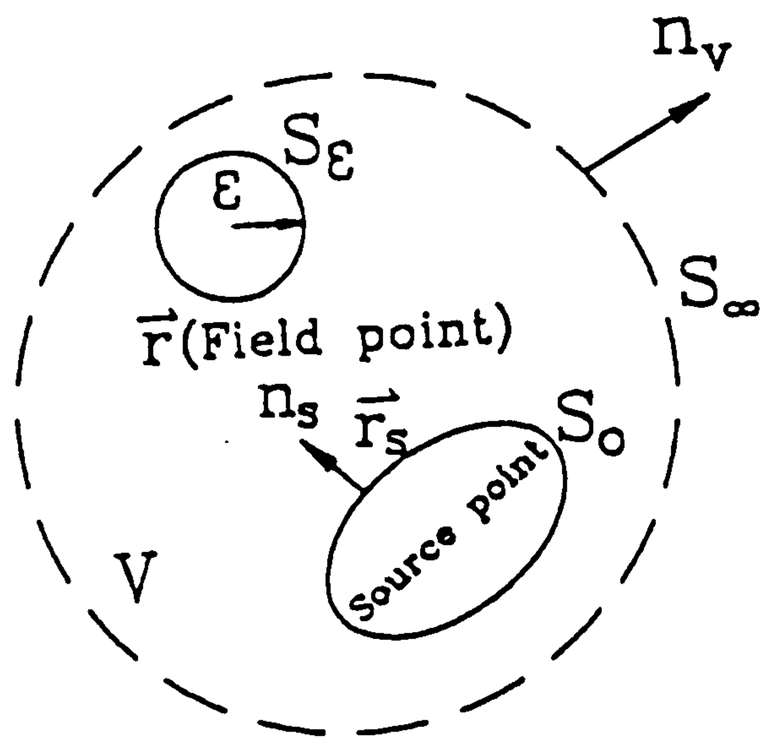

Figure B1. Exterior propagation problem

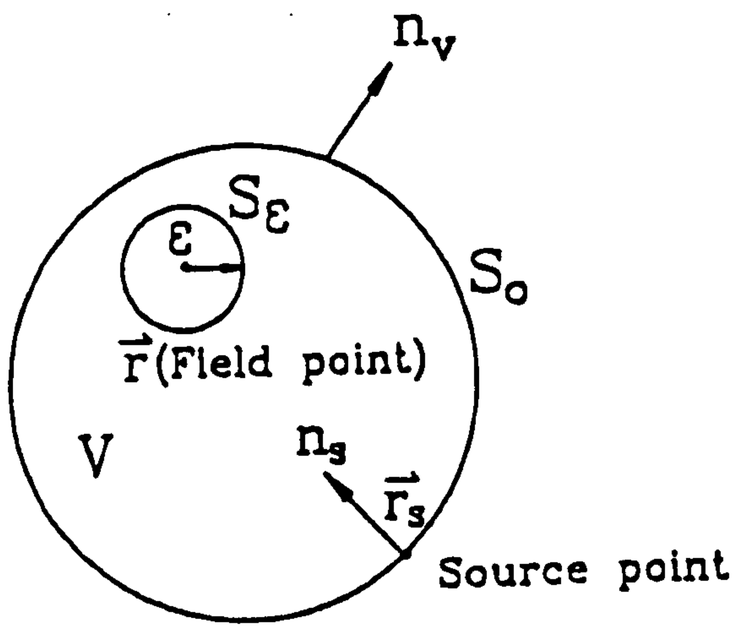

Figure B2. Interior propagation problem

Consider the exterior propagation problem described as in Figure B1, in which $\vec{r}$ means the position vector of a sound field point, S_ε is the spheric surface which encompassing the considered sound field point with a infinitesimal radius ε, S_∞ represents the surface area of the infinite control volume V, n_v is outward normal vector of the surface S_∞, n_S is outward normal vector of the surface of source body. At the source point n_v and n_S have opposite directions, ie, $\frac{\partial}{\partial n_s} = -\frac{\partial}{\partial n_v}$.

From the Green's theorem, equation (B.8) becomes :

$$\int_{S_0+S_\varepsilon+S_\infty} [P(\vec{r}_s)\frac{\partial G(\vec{r},\vec{r}_s)}{\partial n_v} - G(\vec{r},\vec{r}_s)\frac{\partial P(\vec{r}_s)}{\partial n_v}]dS = \int_V (P\nabla G - G\nabla P)dV = 0 \qquad (B.12)$$

in which

$$\int_{S_\varepsilon}[P(\vec{r})\frac{\partial G(\vec{r},\vec{r}_s)}{\partial n_v} - G(\vec{r},\vec{r}_s)\frac{\partial P(\vec{r})}{\partial n_v}]dS(\vec{r}) = 4\pi P(\vec{r})$$

$$\int_{S_\infty}[P(\infty)\frac{\partial G(\vec{r},\vec{r}_s)}{\partial n_v} - G(\vec{r},\vec{r}_s)\frac{\partial P(\infty)}{\partial n_v}]dS(\infty) = 0$$

so that

$$4\pi P(\vec{r}) + \int_{S_0}[P(\vec{r}_s)\frac{\partial G(\vec{r},\vec{r}_s)}{\partial n_v} - G(\vec{r},\vec{r}_s)\frac{\partial P(\vec{r}_s)}{\partial n_v}]dS(\vec{r}_s) = 0 \qquad (B.13)$$

or

$$4\pi P(\vec{r}) = \int_{S_0}[P(\vec{r}_s)\frac{\partial G(\vec{r},\vec{r}_s)}{\partial n_v} - G(\vec{r},\vec{r}_s)\frac{\partial P(\vec{r}_s)}{\partial n_v}]dS(\vec{r}_s) \qquad (B.14)$$

Equation (B.14) is named as the Exterior Helmholtz Integral Equation.

If both the sound source point and sound field point are sited on the boundary surface of the sound source body, then the field point $\vec{r}$ can be only encompassed by an infinitesimal semi-spheric surface. Now equation (B.14) becomes :

$$2\pi P(\vec{r}) = \int_{S_0}[P(\vec{r}_s)\frac{\partial G(\vec{r},\vec{r}_s)}{\partial n_v} - G(\vec{r},\vec{r}_s)\frac{\partial P(\vec{r}_s)}{\partial n_v}]dS(\vec{r}_s) \qquad (B.15)$$

In the exterior propagation problem, if the field point is considered within the source body and is not pertaining to the interior region of the control volume V, then equation (B.13) should be taken account for deleting the surface integral domain S ,ie,

$$\int_{S_0}[P(\vec{r}_s)\frac{\partial G(\vec{r},\vec{r}_s)}{\partial n_v} - G(\vec{r},\vec{r}_s)\frac{\partial P(\vec{r}_s)}{\partial n_v}]dS(\vec{r}_s) = 0 \qquad \text{(B.16)}$$

As for the interior propagation problem, the derivations are the same as the exterior propagation problem except to put n_S and n_V in the same directions.

After summarising various conditions of the $\vec{r}$ positions ,the Helmholtz equation can be expressed as :

$$C(\vec{r})P(\vec{r}) = \int_{S_0}[P(\vec{r}_s)\frac{\partial G(\vec{r},\vec{r}_s)}{\partial n_v} - G(\vec{r},\vec{r}_s)\frac{\partial P(\vec{r}_s)}{\partial n_v}]dS(\vec{r}_s) \qquad \text{(B.17)}$$

where the $C(\vec{r})$ values are listed in Table B.1.

Table B.1 $C(\vec{r})$ values for various $\vec{r}$ position

Position of $\vec{r}$	Exterior propagation	Interior propagation
$\vec{r}$ outside S_0	$C(\vec{r}) = 4\pi$	$C(\vec{r}) = 0$
$\vec{r}$ on S_0	$C(\vec{r}) = 2\pi$	$C(\vec{r}) = 2\pi$
$\vec{r}$ inside S_0	$C(\vec{r}) = 0$	$C(\vec{r}) = 4\pi$

As for other surface boundary like a corner or plane, then $C(\vec{r})$ is taken to be :

$$C(\vec{r}) = 4\pi - \int_{S_0}\frac{\partial(\frac{1}{r(\vec{r},\vec{r}_s)})}{\partial n}dS(\vec{r}_s) \qquad \text{(B.18)}$$

B.3 Fluid-Structure Interaction

As the density of water is much greater than air, the coupling effects of fluid-structure interaction have to be taken into consideration for the vibration problems of an immersed structure. As shown in equation (B.15), $P(\vec{r})$ represents the relative acoustic pressure on the wetted surface of a submerged sturcture in vibration. On the wetted surface there exists the relation :

$$\frac{\partial P(\vec{r}_s)}{\partial n} = i\rho\omega v_n(\vec{r}_s) \tag{B.19}$$

Now the Helmhotz Integral Equation of the submerged body surface can be expressed as :

$$C(\vec{r})P(\vec{r}) = \int_{S_0}[P(\vec{r}_s)\frac{\partial G(\vec{r},\vec{r}_s)}{\partial n_v} + i\rho\omega G(\vec{r},\vec{r}_s)v_n(\vec{r}_s)]dS(\vec{r}_s) \tag{B.20}$$

Utilizing the boundary element discretization technique on the submerged body surface, equation (B.20) can be written as :

$$C(\vec{r})P(\vec{r}) = \sum_e \int_{S_e}[N(\vec{r}_s)P(\vec{r}_s)\frac{\partial G(\vec{r},\vec{r}_s)}{\partial n_v} - i\rho\omega G(\vec{r},\vec{r}_s)N(\vec{r}_s)v_n(\vec{r}_s)]dS_e(\vec{r}_s) \tag{B.21}$$

Equation (B.21) can be expressed in matrix form as :

$$[A]\{P\} = [B]\{V_n\} \tag{B.22}$$

where

$$[A] = C(\vec{r}) - \sum_e \int_{S_e}[N(\vec{r}_s)\frac{\partial G(\vec{r},\vec{r}_s)}{\partial n_v}]dS_e(\vec{r}_s) \tag{B.23}$$

$$[B] = \sum_e \int_{S_e} i\rho\omega G(\vec{r},\vec{r}_s)N(\vec{r}_s)dS_e(\vec{r}_s) \tag{B.24}$$

By assuming that the modal point displacements of the boundary structure elements have the form :

$$\{x_n\} = \{X_n\}e^{i\omega t}$$

then

$$\{v_n\} = \frac{\partial\{x_n\}}{\partial t} = i\omega\{x_n\} \tag{B.25}$$

Substituting into equation (B.22), it becomes

$$[A]\{P\} = i\omega[B]\{x_n\} \tag{B.27}$$

or

$$[A]\{P\} = [G]\{x_n\} \tag{B.28}$$

where

$$[G] = i\omega[B]$$

The fluid interacting forces applied to the nodal points of the wetted structure boundauy surface are :

$$\{f_w\} = \{a\}^T\{P\} = \{a\}^T[A]^{-1}[B]i\omega\{x_n\} = \{a\}^T[A]^{-1}[G]\{x_n\} \tag{B.28}$$

in which {a} represents the area parameters of each nodal point.

Appendix C

Half-Space Green's Function for Helmhotz Equation

Appendix C.

Half-Space Green's Function for Helmhotz Equation

The Green's function in equation (A.7) represents that of the submerged body situated within an unbounded water space. When the body nears or is located at the free surface or the seabed, there exists an infinite plane surface S_p as shown in Figure C1 and C2, the Green's function used in the boundary surface integral equation (B.8) should be changed. In this case the impedance boundary condition should be satisfied on both the submerged body surface S_0 and the infinite plane surface S_p .The impedance boundary condition can be expressed as :

$$ikP + \frac{Z}{\rho_0 c}\frac{\partial P}{\partial n_0} = 0 \qquad (C.1)$$

where Z represents the surface sound impedance and $\rho_0 c$ is the characteristic value of the impedance in the medium. Now the boundary surface integral should be taken over the domains S_0 and S_p . In order to overcome the difficuty of integrating over the unbounded plane surface S_p ,it is intended to choose a Half-Space Green's Function G_h so as to make that

$$\int_{s_p}[P\frac{\partial G_h}{\partial n_0} + G_h\frac{\partial P}{\partial n_0}]dS = 0 \qquad (C.2)$$

and simultaneously to satisfy the impedance boundary condition :

$$ikG_h + \frac{Z}{\rho_0 c}\frac{\partial G_h}{\partial n_0} = 0 \qquad (C.3)$$

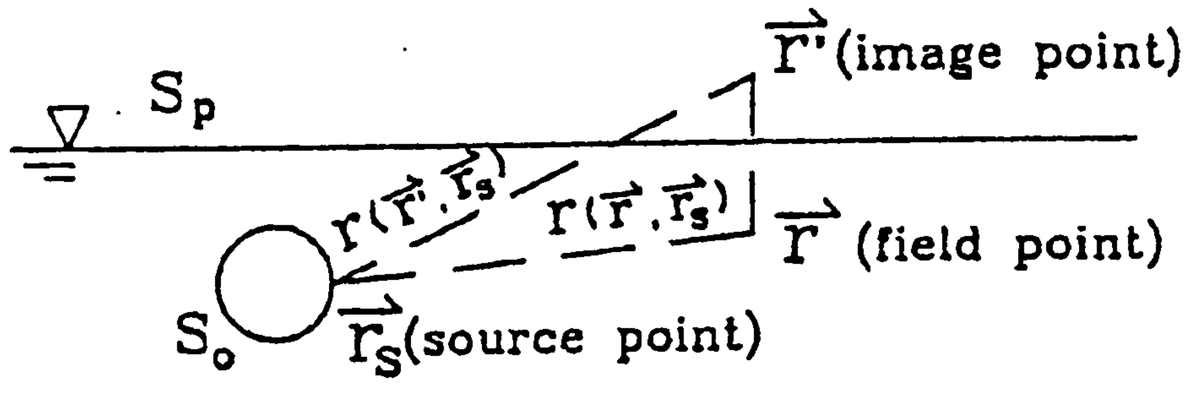

Figure C1 Submerged body nears half-space boundary

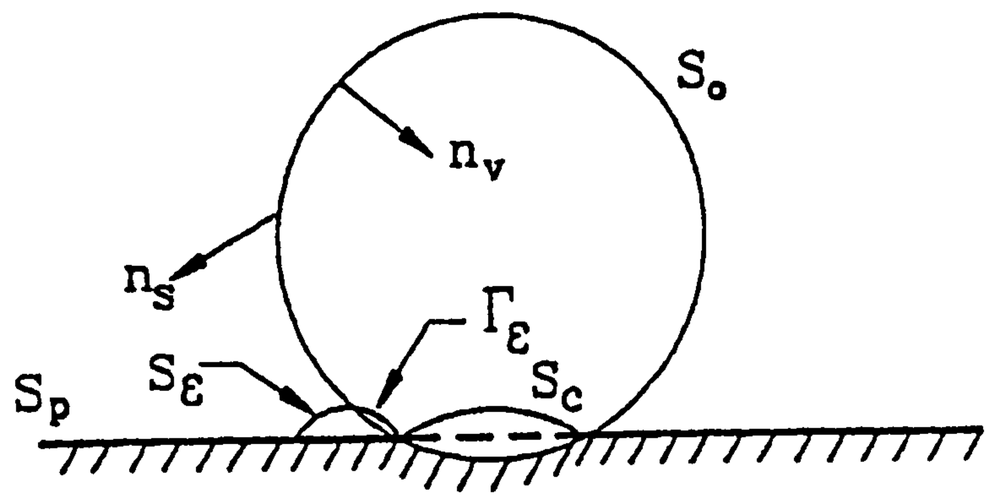

Figure C2 Submerged body situated in half-space

There are different boundary conditions which need to be considered for each type of the half-space propagation problem, and they are :

(a) If the submerged body is near the free surface, then $P = 0$ on S_p.

(b) If the submerged body is situated on the seabed, then $\frac{\partial P}{\partial n_0} = 0$ on S_p .

Choose the Helf-Space Green's Function so considered as :

$$G_h = \frac{e^{ikr}}{r} + R_p \frac{e^{-ikr'}}{r'} \qquad (C.4)$$

The above expression is just to increase an image point $\vec{r}'$ to the field point $\vec{r}$ with respect to the free surface. Where R_p represents the refraction ratio of the plane boundary surface S_p . When $R_P = 1$, ie, in the rigid body surface condition $Z \to \infty$ and $\frac{\partial G_h}{\partial n_0} = 0$ which means the velocity is zero as $\vec{r}_s$ located on S_p. When $R_p = -1$, ie, in the free surface conditions, $Z=0$ and $P=0$. As $\vec{r}_s$ is on S_p, $G_h=0$ .Both the conditions $R_p = 1$ and $R_p = -1$ can satisfy equation (C.2).

Appendix D

Publication Works

The following technical papers related directly to the work of the study have been published during its progress.

1. W.H. Wang, R. Sutton and B. Dobson (1995) "Modelling Mobility and Transmissibility of Sound and Vibration from Machinery to Ship Structure", Journal of the Society of Naval Architects and Marine Engineers, ROC, Vol. 14, No.2, pp. 31-53.(This paper was awarded as to be the outstanding paper on the annual meeting of the Society of Naval Architects and Marine Engineers, ROC, 1995).

2. W.H. Wang, R. Sutton and B. Dobson (1997) "Structure-Borne Noise Control for a Marine Engine", Proceedings of the 10th Symposium of the Acoustical Society, ROC, Taipei, pp. 190-199.

3.W.H. Wang, R. Sutton and B. Dobson (1997) "Behaviour of Structure-Borne Noise Attenuation in a Resilient Mount", Proceedings of TRAM'97 SIMGAPORE, pp. 241-251.

4.W.H. Wang, R. Sutton and B. Dobson (1998) "Behaviour of Structure-Borne Noise Attenuation in a Resilient Mount", Journal the Society of Naval Architects and Marine Engineers, ROC, Vol.17, No.2, pp. 49-62.

5.W.H. Wang, R.J. Shyu and J.R. Chang (1998) "Viscoelastic Passive Damping Technology on Ship's Vibration and Noise Control", Proceedings of PRADS'98, Hague, pp. 943-950.

6.W.H. Wang, and T.C.Yang (1999) "Mobility Analysis of the Improved Bottom Structure by Squeeze Film for Structure-Borne Noise Reduction", Proceedings of Third International Students' Congress of the Asia-Pacific Region Countries, Part II, pp. 7.1-7.18.(This paper was awarded as to be the outstanding paper on the field of ocean engineering and shipbuiding.)

7.W.H. Wang, J.H. Liou, R. Sutton and B. Dobson (2000) "Machine Vibration Induced Underwater Acoustic Radiation", Journal of Marine Science and Technology, Vol.8, No.1, pp. 1-11.

SOME PARTS
EXCLUDED
UNDER
INSTRUCTION
FROM THE
UNIVERSITY

Appendix E

FORTRAN Program for Structure-Borne Noise Propagation Analysis

```
      PROGRAM MAIN
C     ============================================================
C     PURPOSE:THIS PROGRAM IS DEVELOPED TO PREDICT
C     PROPAGATION OF STRUCTURE-BORNE NOISE
C     NW   IS   FREQUENCY
C     A_M   IS   MASS
C     DB     IS THE RIGID OF THE BENDING
C     A_K   IS   K
C     N_FORC(NT,3)   IS THE NUMBER OF THE FORCE
C     N_DISP(NT,2)     IS THE NUMBER OF THE DISPLACE
      IMPLICIT DOUBLE PRECISION (A,B,D-H,O-Y)
      IMPLICIT COMPLEX*16 (C,Z)
      PARAMETER (NT=100,CI=(0.0,1.0),CJ=(1.0,0.0))
      DIMENSION A_NODE(NT,4),N_ELEM(NT,5),CAHM(NT,NT),CHR1(24,24)
     +K(4),N_FORC(NT,3),N_DISP(NT,3),NIN(NT)
C      OPEN(17,FILE='TEST_1.TXT')
      OPEN(18,FILE='T33.TXT')
C     OPEN ELEM,A_NODE FILES
      OPEN(12,FILE='INPUT.TXT')
      READ(12,*) NE,NN,E,U,RO,TH,N_FOR,N_DIS
      CLOSE(12)
      OPEN(13,FILE='ELEM.TXT')
      OPEN(14,FILE='NODE.TXT')
      DO 10 I=1,NE
      READ (13,*) N_ELEM(I,1),N_ELEM(I,2),
     +N_ELEM(I,3),N_ELEM(I,4),N_ELEM(I,5)
10    CONTINUE
      DO 20 I=1,NN
20    READ(14,*) A_NODE(I,1),A_NODE(I,2),A_NODE(I,3),A_NODE(I,4)
      CLOSE(13)
      CLOSE(14)
C     READ THE BOUNDARY CONDITION
C     N_ALL IS THE NUMBER OF ALL NODES
C     N_UKN IS THE NUMBER OF THE UNKNOW DEGREE OF FREEDOM
C     NIN IS THE INDEX AFTER CHANGING THE LOCATION
      OPEN(15,FILE='FORCE.TXT')
      OPEN(16,FILE='DISP.TXT')
      DO 50 I=1,N_FOR
50    READ(15,*) N_FORC(I,1),N_FORC(I,2),N_FORC(I,3)
      DO 51 I=1,N_DIS
51    READ(16,*) N_DISP(I,1),N_DISP(I,2),N_DISP(I,3)
      CLOSE(15)
      CLOSE(16)
      N_ALL = NN*6
      N_UKN = N_ALL-N_DIS
      CALL NINDEX(NT,N_DISP,N_DIS,N_ALL,N_UKN,NIN)
      W = 1
      DO 500 III=1,1000
      A_M = RO*TH
      DB    = E*TH**3/(12*(1-U**2))
      DD  = E/(1-U**2)
      A_K = (W**2*A_M/DB)**0.25
      A_K1= W/SQRT(DD/RO)
      DO 21 J=1,N_ALL
      DO 21 I=1,N_ALL
21    CAHM(I,J)=(0.0,0.0)
      DO 30 L=1,NE
      DO 22 J=1,4
      K(J)=N_ELEM(L,J+1)
22    CONTINUE
      CALL HMATR(W,DB,DD,A_K,A_K1,TH,RO,A_NODE,N_ELEM,CHR1,NT,L)
C     ASSEMBLE THE CHR1 MATRIX
```

```
      DO 40 JJ=1,4
      DO 40 KK=1,4
      DO 40 I=1,6
      DO 40 J=1,6
      CAHM(((K(JJ)-1)*6+I),((K(KK)-1)*6+J))
     + = CAHM(((K(JJ)-1)*6+I),((K(KK)-1)*6+J))
     + +CHR1((I+(JJ-1)*6),(J+(KK-1)*6))
40    CONTINUE
30    CONTINUE
C     PARTITION CAHM
      CALL PARTIT(W,N_FOR,N_DIS,N_UKN,N_ALL,NIN,CAHM,NT,N_FORC,N_DISP)
      W=W+1
500   CONTINUE
C     CLOSE(17)
      CLOSE(18)
      STOP
      END



      SUBROUTINE NINDEX(NT,N_DISP,N_DIS,N_ALL,N_UKN,NIN)
C     THE SUBROUTINE THE INDEX OF THE BOUNDARY CONDITION AFTER
C     REARRANGEMENT
C     N_DISP IS THE LOCATION OF THE DISPLACE
C     N_KN IS THE LOCATION OF THE DIMENSION
      IMPLICIT DOUBLE PRECISION (A,B,D-H,O-Y)
      DIMENSION N_DISP(NT,3),N_KN(N_DIS),N_UN(N_ALL),NIN(NT)
      DO 10 I=1,N_DIS
      N_KN(I)=(N_DISP(I,1)-1)*6+N_DISP(I,2)
10    CONTINUE
C     I SET THE N_UN(I)=0
      DO 20 I=1,N_ALL
      N_UN(I)=I
      DO 30 K=1,N_DIS
      IF (I .EQ. N_KN(K))THEN
      N_UN(I)=0
      END IF
30    CONTINUE
20    CONTINUE
      DO 40 K=(N_ALL-1),1,-1
      DO 50 J=1,K
      IF(N_UN(J) .GT. N_UN(J+1)) THEN
      M = N_UN(J)
      N_UN(J) = N_UN(J+1)
      N_UN(J+1) = M
      END IF
50    CONTINUE
40    CONTINUE
      DO 60 I=1,N_UKN
      N_UN(I)=N_UN(I+N_DIS)
60    CONTINUE
      DO 61 I=1,N_DIS
61    NIN(I)=N_KN(I)
      DO 62 I=1,N_UKN
62    NIN(I+N_DIS)=N_UN(I)
      RETURN
      END



      SUBROUTINE HMATR(W,DB,DD,A_K,A_K1,TH,RO,TN,NTE,CHR1,NT,L)
C     THIS SUBROUTINE IS MOBILITY MATRIX OF FINITE RECTANGULAR
```

```
C       K(4) COULD FIND NODE NUM.
C       T_X,T_Y,T_Z ARE THE GLOBAL COOR.
C       R12 ,R13 AND R14 ARE THE VECTOR FROM 1 TO 2,3 AND 4.
C       RCROS IS R12 X R13.
C       UNIT_X,UNIT_Y,UNIT_Z ARE THE LOCAL UNIT VECTOR.
C       X(I,J) AND Y(I,Y) IS THE MAGNITUDE OF THE UNIT_X AND UNIT_Y
C       FROM NODE I TO NODE J.
C       R(I,J) IS THE DISTANCE FROM NODE I TO NODE J.
        IMPLICIT DOUBLE PRECISION (A,B,D-H,O-Y)
        IMPLICIT COMPLEX*16 (C,Z)
        PARAMETER (CI=(0.0,1.0),CJ=(1.0,0.0),A=1.0E-5,AMP=1.0,
       +PI=3.141592653589793D0)
        DIMENSION NTE(NT,5),TN(NT,4),CHR(24,24),CHR1(24,24)
       +  ,CHL(24,24),CHLB(24,24),CHLL(24,24),CHL1(12,12),CHL2(8,8),K(4)
       +  ,T_X(7),T_Y(7),T_Z(7),R12(3),R13(3),R14(3),R(7,4),X(7,4),Y(7,4)
       +  ,UNIT_X(3),UNIT_Y(3),UNIT_Z(3),RCROS(3),TL(24,24),CTL(24,24)
       +  ,CTTL(24,24)
       +  ,CHZ1(2,2),CHZ2(2,2),CHZ1I(2,2),CHZ2I(2,2),CHAB(2,2),CHEF(2,2)
       +  ,CHAB1(2,2),CHEF1(2,2)
       +  ,CHL2A(8,8),CHL2B(8,8),CHL2C(8,8),IN(8)
        DO 3 J=1,12
        DO 3 I=1,12
3       CHL1(I,J)=(0.0,0.0)
        DO 4 J=1,8
        DO 4 I=1,8
4       CHL2(I,J)=(0.0,0.0)
        DO 1 I=1,3
        RCROS(I)=0
        UNIT_X(I)=0
        UNIT_Y(I)=0
1       UNIT_Z(I)=0
        DO 2 I=1,7
        DO 2 J=1,4
        R(I,J)=0
        X(I,J)=0
2       Y(I,J)=0
C       CALL THE ROTATION TRANSFORMATION MATRIX [T]
C       CTL=TL*i
C       CTTL=CTL TRANSPOSE CTL
        CALL TRANS(TN,NTE,TL,NT,L)
        DO 9 I=1,24
        DO 9 J=1,24
        CHR1(I,J)=(0.0,0.0)
        CTL(I,J)=(0.0,0.0)
9       CTTL(I,J)=(0.0,0.0)
        DO 10 I=1,24
        DO 10 J=1,24
        CTL(I,J)=CJ*TL(I,J)
10      CONTINUE
        CALL TMPY(CTL,CTTL,24,24,24,24)
        DO 20 J=1,4
        K(J)=NTE(L,J+1)
20      CONTINUE
        DO 30 I=1,4
        T_X(I)=TN(K(I),2)
        T_Y(I)=TN(K(I),3)
        T_Z(I)=TN(K(I),4)
30      CONTINUE
C       CALCULATE THE DISTANCE R(I,J)
        DO 31 I=1,4
        DO 31 J=1,4
        D_X=T_X(I)-T_X(J)
```

```
      D_Y=T_Y(I)-T_Y(J)
      D_Z=T_Z(I)-T_Z(J)
      R(I,J)=SQRT(D_X**2+D_Y**2+D_Z**2)
31    CONTINUE
      DO 60 I=1,3
      T_X(I+4)=T_X(I)
      T_Y(I+4)=T_Y(I)
      T_Z(I+4)=T_Z(I)
60    CONTINUE
C     FIND THE VECTOR X AND Y
      DO 70 ID=0,3
      R12(1)=T_X(2+ID)-T_X(1+ID)
      R12(2)=T_Y(2+ID)-T_Y(1+ID)
      R12(3)=T_Z(2+ID)-T_Z(1+ID)
      R13(1)=T_X(3+ID)-T_X(1+ID)
      R13(2)=T_Y(3+ID)-T_Y(1+ID)
      R13(3)=T_Z(3+ID)-T_Z(1+ID)
      R14(1)=T_X(4+ID)-T_X(1+ID)
      R14(2)=T_Y(4+ID)-T_Y(1+ID)
      R14(3)=T_Z(4+ID)-T_Z(1+ID)
      RCROS(1)=R12(2)*R13(3)-R12(3)*R13(2)
      RCROS(2)=R12(3)*R13(1)-R12(1)*R13(3)
      RCROS(3)=R12(1)*R13(2)-R12(2)*R13(1)
      AM_R12=SQRT(R12(1)**2+R12(2)**2+R12(3)**2)
      AM_R13=SQRT(R13(1)**2+R13(2)**2+R13(3)**2)
      AM_RCR=SQRT(RCROS(1)**2+RCROS(2)**2+RCROS(3)**2)
C     CALCULATE THE UNIT_X,UNIT_Y AND UNIT_Z
      DO 40 II=1,3
      UNIT_X(II)=R12(II)/AM_R12
      UNIT_Z(II)=RCROS(II)/AM_RCR
40    CONTINUE
      UNIT_Y(1)=UNIT_Z(2)*UNIT_X(3)-UNIT_Z(3)*UNIT_X(2)
      UNIT_Y(2)=UNIT_Z(3)*UNIT_X(1)-UNIT_Z(1)*UNIT_X(3)
      UNIT_Y(3)=UNIT_Z(1)*UNIT_X(2)-UNIT_Z(2)*UNIT_X(1)
      X(2+ID,1+ID)=UNIT_X(1)*R12(1)+UNIT_X(2)*R12(2)+UNIT_X(3)*R12(3)
      X(3+ID,1+ID)=UNIT_X(1)*R13(1)+UNIT_X(2)*R13(2)+UNIT_X(3)*R13(3)
      X(4+ID,1+ID)=UNIT_X(1)*R14(1)+UNIT_X(2)*R14(2)+UNIT_X(3)*R14(3)
      Y(2+ID,1+ID)=UNIT_Y(1)*R12(1)+UNIT_Y(2)*R12(2)+UNIT_Y(3)*R12(3)
      Y(3+ID,1+ID)=UNIT_Y(1)*R13(1)+UNIT_Y(2)*R13(2)+UNIT_Y(3)*R13(3)
      Y(4+ID,1+ID)=UNIT_Y(1)*R14(1)+UNIT_Y(2)*R14(2)+UNIT_Y(3)*R14(3)
70    CONTINUE
      X(1,2)=X(5,2)
      X(1,3)=X(5,3)
      X(2,3)=X(6,3)
      X(1,4)=X(5,4)
      X(2,4)=X(6,4)
      X(3,4)=X(7,4)
      Y(1,2)=Y(5,2)
      Y(1,3)=Y(5,3)
      Y(2,3)=Y(6,3)
      Y(1,4)=Y(5,4)
      Y(2,4)=Y(6,4)
      Y(3,4)=Y(7,4)
C     CHL1 IS THE MOBILITY MATRIX OF FINITE RECTANGULAR PLATE
C     IN BENDING WAVE
      DO 80 I=1,4
      DO 80 J=1,4
      IF(I.EQ.J) THEN
      CHL1(I,J)=W/(2*DB*A_K**2)*CJ*AMP
      ELSE
      C_A =CJ*A_K*R(I,J)
      C_B = -1*CI*A_K*R(I,J)
```

```
      CALL HAN0(C_A,CHAN_A)
      CALL HAN0(C_B,CHAN_B)
      CHAN=CHAN_A-CHAN_B
      CHL1(I,J)=W/(2*DB*A_K**2)*CHAN*AMP
      END IF
80    CONTINUE
      DO 90 I=5,12
      DO 90 J=1,4
      IF((I-J).EQ.4) THEN
      CHL1(I,J)=0*CJ
      ELSE IF((I-J).EQ.8) THEN
      CHL1(I,J)=0*CJ
      ELSE
      IF((I.GT.4).AND.(I.LE.8)) THEN
      II=I-4
      CALL DHAN0(A_K,R(II,J),CDHANA)
      CALL DHAN1(A_K,R(II,J),CDHANB)
      CDHAN=CDHANA-CDHANB
      CHL1(I,J)=W/(2*DB*A_K**2)*CDHAN*Y(II,J)/R(II,J)*AMP
      ELSE
      II=I-8
      CALL DHAN0(A_K,R(II,J),CDHANA)
      CALL DHAN1(A_K,R(II,J),CDHANB)
      CDHAN=CDHANA-CDHANB
      CHL1(I,J)=W/(2*DB*A_K**2)*CDHAN*X(II,J)/R(II,J)*AMP
      END IF
      END IF
90    CONTINUE
      DO 100 I=1,4
      DO 100 J=5,8
      IF((J-I).EQ.4) THEN
      CHL1(I,J)=0*CJ
      ELSE
      JJ=J-4
      R1=DSQRT((Y(I,JJ)-A)**2+(X(I,JJ))**2)
      R2=DSQRT((Y(I,JJ)+A)**2+(X(I,JJ))**2)
      C_A1 =CJ*A_K*R1
      C_A2 = -1*CI*A_K*R1
      C_B1 =CJ*A_K*R2
      C_B2 = -1*CI*A_K*R2
      CALL HAN0(C_A1,CHANA1)
      CALL HAN0(C_A2,CHANA2)
      CALL HAN0(C_B1,CHANB1)
      CALL HAN0(C_B2,CHANB2)
      CHANA=CHANA1-CHANA2
      CHANB=CHANB1-CHANB2
      CHL1(I,J)=(0.5E+5)*W/(2*DB*A_K**2)*(CHANA-CHANB)*AMP
      END IF
100   CONTINUE
      RGAMA=1.781
      DO 110 I=5,8
      DO 110 J=5,8
      IF((I-J).EQ.0) THEN
      CHL1(I,J)=W/(4*DB)*(1-4*CI/PI*DLOG(RGAMA*A_K*A/2))*AMP
      ELSE
      II=I-4
      JJ=J-4
      R1=SQRT((Y(II,JJ)-A)**2+(X(II,JJ))**2)
      R2=SQRT((Y(II,JJ)+A)**2+(X(II,JJ))**2)
      CALL DHAN0(A_K,R1,CDHA0)
      CALL DHAN1(A_K,R1,CDHA1)
      CALL DHAN0(A_K,R2,CDHB0)
```

```
      CALL DHAN1(A_K,R2,CDHB1)
      CDHA=CDHA0-CDHA1
      CDHB=CDHB0-CDHB1
      CHL1(I,J)=(0.5E+5)*W/(2*DB*A_K**2)*(CDHA*(Y(II,JJ)-A)/R1-
     +CDHB*(Y(II,JJ)+A)/R2)*AMP
      END IF
110   CONTINUE
      DO 120 I=9,12
      DO 120 J=5,8
      IF((I-J).EQ.4) THEN
      CHL1(I,J)=0*CJ
      ELSE
      II=I-8
      JJ=J-4
      R1=SQRT((Y(II,JJ)-A)**2+(X(II,JJ))**2)
      R2=SQRT((Y(II,JJ)+A)**2+(X(II,JJ))**2)
      CALL DHAN0(A_K,R1,CDHA0)
      CALL DHAN1(A_K,R1,CDHA1)
      CALL DHAN0(A_K,R2,CDHB0)
      CALL DHAN1(A_K,R2,CDHB1)
      CDHA=CDHA0-CDHA1
      CDHB=CDHB0-CDHB1
      CHL1(I,J)=(0.5E+5)*W/(2*DB*A_K**2)*(CDHA*X(II,JJ)/R1-
     +CDHB*X(II,JJ)/R2)*AMP
      END IF
120   CONTINUE
      DO 130 I=1,4
      DO 130 J=9,12
      IF((J-I).EQ.8) THEN
      CHL1(I,J)=0*CJ
      ELSE
      JJ=J-8
      R1=SQRT(Y(I,JJ)**2+(X(I,JJ)+A)**2)
      R2=SQRT(Y(I,JJ)**2+(X(I,JJ)-A)**2)
      C_A1 =CJ*A_K*R1
      C_A2 = -1*CI*A_K*R1
      C_B1 =CJ*A_K*R2
      C_B2 = -1*CI*A_K*R2
      CALL HAN0(C_A1,CHANA1)
      CALL HAN0(C_A2,CHANA2)
      CALL HAN0(C_B1,CHANB1)
      CALL HAN0(C_B2,CHANB2)
      CHANA=CHANA1-CHANA2
      CHANB=CHANB1-CHANB2
      CHL1(I,J)=(0.5E+5)*W/(2*DB*A_K**2)*(CHANA-CHANB)*AMP
      END IF
130   CONTINUE
      DO 140 I=5,8
      DO 140 J=9,12
      IF((J-I).EQ.8) THEN
      CHL1(I,J)=0*CJ
      ELSE
      II=I-4
      JJ=J-8
      R1=SQRT((Y(II,JJ))**2+(X(II,JJ)+A)**2)
      R2=SQRT((Y(II,JJ))**2+(X(II,JJ)-A)**2)
      CALL DHAN0(A_K,R1,CDHA0)
      CALL DHAN1(A_K,R1,CDHA1)
      CALL DHAN0(A_K,R2,CDHB0)
      CALL DHAN1(A_K,R2,CDHB1)
      CDHA=CDHA0-CDHA1
      CDHB=CDHB0-CDHB1
```

```
      CHL1(I,J)=(0.5E+5)*W/(2*DB*A_K**2)*(CDHA*Y(II,JJ)/R1-
     +CDHB*Y(II,JJ)/R2)*AMP
      END IF
140   CONTINUE
      DO 150 I=9,12
      DO 150 J=9,12
      IF((I-J).EQ.0) THEN
      CHL1(I,J)=W/(4*DB)*(1-4*CI/PI*DLOG(RGAMA*A_K*A/2))*AMP
      ELSE
      II=I-8
      JJ=J-8
      R1=SQRT((Y(II,JJ))**2+(X(II,JJ)+A)**2)
      R2=SQRT((Y(II,JJ))**2+(X(II,JJ)-A)**2)
      CALL DHAN0(A_K,R1,CDHA0)
      CALL DHAN1(A_K,R1,CDHA1)
      CALL DHAN0(A_K,R2,CDHB0)
      CALL DHAN1(A_K,R2,CDHB1)
      CDHA=CDHA0-CDHA1
      CDHB=CDHB0-CDHB1
      CHL1(I,J)=(0.5E+5)*W/(2*DB*A_K**2)*(CDHA*(X(II,JJ)+A)/R1-
     +CDHB*(X(II,JJ)-A)/R2)*AMP
      END IF
150   CONTINUE
C     CHL2 IS THE MOBILITY MATRIX OF FINITE RECTANGULAR PLATE
C      IN LONGITUDINAL WAVE
C     Z1=SQRT(D*RO)*S1
C     Z2=SQRT(D*RO)*S2
      DIS_A=R(2,1)
      DIS_B=R(4,1)
      AZ1=SQRT(DD*RO)*(0.5*DIS_B*TH)
      AZ2=SQRT(DD*RO)*(0.5*DIS_A*TH)
      CHZ1(1,1) =AZ1*CJ
      CHZ1(1,2) = -1*AZ1*CJ
      CHZ1(2,1) =AZ1*CDEXP(-1*CI*A_K1*DIS_A)
      CHZ1(2,2) = -1*AZ1*CDEXP(CI*A_K1*DIS_A)
      CHZ2(1,1) =AZ2*CJ
      CHZ2(1,2) = -1*AZ2*CJ
      CHZ2(2,1) =AZ2*CDEXP(-1*CI*A_K1*DIS_B)
      CHZ2(2,2) = -1*AZ2*CDEXP(CI*A_K1*DIS_B)
      CALL DLINCG(2,CHZ1,2,CHZ1I,2)
      CALL DLINCG(2,CHZ2,2,CHZ2I,2)
      CHAB1(1,1) = 1*CJ
      CHAB1(1,2) = 1*CJ
      CHAB1(2,1) = CDEXP(-1*CI*A_K1*DIS_A)
      CHAB1(2,2) = CDEXP(CI*A_K1*DIS_A)
      CHEF1(1,1) = 1*CJ
      CHEF1(1,2) = 1*CJ
      CHEF1(2,1) = CDEXP(-1*CI*A_K1*DIS_B)
      CHEF1(2,2) = CDEXP(CI*A_K1*DIS_B)
      CALL AMPY(CHAB1,CHZ1I,CHAB,2,2,2,2,2,2)
      CALL AMPY(CHEF1,CHZ2I,CHEF,2,2,2,2,2,2)
      DO 160 I=1,8
      DO 160 J=1,8
160   CHL2(I,J)=(0.0,0.0)
      CHL2(1,1)=CHAB(1,1)*AMP
      CHL2(1,2)=CHAB(1,2)*AMP
      CHL2(2,1)=CHAB(2,1)*AMP
      CHL2(2,2)=CHAB(2,2)*AMP
      CHL2(3,3)=CHAB(2,1)*AMP
      CHL2(3,4)=CHAB(2,2)*AMP
      CHL2(4,3)=CHAB(1,1)*AMP
      CHL2(4,4)=CHAB(1,2)*AMP
```

```
      CHL2(5,5)=CHEF(1,1)*AMP
      CHL2(5,8)=CHEF(1,2)*AMP
      CHL2(8,5)=CHEF(2,1)*AMP
      CHL2(8,8)=CHEF(2,2)*AMP
      CHL2(6,6)=CHEF(1,1)*AMP
      CHL2(6,7)=CHEF(1,2)*AMP
      CHL2(7,6)=CHEF(2,1)*AMP
      CHL2(7,7)=CHEF(2,2)*AMP
C     CHANGE THE COOR.
C     1 -> 1   , 2 -> 6 , 3 -> 3
C     4 -> 8     , 5 -> 5 , 6 -> 2
C     7 -> 7   , 8 -> 4
C     IN(1)=1
C     IN(2)=6
C     IN(3)=3
C     IN(4)=8
C     IN(5)=5
C     IN(6)=2
C     IN(7)=7
C     IN(8)=4
C     DO 161 I=1,8
C     CHL2A(3,I)=-1.0*CHL2(3,I)
C     CHL2A(4,I)=-1.0*CHL2(4,I)
C     CHL2A(6,I)=-1.0*CHL2(6,I)
C161  CHL2A(7,I)=-1.0*CHL2(7,I)
C     DO 162 I=1,8
C     CHL2B(I,3)=-1.0*CHL2A(I,3)
C     CHL2B(I,4)=-1.0*CHL2A(I,4)
C     CHL2B(I,6)=-1.0*CHL2A(I,6)
C162  CHL2B(I,7)=-1.0*CHL2A(I,7)
C     DO 163 I=1,8
C     DO 163 J=1,8
C163  CHL2C(I,J)=CHL2B(IN(I),J)
C     DO 164 I=1,8
C     DO 164 J=1,8
C164  CHL2(I,J)=CHL2C(I,IN(J))
C     ASSEMBLY OF MOBILITY MATRIX OF PLATE ELEMENT
      DO 170 I=1,24
      DO 170 J=1,24
      CHLL(I,J)=(0.0,0.0)
170   CHL(I,J)=(0.0,0.0)
C     THIS IS LONGITUDINAL WAVE
      DO 180 I=1,8
      DO 180 J=1,8
180   CHL(I,J)=CHL2(I,J)
C     THIS IS BENDING WAVE
      DO 190 I=1,12
      DO 190 J=1,12
190   CHL(I+8,J+8)=CHL1(I,J)
C     GIVE A SMALL NUMBER 1.0E-20
      DO 191 I=21,24
191   CHL(I,I)=1.0E-20
C     CHANGE THE ADDRESS ACCORDING TO NODE 1->4
      DO 200 J=1,24
      CHLB(1,J)=CHL(1,J)
      CHLB(2,J)=CHL(5,J)
      CHLB(3,J)=CHL(9,J)
      CHLB(4,J)=CHL(13,J)
      CHLB(5,J)=CHL(17,J)
      CHLB(6,J)=CHL(21,J)
      CHLB(7,J)=CHL(2,J)
      CHLB(8,J)=CHL(6,J)
```

```
      CHLB(9,J)=CHL(10,J)
      CHLB(10,J)=CHL(14,J)
      CHLB(11,J)=CHL(18,J)
      CHLB(12,J)=CHL(22,J)
      CHLB(13,J)=CHL(3,J)
      CHLB(14,J)=CHL(7,J)
      CHLB(15,J)=CHL(11,J)
      CHLB(16,J)=CHL(15,J)
      CHLB(17,J)=CHL(19,J)
      CHLB(18,J)=CHL(23,J)
      CHLB(19,J)=CHL(4,J)
      CHLB(20,J)=CHL(8,J)
      CHLB(21,J)=CHL(12,J)
      CHLB(22,J)=CHL(16,J)
      CHLB(23,J)=CHL(20,J)
200   CHLB(24,J)=CHL(24,J)
      DO 210 I=1,24
      CHLL(I,1)=CHLB(I,1)
      CHLL(I,2)=CHLB(I,5)
      CHLL(I,3)=CHLB(I,9)
      CHLL(I,4)=CHLB(I,13)
      CHLL(I,5)=CHLB(I,17)
      CHLL(I,6)=CHLB(I,21)
      CHLL(I,7)=CHLB(I,2)
      CHLL(I,8)=CHLB(I,6)
      CHLL(I,9)=CHLB(I,10)
      CHLL(I,10)=CHLB(I,14)
      CHLL(I,11)=CHLB(I,18)
      CHLL(I,12)=CHLB(I,22)
      CHLL(I,13)=CHLB(I,3)
      CHLL(I,14)=CHLB(I,7)
      CHLL(I,15)=CHLB(I,11)
      CHLL(I,16)=CHLB(I,15)
      CHLL(I,17)=CHLB(I,19)
      CHLL(I,18)=CHLB(I,23)
      CHLL(I,19)=CHLB(I,4)
      CHLL(I,20)=CHLB(I,8)
      CHLL(I,21)=CHLB(I,12)
      CHLL(I,22)=CHLB(I,16)
      CHLL(I,23)=CHLB(I,20)
210   CHLL(I,24)=CHLB(I,24)
C     CHR1=[CTL] [CHR] [CTL]
      CALL AMPY(CTTL,CHLL,CHR,24,24,24,24,24,24)
      CALL AMPY(CHR,CTL,CHR1,24,24,24,24,24,24)
      RETURN
      END
```

```
      SUBROUTINE HAN0(Z1,C_HAN)
C     THIS SUBROUTINE IS FOR HANKEL FUNCTION,
C     X IS INPUT REAL NUMBER
C     C_HAN IS OUTPUT COMPLEX NUMBER
C     H0(X)=J0(X)-J*Y0(X)
      IMPLICIT DOUBLE PRECISION (A,B,D-H,O-Y)
      IMPLICIT COMPLEX*16 (C,Z)
      PARAMETER (CI=(0.0,1.0))
      CALL CJY01(Z1,CBJ0,CDJ0,CBJ1,CDJ1,CBY0,CDY0,CBY1,CDY1)
      C_HAN=CBJ0-CI*CBY0
      RETURN
      END
```

```
      DO 25 K=1,30
      W0=W0+1.0D0/K
      R0=-0.25D0*R0/(K*K)*X2
      R=R0*W0
      CS0=CS0+R
      IF (DABS(R).LT.DABS(CS0)*1.0D-15) GO TO 30
25    CONTINUE
30    BY0=RP2*(EC*BJ0-CS0)
      CS1=1.0D0
      W1=0.0D0
      R1=1.0D0
      DO 35 K=1,30
      W1=W1+1.0D0/K
      R1=-0.25D0*R1/(K*(K+1))*X2
      R=R1*(2.0D0*W1+1.0D0/(K+1.0D0))
      CS1=CS1+R
      IF (DABS(R).LT.DABS(CS1)*1.0D-15) GO TO 40
35    CONTINUE
40    BY1=RP2*(EC*BJ1-1.0D0/X-0.25D0*X*CS1)
      ELSE
      DATA A/-.703125000000000D-01,.112152099609375D+00,
     &       -.572501420974731D+00,.607404200127348D+01,
     &       -.110017140269246D+03,.303809051092238D+04,
     &       -.118838426256783D+06,.625295149343479D+07,
     &       -.425939216504766D+09,.364684008070656D+11,
     &       -.383353466139394D+13,.485401468685290D+15/
      DATA B/ .732421875000000D-01,-.227108001708984D+00,
     &        .172772750258446D+01,-.243805296995561D+02,
     &        .551335896122021D+03,-.182577754742932D+05,
     &        .832859304016289D+06,-.500695895319889D+08,
     &        .383625518023043D+10,-.364901081884983D+12,
     &        .421897157028410D+14,-.582724463156691D+16/
      DATA A1/.117187500000000D+00,-.144195556640625D+00,
     &        .676592588424683D+00,-.688391426810995D+01,
     &        .121597891876536D+03,-.330227229448085D+04,
     &        .127641272646175D+06,-.665636771881769D+07,
     &        .450278600305039D+09,-.383385752074279D+11,
     &        .401183859913320D+13,-.506056850331473D+15/
      DATA B1/-.102539062500000D+00,.277576446533203D+00,
     &        -.199353173375130D+01,.272488273112685D+02,
     &        -.603844076705070D+03,.197183759122366D+05,
     &        -.890297876707068D+06,.531041101096852D+08,
     &        -.404362032510775D+10,.382701134659861D+12,
     &        -.440648141785228D+14,.606509135122270D+16/
      K0=12
      IF (X.GE.35.0) K0=10
      IF (X.GE.50.0) K0=8
      T1=X-0.25D0*PI
      P0=1.0D0
      Q0=-0.125D0/X
      DO 45 K=1,K0
      P0=P0+A(K)*X**(-2*K)
45    Q0=Q0+B(K)*X**(-2*K-1)
      CU=DSQRT(RP2/X)
      BJ0=CU*(P0*DCOS(T1)-Q0*DSIN(T1))
      BY0=CU*(P0*DSIN(T1)+Q0*DCOS(T1))
      T2=X-0.75D0*PI
      P1=1.0D0
      Q1=0.375D0/X
      DO 50 K=1,K0
      P1=P1+A1(K)*X**(-2*K)
50    Q1=Q1+B1(K)*X**(-2*K-1)
```

```
      SUBROUTINE GAMMA(X,GA)
C     ==========================================================
C     PURPOSE: COMPUTE GAMMA FUNCTION X)
C     INPUT :   X   --- ARGUMENT X)
C                          ( X IS NOT EQUAL TO 0,-1,-2,   )
C     OUTPUT:   GA --- X)
C     ==========================================================
C     GAMMA(X) FUNCTION IS (X-1)!
      IMPLICIT DOUBLE PRECISION (A-H,O-Z)
      DIMENSION G(26)
      PI=3.1415926535897 93D0
      IF (X.EQ.INT(X)) THEN
      IF (X.GT.0.0D0) THEN
      GA=1.0D0
      M1=X-1
      DO 10 K=2,M1
10    GA=GA*K
      ELSE
      GA=1.0D+300
      ENDIF
      ELSE
      IF (DABS(X).GT.1.0D0) THEN
      Z=DABS(X)
      M=INT(Z)
      R=1.0D0
      DO 15 K=1,M
15    R=R*(Z-K)
      Z=Z-M
      ELSE
      Z=X
      ENDIF
      DATA G/1.0D0,0.5772156649015329D0,
     &-0.6558780715202538D0, -0.420026350340952D-1,
     &0.166538611382291 5D0,-.421977345555443D-1,
     &-.962197152787 70D-2, .721894324666 30D-2,
     &-.116516759185 91D-2, -.215241674114 9D-3,
     &.128050282388 2D-3, -.201348547807D-4,
     &-.125049348 21D-5, .113302723 20D-5,
     &-.205633841 7D-6, .611609 50D-8,
     &.500200 75D-8, -.118127 46D-8,
     &.104342 7D-9, .778 23D-11,
     &-.369 68D-11, .51D-12,
     &-.206D-13, -.54D-14, .14D-14, .1D-15/
      GR=G(26)
      DO 20 K=25,1,-1
20    GR=GR*Z+G(K)
      GA=1.0D0/(GR*Z)
      IF (DABS(X).GT.1.0D0) THEN
      GA=GA*R
      IF (X.LT.0.0D0) GA=-PI/(X*GA*DSIN(PI*X))
      ENDIF
      ENDIF
      RETURN
      END
      SUBROUTINE DHAN0(X,Y,CDHAN0)
C     THIS IS THE DERIVATIVE OF HANKEL FUNCTION WITH
C     RESPECT TO KR.
C     X IS K
C     Y IS R
C     C_DHAN IS THE RESULT
```

```
      IMPLICIT DOUBLE PRECISION (A,B,D-H,O-Y)
      IMPLICIT COMPLEX*16 (C,Z)
      PARAMETER (CI=(0.0,1.0),CJ=(1.0,0.0),PI=3.1415926535897 93D0,
     +ERR = 10E-15)
      H1   = 0.0
      H4   = 0.0
C     ADD IS GAIN NUMBER
C     IF ADD IS SMALLER THAN ERR
C     THEN THE FUNCTION WILL EXIT   DO-LOOP
C     ERR IS DEFINED AS 10E-15
      DO 10 I=1,100
      G_I=I+1
      CALL GAMMA(G_I,GA)
      A=2.0**(I*2.0)
      ADD= (-1)**I*(2*I)*(X)*(X*Y)**(2*I-1)/(A*GA**2)
      H1 = H1 + ADD
      IF (ABS(ADD) .LT. ERR) GOTO 40
10    CONTINUE
40    C_H1 =CJ*H1
      Z    = X*Y*CJ
      CALL CJY01(Z,CBJ0,CDJ0,CBJ1,CDJ1,CBY0,CDY0,CBY1,CDY1)
      C_H2 = -2*CI/PI*CBJ0/Y
      C_H3 = -2*CI/PI*(DLOG(X*Y/2)+0.5772)*H1
      DO 20 I=1,100
      A_H = 0.0
      DO 30 J=1,I
      A_H= A_H + 1.0/J
30    CONTINUE
      G_I=I+1
      CALL GAMMA(G_I,GA)
      ADD = (-1)**(I-1)*A_H*2*I*X*(X*Y)**(2*I-1)
     +/(2.0**(2.0*I)*GA**2.0)
      H4=H4+ ADD
      IF (ABS(ADD) .LT. ERR) GOTO 50
20    CONTINUE
50    C_H4 = -2.0*CI/PI*H4
      CDHAN0 = C_H1+C_H2+C_H3+C_H4
      RETURN
      END



      SUBROUTINE DHAN1(X,Y,CDHAN1)
C     THIS IS THE DERIVATIVE OF hANKEL FUNCTION WITH
C     RESPECT TO -JKR.
C     X IS K
C     Y IS R
C     C_DHAN IS THE RESULT
C     C_K =-CI*X
      IMPLICIT DOUBLE PRECISION (A,B,D-H,O-Y)
      IMPLICIT COMPLEX*16 (C,Z)
      PARAMETER (CI=(0.0,1.0),CJ=(1.0,0.0),PI=3.1415926535897 93D0,
     +ERR = 10E-15)
      C_K = -1*CI*X
      C_H1   = (0.0,0.0)
      C_H4   = (0.0,0.0)
C     ADD IS GAIN NUMBER
C     IF ADD IS SMALLER THAN ERR
C     THEN THE FUNCTION WILL EXIT   DO-LOOP
C     ERR IS DEFINED AS 10E-15
      DO 10 I=1,100
      G_I=I+1
```

```
      CALL GAMMA(G_I,GA)
      A = 2.0**(I*2.0)
      ADD = (-1)**I*(2*I)*(C_K)*(C_K*Y)**(2*I-1)/(A*GA**2)
      C_H1=C_H1+ ADD
      IF (ABS(ADD) .LT. ERR) GOTO 40
10    CONTINUE
40    Z   = C_K*Y*CJ
      CALL CJY01(Z,CBJ0,CDJ0,CBJ1,CDJ1,CBY0,CDY0,CBY1,CDY1)
      C_H2 = -2.0*CI/PI*CBJ0/Y
      C_H3 = -2*CI/PI*(CDLOG(C_K*Y/2)+0.5772156649)*C_H1
      DO 20 I=1,100
      A_H = 0.0
      DO 30 J=1,I
      A_H= A_H + 1.0/J
30    CONTINUE
      G_I=I+1
      CALL GAMMA(G_I,GA)
      ADD= (-1)**(I-1)*A_H*2*I*C_K*(C_K*Y)**(2*I-1)
     +/(2.0**(2.0*I)*GA**2.0)
      C_H4 = C_H4 + ADD
      IF (ABS(ADD) .LT. ERR) GOTO 50
20    CONTINUE
50    C_H4 = -2.0*CI/PI*C_H4
      CDHAN1 = C_H1 + C_H2 + C_H3 + C_H4
      RETURN
      END



      SUBROUTINE TRANS(TN,NTE,TL,NT,L)
C     THIS PROGRAM TRANSFER LOCAL COOR. TO GLOBAL COOR.
C     M(4) COULD FIND NODE NUM.
C     T_X,T_Y,T_Z ARE THE GLOBAL COOR.
C     R12 ,R13 ARE THE VECTOR FROM 1 TO 2 OR 3
C     RCROS IS R12 X R13
C     UNIT_X,UNIT_Y,UNIT_Z ARE THE LOCAL UNIT VECTOR
      IMPLICIT DOUBLE PRECISION (A,B,D-H,O-Y)
      IMPLICIT COMPLEX*16 (C,Z)
      DIMENSION NTE(NT,5),TN(NT,4),TL(24,24),K(4),T_X(6)
     +,T_Y(6),T_Z(6),R12(3),R13(3),UNIT_X(3),UNIT_Y(3),
     +UNIT_Z(3),RCROS(3)
      DO 1 J=1,24
      DO 1 I=1,24
1     TL(I,J)=0
      DO 20 J=1,4
      K(J)=NTE(L,J+1)
20    CONTINUE
      DO 30 I=1,4
      T_X(I)=TN(K(I),2)
      T_Y(I)=TN(K(I),3)
      T_Z(I)=TN(K(I),4)
30    CONTINUE
      DO 60 I=1,2
      T_X(I+4)=T_X(I)
      T_Y(I+4)=T_Y(I)
      T_Z(I+4)=T_Z(I)
60    CONTINUE
      DO 70 ID=0,3
      R12(1)=T_X(2+ID)-T_X(1+ID)
      R12(2)=T_Y(2+ID)-T_Y(1+ID)
      R12(3)=T_Z(2+ID)-T_Z(1+ID)
      R13(1)=T_X(3+ID)-T_X(1+ID)
```

```
      R13(2)=T_Y(3+ID)-T_Y(1+ID)
      R13(3)=T_Z(3+ID)-T_Z(1+ID)
      RCROS(1)=R12(2)*R13(3)-R12(3)*R13(2)
      RCROS(2)=R12(3)*R13(1)-R12(1)*R13(3)
      RCROS(3)=R12(1)*R13(2)-R12(2)*R13(1)
      AM_R12=SQRT(R12(1)**2+R12(2)**2+R12(3)**2)
      AM_R13=SQRT(R13(1)**2+R13(2)**2+R13(3)**2)
      AM_RCR=SQRT(RCROS(1)**2+RCROS(2)**2+RCROS(3)**2)
      DO 40 II=1,3
      UNIT_X(II)=R12(II)/AM_R12
      UNIT_Z(II)=RCROS(II)/AM_RCR
40    CONTINUE
      UNIT_Y(1)=UNIT_Z(2)*UNIT_X(3)-UNIT_Z(3)*UNIT_X(2)
      UNIT_Y(2)=UNIT_Z(3)*UNIT_X(1)-UNIT_Z(1)*UNIT_X(3)
      UNIT_Y(3)=UNIT_Z(1)*UNIT_X(2)-UNIT_Z(2)*UNIT_X(1)
      DO 50 IA=1,3
      TL(1+ID*6,IA+ID*6)=UNIT_X(IA)
      TL(2+ID*6,IA+ID*6)=UNIT_Y(IA)
      TL(3+ID*6,IA+ID*6)=UNIT_Z(IA)
      TL(4+ID*6,IA+3+ID*6)=UNIT_X(IA)
      TL(5+ID*6,IA+3+ID*6)=UNIT_Y(IA)
      TL(6+ID*6,IA+3+ID*6)=UNIT_Z(IA)
50    CONTINUE
70    CONTINUE
      RETURN
      END



      SUBROUTINE MOMENT_1(X,W,Y,CMO1)
C     THIS IS THE FUNCTION (A-29).
C     EXPANDING THE HANKEL FUNCTION H0(KR1) WITH RESPECT TO K(Y+A)
C     X IS K
C     Y IS R
C     W  IS X

      IMPLICIT DOUBLE PRECISION (A,B,D-H,O-Y)
      IMPLICIT COMPLEX*16 (C,Z)
      PARAMETER (CI=(0.0,1.0),CJ=(1.0,0.0),PI=3.141592653589793D0,
     +ERR = 10E-15)
C     THIS IS (A-29)
      A = 10E-5
      R1 = SQRT((Y-A)**2+W**2)
      R2 = SQRT((Y+A)**2+W**2)
      CR11= X*R1*CJ
      CR12= X*R1*(-1)*CI
      CALL HAN0(CR11,CH11)
      CALL HAN0(CR12,CH12)
      CANS1=CH11-CH12
C     THIS IS (A-29)
      CX1 = -0.25-CI/(PI*2)
      CX2 = CI/(2*PI)
      R = 1.781
      CMO1= 1.0+2*X**2*(Y-A)**2*(CX1+
     +CX2*DLOG(0.5*R*X*(Y-A))-0.5*CX2*CDLOG(-1*CI))
      RETURN
      END



      SUBROUTINE CJY01(Z,CBJ0,CDJ0,CBJ1,CDJ1,CBY0,CDY0,CBY1,CDY1)
C     ═══════════════════════════════════════════════════════════
```

```
C       Purpose: Compute Bessel functions J0(z), J1(z), Y0(z),
C                Y1(z), and their derivatives for a complex
C                argument
C       Input :  z --- Complex argument
C       Output:  CBJ0 --- J0(z)
C                CDJ0 --- J0'(z)
C                CBJ1 --- J1(z)
C                CDJ1 --- J1'(z)
C                CBY0 --- Y0(z)
C                CDY0 --- Y0'(z)
C                CBY1 --- Y1(z)
C                CDY1 --- Y1'(z)
C       ================================================================
        IMPLICIT DOUBLE PRECISION (A,B,E,P,R,W)
        IMPLICIT COMPLEX*16 (C,Z)
        DIMENSION A(12),B(12),A1(12),B1(12)
        PI=3.141592653589793D0
        EL=0.5772156649015329D0
        RP2=2.0D0/PI
        CI=(0.0D0,1.0D0)
        A0=CDABS(Z)
        Z2=Z*Z
        Z1=Z
        IF (A0.EQ.0.0D0) THEN
        CBJ0=(1.0D0,0.0D0)
        CBJ1=(0.0D0,0.0D0)
        CDJ0=(0.0D0,0.0D0)
        CDJ1=(0.5D0,0.0D0)
        CBY0=-(1.0D300,0.0D0)
        CBY1=-(1.0D300,0.0D0)
        CDY0=(1.0D300,0.0D0)
        CDY1=(1.0D300,0.0D0)
        RETURN
        ENDIF
        IF (REAL(Z).LT.0.0) Z1=-Z
        IF (A0.LE.12.0) THEN
        CBJ0=(1.0D0,0.0D0)
        CR=(1.0D0,0.0D0)
        DO 10 K=1,40
        CR=-0.25D0*CR*Z2/(K*K)
        CBJ0=CBJ0+CR
        IF (CDABS(CR).LT.CDABS(CBJ0)*1.0D-15) GO TO 15
10      CONTINUE
15      CBJ1=(1.0D0,0.0D0)
        CR=(1.0D0,0.0D0)
        DO 20 K=1,40
        CR=-0.25D0*CR*Z2/(K*(K+1.0D0))
        CBJ1=CBJ1+CR
        IF (CDABS(CR).LT.CDABS(CBJ1)*1.0D-15) GO TO 25
20      CONTINUE
25      CBJ1=0.5D0*Z1*CBJ1
        W0=0.0D0
        CR=(1.0D0,0.0D0)
        CS=(0.0D0,0.0D0)
        DO 30 K=1,40
        W0=W0+1.0D0/K
        CR=-0.25D0*CR/(K*K)*Z2
        CP=CR*W0
        CS=CS+CP
        IF (CDABS(CP).LT.CDABS(CS)*1.0D-15) GO TO 35
30      CONTINUE
35      CBY0=RP2*(CDLOG(Z1/2.0D0)+EL)*CBJ0-RP2*CS
```

```
      W1=0.0D0
      CR=(1.0D0,0.0D0)
      CS=(1.0D0,0.0D0)
      DO 40 K=1,40
      W1=W1+1.0D0/K
      CR=-0.25D0*CR/(K*(K+1))*Z2
      CP=CR*(2.0D0*W1+1.0D0/(K+1.0D0))
      CS=CS+CP
      IF (CDABS(CP).LT.CDABS(CS)*1.0D-15) GO TO 45
40    CONTINUE
45    CBY1=RP2*((CDLOG(Z1/2.0D0)+EL)*CBJ1-1.0D0/Z1-.25D0*Z1*CS)
      ELSE
      DATA A/-.703125D-01,.112152096093 75D+00,
     &       -.572501420974731 4D+00,.607404200127348 3D+01,
     &       -.110017140269246 7D+03,.303809051092238 4D+04,
     &       -.118838426256783 2D+06,.625295149343479 7D+07,
     &       -.425939216504766 9D+09,.364684008070655 6D+11,
     &       -.383353466139394 4D+13,.485401468685290 1D+15/
      DATA B/ .732421875D-01,-.227108001708984 4D+00,
     &       .172772750258445 7D+01,-.243805296995560 6D+02,
     &       .551335896122020 6D+03,-.182577554742931 8D+05,
     &       .832859304016289 3D+06,-.500695895319889 3D+08,
     &       .383625518023043 3D+10,-.364901081884983 3D+12,
     &       .421897157028409 6D+14,-.582724463156690 7D+16/
      DATA A1/.1171875D+00,-.144195556406 25D+00,
     &        .676592588424682 6D+00,-.688391426810994 7D+01,
     &        .121597891876535 9D+03,-.330227229448085 2D+04,
     &        .127641272646174 6D+06,-.665636771881768 8D+07,
     &        .450278600305039 3D+09,-.383385752074279 0D+11,
     &        .401183859913319 8D+13,-.506056850331472 7D+15/
      DATA B1/-.1025390625D+00,.277576446533203 1D+00,
     &        -.199353173375129 7D+01,.272488273112685 4D+02,
     &        -.603844076705070 2D+03,.197183759122366 3D+05,
     &        -.890297876707067 8D+06,.531041101096852 2D+08,
     &        -.404362032510775 4D+10,.382701134659860 5D+12,
     &        -.440648141785227 8D+14,.606509135122269 9D+16/
      K0=12
      IF (A0.GE.35.0) K0=10
      IF (A0.GE.50.0) K0=8
      CT1=Z1-.25D0*PI
      CP0=(1.0D0,0.0D0)
      DO 50 K=1,K0
50    CP0=CP0+A(K)*Z1**(-2*K)
      CQ0=-0.125D0/Z1
      DO 55 K=1,K0
55    CQ0=CQ0+B(K)*Z1**(-2*K-1)
      CU=CDSQRT(RP2/Z1)
      CBJ0=CU*(CP0*CDCOS(CT1)-CQ0*CDSIN(CT1))
      CBY0=CU*(CP0*CDSIN(CT1)+CQ0*CDCOS(CT1))
      CT2=Z1-.75D0*PI
      CP1=(1.0D0,0.0D0)
      DO 60 K=1,K0
60    CP1=CP1+A1(K)*Z1**(-2*K)
      CQ1=0.375D0/Z1
      DO 65 K=1,K0
65    CQ1=CQ1+B1(K)*Z1**(-2*K-1)
      CBJ1=CU*(CP1*CDCOS(CT2)-CQ1*CDSIN(CT2))
      CBY1=CU*(CP1*CDSIN(CT2)+CQ1*CDCOS(CT2))
      ENDIF
      IF (REAL(Z).LT.0.0) THEN
      IF (DIMAG(Z).LT.0.0) CBY0=CBY0-2.0D0*CI*CBJ0
      IF (DIMAG(Z).GT.0.0) CBY0=CBY0+2.0D0*CI*CBJ0
```

```
IF (DIMAG(Z).LT.0.0) CBY1=-(CBY1-2.0D0*CI*CBJ1)
IF (DIMAG(Z).GT.0.0) CBY1=-(CBY1+2.0D0*CI*CBJ1)
CBJ1=-CBJ1
ENDIF
CDJ0=-CBJ1
CDJ1=CBJ0-1.0D0/Z*CBJ1
CDY0=-CBY1
CDY1=CBY0-1.0D0/Z*CBY1
RETURN
END


      SUBROUTINE JY01A(X,BJ0,DJ0,BJ1,DJ1,BY0,DY0,BY1,DY1)
C     ===========================================================
C     Purpose: Compute Bessel functions J0(x), J1(x), Y0(x),
C              Y1(x), and their derivatives
C     Input :  x     --- Argument of Jn(x) & Yn(x) ( x ?0 )
C     Output:  BJ0 --- J0(x)
C              DJ0 --- J0'(x)
C              BJ1 --- J1(x)
C              DJ1 --- J1'(x)
C              BY0 --- Y0(x)
C              DY0 --- Y0'(x)
C              BY1 --- Y1(x)
C              DY1 --- Y1'(x)
C     ===========================================================
      IMPLICIT DOUBLE PRECISION (A-H,O-Z)
      DIMENSION A(12),B(12),A1(12),B1(12)
      PI=3.141592653589793D0
      RP2=0.63661977236758D0
      X2=X*X
      IF (X.EQ.0.0D0) THEN
      BJ0=1.0D0
      BJ1=0.0D0
      DJ0=0.0D0
      DJ1=0.5D0
      BY0=-1.0D+300
      BY1=-1.0D+300
      DY0=1.0D+300
      DY1=1.0D+300
      RETURN
      ENDIF
      IF (X.LE.12.0D0) THEN
      BJ0=1.0D0
      R=1.0D0
      DO 5 K=1,30
      R=-0.25D0*R*X2/(K*K)
      BJ0=BJ0+R
      IF (DABS(R).LT.DABS(BJ0)*1.0D-15) GO TO 10
5     CONTINUE
10    BJ1=1.0D0
      R=1.0D0
      DO 15 K=1,30
      R=-0.25D0*R*X2/(K*(K+1.0D0))
      BJ1=BJ1+R
      IF (DABS(R).LT.DABS(BJ1)*1.0D-15) GO TO 20
15    CONTINUE
20    BJ1=0.5D0*X*BJ1
      EC=DLOG(X/2.0D0)+0.5772156649015329D0
      CS0=0.0D0
      W0=0.0D0
      R0=1.0D0
```

```
      CU=DSQRT(RP2/X)
      BJ1=CU*(P1*DCOS(T2)-Q1*DSIN(T2))
      BY1=CU*(P1*DSIN(T2)+Q1*DCOS(T2))
      ENDIF
      DJ0=-BJ1
      DJ1=BJ0-BJ1/X
      DY0=-BY1
      DY1=BY0-BY1/X
      RETURN
      END

      SUBROUTINE PARTIT(W,N_FOR,N_DIS,N_UKN,N_ALL,NIN,CAHM,
     +NT,N_FORC,N_DISP)
C     THIS IS THE PARTITION OF THE MATRIX
C      GET CH11,CH12,CH21,CH22
C      CIH22 IS THE INVERSE OF THE CH22
C      CHA=CH11-CH12*INV(CH22)*CH21
C      CHB=CH12*INV(CH22)
C      CHC=-INV(CH22)*CH21
C      CHD=INV(CH22)
       IMPLICIT DOUBLE PRECISION (A,B,D-H,O-Y)
       IMPLICIT COMPLEX*16 (C,Z)
       PARAMETER (CI=(0.0,1.0),CJ=(1.0,0.0))
       DIMENSION CAHM(NT,NT),NIN(NT),C_AHM(N_ALL,N_ALL),N_IN(N_ALL),
     +CCAHM1(N_ALL,N_ALL),CCAHM2(N_ALL,N_ALL),
     +CH11(N_DIS,N_DIS),CH12(N_DIS,N_UKN),CH21(N_UKN,N_DIS),
     +CH22(N_UKN,N_UKN),CH22I(N_UKN,N_UKN),
     +CHA(N_DIS,N_DIS),CHB(N_DIS,N_UKN),CHC(N_UKN,N_DIS),
     +CHD(N_UKN,N_UKN),
     +CHA1(N_DIS,N_UKN),CHA2(N_DIS,N_DIS),CHC1(N_UKN,N_DIS),
     +CAM(N_ALL,N_ALL),CAMI(N_ALL,N_ALL),
     +N_FORC(NT,3),N_DISP(NT,3),A_NN(N_DIS),CA_NU(N_UKN),
     +A_FN(N_UKN),CA_FU(N_DIS),A_NFN(N_ALL),A_F(N_ALL),
     +CNODE(N_ALL),CFORC(N_ALL)
C      SET C_AHM(N_ALL,N_ALL) IS THE SAME AS CAHM(1->N_ALL,1->N_ALL)
C      SET N_IN(N_ALL) IS THE SAME AS NIN(1->N_ALL)
       DO 10 I=1,N_ALL
       N_IN(I) = NIN(I)
       DO 10 J=1,N_ALL
10     C_AHM(I,J)= CAHM(I,J)
       DO 20 I=1,N_ALL
       DO 20 J=1,N_ALL
20     CCAHM1(I,J)=C_AHM(N_IN(I),J)
       DO 30 I=1,N_ALL
       DO 30 J=1,N_ALL
30     CCAHM2(I,J)=CCAHM1(I,N_IN(J))
C      SET CH11,CH12,CH21,CH22
       DO 40 I=1,N_DIS
       DO 40 J=1,N_DIS
40     CH11(I,J)=CCAHM2(I,J)
       DO 50 I=1,N_DIS
       DO 50 J=1,N_UKN
50     CH12(I,J)=CCAHM2(I,N_DIS+J)
       DO 60 I=1,N_UKN
       DO 60 J=1,N_DIS
60     CH21(I,J)=CCAHM2(N_DIS+I,J)
       DO 70 I=1,N_UKN
       DO 70 J=1,N_UKN
70     CH22(I,J)=CCAHM2(N_DIS+I,N_DIS+J)
C      CALCULATE CHA=CH11-CH12*INV(CH22)*CH21
C      CHB=CH12*INV(CH22)
C      CHC=-INV(CH22)*CH21
```

```
C       CHD=INV(CH22)
        CALL DLINCG(N_UKN,CH22,N_UKN,CH22I,N_UKN)
        CALL AMPY1(CH12,CH22I,CHA1,N_DIS,N_UKN,N_UKN)
        CALL AMPY1(CHA1,CH21,CHA2,N_DIS,N_UKN,N_DIS)
        DO 80 I=1,N_DIS
        DO 80 J=1,N_DIS
80      CHA(I,J)=CH11(I,J)-CHA2(I,J)
        CALL AMPY1(CH12,CH22I,CHB,N_DIS,N_UKN,N_UKN)
        CALL AMPY1(CH22I,CH21,CHC1,N_UKN,N_UKN,N_DIS)
        DO 90 I=1,N_UKN
        DO 90 J=1,N_DIS
90      CHC(I,J)=-1*CHC1(I,J)
        DO 100 I=1,N_UKN
        DO 100 J=1,N_UKN
100     CHD(I,J)=CH22I(I,J)
C       ASSEMBLE CHA,CHB,CHC,CHD
        DO 110 I=1,N_ALL
        DO 110 J=1,N_ALL
110     CAM(I,J)=(0.0,0.0)
        DO 120 I=1,N_DIS
        DO 120 J=1,N_DIS
120     CAM(I,J)=CHA(I,J)
        DO 130 I=1,N_DIS
        DO 130 J=1,N_UKN
130     CAM(I,J+N_DIS)=CHB(I,J)
        DO 140 I=1,N_UKN
        DO 140 J=1,N_DIS
140     CAM(I+N_DIS,J)=CHC(I,J)
        DO 150 I=1,N_UKN
        DO 150 J=1,N_UKN
150     CAM(I+N_DIS,J+N_DIS)=CHD(I,J)
C       A_NN IS KNOWN NODE VALUE
C       A_FN IS KNOWN FORCE VALUE
C       A_NFN ASSEMBLE A_NN AND A_FN
        DO 160 I=1,N_DIS
160     A_NN(I)=N_DISP(I,3)
        DO 170 I=1,N_ALL
170     A_F(I)=0.0
        DO 180 I=1,N_FOR
180     A_F(6*(N_FORC(I,1)-1)+N_FORC(I,2))=N_FORC(I,3)
        DO 190 I=1,N_UKN
190     A_FN(I)=A_F(N_IN(N_DIS+I))
        DO 200 I=1,N_DIS
200     A_NFN(I)=A_NN(I)
        DO 210 I=1,N_UKN
210     A_NFN(I+N_DIS)=A_FN(I)
        CALL DLINCG(N_ALL,CAM,N_ALL,CAMI,N_ALL)
C       CALCULATE THE UNKNOWN VALUE A_FU,A_NU
        DO 220 I=1,N_DIS
220     CA_FU(I)=(0.0,0.0)
        DO 230 I=1,N_UKN
230     CA_NU(I)=(0.0,0.0)
        DO 240 I=1,N_DIS
        DO 240 J=1,N_ALL
240     CA_FU(I)=CA_FU(I)+CAMI(I,J)*A_NFN(J)
        DO 250 I=1,N_UKN
        DO 250 J=1,N_ALL
250     CA_NU(I)=CA_NU(I)+CAMI(I+N_DIS,J)*A_NFN(J)
C       THE SOLUTION OF THE NODE AND THE FORCE ARE
C       CNODE AND CFORC
        DO 260 I=1,N_ALL
        CFORC(I)=(0.0,0.0)
```

```
260     CNODE(I)=(0.0,0.0)
        DO 270 I=1,N_DIS
        CFORC(N_IN(I))=CA_FU(I)
270     CNODE(N_IN(I))=A_NN(I)*CJ
        DO 280 I=1,N_UKN
        CFORC(N_IN(I+N_DIS))=A_FN(I)*CJ
280     CNODE(N_IN(I+N_DIS))=CA_NU(I)
        ANS=cdabs(CNODE(33))/1.0
        WRITE(18,*) W,ANS
        RETURN
        END



        SUBROUTINE AMPY1(CAA,CAB,CAC,N,M,L)
C       THIS IS MATRIX A * B = C
        IMPLICIT DOUBLE PRECISION (A,B,D-H,O-Y)
        IMPLICIT COMPLEX*16 (C,Z)
        PARAMETER (CI=(0.0,1.0),CJ=(1.0,0.0))
        DIMENSION CAA(N,M),CAB(M,L),CAC(N,L)
        DO 9 J=1,L
        DO 9 I=1,N
        CAC(I,J)=0*CI
        DO 9 K=1,M
9       CAC(I,J)=CAC(I,J)+CAA(I,K)*CAB(K,J)
        RETURN
        END



        SUBROUTINE AMPY(CAA,CAB,CAC,N,M,L,NA,NB,NC)
C       THIS IS MATRIX A * B = C
        IMPLICIT DOUBLE PRECISION (A,B,D-H,O-Y)
        IMPLICIT COMPLEX*16 (C,Z)
        PARAMETER (CI=(0.0,1.0),CJ=(1.0,0.0))
        DIMENSION CAA(NA,NA),CAB(NB,NB),CAC(NC,NC)
        DO 10 J=1,L
        DO 10 I=1,N
        CAC(I,J)=0*CI
        DO 10 K=1,M
10      CAC(I,J)=CAC(I,J)+CAA(I,K)*CAB(K,J)
        RETURN
        END



        SUBROUTINE TMPY(CA,CB,M,N,NA,NB)
C       THIS IS THE TRANSPOSE OF MATRIX
C       B=A'
        IMPLICIT DOUBLE PRECISION (A,B,D-H,O-Y)
        IMPLICIT COMPLEX*16 (C,Z)
        DIMENSION CA(NA,NA),CB(NB,NB)
        DO 100 J=1,M
        DO 100 I=1,N
100     CB(I,J)=CA(J,I)
        RETURN
        END



        PROGRAM MAIN
        IMPLICIT DOUBLE PRECISION (A,B,D-H,O-Y)
```

```
      IMPLICIT COMPLEX*16 (C,Z)
      PARAMETER (NT=6,CI=(0.0,1.0),CJ=(1.0,0.0))
      DIMENSION A_NODE(NT,2),N_ELEM(NT,3),CAHM(NT,NT),CHR1(4,4)
     +,N_FORC(NT,3),C_FOR(NT),CAHMI(NT,NT)
      PI=DACOS(-1.0d0)
      OPEN(12,FILE='INPUT.TXT')
      READ(12,*) NE,NN,E,U,RO,THO,THI,N_FOR
      CLOSE(12)
      OPEN(13,FILE='ELEM.TXT')
      OPEN(14,FILE='NODE.TXT')
      OPEN(118,FILE='N3.DAT')
      OPEN(119,FILE='N4.DAT')
      DO 10 I=1,NE
   10 READ (13,*) N_ELEM(I,1),N_ELEM(I,2),N_ELEM(I,3)
      DO 20 I=1,NN
   20 READ(14,*) A_NODE(I,1),A_NODE(I,2)
      CLOSE(13)
      CLOSE(14)
      N_ALL = NN*2
      A_L = A_NODE(2,2)-A_NODE(1,2)
      A_I = 0.25*PI*((THO/2.0)**4-(THI/2.0)**4)
      A_S = PI*((THO/2.0)**2-(THI/2.0)**2)
      A_M = RO*A_S
      A_B= E*A_I
C     A_Z= (E*RO)**0.5*A_S
      DO 49 I=1,N_ALL
   49 C_FOR(I)=(0.0,0.0)
      OPEN(15,FILE='FORCE.TXT')
      DO 50 I=1,N_FOR
   50 READ(15,*) N_FORC(I,1),N_FORC(I,2),N_FORC(I,3)
      CLOSE(15)
      C_FOR((N_FORC(1,1)-1)*2+N_FORC(1,2))=CJ*N_FORC(1,3)
      F = 1.0
      DO 500 III=1,800
      W=2.0*PI*F
C     A_G = E/(2*(1+U))
C     A_KK= 1.18
C     A_K = A_G*A_S/A_KK
      A_K = (W**2*A_M/A_B)**0.25
      DO 21 J=1,N_ALL
      DO 21 I=1,N_ALL
   21 CAHM(I,J)=(0.0D0,0.0D0)
      DO 22 J=1,4
      DO 22 I=1,4
   22 CHR1(I,J)=(0.0D0,0.0D0)
      CALL HMATR(A_B,A_K,A_L,CHR1)
      DO 30 L=1,NE
C      ASSEMBLE THE CHR1 MATRIX
      DO 40 I=1,4
      DO 40 J=1,4
      CAHM(I+2*(L-1),J+2*(L-1))
     += CAHM(I+2*(L-1),J+2*(L-1))+CHR1(I,J)
   40 CONTINUE
   30 CONTINUE
      CALL DLINCG(N_ALL,CAHM,N_ALL,CAHMI,N_ALL)
      CALL SOLVE(F,N_ALL,CAHMI,C_FOR,NT)
      F=F+1.0
  500 CONTINUE
      STOP
      END
```

```
      SUBROUTINE HMATR(A_B,A_K,A_L,CHR1)
      IMPLICIT DOUBLE PRECISION (A,B,D-H,O-Y)
      IMPLICIT COMPLEX*16 (C,Z)
      PARAMETER (CI=(0.0,1.0D0),CJ=(1.0D0,0.0))
      DIMENSION CHR1(4,4),CB1(4,4),CB(4,4),CB2(4,4),CB2I(4,4)
     +,CB1I(4,4),CBT(4,4)
      PI=DACOS(-1.0d0)
      DO 10 I=1,4
      DO 10 J=1,4
10    CHR1(I,J)=(0.0D0,0.0D0)
      B_SS=DSIN(A_K*A_L)
      B_LS=DSINH(A_K*A_L)
      B_SC=DCOS(A_K*A_L)
      B_LC=DCOSH(A_K*A_L)
      CB1(1,1)=0*CJ
      CB1(1,2)=1.0D0*CJ
      CB1(1,3)=0*CJ
      CB1(1,4)=1.0D0*CJ
      CB1(2,1)= A_K
      CB1(2,2)= 0.0
      CB1(2,3)= A_K
      CB1(2,4)= 0.0
      CB1(3,1)=B_SS
      CB1(3,2)=B_SC
      CB1(3,3)=B_LS
      CB1(3,4)=B_LC
      CB1(4,1)= A_K*B_SC
      CB1(4,2)=-1*A_K*B_SS
      CB1(4,3)= A_K*B_LC
      CB1(4,4)= A_K*B_LS
C     DO 20 J=1,4
C20   CB1(3,J)=-1.0*CB1(3,J)
C20   CB1(4,J)=-1.0*CB1(4,J)
      CB2(1,1)= -1*A_K**3
      CB2(1,2)= 0.0
      CB2(1,3)= A_K**3
      CB2(1,4)= 0.0
      CB2(2,1)= 0.0
      CB2(2,2)= A_K**2
      CB2(2,3)= 0.0
      CB2(2,4)= -1*A_K**2
      CB2(3,1)= A_K**3*B_SC
      CB2(3,2)= -1*A_K**3*B_SS
      CB2(3,3)= -1*A_K**3*B_LC
      CB2(3,4)= -1*A_K**3*B_LS
      CB2(4,1)= -1*A_K**2*B_SS
      CB2(4,2)= -1*A_K**2*B_SC
      CB2(4,3)= A_K**2*B_LS
      CB2(4,4)= A_K**2*B_LC
      DO 25 I=1,4
      DO 25 J=1,4
25    CB2(I,J)=A_B*CB2(I,J)
C     DO 29 J=1,4
C     CB2(3,J)=-1.0*CB2(3,J)
C29   CB2(4,J)=-1.0*CB2(4,J)
      CALL DLINCG(4,CB2,4,CB2I,4)
      CALL DLINCG(4,CB1,4,CB1I,4)
C     CALL cinvs(CB2,CB2I,4)
      CALL AMPY1(CB1,CB2I,CB,4,4,4)
      CALL AMPY1(CB2,CB1I,CBT,4,4,4)
C     DO 29 J=1,4
```

```
C       CB(3,J)=-1.0*CB(3,J)
C29     CB(4,J)=-1.0*CB(4,J)
        DO 50 I=1,4
        DO 50 J=1,4
50      CHR1(I,J)=CBT(I,J)
        RETURN
        END



        SUBROUTINE AMPY1(CAA,CAB,CAC,N,M,L)
C       THIS PROGRAM IS MATRIX A * B = C
        IMPLICIT DOUBLE PRECISION (A,B,D-H,O-Y)
        IMPLICIT COMPLEX*16 (C,Z)
        PARAMETER (CI=(0.0,1.0),CJ=(1.0,0.0))
        DIMENSION CAA(N,M),CAB(M,L),CAC(N,L)
        DO 9 J=1,L
        DO 9 I=1,N
        CAC(I,J)=0*CI
        DO 9 K=1,M
9       CAC(I,J)=CAC(I,J)+CAA(I,K)*CAB(K,J)
        RETURN
        END



        SUBROUTINE AMPY(CAA,CAB,CAC,N,M,L,NA,NB,NC)
C       THIS PROGRAM IS MATRIX A * B = C
        IMPLICIT DOUBLE PRECISION (A,B,D-H,O-Y)
        IMPLICIT COMPLEX*16 (C,Z)
        PARAMETER (CI=(0.0,1.0),CJ=(1.0,0.0))
        DIMENSION CAA(NA,NA),CAB(NB,NB),CAC(NC,NC)
        DO 10 J=1,L
        DO 10 I=1,N
        CAC(I,J)=0*CI
        DO 10 K=1,M
10      CAC(I,J)=CAC(I,J)+CAA(I,K)*CAB(K,J)
        RETURN
        END



        SUBROUTINE TMPY(CA,CB,M,N,NA,NB)
C       THIS IS FOR MATRIX TRANSPOSE
C       B=A'
        IMPLICIT DOUBLE PRECISION (A,B,D-H,O-Y)
        IMPLICIT COMPLEX*16 (C,Z)
        DIMENSION CA(NA,NA),CB(NB,NB)
        DO 100 J=1,M
        DO 100 I=1,N
100     CB(I,J)=CA(J,I)
        RETURN
        END



        SUBROUTINE CINVS(H,HINVS,N)
C       FIND INVERSE (HINVS) OF COMPLEX MATRIX H
        COMPLEX*16 H(N,N),HINVS(N,N),A(N,N),B(N,N),SUM
        CALL CSUBN(H,A,N)
        NM1=N-1
        DO 40 I=1,NM1
        SUM=(0.0,0.0)
```

```
      DO 41 K=1,N
41    SUM=SUM+A(K,K)
      SUM=SUM/I
      DO 42 J=1,N
42    A(J,J)=A(J,J)-SUM
      IF (I .EQ. NM1) CALL CSUBN(A,HINVS,N)
      CALL CMPLY(H,A,B,N)
40    CALL CSUBN(B,A,N)
      DO 43 I=1,N
      DO 43 J=1,N
43    HINVS(I,J)=HINVS(I,J)/A(1,1)
      RETURN
      END

      SUBROUTINE CSUBN(A,B,N)
      COMPLEX*16 A(N,N),B(N,N)
      DO 50 I=1,N
      DO 50 J=1,N
50    B(I,J)=A(I,J)
      RETURN
      END
C     REAL MATRIX MULTIPLICATION:C=A*B
      SUBROUTINE CMPLY(A,B,C,N)
      COMPLEX*16 A(N,N),B(N,N),C(N,N)
      DO 60 I=1,N
      DO 60 J=1,N
      C(I,J)=0
      DO 60 K=1,N
60    C(I,J)=C(I,J)+A(I,K)*B(K,J)
      RETURN
      END


      SUBROUTINE SOLVE(F,N_ALL,CAHM,C_FOR,NT)
      IMPLICIT DOUBLE PRECISION (A,B,D-H,O-Y)
      IMPLICIT COMPLEX*16 (C,Z)
      PARAMETER (CI=(0.0,1.0),CJ=(1.0,0.0),IPATH=1)
      DIMENSION CAHM(NT,NT),C_FOR(NT),CA(N_ALL,N_ALL),
     +CB(N_ALL),CX(N_ALL)
      PI=DACOS(-1.0d0)
      DO 9 I=1,N_ALL
9     CX(I)=0*CJ
      DO 10 I=1,N_ALL
      DO 10 J=1,N_ALL
10    CA(I,J)=CAHM(I,J)
      DO 20 I=1,N_ALL
20    CB(I)=C_FOR(I)
C     CALL DLSLCG (N_ALL,CA,N_ALL,CB,IPATH,CX)
      DO 30 I=1,N_ALL
      DO 30 J=1,N_ALL
30    CX(I)=CX(I)+CA(I,J)*CB(J)
      ANS=CDABS(CX(29))
C     ANS=CDABS(CX(8))
C     WRITE(118,*) F,20*LOG10(CDABS(CX(29)/10E+20))
      WRITE(118,*) F,ANS
C     WRITE(119,*) F,20*LOG10(CDABS(CX(6)))
C     WRITE(119,*) F,CDABS(CX(6))
      WRITE(119,*) F,CDABS(CX(30))
      RETURN
      END
```